

## **SHEAR STRENGTH OF HEAT-TREATED SOLID WOOD BONDED WITH POLYVINYL-ACETATE REINFORCED BY NANOWOLLASTONITE**

HAMID R. TAGHIYARI<sup>1</sup>, AYOUB ESMAILPOUR<sup>1</sup>, STERGIOS ADAMOPOULOS<sup>2</sup>, KUROSH ZERESHKI<sup>1</sup>, REZA HOSSEINPOURPIA<sup>2</sup>

<sup>1</sup>SHAHID RAJAEI TEACHER TRAINING UNIVERSITY, TEHRAN, IRAN

<sup>2</sup>LINNAEUS UNIVERSITY, VÄXJÖ, SWEDEN

(RECEIVED MAY 2019)

### **ABSTRACT**

This study investigated the shear strength of heat-treated solid wood of three species (beech, poplar, and fir) bonded with polyvinyl-acetate (PVA) adhesive reinforced by nanowollastonite (NW). Wood specimens were heat-treated at 165°C and 185°C, and then bonded using PVA reinforced by 5% and 10% of NW. Shear strength tests parallel to the grain of bonded specimens were performed according to ASTM D143-14 (2014). The results demonstrated that the shear strength was significantly dependent upon the density of the specimens. Heat treatment decreased the shear strength of the bonded specimens considerably. This was attributed to several factors, such as a reduction in polar groups in the cell wall, increased stiffness of the cell wall after heat treatment, and a reduction in the wettability of treated wood. However, NW acted as a reinforcement agent or extender in the complex, and eventually improved the shear bond strength. Moreover, the density functional theory (DFT) proved the bond formation between calcium atoms in the NW and hydroxyl groups of cell wall polymers. The overall results indicated the potential of NW to improve the bonding strength of heat-treated wood.

**KEYWORDS:** Heat treatment, nano-suspensions, polyvinyl-acetate adhesive (PVA), shear bond strength, wollastonite.

### **INTRODUCTION**

Wood is a renewable raw material for numerous industrial sectors; however, it is susceptible to abiotic and biological degradations. Wood modification is an established, environmentally friendly technology that decreases the hygroscopicity of wood and, consequently, diminishes the moisture-induced deformation processes and abiotic and biotic damages, such as those caused by

weathering and fungal decay (Hosseinpourpia et al. 2016, Ayata et al. 2017, Behr et al. 2018). Chemical modification, such as acetylation, involves a reaction between a chemical reagent and the reactive parts (mainly hydroxyl groups) of wood components. As a result, covalent bonds are formed and the basic chemistry and properties of the wood's cell wall polymers are changed (Papadopoulos and Hill 2002, 2003, Hill 2006, 2008). Impregnation modification of wood with thermosetting resins, such as melamine-formaldehyde and phenol formaldehyde, alters its material properties, but the chemical structure of the cell wall polymer remains unchanged (Mahnert et al. 2013, Kielmann et al. 2014, Hosseinpourpia and Mai 2016a,b,c). Thermal modification improves wood properties by altering its chemical structure, mainly hemicelluloses (Kato and Cameron 1999, Borrega and Karenlampi 2010, Suchy et al. 2010, Hosseinpourpia et al. 2018). However, this method results in a reduction in the mechanical strength of modified wood, particularly impact bending (Hill 2006). Wood degradation starts at temperatures of approximately 120°C (Kollmann and Fengel 1965) with cleavage of the ether linkages of hemicelluloses and the formation of carboxylic acids (Tjeerdsma et al. 1998, Garrote et al. 2001, Tjeerdsma and Militz 2005, Sundqvist et al. 2006). The latter catalyzes the further degradation of polysaccharides (Tjeerdsma et al. 1998), and releases formaldehyde and other aldehydes (Peters et al. 2008, 2009). Lignin is a more stable polymer during thermal degradation when compared to polysaccharides, but its chemical structure alters through the demethoxylation of ether bonds, auto-condensation reactions, and cross-linking (Mahnert et al. 2013, Tjeerdsma et al. 1998, Sivonen et al. 2002, Wikberg and Maaunu 2004, Nuopponen et al. 2005, Hosseinpourpia et al. 2017).

Alterations in the chemical structure of wood due to the thermal modification might affect its gluing and painting ability (Kamdern et al. 2002, Inari et al. 2007, Bastani et al. 2015). It was shown previously that the penetration of a polyvinyl-acetate (PVA) adhesive increased considerably into Scots pine and beech wood treated at 195°C (Bastani et al. 2016a). The authors argued that thermal modification creates some free spaces in the wood structure through the cell wall deterioration, like cracking and/or the decomposition of some chemical compounds inside lumens, such as extractives, which results in the development of additional flow pathways for the adhesive.

The thermal conductivity of nanofluids containing dispersed metallic nanoparticles has been widely studied. In general, these nanofluids increase wood's thermal conductivity due to the enhancement of heat transfer (Majidi 2016, Harsini et al. 2017, Sandeep et al. 2017). Metal and mineral nanoparticles and nanofibers have been used to increase the heat-transfer and resistance to fungal deterioration in solid wood and wood-based composites (Mantanis and Papadopoulos 2010, Akhtari et al. 2013, Haghighi et al. 2014, Taghiyari et al. 2014a,b, Soltani et al. 2016).

Wollastonite is a silicate mineral compound ( $\text{CaSiO}_3$ ) that can be found in many countries including the USA, China, and Iran. A number of studies have investigated the influence of nanowollastonite impregnation on the properties of wood and wood-based composites (Haghighi et al. 2014, Soltani et al. 2016, Schmidt 2006, Maresi et al. 2013, Taghiyari et al. 2013, 2016a, Taghiyari and Moradi Malek 2014, Kumar et al. 2020). The formation of bonds between the nanowollastonite (NW) and wood components resulted in the engagement of hydroxyl groups in wood, eventually improving the dimensional stability. Additionally, its high thermal conductivity coefficient accelerates resin-curing, resulting in an improvement in the wood's physical and mechanical properties. The NW acted as a physical barrier towards the penetration of fire, increasing fire-retardancy in both solid wood and wood-composites. Furthermore, its growth-reducing effects on some pathogens, including fungi, improved biological resistance to some wood-deteriorating fungi (Haghighi et al. 2014, Soltani et al. 2016, Schmidt 2006, Maresi et al. 2013, Taghiyari et al. 2013, 2016a, Taghiyari and Moradi Malek 2014).

As the use of wollastonite nanomaterials has become more popular to improve the technological properties of wood and wood-based composites during the last few years, it is important to expand the knowledge of their influence on the bonding behavior of solid wood adhesives. Therefore, the present study aims to investigate the tensile shear strength of untreated and heat-treated beech, poplar, and fir wood bonded with a nanowollastonite reinforced PVA adhesive.

## MATERIAL AND METHODS

### Material

#### *Specimen preparation*

Beech (*Fagus orientalis* L. collected from Chalous, Iran), poplar (*Populus nigra* L.; collected from Chalous, Iran), and Silver fir (*Abies alba* Mill. imported from Russia) were selected as the test wood species based on their importance in various industrial applications in Iran. Ninety specimens, free from knots, cracks, and other physical or fungal damages were prepared for each wood species. In total, 270 specimens were prepared for all three wood species, as shown in Fig. 1.

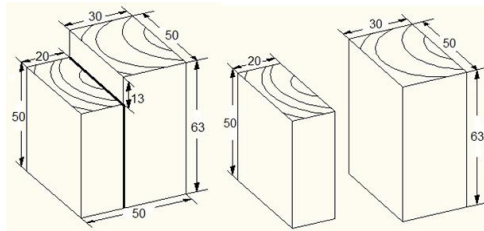


Fig. 1: Details of sample preparation for the shear strength testing. From right to the left: dimensions of the large and small pieces to be glued and final sample size showing a thicker glue line (dimensions in mm).

The specimens were randomly divided into three treatments, including untreated (UT), and heat-treated at 165°C (HT-165) and 185°C (HT-185). Then, the specimens were divided into three sub-groups for gluing with polyvinyl acetate adhesive (PVA), and with polyvinyl acetate containing 5% (PVA-5NW) and 10% nanowollastonite (PVA-10NW). The PVA adhesive was purchased from Shomal Resin & Adhesive Co. (Tehran, Iran), with a viscosity of  $500 \pm 20$ , and  $50 \pm 5\%$  solid content. Ten specimens were used for each treatment condition.

#### *Heat treatment process*

Specimens of each heat-treatment temperature were randomly arranged in an oven and heated for 5 h at 165°C and at 185°C for HT-165 and HT-185 treatments, respectively. The treatment initiated when the internal temperature of the oven reached the target temperatures (165 or 185°C). The specimens were weighed both before and after the heat treatment by a digital scale (with 0.0001 g precision) to assess the mass changes during the process.

#### *Aqueous NW addition*

Aqueous NW gel with 70% to 75% solid content and a size range of 30 to 110 nm was purchased from Lotfali-Zade Mehrabadi Manufacturing Company of Mineral and Industrial Products, Tehran, Iran. The compound contents of NW are summarized in Tab. 1.

Tab. 1: Compounds and formulations of the wollastonite nanosuspension (Taghiyari et al. 2016a, 2014ab, Esmailpour et al. 2019ab).

Nanowollastonite compounds	Mixing ratio by mass (% wt.)
CaO	39.77
SiO <sub>2</sub>	46.96
Al <sub>2</sub> O <sub>3</sub>	3.95
Fe <sub>2</sub> O <sub>3</sub>	2.79
TiO <sub>2</sub>	0.22
K <sub>2</sub> O	0.04
MgO	1.39
Na <sub>2</sub> O	0.16
SO <sub>3</sub>	0.05
Water	4.67

Based on the dry weight of PVA, 5% and 10% of NW gel were added to produce PVA-5NW and PVA-10NW gluing systems, respectively. The mixtures were blended for 30 min with a magnetic stirrer for an even dispersion of NW.

## Methods

### *Shear strength parallel to grain*

After the heat treatments, the samples were prepared for their determination of shear strength parallel to grain. Dimensions of the specimens and testing method were performed according to the ASTM D143-14 (2014) standard. Two pieces (small and large) were prepared according to the standard from the UT, HT-165, and HT-185 specimen collectives and subsequently bonded with PVA, PVA-5NW, and PVA-10NW gluing systems (Fig. 1). Then, the glued samples were stored at room conditions ( $25 \pm 2^\circ\text{C}$ ,  $40 \pm 3\%$  RH) for eight weeks to complete the polymerization of the adhesive. Determination of shear strength was carried out using an Instron 4486 universal testing machine (Norwood, MA, USA). The loading was applied continuously throughout the test at a rate of motion of  $0.6 \text{ mm}\cdot\text{min}^{-1}$ . The testing for each specimen was discontinued after the first sudden drop of the loading force.

### *Theoretical analysis*

Density functional theory (DFT) was carried out with OpenMX 3.6 package (Ozaki Group, Tokyo, Japan) to study the adsorption of NW on the cellulose surface (Perdew et al. 1996, Grimme 2006). The generalized gradient approximation (GGA) function with the Perdew-Burke-Ernzerhof (PBE) correction was used to describe the exchange-correlation energy functional (Perdew et al. 1996). The Van der Waals (vdW) interactions were included in the density functional theory (DFT) approach proposed by Grimme (2006).

### *Statistical analysis*

Statistical analysis was conducted using the SPSS software program, version 18 (Chicago, USA). A one-way analysis of variance (ANOVA) was performed to discern significant differences at a 95% confidence level among the different treatments, as described previously (Hosseinpourpia et al. 2019a,b). Fitted-line and surface plots were made using the Minitab software, version 16.2.2 (Minitab Inc., State College, PA, USA).

## RESULTS AND DISCUSSION

The mean mass loss of the heat-treated samples increased with increasing temperature (Fig. 2), due to the higher degradation of wood polysaccharides, mainly hemicelluloses, and the evaporation of extractives (Zaman et al. 2000, Alen et al. 2002, Mahnert et al. 2013, Hosseinpourpia et al. 2016c).

The highest weight loss was 14.8%, which was obtained for the HT-185 beech specimens. This might have been attributed to the higher density and the higher polymer compounds contained in beech as compared to poplar and fir. The density of unheated beech was measured at  $0.7 \text{ g}\cdot\text{cm}^{-3}$  in comparison to those of poplar ( $0.4 \text{ g}\cdot\text{cm}^{-3}$ ) and fir ( $0.38 \text{ g}\cdot\text{cm}^{-3}$ ).

The shear strength results of the untreated specimens showed that the highest and the lowest values were found for beech and fir at 8.3 MPa and 4.8 MPa, respectively (Fig. 3). Poplar exhibited greater shear strength (6.7 MPa) than fir (4.8 MPa). The transversal permeability of poplar and fir were reported as  $0.0028$  and  $0.0004 \times 10^{-13} \text{ m}^3\cdot\text{m}^{-1}$ , respectively (Taghiyari et al. 2016b). The higher permeability may have provided better penetration of the PVA adhesive into the wood structure, which resulted in the greater shear strength of poplar as compared to fir. However, the adhesive penetration needs to be measured and analyzed in further studies for a final conclusion on the possible correlation between the shear strength of adhesives and the permeability of untreated wood.

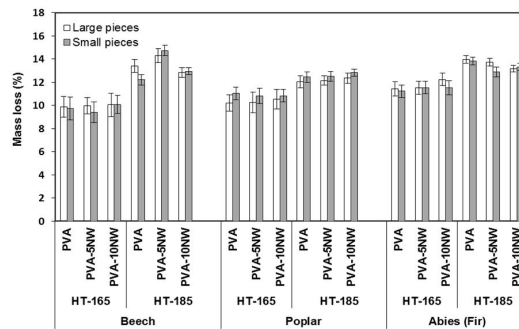


Fig. 2: Mass loss (%) of beech, poplar, and fir samples treated at  $165^\circ\text{C}$  (HT-165) and  $185^\circ\text{C}$  (HT-185).

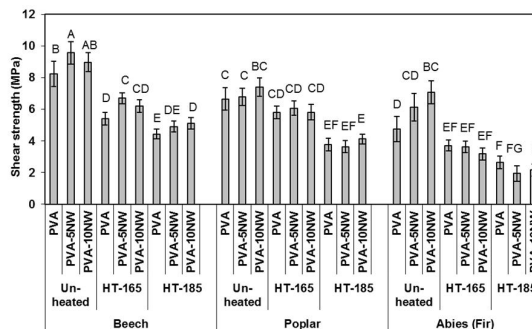


Fig. 3: Shear strength of untreated and heat-treated beech, poplar, and fir bonded with PVA reinforced with NW. The standard deviation was based on the entire population, and the statistical differences were tested with ANOVA and a Duncan test. The labeled values were statistically equal at an error probability of  $\alpha = 0.05$ .

Heat treatment reduced the shear strength for all three wood species; a higher temperature resulted in greater shear strength loss (Fig. 3). The highest and lowest losses in shear strength as a result of heat treatment were observed in HT-185 beech with PVA resin (86%) and poplar HT-165 (79%) with 5% NW content, respectively. This was in accordance to Sahin Kol and co-workers (2009) and Bastani and colleagues (2016b), who found that the bonding strength was reduced in heat-treated wood samples. The shear strength reduction of heat-treated wood can be attributed to: (a) a reduction of polar groups in the cell wall due to the degradation of amorphous polysaccharides by the heat treatment, resulting in less sites available for bonding (Inari et al. 2007, Goli et al. 2014), (b) an increased stiffness of the cell wall after heat treatment (Altgen et al. 2016), which results in a reduction of internal surfaces for chemical bonding or mechanical interlocking of adhesives (Bastani et al. 2015); and (c) a reduction in wettability that may hamper the proper curing of water-based adhesives such as PVA (Bastani et al. 2015). The formation of micro-cracks and checks due to the heat treatment at temperatures above 180°C might also contribute to a declined shear strength of heat-treated wood (Taghiyari and Moradi Malek 2014).

The addition of NW to PVA adhesive resulted in an improvement of shear strength for the untreated samples of all three species (Fig. 3). This positive effect could be partly attributed to the formation of bonds between the wood cell compounds and NW. By means of density functional theory, Taghiyari and co-workers (2016) calculated an optimal adsorption distance and adsorption energy for NW of 1.7 Å and -6.6 eV, respectively. In fact, this rather large adsorption energy obviously indicated a formation of additional bonds between the calcium atoms of NW and the oxygen atoms of hydroxyl groups of the wood cell wall polymers (Fig. 4).

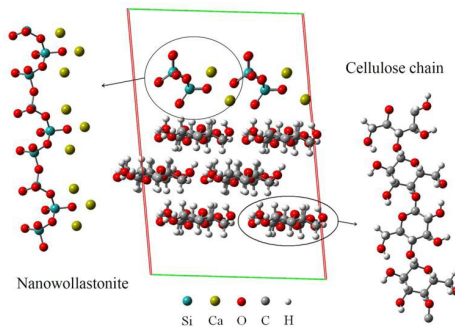
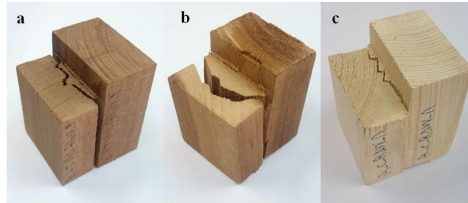


Fig. 4: Schematic representation of bond formation between calcium atoms of NW and oxygen atoms of cell wall cellulose chains.

This could eventually contribute to higher shear strength of samples bonded with PVA-NW systems than with PVA alone. The formation of similar bonds was the main cause of an increased thermal conductivity coefficient and of improved physical and mechanical properties of medium-density fiberboard, in which the resin was treated with NW before being sprayed on the fibers (Taghiyari et al. 2013, 2014a,b). The hardness of wollastonite is relatively high, around 4.5 to 5 based on Mohs scale of mineral hardness. This may have enabled NW fibers to act as reinforcement filler in the glue layer between the two wood pieces, and eventually have fortified their bonding. In the heat-treated samples, the addition of NW to PVA adhesive improved the shear strength of beech specimens. However, it did not change the shear strength of the poplar samples. In the case of fir specimens, the addition of NW to PVA adhesive even slightly reduced the shear strength. This might have been attributed to an increased availability of bonding sites

in beech wood due to the higher density, even after heat-treatment, when compared to poplar and fir.

Macroscopic observation of the tested specimens revealed that most of the failures, in sole PVA adhesive, occurred along the glue line rather than in the wood structure. This was true for both treated and untreated wood samples. However, reinforcement of the PVA with NW provided stronger bonds than solely PVA, which caused the failure in the wood structure (Fig. 5).



*Fig. 5: Wood failures of heat-treated beech at 185°C bonded with PVA-10NW (a), heat-treated poplar at 185°C bonded with PVA-5NW (b), and control fir bonded with PVA (c).*

A long service life of glued wood elements requires tolerant adhesives under different temperature and humidity conditions, and therefore, further studies should be carried out to explore such effects on the performance of NW-reinforced adhesives.

## CONCLUSIONS

(1) For all of the wood species, the shear strength of the heat-treated samples bonded with PVA adhesive were significantly lower than that of the untreated ones, at a 95% statistical confidence level.

(2) The shear strength of untreated beech, poplar, and fir specimens bonded with PVA adhesive was improved by the addition of NW. It was suggested that NW acted as a reinforcement agent in the adhesive.

(3) Although the shear strength of the heat-treated beech increased by adding NW to PVA adhesive, a clear trend was not observed in shear strength of heat-treated poplar and fir specimens by adding NW.

## ACKNOWLEDGMENTS

The first author acknowledges the constant scientific support of his mentor, Mr. Jack Norton (Retired, Horticulture and Forestry Science, Queensland Department of Agriculture, Forestry and Fisheries, Brisbane, Australia). Technical drawing by Engr. Afroz Ghayasvand is also appreciated.

## REFERENCES

1. Akhtari, M., Taghiyari, H.R., Ghorbani Kokandeh, M., 2013: Effect of some metal nanoparticles on the spectroscopy analysis of Paulownia wood exposed to white-rot fungus. *European Journal of Wood and Wood Products* 71(2): 283-285.

2. Alen, R., Kotilainen, R., Zaman, A., 2002: Thermochemical behavior of Norway spruce (*Picea abies*) at 180-225°C. *Wood Science and Technology* 36(2): 163-171.
3. Altgen, M., Hofmann, T., Militz, H., 2016: Wood moisture content during the thermal modification process affects the improvement in hygroscopicity of Scots pine sapwood. *Wood Science and Technology* 50(6): 1181-1195.
4. Ayata, U., Akcay, C., Esteves, B., 2017: Determination of decay resistance against *Pleurotus ostreatus* and *Coniophora puteana* fungus of heat-treated Scotch pine, oak and beech wood species. *Maderas: Ciencia y tecnología* 19: 309-316.
5. ASTM D143-14, 2014: Standard test methods for small clear specimens of timber.
6. Bastani, A., Adamopoulos, S., Militz, H., 2015: Effect of open assembly time and equilibrium moisture content on the penetration of polyurethane adhesive into thermally modified wood. *Journal of Adhesion* 93(7): 575-583.
7. Bastani, A., Adamopoulos, S., Koddenberg, T., Militz, H., 2016a: Study of adhesive bondlines in modified wood with fluorescence microscopy and X-ray micro-computed tomography. *International Journal of Adhesion and Adhesives* 68: 351-358.
8. Bastani, A., Adamopoulos, S., Militz, H., 2016b: Shear strength of furfurylated, N-methylol melamine and thermally modified wood bonded with three conventional adhesives. *Wood Material Science & Engineering* 12(4): 236-241.
9. Behr, G., Bollmus, S., Gellerich, A., Militz, H., 2018: Improvement of mechanical properties of thermally modified hardwood through melamine treatment. *Wood Material Science & Engineering* 13(5): 262-270.
10. Borrega, M., Karenlampi, P.P., 2010: Hygroscopicity of heat-treated Norway spruce (*Picea abies*) wood. *European Journal of Wood and Wood Products* 68(2): 233-235.
11. Esmailpour, A., Taghiyari H. R., Majidi Najafabadi, R., Kalantari, A., Papadopoulos, A. N., 2019a: Fluid flow in cotton textile: Effects of wollastonite nanosuspension and *Aspergillus niger* fungus. *Processes* 7(12): 901..
12. Esmailpour, A., Taghiyari, H. R., Majidi, R., Morrell, J. J., Mohammad-Panah, B., 2019b: Nano-wollastonite to improve fire retardancy in medium-density fiberboard (MDF) made from wood fibers and camel-thorn. *Wood Material Science & Engineering*, published online: doi 10.1080/17480272.2019.1641838.
13. Garrote, G., Domínguez, H., Parajó, J. C., 2001: Study on the deacetylation of hemicelluloses during the hydrothermal processing of Eucalyptus wood. *Holz als Roh- und Werkstoff* 59(1-2): 53-59.
14. Goli, G., Cremonini, C., Negro, F., Zanuttini, R., Fioravanti, M., 2014: Physical-mechanical properties and bonding quality of heat treated poplar (I-214) and ceiba plywood. *iForest* 8: 687-692.
15. Grimme, S., 2006: Semiempirical GGA-type density functional constructed with a long-range dispersion correction. *Journal of Computational Chemistry* 27(15): 1787-1799.
16. Harsini, I., Matalkah, F., Soroushian, P., Balachandra, A.M., 2017: Robust, carbon nanotube/polymer nanolayered composites with enhanced ductility and strength. *Journal of Nanomaterials & Molecular Nanotechnology* 6(3): 1-6.
17. Haghghi, A.P., Taghiyari, H.R., Karimi, A.N., 2014: Fire-retarding properties of nano-wollastonite in solid wood. *Philippine Agricultural Scientist* 97(1): 52-59.
18. Hill, C.A.S., 2006: *Wood modification chemical, thermal and other processes*. John Wiley and Sons, Ltd., Chichester, West Sussex, England, 238 pp.
19. Hill, C.A.S., 2008: The reduction in the fibre saturation point of wood due to chemical modification using anhydride reagents: A reappraisal. *Holzforschung* 62(4): 423-428.

20. Hosseinpourpia, R., Adamopoulos, S., Mai, C., 2016: Dynamic vapour sorption of wood and holocellulose modified with thermosetting resins. *Wood Science and Technology* 50(1): 165-178.
21. Hosseinpourpia, R., Mai, C., 2016a: Mode of action of brown rot decay resistance of acetylated wood: Resistance to Fenton's reagent. *Wood Science and Technology* 50: 413-426.
22. Hosseinpourpia, R., Mai, C., 2016b: Mode of action of brown rot decay resistance in phenol-formaldehyde-modified wood: Resistance to Fenton's reagent. *Holzforschung* 70(3): 253-259.
23. Hosseinpourpia, R., Mai, C., 2016c: Mode of action of brown rot decay resistance of thermally modified wood: Resistance to Fenton's reagent. *Holzforschung* 70(7): 691-697.
24. Hosseinpourpia, R., Adamopoulos, S., Holstein, N., Mai, C., 2017: Dynamic vapour sorption and water-related properties of thermally modified Scots pine (*Pinus sylvestris* L.) wood pre-treated with proton acid. *Polymer Degradation and Stability* 138: 161-168.
25. Hosseinpourpia, R., Adamopoulos, S., Mai, C., 2018: Effects of acid pre-treatments on the swelling and vapor sorption of thermally modified Scots pine (*Pinus sylvestris* L.) wood. *BioResources* 13(1): 331-345.
26. Hosseinpourpia, R., Adamopoulos, S., Parsland, C., 2019a: Utilization of different tall oils for improving the water resistance of cellulosic fibers. *Applied Polymer Science* 136(13): 47303.
27. Hosseinpourpia, R., Adamopoulos, S., Mai, C., Taghiyari, H.R., 2019b: Properties of medium-density fibreboards bonded with dextrin-based wood adhesive. *Wood Research* 64(2): 185-194.
28. Inari, G.N., Petrissans, M., Gerardin, P. 2007: Chemical reactivity of heat-treated wood. *Wood Science and Technology* 41(2): 157-168.
29. Kato, K.L., Cameron, R.E., 1999: A review of the relationship between thermally-accelerated ageing of paper and hornification. *Cellulose* 6(1): 23-40.
30. Kamdem, D.P., Pizzi, A., Jermannaud, A., 2002: Durability of heat-treated wood. *Holz als Roh- und Werkstoff* 60(1): 1-6.
31. Kielmann, B.C., Adamopoulos, S., Militz, H., Mai, C., 2014: Decay resistance of ash, beech and maple wood modified with N-methylol melamine and a metal complex dye. *International Biodeterioration & Biodegradation* 89: 110-114.
32. Kollmann, F., Fengel, D., 1965: Änderungen der chemischen Zusammensetzung von Holz durch thermische Behandlung (Changes in the chemical composition of wood by thermal treatment). *Holz als Roh- und Werkstoff* 23(12): 461-468.
33. Kumar, A., Jyske, T., Möttönen, V., 2020: Properties of injection molded biocomposites reinforced with wood particles of short-rotation aspen and willow. *Polymers* 12(2): 257.
34. Mahnert, K.C., Adamopoulos, S., Koch, G., Militz, H., 2013: Topochemistry of heat-treated and N-methylol melamine modified wood of Koto (*Pterygota macrocarpa* K. Schum.) and Limba (*Terminalia superba* Engl. et Diels). *Holzforschung* 67(2): 137-146.
35. Majidi, R., 2016: Electronic properties of graphyne nanotubes filled with small fullerenes: A density functional theory study. *Journal of Computational Electronics* 15(4): 1263-1268.
36. Mantanis, G. I., Papadopoulos, A. N., 2010: Reducing the thickness swelling of wood based panels by applying a nanotechnology compound. *European Journal of Wood and Wood Products* 68(2): 237-239.
37. Maresi, G., Oliveira Longa, C.M., Turchetti, T., 2013: Brown rot on nuts of *Castanea sativa* Mill: An emerging disease and its causal agent. *iForest* 6: 294-301.

38. Nuopponen, M., Vuorinen, T., Jämsä, S., Viitaniemi, P., 2005: Thermal modifications in softwood studied by FT-IR and UV resonance Raman spectroscopies. *Journal of Wood Chemistry and Technology* 24(1): 13-26.
39. Papadopoulos, A.N., Hill, C.A.S., 2002: The biological effectiveness of wood modified with linear chain carboxylic acid anhydrides against *Coniophora puteana*. *Holz als Roh- und Werkstoff* 60(5): 329-332.
40. Papadopoulos, A.N., Hill, C.A.S., 2003: The sorption of water vapour by anhydride modified softwood. *Wood Science and Technology* 37(3-4): 221-231.
41. Perdew, J.P., Burke, K., Ernzerhof, M., 1996: Generalized gradient approximation made simple. *Physical Review Letters* 77(18): 3865-3868.
42. Peters, J., Fischer, K., Fischer, S., 2008: Characterization of emissions of thermally modified wood and their reduction by chemical treatment. *BioResources* 3(2): 491-502.
43. Peters, J., Pfriem, A., Horbens, M., Fischer, S., Wagenführ, A., 2009: Emissions from thermally modified beech wood, their reduction by solvent extraction and fungicidal effect of the organic solvent extracts. *Wood Material Science & Engineering* 4(1-2): 61-66.
44. Sahin Kol, H., Özbay, G., Altun, S., 2009: Shear strength of heat-treated tali (*Erythrophloeum ivorense*) and iroko (*Chlorophora excelsa*) woods, bonded with various adhesives. *BioResources* 4(4): 1545-1554.
45. Sandeep, N., Sulochana, C., Kumar, B.R., 2017: Flow and heat transfer in MHD dusty nanofluid past a stretching/shrinking surface with non-uniform heat source/sink. *Walailak Journal of Science and Technology* 14(2): 117-140.
46. Schmidt, O., 2006: *Wood and tree fungi: Biology, damage, protection, and use*. Springer-Verlag Berlin Heidelberg, Berlin, 334 pp.
47. Sivonen, H., Maunum, S.L., Sundholm, F., Jämsä, S., Viitaniemi, P., 2002: Magnetic resonance studies of thermally modified wood. *Holzforschung* 56(6): 648-654.
48. Soltani, A., Hosseinpourpia, R., Adamopoulos, S., Taghiyari, H.R., Ghaffari, E., 2016: Effects of heat-treatment and nano-wollastonite impregnation on fire properties of solid wood. *BioResources* 11(4): 8953-8967.
49. Suchy, M., Kontturi, E., Vuorinen, T., 2010: Impact of drying on wood ultrastructure: Similarities in cell wall alteration between native wood and isolated wood-based fibers. *Biomacromolecules* 11(8): 2161-2168.
50. Sundqvist, B., Karlsson, O., Westermarck, U., 2006: Determination of formic-acid and acetic acid concentrations formed during hydrothermal treatment of birch wood and its relation to colour, strength and hardness. *Wood Science and Technology* 40(7): 549-561.
51. Taghiyari, H.R., Mobini, K., Sarvari Samadi, Y., Doosti, Z., Karimi, F., Asghari, M., Jahangiri, A., Nouri, P., 2013: Effects of nano-wollastonite on thermal conductivity coefficient of medium-density fiberboard. *Journal of Nanomaterials & Molecular Nanotechnology* 2(1): 1-5.
52. Taghiyari, H.R., Bari, E., Schmidt, O., Tajick Ghanbary, M. A., Karimi, A., Tahir, P.M.D., 2014a: Effects of nanowollastonite on biological resistance of particleboard made from wood chips and chicken feather against *Antrodia vaillantii*. *International Biodeterioration & Biodegradation* 90: 93-98.
53. Taghiyari, H.R., Ghorbanali, M., Tahir, P.M.D., 2014b: Effects of the improvement in thermal conductivity coefficient by nano-wollastonite on physical and mechanical properties in medium-density fiberboard (MDF). *BioResources* 9(3): 4138-4149.
54. Taghiyari, H.R., Moradi Malek, B., 2014: Effect of heat treatment on longitudinal gas and liquid permeability of circular and square-shaped native hardwood specimens. *Heat and Mass Transfer* 50(8): 1125-1136.

55. Taghiyari, H.R., Majidi, R., Jahangiri, A., 2016a: Adsorption of nanowollastonite on cellulose surface: Effects on physical and mechanical properties of medium-density fiberboard (MDF). *Cerne* 22(2): 215-222.
56. Taghiyari, H.R., Esmailpour, A., Zolfaghari, H., 2016b: Effects of nanosilver on sound absorption coefficients in solid wood species. *IET Nanobiotechnology* 10(3): 147-153.
57. Tjeerdsma, B.F., Boonstra, M., Pizzi, A., Tekely, P., Militz, H., 1998: Characterization of thermally modified wood: Molecular reasons for wood performance improvement. *Holz als Roh- und Werkstoff* 56(3): 149-153.
58. Tjeerdsma, B.F., Militz, H., 2005: Chemical changes in hydrothermal treated wood: FTIR analysis of combined hydrothermal and dry heat-treated wood. *Holz als Roh- und Werkstoff* 63(2): 102-111.
59. Wikberg, H., Maaunu, L.S., 2004: Characterization of thermally modified hard- and softwoods by <sup>13</sup>C CP/MAS NMR. *Carbohydrate Polymer* 58(4): 461-466.
60. Zaman, A., Alén, R., Kotilainen, R., 2000: Thermal behavior of scots pine (*Pinus sylvestris*) and silver birch (*Betula pendula*) at 200°C-230°C. *Wood and Fiber Science* 32(2): 138-143.

HAMID REZA TAGHIYARI  
 SHAHID RAJAEI TEACHER TRAINING UNIVERSITY  
 FACULTY OF MATERIALS ENGINEERING & NEW TECHNOLOGIES  
 WOOD SCIENCE AND TECHNOLOGY DEPARTMENT  
 TEHRAN  
 IRAN

AYOUB ESMAILPOUR  
 SHAHID RAJAEI TEACHER TRAINING UNIVERSITY  
 DEPARTMENT OF PHYSICS  
 FACULTY OF SCIENCES  
 TEHRAN  
 IRAN

STERGIOS ADAMOPOULOS  
 LINNAEUS UNIVERSITY  
 DEPARTMENT OF FORESTRY AND WOOD TECHNOLOGY  
 LÜCKLIGS PLATS 1  
 35195 VÄXJÖ  
 SWEDEN

KUROSH ZERESHKI  
 SHAHID RAJAEI TEACHER TRAINING UNIVERSITY  
 FACULTY OF MATERIALS ENGINEERING & NEW TECHNOLOGIES  
 WOOD SCIENCE AND TECHNOLOGY DEPARTMENT  
 TEHRAN  
 IRAN

\*REZA HOSSEINPOURPIA  
LINNAEUS UNIVERSITY  
DEPARTMENT OF FORESTRY AND WOOD TECHNOLOGY  
LÜCKLIGS PLATS 1  
35195 VÄXJÖ  
SWEDEN

\*Corresponding author: reza.hosseinpourpia@lnu.se

## **HEARTWOOD AND SAPWOOD FEATURES OF *SORBUS* *TORMINALIS* GROWN IN IRANIAN FORESTS**

MOHSEN BAHMANI  
SHAHREKORD UNIVERSITY  
SHAHREKORD, IRAN

LEILA FATHI  
UNIVERSITY OF HAMBURG  
HAMBURG, GERMANY

GERALD KOCH  
THÜNEN INSTITUTE OF WOOD RESEARCH  
HAMBURG, GERMANY

FARHAD KOOL  
UNIVERSITY OF ZABOL  
ZABOL, IRAN

HAMED AGHAJANI  
IRAN SARI AGRICULTURE SCIENCE AND NATURAL RESOURCES UNIVERSITY  
SARI, IRAN

MIHA HUMAR  
UNIVERSITY OF LJUBLJANA  
LJUBLJANA, SLOVENIA

(RECEIVED MARCH 2019)

### **ABSTRACT**

In the present study anatomical, histometrical, chemical and physical properties of the wood of 45-year old trees were determined. For this purpose, three trees were randomly cut at Sangdeh-Mazdaran located in the northern part of Iran. Disks and logs were removed at breast height to study the respective wood properties. Fiber length, fiber diameter, fiber lumen diameter, cell wall thickness as well as lignin and cellulose content of sapwood are superior to those of heartwood. Growth rings boundaries are fairly distinct and can be distinguished by only two to three compact fiber layers. The wood is diffuse-porous and vessels are small and predominately solitary, hardly visible to the naked eye on transverse sections. Most rays are 2-seriate interspersed with only few 3-seriate and uniseriate rays, and composed of procumbent body cells with occasional marginal rows of upright and/or square cells.

KEYWORDS: *Sorbus torminalis*, wood structure, heartwood-sapwood relationship, chemical and physical properties.

## INTRODUCTION

*Sorbus torminalis* (L.) Crantz is an important commercial species growing in the northern forests of Iran from Astara to Golidaghi. In Iran the tree is known as 'Barank', other names are 'Wild service tree' or 'Mountain ash' (GB), alisier des bois (FR) and 'Elsbeere' (DE). According to Espahbodi et al. (2008) and Tabandeh et al. (2007), it grows in mixed stands with beech (*Fagus orientalis*), hornbeam (*Carpinus betulus*) and chestnut-leaved oaks (*Quercus castaneifolia*). The distribution of *Sorbus torminalis* in Eurasia covers a wide range, from the north of the Maghreb to the south of Sweden and from eastern Great Britain to northern Iran (Demersure et al. 2000). Trees grow to a height of 15 to 25 m with a diameter at breast height (DBH) from 60 to 90 cm (Welk et al. 2016). The wood has a fine texture and is often used for manufacturing highly valued artistic objects and musical instruments. Medicinal uses of the *Sorbus* species are also known (Termentzi et al. 2006). In Iran, studies on this species are mainly related to tree-physiology and ecology (Espahbodi et al. 2008). Golbabaee et al. (2015) determined some strength properties (static bending, compression parallel to grain, impact bending and shear) of *S. torminalis* from different regions in the north of Iran. Studies of the anatomical, biometrical, chemical and physical properties are very rare in Iran (Aghajani et al. 2019). Kol et al. (2009) reported that physical and mechanical properties of *S. aucuparia* are sufficient to produce an acceptable product and that this species constitutes a suitable alternative for alder (*Alnus* spp.) and beech. However, it is quite different from *S. torminalis* and its wood properties should not be taken as equivalent.

*S. torminalis* and *S. domestica* are naturally distributed and available in Europe. Although both species belong to the same genus, from the point of view of dendrology and wood quality they are quite different. Schoch et al. (2014) reported that the wood of *S. torminalis* is diffuse to semi-ring-porous, rays almost homocellular and generally 2-seriate, vessels with simple perforation plates and intervessel pits opposite. Đurković et al. (2011) studied some anatomical and chemical properties of the genus *Sorbus* except *S. torminalis*. They reported that most are semi-ring-porous with simple perforation plates, with the exception of *S. aria*. Richter and Dallwitz (2018) described the wood of *S. torminalis* as diffuse porous, vessels arranged in no specific pattern, exclusively solitary or with few multiples, medium fiber cell wall thickness, axial parenchyma in narrow marginal bands, apotracheal diffuse and paratracheal scanty; rays multiseriate, generally 2-3 cells wide.

*S. torminalis* is tolerant to direct sunlight and short-time water deficit in the soil, therefore it is considered suitable for afforestation on arid and warm sites and constitutes a valid option for wider utilization in forestry and landscape management. As *S. torminalis* in Iranian forests has considerable potential, the aim of the current study is to investigate wood structural features, fiber morphology, physical and chemical properties of this species.

## MATERIAL AND METHODS

The raw material was obtained from 45-year-old *S. torminalis* trees grown on an experimental site of the Paradukale forestry project located at the Shirin-e-Rud river basin No. 66 watershed, and cut down in June 2018. The 2347 ha plot is about 60 kilometres from the city of Sari.

The altitude of this site is 350 m, the climate is mild, generally warm and temperate, with an annual precipitation of 690 mm and a mean temperature 16.7°C. October and November are the rainy season in this area. The temperature reaches its maximum in June, July and August.

### Physical properties

5-cm thick discs were cut from three 3-m logs with base diameter 60 cm for determination of physical properties (dry density, basic density and volumetric shrinkage and swelling,  $n = 60$ ). In order to determine the physical properties, test specimens with dimensions of  $3 \times 2 \times 2$  cm were prepared from heartwood and sapwood according to ISO 13061-2. Specimen dimensions were measured in green (saturated) and oven-dry condition with a slide calliper; oven-dry mass was determined with an electric balance to an accuracy of 0.01 g. Shrinkage was calculated using the dimensional change from the green to oven-dry condition. The physical properties were calculated by the following Eqs. 1-4.

$$D_0 = P_0 / V_0 \quad (1)$$

$$D_b = P_0 / V_s \quad (2)$$

$$\beta_v = (V_s - V_0) / V_s \quad (3)$$

$$\alpha_v = (V_s - V_0) / V_0 \quad (4)$$

where:  $D_0$  - oven dry density ( $\text{g}\cdot\text{cm}^{-3}$ ),  
 $D_b$  - basic density ( $\text{g}\cdot\text{cm}^{-3}$ ),  
 $\beta_v$  - volumetric shrinkage (%),  
 $\alpha_v$  - volumetric swelling (%),  
 $V_s$  - volume in state of saturate (cm),  
 $V_0$  - volume in state of oven-dry (cm),  
 $P_0$  - weight in state of oven dry (g),  
 $P_s$  - weight in state of saturate (g).

### Biometric properties

Thirty specimens were prepared for fiber dimension ( $15 \times 10 \times 2$  mm) like fiber length, fiber diameter, lumen diameter and cell wall thickness ( $n = 50$ ). Franklin (1945) method was applied for separation of wood fibers. Samples for measuring fiber dimensions were macerated in a mixture (1:1) of 30% hydrogen peroxide and glacial acid in an oven at 64°C oven for 24 hours. After that, the samples were washed with distilled water. The fiber dimensions were determined by using Leica Image Analysis System. For this test, it was necessary to measure 20 fiber dimensions per sub-samples.

### Chemical compounds

The chemical analysis was performed according to TAPPI test methods, cellulose (T 257 cm-85), lignin (T 222 om-98), ash (T 211 om-93), solubility in alcohol-acetone (T 204 cm-88). All measurements were repeated three times and the mean values calculated.

### Wood anatomical parameters

Small blocks of approximately 1 (L)  $\times$  1 (R)  $\times$  1 (T) cm were cut from each disk. The wood was softened by boiling to remove excess air, followed by immersion in distilled water. 20-30  $\mu\text{m}$  thin transverse, radial and tangential sections were cut with a sliding microtome, bleached, stained with safranin red and rinsed in an ethanol series (50, 95 and 100%) until all traces of excess stain

and water were removed. After bleaching, staining and dehydrating, sections were mounted in Canada balsam for subsequent microscopic examination using Olympus BH-2 microscope in different magnification (4x, 10x, 20x and 40x). The description of the anatomical characters followed the IAWA "List of Microscopic Features for Hardwood Identification" (IAWA 1989).

## RESULTS AND DISCUSSION

### Physical properties

Fig. 1 shows the results for oven-dry density, basic density, volumetric shrinkage and volumetric swelling for heartwood and sapwood. The results reveal that there are significant differences between sapwood and heartwood, all determined properties being higher in heartwood than in sapwood. The corresponding numerical values of mean oven-dry density, basic density, volumetric shrinkage, and volumetric swelling values are as follows:

Heartwood:  $887 \pm 49.2 \text{ kg}\cdot\text{cm}^{-3}$ ,  $634 \pm 37.2 \text{ kg}\cdot\text{cm}^{-3}$ ,  $16.60 \pm 2.5\%$  and  $20.4 \pm 3.6\%$ , respectively. Sapwood:  $721 \pm 20.4 \text{ kg}\cdot\text{cm}^{-3}$ ,  $567 \pm 12.7 \text{ kg}\cdot\text{cm}^{-3}$ ,  $15.1 \pm 1.44\%$  and  $17.7 \pm 1.9\%$ , respectively.

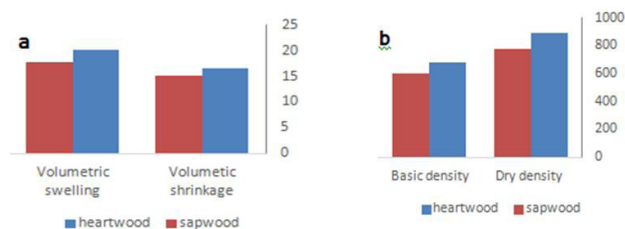


Fig. 1: (a) Volumetric shrinkage and volumetric swelling (%), (b) average of wood density ( $\text{kg}\cdot\text{m}^{-3}$ ) of *Sorbus torminalis* in heartwood and sapwood.

Generally, the wood can be classified as heavy with oven-dry and basic density of  $831 \text{ kg}\cdot\text{m}^{-3}$  and  $643 \text{ kg}\cdot\text{m}^{-3}$ , respectively. The oven-dry density measured in the present study is much higher than reported by Gholbabei et al. (2014). It is comparable with the values reported by Richter and Dallwitz (2018) ( $750 \text{ kg}\cdot\text{m}^{-3}$ ). Moreover, the density is higher than that reported for Persian ironwood ( $820 \text{ kg}\cdot\text{m}^{-3}$ , Enayati 2010) and hornbeam ( $800 \text{ kg}\cdot\text{m}^{-3}$ , Khalkhali 2013) but lower than that of Persian oak ( $0.99 \text{ kg}\cdot\text{cm}^3$ , Saedi et al. 2017). For comparison, oven-dry and basic density of *S. aucuparia* are  $737 \text{ kg}\cdot\text{m}^{-3}$  and  $635 \text{ kg}\cdot\text{m}^{-3}$ , respectively (Korkut et al. 2009).

### Chemical composition

Tab. 1 shows the mean values of the chemical constituents of *S. torminalis*. On average, hardwood is composed of 40-45% cellulose, 17-25% lignin and less than 10% of extractives (Efhamisizi et al. 2009). In other *Sorbus* species such as *S. aria*, *S. zuzanae*, *S. montisalpa*, *S. haljamovae*, *S. chamaemmespilus* and *S. aucuparia*, the lignin content is 16-19%, that of cellulose 28-30%, and that of extractives 3-5% (Đurković et al. 2011). By comparison, for *S. torminalis* from the northern forests of Iran, cellulose content is somewhat lower, extractives content somewhat higher and lignin content about equal. Such differences could be related to site, growth conditions and forest management practices (Zobel and Buijtenen 1989, Bahmani et al. 2018). Overall, the lignin content of *S. torminalis* is less than the average of most hardwoods, whereas the cellulose content does not differ significantly.

Tab. 1: The average chemical composition of heartwood and sapwood of *S. torminalis* (according to TAPPI test methods).

Area	Cellulose (%)	Lignin (%)	Extractives (%)	Ash (%)
Sapwood	49.8	17.8	1.6	0.6
Heartwood	47.9	19.2	2.7	0.8
Combined	48.9 ± 3.5	18.5 ± 1.2	2.2 ± 0.6	0.7 ± 0.2

### Histometrical parameters

Sapwood has longer fibers than heartwood (Tab. 2). Similar results were previously reported by several researchers (Mariana et al. 2005, Rayirath and Avramidis 2008, Saraeian et al. 2011). On the other hand, sapwood has fibers with larger lumens and thicker walls. Longer fibers in sapwood were reported by Ay and Şahin (1998) and Mariani et al. (2005). Thicker fibers in sapwood were reported by Mariana et al. (2005) and Liukkonen et al. (2007).

Tab. 2: The average biometric features of heartwood and sapwood of *S. torminalis*.

Area	Fiber length (µm)	Fiber diameter (µm)	Lumen diameter (µm)	Cell wall thickness (µm)
Sapwood	1725	25.2	6.6	10.3
Heartwood	1414	22.9	4.1	8.7
Combined	1570 ± 182.1	24.1 ± 2.4	5.4 ± 1.9	9.5 ± 1.6

Fibers are classified into three groups (IAWA 1989):

- short fibers with a length less 900 microns;
- fibers of medium length between 900-1900 microns including *S. torminalis* with an average fiber length of 1570 microns;
- fibers longer than 1900 microns.

The average fiber length of *S. torminalis* is higher than that reported for most hardwoods (Khalkhali 2013). Among Iranian wood species cell wall thickness is high compared to *Populus* species (5 µm) and about equal to that of Persian oak with 9 µm (Efhamisisi 2009, Saedi et al. 2017).

### Wood anatomy

According to the standardized description of the "List of microscopic features for hardwood identification" (IAWA 1989) following microscopic characters were determined for the individual cell types (tissue):

*Vessels*: wood diffuse porous, vessels commonly in short (2-3) radial rows. Average tangential vessel diameter 50 µm, average number of vessels/mm<sup>2</sup> 40-100. Perforations mainly simple; in very narrow vessels occasionally with scalariform to reticulate perforations. Vessel-ray pits with distinct borders, similar to intervessel pits. Helical thickenings present, in narrow and wide vessel elements, throughout the body of vessel elements.

*Tracheids and fibres*: Fibres of medium wall thickness. Average fibre length 900-1600 µm. Fibre pits common in both radial and tangential walls, distinctly bordered.

*Axial parenchyma*: Axial parenchyma banded or diffuse-in aggregates, bands are marginal or seemingly marginal.

*Rays*: Rays 8-12 per tangential mm, multiseriate, even if only few, 1-3 cells wide, narrow (2-4 seriate). Height of large rays more than 1 mm. Rays composed of a single cell type (homocellular), or two or more cell types (heterocellular); heterocellular rays with square and

upright cells restricted to marginal rows, mostly 1 marginal row of upright or square cells.

The following microscopic images show representative transverse sections of *S. torminalis* (Fig. 2). The wood is diffuse-porous with no specific pattern in vessel arrangement. The vessels are predominantly solitary with a mostly rounded, rarely angular outline. The ground tissue fibers are relatively thick-walled and can be clearly distinguished from the thinner-walled apotracheal parenchyma which is banded or diffuse-in aggregates (Fig. 2 left and center).

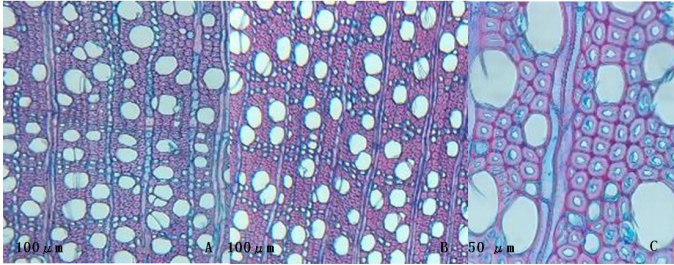


Fig 2: Transverse section of *Sorbus torminalis* L.

The tangential sections (Fig. 3) show the characteristic arrangement of the predominantly 2-seriate rays. Rays either homocellular and composed of procumbent cells or, more frequently, heterocellular with one or more marginal rows of square to upright cells. Ray cells round to slightly oval-elongated; large rays up to 500 µm high; sheath and tile cells absent.

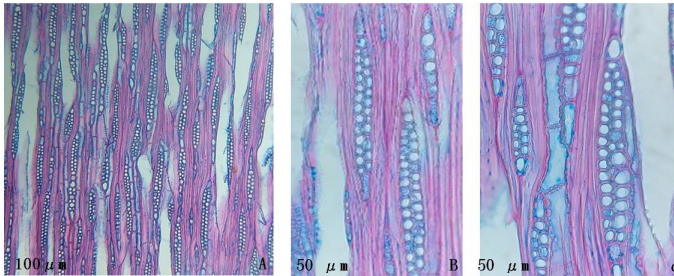


Fig 3: Tangential section of *Sorbus torminalis* L.

The radial sections (Fig. 4) show a heterocellular ray with one marginal row of upright cells (left) or up to 3 square cells (right). The intervessel pits are opposite or alternate with an average diameter (vertical) of 5-7 µm. The vessel-ray pits have distinct borders, similar to intervessel pits (Fig. 4 right). Scalariform to sometimes reticulate perforations are occasionally present in narrow vessel elements (Fig. 4 center); narrow and wide vessel elements with helical thickenings.

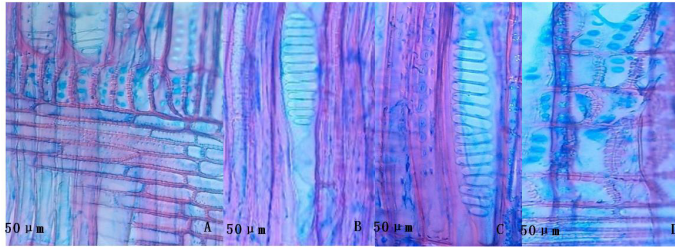


Fig 4: Radial section of *Sorbus torminalis* L.

There is agreement between these results and the wood description of *S. torminalis* by Richter and Dallwitz (2000). Noteworthy anatomical similarities include: growth ring boundaries distinct; wood diffuse porous, vessels solitary or in multiples, the latter few and commonly in short (2–3 vessels) radial rows; perforation plates simple, occasionally with scalariform to reticulate perforations, axial parenchyma present, helical thickenings in vessels present, tyloses absent, sheath and tile cells absent.

## CONCLUSIONS

*Sorbus torminalis* grown in Iran is a diffuse porous wood with a very high density. It can be utilized in various industrial applications. Its anatomical features do not differ significantly from congeneric. Cellulose content is in the range of other hardwoods but the lignin content is lower. It is suggested that in further studies additional properties such as the natural durability of Iranian *S. torminalis* wood against fungi, molds, insects, and termites be investigated.

## REFERENCES

1. Aghajani, H., Bahmani, M., Raesi, Gahrooei, M., Efhamisisi, D., Kool, F., 2019: Anatomical, biometrical, physical and chemical properties of wild service (*Sorbus torminalis* L.) wood (Case study: Sangdeh forests of Mazandaran). *Iranian Journal of Wood and Paper Industries* 24(3): 171-182.
2. Ay, N., Şahin, H., 1998: An investigation of internal morphological properties of sapwood and heartwood of oriental spruce (*Picea orientalis* (L.) Link.). *Turkish Journal of Agriculture and Forestry* 22(2): 203–207.
3. Bahmani, M., Saeidi, S., Humar, M., Kool, F., 2018: Effect of tree diameter classes on the properties of Persian oak (*Quercus brantii* lindl.) wood. *Wood Research* 63(5): 755-762.
4. Demersure, B., Le Guerroue, B., Lucchi, G., Part, D., Petit, R.J., 2000: Genetic variability of a scattered temperate forest tree: *Sorbus torminalis* L. *Annals Forest Science* 57(1): 63-71.
5. Đurković, J., Kardošová, M., Kačík, F., Masaryková, M., 2011: Wood traits in parental and hybrid species of *Sorbus*. *Botany* 89(8): 559-572.
6. Espahbodi, K., Mirzaie-Nodoushan, H., Tabari, M., Akbarinia, M., Dehghan-Shuraki, Y., Jalali, S.G., 2008: Genetic variation in early growth characteristics of two populations of wild service tree (*Sorbus torminalis* L. Crantz) and their interrelationship. *Silvae Genetica* 57(6): 340-348.

7. Franklin, G.L., 1945: Preparation of thin sections of synthetic resins and wood-resin composites, and a new macerating method for wood. *Nature* 155(51): 3924.
8. Golbabaie, F., Hosseinkhani, H., Euring, M., Kharazipour, A., 2014: Principle of mechanical properties of wild service tree (*Sorbus torminalis* L.) at different regions of northern part of Iran. *Holztechnologie* 55(3): 27-31.
9. IAWA Committee, 1989: IAWA list of microscopic features for hardwood identification by an IAWA Committee. E.A. Wheeler, P. Baas and P.E. Gasson (eds.) *IAWA Bull.* n.s. 10(3): 219-332.
10. ISO 13061-14., 2016: Physical and mechanical properties of wood. Test methods for small clear wood specimens. Part 14: Determination of volumetric shrinkage.
11. Khalkhali, M.B., 2013: A comparative study on wood density and pH of oak, maple and Iron trees in the North of Iran. *Technical Journal of Engineering and Applied Sciences* 3(22): 3098-3101.
12. Kol, H.S., Keskin, H., Korkut, S., Akbulut, T., 2009: Laminated veneer lumber from Rowan (*Sorbus aucuparia* Lipsky). *African Journal of Agricultural Research* 4(10): 1101-1105.
13. Korkut, S., Guller, B., Aytin, A., Kök, M.S., 2009: Turkey's native wood species: Physical and mechanical characterization and surface roughness of Rowan (*Sorbus aucuparia* L.). *Wood Research* 54(2): 19-30.
14. Liukkonen, S., Vehniainen, A., Sirvio, J., 2007: Selection of raw material offers new energy-property combinations for mechanical pulp. *International Mechanical Pulping Conference, Minnesota, USA*, Pp 1-9.
15. Mariani, S., Torres, M., Fernandez, A., Morales, E., 2005: Effects of *Eucalyptus nitens* heartwood in kraft pulping. *Tappi Journal* 4(2): 8-10.
16. Rayirath, P., Avramidis, S., 2008: Some aspects of western hemlock air permeability. *Maderas. Ciencia y tecnología* 10(3): 185-193.
17. Richter, H.G., Dallwitz, M.J., 2000: Commercial timbers: Descriptions, illustrations, identification, and information retrieval. Retrieval. <http://www.biodiversity.uno.edu/delta/> (accessed on 18.04.10).
18. Rowell, R.M., Young, R.A., Rowell, J.K., 1997: Paper and composites from Agro-based resource, CRC Lewis publisher, Boca Raton, FL, USA. 446 pp.
19. Saedi, S., Bahmani, M., Kool, F., Iranmanesh, Y., Abbasi, M., 2017: Investigation on physical, chemical and biometrical properties of Persian oak (*Quercus brantii* Lindl.) (Case study: Lordegan Township). *Journal of Wood & Forest Science and Technology* 24(3): 171-182.
20. Saraeian, A.R., Khalili, G.R.A., Aliabadi, M., Dahmardeh, G.N.M., 2011: Comparison of soda and kraft pulp properties of *Populus deltoides* sapwood and heartwood. *Journal of Wood & Forest Science and Technology* 10(17): 125-137.
21. Schoch, W., Heller, I., Schweingruber, F.H., Kienast, F., 2004: Wood anatomy of central European species. Online version: [www.woodanatomy.ch](http://www.woodanatomy.ch), 4 pp.
22. Tappi test method T 222 om-98, 1998: Standard test methods for acid-insoluble lignin in wood and pulp.
23. Tappi test method T 211 om 02, 2002: Standard test methods for ash in wood, pulp, paper, and paperboard.
24. Tappi test method T 257 cm-85, 1988: Standard test methods for sampling and preparing wood for analysis.

25. Tappi test method T 204 om-88, 1988: Standard test methods for solvent extractives of wood and pulp.
26. Tabandeh, A., Tabari, M., Nadoushan, H.M., Espahbodi, K., 2007: Heritability of some characteristics of *Sorbus torminalis* seedling. Pakistan Journal of Biological Sciences: PJBS 10(16): 2760-2763.
27. Termentzi, A., Kefalas, P., Kokkalou, E., 2006: Antioxidant activities of various extracts and fractions of *Sorbus domestica* fruits at different maturity stages. Food Chemistry 98: 599–608.
28. Welk, E., de Rigo, D., Caudullo, G., 2016: *Sorbus torminalis* in Europe: distribution, habitat, usage and threats. In: San-Miguel- Ayanz, J., de Rigo, D., Caudullo, G., Houston Durrant, T., Mauri, A. (Eds.): European atlas of forest tree species. Publ. Off. EU, Luxembourg, Pp e01090d.
29. Zobel, B., Van Buijtenen, J.P., 1989: Wood variation: Its causes and control. Springer-Verlag, Berlin, Germany, 363 pp.

MOHSEN BAHMANI\*  
SHAHREKORD UNIVERSITY  
DEPARTMENT OF NATURAL RESOURCES AND EARTH SCIENCES  
SHAHREKORD, IRAN

\*Corresponding author: bahmani\_mohsen\_j@yahoo.com, mohsen.bahmani@sku.ac.ir

LEILA FATHI  
UNIVERSITY OF HAMBURG  
CENTER OF WOOD SCIENCE AND TECHNOLOGY  
HAMBURG, GERMANY

GERALD KOCH  
THÜNEN INSTITUTE OF WOOD RESEARCH  
LEUSCHNERSTR 91  
21031 HAMBURG, GERMANY

FARHADH KOOL  
UNIVERSITY OF ZABOL  
DEPARTMENT OF WOOD AND WOOD PAPER SCIENCE AND TECHNOLOGY  
ZABOL, IRAN

HAMED AGHAJANI  
IRAN SARI AGRICULTURE SCIENCE AND NATURAL RESOURCES UNIVERSITY  
DEPARTMENT OF FORESTRY  
SARI, IRAN

MIHA HUMAR  
UNIVERSITY OF LJUBLJANA  
BIOTECHNICAL FACULTY  
LJUBLJANA, SLOVENIA



## **SIZE REDUCTION DOWNCYCLING OF WASTE WOOD. REVIEW**

VLADIMÍR IHNÁT, HENRICH LÜBKE  
SLOVAK FOREST PRODUCTS RESEARCH INSTITUTE  
BRATISLAVA, SLOVAK REPUBLIC

JOZEF BALBERČÁK, VLADIMÍR KUŇA  
PULP AND PAPER RESEARCH INSTITUTE  
BRATISLAVA, SLOVAK REPUBLIC

(RECEIVED SEPTEMBER 2019)

### **ABSTRACT**

The article includes research related to utilization of waste wood which is primarily size reduced due to its voluminity for next processing for lower value added products for about last twenty years. Procedures and results obtained by different authors were considered in one study. In this review a wood waste downcycling was consider as a process of transformation of large size wood products over their lifetime to the new products, where a size reduction is one of the first operations needed to achieve to. Incineration of each way was excluded from the present review, but second-generation biofuels are considered as potential products for the future. Two points of research selection according to origin and according to products made of waste wood was applied in this review. Comparison shown that the most industrially applicable implementation of treated particles obtained from waste wood is intended to the composite materials production as particleboards, fibreboards, cement-bonded and wood-plastics.

**KEYWORDS:** Downcycling, upcycling, wood, waste recycle, size reduction, wood particles.

### **INTRODUCTION**

Wood waste potential depends on many factors, its next processing is mainly depended on the high voluminity and possible content of harmful substances. The estimation of the waste wood statistics in the EU is provided basically on a) wood waste from municipal waste b) construction and demolition wood, and c) waste wood from industry (by products). The most valuable and detailed data on waste management in Europe come from Eurostat. The data show orientations in terms of valorization or elimination of wood waste. However, these data don't consider certain bad practices like household heating or open burning. In 2018 European Commission published the

Guidance on cascading use of biomass with selected good practice examples on woody biomass. The Circular Economy Action Plan adopted in 2015 aims to turn Europe's economy into a more sustainable economy, promoting sustainable economic growth and generating new jobs. The actions in the plan seek to close the life-cycle loop of products and materials by keeping their value in the economy if possible, minimizing the generation of waste and maximizing recycling and reuse. These benefits both the environment and the economy.

Although the idea of wood waste recycling has only begun to become more serious in recent decades, researchers have been dealing with the issue of wood recycling in the past. But practical application in industry has been progressively and over time, considering more economic (Zeng et al. 2018) as environmental benefits (Michanickl 1996). The European wood-based panel industry relies primarily on the softwood timber supply, so waste wood and recovered wood assortments are becoming more important (Janiszewska et al. 2015, Meinschmidt 2016). Recovered waste wood particles can be used for production of eco-friendly wood composite materials bonded by bio-based adhesives (Antov et al. 2020).

Recycling of wood waste is difficult due to a content of harmful chemicals contained both in glue used during a manufacture process (Risholm-Sundman and Vestin 2005) and in additives which originally served to protect it from moisture content, wood decaying fungi, to increase fire resistance and so on (Erbreich 2004). Different authors have used different techniques to determine the content of chemicals contained in waste wood, as for example, laser-induced breakdown spectroscopy (Uhl et al. 2001). Moskal and Haln (2002) suggested the online detector system using laser-induced breakdown spectroscopy for the analysis of copper chromated arsenate (CCA) treated wood products from the waste stream at a construction and demolition debris recycling center. Accuracy of handheld XRF analyzers on wood that has been treated with a preservative containing arsenic was determined by Block et al. (2007). Concentrations of wood preservatives in the wood chips produced in wood-waste processing facilities around 2000 in Japan was investigated by Kurata et al. (2005). Concentration levels depended on the sources of the wood wastes.

Methods of recycling the wood particles from waste wood-based materials were suggested previously by Michanickl and Boehme (1996). Several authors had been devoted to issue of a further processing of large-scale wood-based materials (Riddiough and Kearley 2001, Riddiough 2002). There are many opportunities for composites made from recycled wood-based waste resources. Research in these areas could result in a new product range in combination with other materials that are cost effective, designed to meet demands of end-use, and environmentally friendly (Boehme 2003, Wolff and Siempelkamp 2000, Rowell et al. 1993).

### **Review studies of wood waste carried out**

After 2000, several studies were conducted that dealt with wood in the form of waste or use of wood residues. Several review studies that directly or partially (Jeffrey 2011) deal with waste wood have been published. Tam V. and Tam C. (2006) published a study related to the technology on the construction waste recycling and their viability. Timber recycling technology has been also considered, as well as other materials suitable for recycling (asphalt, brick, concrete, ferrous metal, glass, masonry, non-ferrous metal, paper and cardboard and plastic). Kartal and Imamura (2003) published a review on chemical and biological remediations of CCA-treated (chromium, copper, and arsenic) waste wood. Chemical extraction using inorganic and organic acids and bioremediation using bacteria and fungi were summarized. Several alternative methods for the disposal of CCA treated wood waste have been published also by Helsen and Van den Bulck (2005). Alternative disposal methods include recycling and recovery, chemical

extraction, bioremediation, electrodialytic remediation and thermal destruction. Dias et al. (2007) determined waste wood as one of precursors of activated carbon (AC), which is a preferred adsorbent for the removal of micropollutants from the aqueous phase. AC can be prepared from conventional waste from wood industry to remove organic pollutants, dyes, volatile organic compounds, and heavy metals. Required high surface areas can be obtained using either physical or chemical activation.

The main reason to build this review study was to describe attitudes of different researchers to a waste wood processing in points of selection according to its origin and according to products made of it, sorting the industrially applicable implementations in large scale as well.

### Source of wood waste

Many studies solve a problem of accumulation of waste in the place of its origin. Usually large amounts of this waste end up in dumps every day with the highest environmental impacts (Di Maria et al. 2018). Authors distinguish municipal wood waste from land fields (Stahl et al. 2002), wood waste from construction site (Wang et al. 2016, 2017), demolition waste (Asari et al. 2004, Huang et al. 2002, Rautkoski et al. 2016), and wood industrial waste (Ahmed et al. 1998), also closely specified by type, f. e. hardwood residue (Shulga et al. 2014), untraditional softwood residue (Ozaki et al. 2005, Al Maadeed et al. 2014), or used railway sleepers (Ashori et al. 2012). Some atypical solutions are mentioned as well, as pruning residuals in olive groves and vineyards (Recchia et al. 2009). The bark is not a typical wood waste but since it is produced in parallel as byproduct from sawmills many authors are concerned with this issue, not preferring its direct energy use (Andres et al. 2010, Ghitescu et al. 2015, Medved' et al. 2019, Mirski et al. 2020). Generally, bark has often had three main uses: an animal bedding, an energy recovery and a mulching (in gardening and landscaping). These are generally low values uses.

A great source of wood waste are agglomerated materials as particle boards (PB) mainly from old furniture (Ihnát et al. 2017, 2018, Balberčák et al. 2017, 2018, Wan et al. 2014), oriented strand boards (OSB) (Schoo et al. 2003, Wan et al. 2014, Ihnát et al. 2017, 2018, Zeng et al. 2018), and middle density fiberboards (MDF) (Wan et al. 2014, Ihnát et al. 2018, Petar and Savov 2019).

### Size reduction and wood waste downcycling

Regarding to the wood waste processing in the terms of sequence: reduce-reuse-recycle (Falk 1997), a cascading utilization of resources is encouraged (Höglmeier et al. 2014). Basically, wood recycling is almost always associated with the disintegration (size reduction) of bulk wood waste into small particles (chips, fiber, etc.,) which are reused to produce composite materials (Ihnát et al. 2015). The particles obtained have mostly reduced mechanical and other properties (Buyuksari et al. 2010) and therefore added just in certain proportions (Chen et al. 2006). The process whereby a product is recycled to obtain a new product with a lower added value (technical or utility) is called downcycling and is a frequent phenomenon in the processing of waste wood. Upcycling of this waste material group is unique (Meinlschmidt and Mauruschat 2015, Russ et al. 2013) and almost impossible to apply in a mass production.

### Methods of the size reduced particles treatment

Attention was focused on methods of removing chemical loads from waste wood. Kabir et al. (2006) found out that most of the CCA components could be extracted by 10% H<sub>2</sub>O<sub>2</sub> at 50°C in 6 hours with an average extraction efficiency of 95% for Cr, 94% for Cu and 98% for As. The extract containing Cr<sup>III</sup>, Cu<sup>II</sup> and As<sup>V</sup> could be oxidized in several stages by aqueous 2.5%

w/w H<sub>2</sub>O<sub>2</sub> in less than 2 h. Shupe et al. (2006) used steam treatment to remove residual creosote content of sawdust obtained from weathered, out-of-service poles. Steaming was successful in reducing the creosote content to a level of 1.31%. Hse et al. (2013) provided a recovery of metals from CCA treated southern pine wood particles by the extraction in a microwave reactor with the binary combinations of an acetic acid and phosphoric acid. The highest recovery rate of metals achieved with a mixture of 2.75% phosphoric acid and 0.5% AA at 130°C in 10 min in the microwave oven.

Special attention has been paid to recycling of panelboards. In generally, three different principles can be applied for disintegration of panelboards: mechanical, thermo-hydrolytic and chemical, or combinations thereof (Kharazipour and Kües 2007). These processes were mostly described before 2000 and improved or novelized later. Fleischer and Marutzky (2000) were addressed to degradation of glued UF joints in waste particleboards. Lykidis and Grigoriou (2008) provided four different hydrothermal treatments applied in order to recover wood particles from waste particleboards and use them in the production of new (recycled) ones. It was found that other recycling cycles caused the deterioration in the quality of the recycled boards as regards their mechanical properties. Lykidis and Grygoriou (2011) concluded that the optimum hydrothermal recovery parameters were 45% water retention, 150°C temperature, and 10 min duration. Roffael and Hüster (2012) provided thermohydrolytic treatment of chips from waste UF-bonded particleboards using the flask method at 103°C for the reaction period of 24 h due to degradation of the UF-resin. Wan et al. 2014 subjected medium density fiberboard (MDF), particleboard (PB), and oriented strandboard (OSB) panels to steam explosion treatment. Downgraded panels were treated with thermal chemical impregnation using 0.5% butanetetracarboxylic acid (BTCA) to disintegrate UF bonds and were processed with mechanical hammermilling. The hammermilling of recycled PB was less likely to break particles down into sizes less than 1 mm<sup>2</sup>. Moezzipour et al. (2017) investigated the changes in the chemical properties of wood fibers after hydrothermal recycling of MDF wastes as an important aspect of recycling process which may be efficient on quality of recycled MDF boards. Hydrothermal recycling was done at different temperature (105, 125 and 150°C) in which subsequently defibrillation step was performed.

### **Recycling of heavily contaminated wood**

Recycling of CCA, or creosote-protected products forms a separate category of recycling due to classification as hazardous waste (Humar et al. 2011). Also, common disposal of wood treated with the chromated copper borate (CCB) due to toxic elements (Cu, Cr, and B) is not considered as environmentally sound solutions (Humar et al. 2004). Mengeloglu and Gardner (2000) evaluated flakeboards produced from recycled CCA treated and untreated southern pine (*Pinus* spp.) using two adhesives (polymeric methylene diphenyl diisocyanate and liquid phenol-formaldehyde) and two common flaking techniques (ring and disc flakes). Clausen et al. (2001) remediated CCA-treated southern yellow pine chips utilizing acid extraction alone and using acid extraction followed by bioleaching with the metal-tolerant bacterium *Bacillus licheniformis*. Chips were used to make particleboard with 10 percent urea-formaldehyde resin. Reduction of the strength properties was observed. Kartal and Clausen (2001) evaluated the effect of remediation processes with oxalic acid (OA) extraction and *Bacillus licheniformis* fermentation, on leaching of copper, chromium, and arsenic from particleboards made from remediated wood particles. The particleboard containing OA-extracted and bioremediated particles showed generally high leaching losses of remaining elements. Exposure of particleboards to decay fungi in soil block tests indicated that boards containing CCA-treated particles were most resistant to fungal degradation. Zhou and Kamdem (2002) investigated effect of Portland cement/ particles

from CCA treated red pine ratio on properties of result products and this was determined as a ratio of 3. Catallo and Shupe (2003) described the treatment of 15 years old creosote-treated pine utility pole wood in an anoxic supercritical water. The creosote-derived hydrocarbon residues in the chipped wood were nearly completely recovered, and the wood itself was transformed into a mixture of hydrocarbons including substituted benzenes, phenolics, and light PAHs. Kamdem et al. 2004 studied the feasibility of using recycled plastic and wood particles from CCA-treated wood removed from service. CCA pressure-treated red pine lumber removed from service after 21 years utilization was milled to the wood flour and blended with virgin or recycled high-density polyethylene at 50:50 wood flour-to-plastic weight ratio. Effects of different ratios of recycled CCA-treated wood and untreated virgin wood on flakeboard properties were compared by Li et al. (2004). Clausen et al. (2006) fabricated particleboard and flakeboard panels from remediated CCA-treated southern yellow pine. Treated wood, flaked or comminuted into particles, was remediated using oxalic acid extraction, followed by bioleaching with the metal-tolerant bacterium *Bacillus licheniformis* in trial experiment. Remediation resulted in removal of 80% Cu, 71% Cr, and 89% As for the particulate material and 83%Cu, 86%Cr, and 95% As for the flaked material.

### New downcycled wood waste products

New value added (technical or economical) of new products made of wood particles treated from waste wood is a measure of a sufficiency of its downcycling. Second generation biofuels made from waste wood (Okuda et al. 2008, Shi et al. 2009) are considered for future industrial production with a high potential. Secondary downcycling was provided, the possibility to utilize fiber sludge, waste fibers from pulp mills for combined production of liquid biofuel was investigated by Cavka et al. (2011). Laboratory production of ethanol from sawdust was provided by Chen et al. (2017), also by Afzal et al. (2018). In 2016 the first industrial-scale production of its kind in the world has been launched in Finland. Different pretreatment methods had been studied as a dilute acid pre-treatment on wood dust (Akhavue et al. 2019) or steam explosion on wood particles from waste boards (Pažitný 2019). Iakovlev et al. (2020) used two grades of recycled wood to fractionate on a pilot scale the monomeric sugars, lignin and lignosulfonates using SO<sub>2</sub>-Ethanol-Water (AVAP®) technology, including pretreatment, separation of cellulosic and hemicellulosic streams, and saccharification.

Different example of waste wood downcycling was shown by Bekhta et al. (2019), who examined lignocellulosic waste fibers obtained from fiberboard wet process, recycled paper process, and cellulose process as adhesive additives on some physical and mechanical properties and formaldehyde emission of adhesives and plywood panels. Reduction of formaldehyde emissions by up to 27.8, 24.9, and 19.4%, respectively compared with control panels was achieved. The shear strength of plywood panels with all investigated sludges met the requirements of the EN 314-2 standard.

Janiszewska et al. (2016) liquefied mixed hardwood-softwood powder and bark and tested as binders for particleboards made of recycled wood. The liquefaction reaction was carried out with a mixture of solvents from polyhydroxyl alcohols and p-toluenesulfonic acid as a catalyst. Then the liquefied waste from woods were characterized production as a partial substitute for synthetic urea-formaldehyde resin. It was demonstrated that the substitution of UF resin up to 20% did not have a significant effect on the mechanical properties.

Li et al. 2020 produced polyhydroxyalkanoate (PHA) via mixed a microbial consortia as a green alternative to replace the traditional petroleum-based polymers. Authors synthesized PHA using a volatile fatty acids (VFAs) obtained from the co-fermentation of pretreated wood waste

and sewage as carbon source. High PHA yield of 0.71 g COD PHA/g COD VFAs and PHA content of 50.3 g PHA/100 g VSS were obtained at VFAs ratio (even:odd) of 88:12 after seven cycles cultivation.

Also, biochar may be stated in this review in a different position as wooden pellets and briquettes directly intended for combustion. As biochar understood as high-value, climate-friendly soil improvement material made from woody biomass. When used in soil, biochar reduces the need to use energy-intensive soil fertilizers, since it provides excellent nutrients for plants in the right form and can also substitute peat as a growth and water-retaining medium. Biochar is a product made via pyrolysis or torrefaction, means a process where waste wood is exposed to high temperature and oxygen deficiency (Yargicoglu et al. 2015).

Wood waste may be a bit an interesting source of raw material for pulp and paper industry as well. But environmental aspects would have to outnumber the economic ones. Kraft pulp from industrial wood waste was evaluated and compared with softwood and hardwood pulp by Ahmed et al. (1998). Pulp bleachability was also evaluated. Compared to loblolly pine pulp, industrial wood waste pulp needed less cooking time to achieve the same kappa number and achieved a higher pulp yield for a similar kappa number. Balberčák et al. (2017) described a method of the evaluation and preparation of fluting liners produced from semichemical pulp made of waste wood particleboards and oriented strand boards (OSB). Combination with old corrugated cardboards (OCC) used to improve their strength properties. The semichemical pulp was obtained by a mildly alkaline boiling process. Properties as thickness, bulk density, Gurley, tensile strength, tensile index, breaking length, burst index, CMT30 and SCT were monitored on lab sheets 127 g·m<sup>-2</sup> and 170 g·m<sup>-2</sup>. Values of pH and residual NaOH and Na<sub>2</sub>CO<sub>3</sub> were determined in batch leachate. In the next study (Balberčák et al. 2018) authors described an alkaline cooking process from a sorted fraction of the 4-8 mm chips obtained from same waste sources. Pulp industry uses recycling in broad range. Virgin southern pine fibers and recycled old corrugated cardboard (OCC) were used to produce fiberboards. The virgin fiber was generated using a Kraft process (Hwang et al. 2005). Bending properties and dimensional stability were linearly dependent on virgin fiber ratios. Authors note that all panels with recycled fiber content greater than 40% failed to meet any commercial requirement.

Irle et al. (2019) aimed to generate high-value products from recovered wood to achieve even higher rates of wood recycling. Authors described the extraction of nano-crystalline cellulose from waste MDF and produced laminated beams from recovered wood.

But even though a cases mentioned above the downcycling of wood waste is most economically advantageous for the production of composite materials. For this reason, we will describe in detail the research carried out in the areas of production: particleboards, fiberboards, wood-plastic and cement-bonded composites:

#### *Particleboards (PB)*

Wang et al. (2007) manufactured a low formaldehyde emission particleboard from recycled wood waste chips using polymeric 4,4' methylene-diphenyl isocyanate (PMDI) and phenol-formaldehyde (PF) resins for use in indoor environments. The results showed that the formaldehyde emission released decreased linearly with increasing PMDI/PF particle ratio linearly. It was found that the increasing of PMDI/PF particle ratio positive influences on bending strength, internal bonding strength and screw holding. Ihnát et al. (2017) described a method of the particles preparation from waste particleboards (chipboards) and oriented strand boards (OSB). Method of the waste boards destruction, depending on the glue base urea-formaldehyde (UF) or melamine-urea formaldehyde (MUF), further processing and final particle characterization were determined.

Merrild and Christensen 2009 showed that the greenhouse gas emissions (GHG) related to upstream activities (5 - 41 kg CO<sub>2</sub> equivalents to one tonne of wood waste) are negligible compared to the downstream processing (560 - 120 kg). Savings in GHG emissions downstream are mainly related to savings in energy consumption for drying of fresh wood for particleboard production. Merrild and Christensen (2009) issued a potentially large downstream GHG emissions savings, which can be achieved by recycling of waste wood (1.9 - 1.3 tonnes). However, the GHG account highly depends on the choices made in the modelling of the downstream system. Kim and Song (2014) quantified the environmental impacts per tonne of wood wastes. The results showed that the particleboard from wood wastes produces 428 kg CO<sub>2</sub> eq compared to particleboard from fresh woods.

#### *Fiberboards (MDF)*

Recycled fibre material might be further used in paper making or in fibreboard production (Dix et al. 2001a,b), although it is dark and not as sufficient as other pulps. Mantanis et al. (2004) described a process based on refiner techniques and allows the use of mixtures of fresh wood and waste panel chips as a raw material for dry-process fiberboard production. Testing results revealed that under conventional gluing and pressing conditions, the process effectively recycles the waste boards at a wood substitution level of at least 25%. Ju and Roh (2017) used recycling wood fiber from waste MDF for the manufacturing of interior decorative accessories. Coloristic analyze was provided on fibers dyed by using different reactive dyes. The recycling fiber looked a little darker than the virgin fiber, also the recycling fiber showed a little higher values of color yields. Ihnát et al. (2018) described a process for the preparation of fibre from waste wood particleboards, oriented strand chipboard and medium density fibreboard (MDF). The obtained wood particles were characterized by the fractional composition of chips and subsequently mechanically defibred with subsequent characterization of fiber obtained for its reuse in the manufacture of MDF. A quantity of formaldehyde released into the water when cooking waste MDF and PB was set up depending on the cooking time. Lubis et al. 2018 studied the effect of recycled fiber content on the recycling properties of MDF. Statistical analysis indicates that the minimum of 10% recycle fibers can be used without diminishing the properties of recycled MDF. Fiber length of the recycled fibers obtain from recycled MDF is about 12% shorter than that of the virgin fibers and the percentage of shorter fibers is higher ( $\leq 0.68$  mm) for the former than the latter (Zeng et al. 2018).

#### *Wood-plastic composites*

To reduce the energy input for residue milling for obtaining a lignocellulosic filler as well as to activate its surface for the further modification, the optimal parameters of low temperature acid hydrolysis of the hardwood residue under mild conditions were used (Shulga et al. 2014). Recycling wood and plastic waste into wood-plastic composites (WPCs) was discussed by Wang et al. (2017b). Flexural strength, thickness swelling, water absorption and thermal insulation were observed. Melamine resin was adopted for impregnating anti-microbial agents on the surface. Poly-diallyl-dimethyl-ammonium chloride (PolyDADMAC) and silver were used as well. All the agents showed excellent bactericidal rate against to the *Escherichia coli*. In terms of weight loss and strength reduction due to fungal decay (*Coriolus versicolor*), polydiallyldimethylammonium chloride, silver and cetyltrimethylammonium bromide (CTAB) provided the highest resistance. PolyDADMAC and copper provided the most protection against an algal growth (*Chlorella vulgaris*). Lyuty et al. (2017) determined the release of formaldehyde, phenol, and ammonia from flat pressed WPC obtained from recycled polyethylene and wood particles by chamber method in a laboratory scale. It was found that formaldehyde, phenol and ammonia emission of flat pressed WPC are much lower than steady-state emission.

*Cement-bonded particleboards*

Some authors prefer cement composite materials that are a significant solution to the problem lignocellulosic wastes, generated worldwide, from various sources such as agriculture, construction, wood and furniture industries leading to environmental concerns. However, in this effort there are various restraints like compatibility of these wastes with cement, their toxicity, and limited composite strength (Karade 2010). Bao et al. (2001) used charcoal obtained from wood-based waste materials to determine the properties of charcoal-cement composite boards. Thirteen types of mixture ratios of charcoal to cement were used to produce 10mm-thick composite boards. The flexural strength of the board showed the maximum at the charcoal/cement mix ratio of 0.05, and then decreased as the mix ratio increased. The possibility of recycling waste medium density fiberboard (MDF) into wood-cement composites was evaluated by Qi et al. (2006). New fibers and recycled steam exploded MDF fibers had poor compatibility with cement so a rapid hardening process with carbon dioxide injection was adopted. After 3–5 min of carbon dioxide injection, the composites reached 22–27% of total carbonation and developed 50–70% of their final (28-day) strength. Wang et al. (2016) developed a practicable technology for recycling construction waste wood into formaldehyde-free cement-bonded particleboards. A high strength, light weight, and thermal/noise insulation are value-added features of new products at density of the particleboards to  $1.54 \text{ g cm}^{-3}$  and the volume of capillary pores was effectively reduced from  $0.16 \text{ mL g}^{-1}$  to  $0.02 \text{ mL g}^{-1}$ . The high fracture energy at  $6.57 \text{ N mm}^{-1}$  and flexural strength of  $12.9 \text{ MPa}$  were achieved as well. The particleboards also manifested outstanding structure-borne noise reduction (at 32-100 Hz) and low thermal conductivity ( $0.29 \text{ W m}^{-1} \text{ K}^{-1}$ ). X-ray diffraction, thermogravimetry, and mercury intrusion porosimetry were used for analyses. It was found that the use of 2%  $\text{CaCl}_2$  improve the wood-cement compatibility at wood-to-cement ratio of 3:7 by weight. Wang et al. (2017a) proposed a novel use of alumina and red mud to improve water resistance of magnesia-phosphate cement (MPC) particleboards. Addition of alumina or red mud (Mg/Al or Mg/Fe at optimal molar ratio of 10:1) facilitated formation of amorphous Mg/Al or Mg/Al/Fe phosphate gel, with enhanced compressive strength. Alumina improved short-term water resistance, whereas red mud provided a better long-term water resistance. Red mud-MPC binder enhanced strength retention (by 22.8%) and reduced water absorption (by 26.4%) of particleboards after 72 h water immersion. The X-ray diffraction analyses and scanning electron microscopy were used for analyze.

## CONCLUSIONS

Wood waste is becoming a substitute for raw wood on an increasingly wide scale, not only in Europe. Until recently, economic reasons outnumbered environmental ones. Downcycling of waste wood, after its size reduction, has a major application in re-incorporation into wood based composite materials. However, the results of the studies show that recycled wood particles have lower mechanical properties than primarily obtained from fresh wood, or some other restrictions exist and therefore the principle of addition to a certain limit must be maintained. New progressive materials and other ways of using of waste wood, mainly chemically treated, need to be developed in the future.

## ACKNOWLEDGMENTS

This research was supported by the Slovak Research and Development Agency under the contract No. APVV-17-0330.

## REFERENCES

1. Almaadeed, M.A., Nógellová, Z., Mičušík, M., Novák, I., Krupa, I., 2014: Mechanical, sorption and adhesive properties of composites based on low density polyethylene filled with date palm wood powder. *Materials & Design* 53: 29-37.
2. Afzal, A., Fatima, T., Tabassum, M., Nadeem, M., Irfan, M., Syed, Q., 2018: Bioethanol Production from saw dust through simultaneous saccharification and fermentation. *Punjab University Journal of Zoology* 33(2): 145-148.
3. Ahmed, A., Akhtar, A., Myers, G.C., Scott, G.M., 1998: Kraft pulping of industrial wood waste. *TAPPI Pulping Conference, Montreal*, Pp 993-1000.
4. Akhabue, C., Otoikhian, K.S., Bello, D., Adeniyi, A.G., Ighalo, J.O., 2019: Effect of dilute acid pre-treatment on the functional complexes and surface morphology of wood sawdust for bioethanol production. *Proceeding of the 18<sup>th</sup> Annual International Materials Congress for the Materials Society of Nigeria (MSN)*, 18 - 22<sup>nd</sup> November, Nigeria. Pp 318-322.
5. Andres, Y., Dumont, E., Le Cloirec, P., Ramirez-Lopez E., 2010: Wood bark as packing material in a biofilter used for air treatment. *Environmental Technology* 27(12): 1297-1301.
6. Antov, P., Savov, V., Neykov, N., 2020: Sustainable bio-based adhesives for eco-friendly wood composites. A review. *Wood Research* 65(1): 51-62.
7. Asari, M., Takatsuki, H., Yamazaki, M., Azuma, T., Takigami, H., Sakai, S.I., 2004: Waste wood recycling as animal bedding and development of bio-monitoring tool using the CALUX assay. *Environment International* 30(5): 639-649.
8. Ashori, A., Tabarsa, T., Amosi, F., 2012: Evaluation of using waste timber railway sleepers in wood-cement composite materials. *Construction and Building Materials* 27(1): 126-129.
9. Balbercak, J., Bohacek, S., Medo, P., Ihnat, V., Lubke, H., 2017: Chemical processing of waste wood based agglomerates Part I: Evaluation of properties of fluting liners made of semichemical pulp obtained by a mildly alkaline sulphur-free cooking process. *Wood Research* 62(5): 715-726.
10. Balbercak, J., Bohacek, S., Pazitny, A., Ihnat, V., Lubke, H., 2018: Chemical processing of waste wood based agglomerates part II: Evaluation of properties of fluting liners made of semichemical pulp obtained by an alkaline cooking process. *Wood Research* 63(1): 35-44.
11. Bao, M.Q., Morita, M., Higuchi, M., 2001: Utilization of charcoal from wood waste. I. Properties of charcoal-cement composite boards. *Journal of the Faculty of Agriculture Kyushi University* 46(1): 93-102.
12. Bekhta, P., Sedliačik, J., Kačík, F., Noshchenko, G., Kleinová, A., 2019: Lignocellulosic waste fibers and their application as a component of urea-formaldehyde adhesive composition in the manufacture of plywood. *European Journal of Wood and Wood Products* 77: 495-508.
13. Block, C.N., Shibata, T., Solo-Gabriele, H.M., Townsend, T.G., 2007: Use of handheld X-ray fluorescence spectrometry units for identification of arsenic in treated wood. *Environmental Pollution* 148(2): 627-633.

14. Boehme, C., 2003: Waste wood is important for the wood-based products industry. *HolzZentralblatt* 4: 101.
15. Buyuksari, U., Ayrimis, N., Avci, E., Koc, E., 2010: Evaluation of the physical, mechanical properties and formaldehyde emission of particleboard manufactured from waste stone pine (*Pinus pinea* L.) cones. *Bioresource Technology* 101(1): 255-259.
16. Catallo, W.J., Shupe, T.F., 2003: Hydrothermal treatment of creosote-impregnated wood. *Wood and Fiber Science* 35(4): 524-531.
17. Cavka, A., Alriksson, B., Rose, S.H., Van Zyl, W.H., Jönsson, L.J., 2011: Biorefining of wood: combined production of ethanol and xylanase from waste fiber sludge. *Journal of Industrial Microbiol & Biotechnology* 38: 891-899.
18. Clausen, C.A., Kartal, S.N., Muehl, J., 2001: Particleboard made from remediated CCA-treated wood: evaluation of panel properties. *Forest Products Journal* 51: 61-64.
19. Clausen, C.A., Muehl, J.H., Krzysik, A.M., 2006: Properties of structural panels fabricated from bio-remediated CCA-treated wood: pilot scale. *Forest Products Journal* 56: 32-35.
20. Chen, W.C., Lin, Y.Ch., Ciou, Y.L., Chu, I.M., Tsai, S.L., Lan, J.C.W., Chang, Y.K., Wei, Y.H., 2017: Producing bioethanol from pretreated-wood dust by simultaneous saccharification and co-fermentation process. *Journal of the Taiwan Institute of Chemical Engineers* 79: 43-48
21. Chen, H., Chen, T., Hsu, C., 2006: Effects of wood particle size and mixing ratios of HDPE on the properties of the composites. *European Journal of Wood and Wood Products* 64: 172-177.
22. Di Maria, A., Eyckmans, J., Van Acker, K., 2018: Downcycling versus recycling of construction and demolition waste: Combining LCA and LCC to support sustainable policy making. *Waste Management* 75: 3-21.
23. Dias, J.M., Alvim-Ferraz, M.C.M., Almeida, M.F., Rivera-Utrilla, J., Sánchez-Polo, M., 2007: Waste materials for activated carbon preparation and its use in aqueous-phase treatment: A review. *Journal of Environmental Management* 85: 833-846.
24. Dix, B., Schäfer, M., Roffael, E., 2001a: Use of thermochemically defibered pulps from waste fiberboards for manufacturing of medium-density fiberboards (MDF). *European Journal of Wood and Wood Products* 59(4): 276.
25. Dix, B., Schäfer, M., Roffael, E., 2001b: Use of fiber pulps from chemo-thermo-mechanical pulping, waste fiber and particleboards for manufacturing medium density fiberboards. *European Journal of Wood and Wood Products* 59(4): 299-300.
26. Erbreich, M., 2004: Die Aufbereitung und Wiederverwendung von Altholz zur Herstellung von Mitteldichtden Faserplatten (MDF), Dissertation. Universität Hamburg Fachbereich Biologie, 255 pp.
27. Falk, B., 1997: Opportunities for the Wood waste resource: *Forest Products Journal* 47(6): 17-22.
28. Fleischer, O., Marutzky, R., 2000: Hydrolysis of urea-formaldehyde resins: Disintegration of wood-based panels due to hydrolytic degradation of the glue-joint. *Journal of Wood and Wood Products* 58(5): 295-300.
29. Ghitescu, R.E., Volf, I., Carausu, C., Bühlmann, A.M., Gilca, I.A., Popa, V.I., 2015: Optimization of ultrasound-assisted extraction of polyphenols from spruce wood bark. *Ultrasonics Sonochemistry* 22: 535-541.
30. Helsen, L., Van den Bulck, E., 2005: Review of disposal technologies for chromated copper arsenate (CCA) treated wood waste, with detailed analyses of their thermomechanical conversion processes. *Environmental Pollution* 134(2): 301-314.

31. Höglmeier, K., Weber-Blaschke, G., Richter, K., 2014: Utilization of recovered wood in cascades versus utilization of primary wood. A comparison with life cycle assessment using system expansion. *The International Journal of Life Cycle Assessment* 19: 1755–1766.
32. Hwang, C.Y., Hse, C.Y., Shupe, T.F., 2005: Effects of recycled fiber on the properties of fiberboard panels. *Forest Products Journal* 55(11): 60–64.
33. Huang, W.L., Lin, D.H., Chang, N.B., Lin, K.S., 2002: Recycling of construction and demolition waste via a mechanical sorting process. *Resources, Conservation and Recycling* 37(1): 23–37.
34. Humar, M., Pohleven, F., Šentjurc, M., 2004: Effect of oxalic, acetic acid, and ammonia on leaching of Cr and Cu from preserved wood. *Wood Science and Technology* 37: 463–473.
35. Humar, M., Budija, F., Hraštnik, D., 2011: Potentials of liquefied CCB treated waste wood for wood preservation. *Drvna industrija* 62(3): 213–218.
36. Hse, C.Y., Shupe, T.F., Yu, B., 2013: Rapid microwave-assisted acid extraction of southern pine waste wood to remove metals from chromated copper arsenate (CCA) treatment. *Holzforschung* 67(3): 285–290.
37. Iakovlev, M., Survase, S., Hill, L., Sideri, S., Rouzinou, S., Kroff, P., Pylkkanen, V., Rutherford, S., Retsina, T., 2020: Pilot scale sulfur dioxide-ethanol-water fractionation of recycled wood to sugars, bioethanol, lignin and lignosulfonates: Carbohydrate balance. *Bioresource Technology* 307: 123240.
38. Ihnat, V., Lubke, H., Boruvka, V., Russ, A., 2017: Waste agglomerated wood materials as a secondary raw material for chipboards and fibreboards. Part I: Preparation and characterization of wood chips in term of their reuse. *Wood Research* 62(1): 45–56.
39. Ihnat, V., Lübke, H., Russ, A., Pažitný, A., Borůvka, V., 2018: Waste agglomerated wood materials as a secondary raw material for chipboards and fibreboards. Part II: Preparation and characterization of wood fibres in terms of their reuse. *Wood Research* 63(3): 431–442.
40. Ihnat, V., Boruvka, V., Lubke, H., Babiak, M., Schwartz, J., 2015: Straw pulp as a secondary lignocellulosic raw material and its impact on properties of properties of insulating fiberboards. Part III. Preparation of insulating fiberboards from separately milled lignocellulosic raw materials. *Wood Research* 60(3): 457–466.
41. Irlé, M., Privat, F., Couret, L., Belloncle, Ch., Dérubaix, G., Bonnin E., Cathala, B., 2019: Advanced recycling of post-consumer solid wood and MDF. *Wood Material Science & Engineering* 14(1): 19–23.
42. Janiszewska, D., Frąckowiak, I., Andrzejak, C., 2015: Some aspects of using post-consumer wood in particleboard production. In: *Wood 2015: Innovations in wood materials and processes* Brno, Czech Republic, 19–22 May 2015, Pp 159–160.
43. Janiszewska, D., Frąckowiak, I., Mytko, K., 2016: Exploitation of liquefied wood waste for binding recycled wood particleboards. *Holzforschung* 70(12): 1135–1138.
44. Jeffrey, C., 2011: Construction and demolition waste recycling. A literature review. *Dalhousie University's Office of Sustainability*. 35 pp.
45. Ju, S.G., Roh, J., 2017: Manufacture of dyed recycling wood fiber using waste MDF. *Journal of The Korean Wood Science and Technology* 45(3): 297–307.
46. Kabir, F., Kazi, M., Cooper, P.A., 2006: Method to recover and reuse chromated copper arsenate wood preservative from spent treated wood. *Waste Management* 26(2): 182–188.
47. Kamdem, D.P., Jiang, H.H., Cui, W.N., Freed, J., Matuana, L.M., 2004: Properties of wood plastic composites made of recycled HDPE and wood flour from CCA-treated wood removed from service. *Composites Part A - Applied Science and Manufacturing* 35(3): 347–355.

48. Karade, S.R., 2010: Cement-bonded composites from lignocellulosic wastes. *Construction and Building Materials* 24(8): 1323-1330.
49. Kartal, S. N., Imamura, Y., 2003: Chemical and biological remediation of CCA-treated waste wood. *Wood research: bulletin of the Wood Research Institute Kyoto University* 90: 111-115.
50. Kartal, S.N., Clausen, C.A., 2001: Leachability and decay resistance of particleboard made from acid extracted and bioremediated CCA-treated wood. *International Biodeterioration & Biodegradation* 47: 183-191.
51. Kharazipour, A., Kües, U., 2007: Recycling of wood composites and solid wood products. In: *Wood production, wood technology, and biotechnological impacts*. Chapter: Recycling of wood composites and solid wood products. Publisher: Universitätsverlag Göttingen, Editors: Ursula Kües, Pp 509-533.
52. Kim, M.H., Song, H.B., 2014: Analysis of the global warming potential for wood waste recycling systems. *Journal of Cleaner Production* 69(15): 199-207.
53. Kurata, Y., Watanabe, Y., Ono, Y., Kawamura, K., 2005: Concentrations of organic wood preservatives in wood chips produced from wood wastes. *Journal of Material Cycles and Waste Management* 7: 38-47.
54. Li, W., Shupe, T.F., Hse, C.Y., 2004: Physical and mechanical properties of flakeboard produced from recycled CCA-treated wood. *Forest Products Journal* 54: 89-94.
55. Li, D., Yin, F., Ma, X., 2020: Towards biodegradable polyhydroxyalkanoate production from wood waste: Using volatile fatty acids as conversion medium. *Bioresource Technology* 299: 122629.
56. Lykidis C., Grigoriou A., 2008: Hydrothermal recycling of waste and performance of the recycled wooden particle-boards. *Waste Management* 28(1): 57-63.
57. Lykidis, C., Grygoriou, A., 2011: Quality characteristics of hydrothermally recycled particleboards using various wood recovery parameters. *International Wood Products Journal* 2(1): 38-43.
58. Lyuty, P., Bekhta, P., Ortyńska, G., Sedláčik, J., 2017: Formaldehyde, phenol and ammonia emissions from wood/recycled polyethylene composites. *Acta Facultatis Xylogiae Zvolen* 59(1): 107-112.
59. Lubis, M.A.R., Hong, M.K., Park, B.D., Lee, S.M., 2018: Effects of recycled fiber content on the properties of medium density fibreboard. *European Journal of Wood and Wood Products* 76: 1515-1526.
60. Mantanis, G., Athanassiadou, E., Nakos, P., Coutinho, A., 2004: A new process for recycling waste fiberboards. In: *Proceedings of the XXXVIII International Wood Composites Symposium*. Pullman, USA, Pp 119-122.
61. Medved, S., Gajšek, U., Tudor, E.M., Barbu, M.C., Antonović, A., 2019: Efficiency of bark for reduction of formaldehyde emission from particleboards.. *Wood Research* 64(2): 307-316.
62. Meinschmidt, P., Mauruschat, D., 2015: Up- and down-cycling of waste wood in Europe. In: *Wood2015: Innovations in wood materials and processes* Brno, Czech Republic, 19-22 May 2015, Pp 161-162.
63. Meinschmidt, P., Mauruschat, D., Briesemeister, R., 2016: Waste wood situation in Europe and Germany. *Chemie Ingenieur Technik* 88(4): 475-482.
64. Mengelöglu, F., Gardner, D.J., 2000: Recycled CCA-treated lumber in flakeboards: evaluation of adhesives and flakes. *Forest Products Journal* 50: 41-45.

65. Merrill, H., Christensen, T.H., 2009: Recycling of wood for particle board production: accounting of greenhouse gases and global warming contributions. *Waste Management and Research* 27(8): 781-788.
66. Michanickl, A., Boehme, C., 1996: Recovery of particles and fibers from wood-based products), Sonderdruck aus HK Holz - und Kunststoffverarbeitung 4: 50-55.
67. Michanickl, A., 1996: Recovery of fibers and particles from wood based products. In: Proceedings No 7286: Wood and Paper in Building Applications, Forest Products Society, Pp 115-119.
68. Mirski, R., Kawalerczyk, J., Dziurka, D., Wieruszewski, M., Trociński, A., 2020: Effects of using bark particles with various dimensions as a filler for urea-formaldehyde resin in plywood. *BioResources* 15(1): 1692-1701.
69. Moezzi-pour, B., Ahmadi, M., Abdolkhani, A., Doosthoseini, K., 2017: Chemical changes of wood fibers after hydrothermal recycling of MDF wastes. *Journal of the Indian Academy of Wood Science* 14(2): 133-138.
70. Moskal, T.M., Hahn, D.W., 2002: On-line sorting of wood treated with chromated copper arsenate using laser-induced breakdown spectroscopy. *Applied Spectroscopy* 56(10): 1337-1344.
71. Okuda, N., Ninomiya, K., Katakura, Y., Shioya, S., 2008: Strategies for reducing supplemental medium cost in bioethanol production from waste house wood hydrolysate by ethanologenic *Escherichia coli*: Inoculum size increase and coculture with *Saccharomyces cerevisiae*. *Bioengineering* 105(2): 90-96.
72. Ozaki, S.K., Monteiro, M.B.B., Yano, H., Imamura, Y., Souza, M.F., 2005: Biodegradable composites from waste wood and poly(vinyl alcohol). *Polymer Degradation and Stability* 87(2): 293-299.
73. Pažitný, A., 2019: Steam explosion of wood particles from fibreboard and particle board with indirect control by enzymatic hydrolysis. *Acta Chimica Slovaca* 12(2): 185-191.
74. Petar, A., Savov, V., 2019: Possibilities for manufacturing eco-friendly medium density fibreboards from recycled fibres. A Review. In: 30<sup>th</sup> International Conference on Wood Science and Technology - ICWST 2019 "Implementation of wood science in woodworking sector" and 70<sup>th</sup> anniversary of Drvna industrija Journal, 7 pp.
75. Rautkoski, H., Vähä-Nissi, M., Kataja, K., Gestranus, M., Liukkonen, S., Määttänen, M., Liukkonen J., Kouko, J., Asikainen, S., 2016: Recycling of contaminated construction and demolition wood waste. *Waste and Biomass Valorisation* 7: 615-624.
76. Recchia, L., Daou, M., Rimediotti, M., Cini, E., Vieri, M., 2009: New shredding machine for recycling pruning residuals. *Biomass and Bioenergy* 33(1): 149-154.
77. Riddiough, S., Kearley, V., 2001: Wood based panels: real potential for recycling success. In: Proceedings of the 5<sup>th</sup> Panel Products Symposium, Llandudno, Wales, UK. Pp 321-327.
78. Riddiough, S., 2002: Wood panel recycling: an introduction to the fiber solve process. In: Proceedings of the 6<sup>th</sup> Panel Products Symposium, Llandudno, Wales, UK. Pp 159-166.
79. Risholm-Sundman, M., Vestin, E., 2005: Emissions during combustion of particleboard and glued veneer. *European Journal of Wood and Wood Products* 63: 179-185.
80. Roffael, E., Hüster, H.G., 2012: Complex chemical interactions on thermo hydrolytic degradation of urea formaldehyde resins (UF-resins) in recycling UF-bonded boards. *European Journal of Wood and Wood Products* 70: 401-405.
81. Rowell, R., Spelter, H., Arola, R., Davis, P., Friberg, T., Hemingway, R., Rials, T., Luneke, D., Narayan, R., Simonsen, J., White, D., 1993: Opportunities for composites from recycled wastewood-based resources: a problem analysis and research plan. *Forest Products Journal* 43 (1): 55-63.

82. Russ, A., Schwartz, J., Boháček, Š., Lübke, H., Ihnat, V., Pažitný, A., 2013: Reuse of old corrugated cardboard in constructional and thermal insulating boards. *Wood Research* 58(3): 505-510.
83. Qi, H., Cooper, P.A., Wan, H., 2006: Effect of carbon dioxide injection on production of wood cement composites from waste medium density fiberboard (MDF). *Waste Management* 26(5): 509-515.
84. Shi, J., Ebrik, M., Yang, B., Wyman, Ch.E., 2009: The potential of cellulosic ethanol production from municipal solid waste: A technical and economic evaluation. University of California Energy Institute, 38 pp.
85. Shulga, G., Neiberte, B., Verovkins, A., Jaunslavietis, J., Shakels, V., Vitolina, S., Sedliačik, J., 2016: Eco-friendly constituents for making wood-polymer composites. *Key Engineering Materials* 688: 122-130.
86. Shupe, T.F., Hse, Ch.Y., Roliadi, H., 2006: Removal of creosote from wood particles at different horizontal and vertical locations of decommissioned poles using steam treatment. *Wood and Fiber Science* 38(2): 345 – 350.
87. Schoo, A., Roffael, E., Uhde, M., 2003: Medium density fibre boards (MDF) from recovered oriented strand boards (OSB). *European Journal of Wood and Wood Products* 61: 390-391.
88. Stahl, D.C., Skoraczewski, G., Arena, P., Stempsko, B., 2002: Lightweight concrete masonry with recycled wood aggregate. *Journal of Materials in Civil Engineering* 14(2): 116-121.
89. Tam, V.W.Y., Tam, C.M., 2006: A review on the viable technology for construction waste recycling. *Resources, Conservation and Recycling* 47(3): 209-221.
90. Uhl, A., Loebe, K., Kreuchwig, L., 2001: Fast analysis of wood preservers using laser induced breakdown spectroscopy. *Spectrochimica Acta Part B: Atomic Spectroscopy* 56(6): 795-806.
91. Wan, H., Wang, X.M., Barry, A., Shen, J., 2014: Recycled wood composite panels: Characterizing recycled materials. *BioResources* 9(4): 7554-7565.
92. Wang, S.Y., Yang, T.H., Lin, L.T., Lin, C.J., Tsai, M.J., 2007: Properties of low-formaldehyde-emission particleboard made from recycled wood-waste chips sprayed with PMDI/PF resin. *Building and Environment* 42(7): 2472-2479.
93. Wang, L., Chen, S.S., Tsang, D.C.W., Poon, Ch.S., Shih, K., 2016: Value-added recycling of construction waste wood into noise and thermal insulating cement-bonded particleboards. *Construction and Building Materials* 125(30): 316-325.
94. Wang, L., Yu, I.K.M., Tsang, D.C.W., Li, S., Li, J.-s., Sun, Poon, Ch.S., Wang, Y.S., Dai, J.-G., 2017a: Transforming wood waste into water-resistant magnesia-phosphate cement particleboard modified by alumina and red mud. *Journal of Cleaner Production* 168: 452-462.
95. Wang, L., Chen, S.S., Tsang, D.C.W., Poon, Ch., S., Ok, Y.S., 2017b: Enhancing antimicrobial properties of wood-plastic composites produced from timber and plastic wastes. *Environmental Science and Pollution Research* 24: 12227-12237.
96. Wolff, S., Siempelkamp, G., 2000: Post-consumer wood waste as raw material for particleboard and MDF. In: *Proceedings of the 5<sup>th</sup> Pacific Bio-Based Composites Symposium*, Canberra, Australia. Pp 572-579.
97. Zeng, Q., Lu, Q., Zhou, Y., Chen, N., Rao, J., Fan, M., 2018: Circular development of recycled natural fibers from medium density fiberboard wastes. *Journal of Cleaner Production* 202: 456-464.

98. Zhou, Y.G., Kamdem, D.P., 2002: Effect of cement/wood ratio on the properties of cement-bonded particleboard using CCA-treated wood removed from service. *Forest Products Journal* 52: 77- 81.
99. Yargicoglu, E.N., Sadasivam, B.Y., Reddy, K.R., Spokas, K., 2015: Physical and chemical characterization of waste wood derived biochars. *Waste Management* 36: 256-268.

VLADIMIR IHNAT, HENRICH LÜBKE\*  
SLOVAK FOREST PRODUCTS RESEARCH INSTITUTE  
DUBRAVSKA CESTA 14  
841 04 BRATISLAVA  
SLOVAK REPUBLIC

\*Corresponding author: lubke.sdvu@vupc.sk

JOZEF BALBERČAK, VLADIMÍR KUŇA  
PULP AND PAPER RESEARCH INSTITUTE  
DUBRAVSKA CESTA 14  
841 04 BRATISLAVA  
SLOVAK REPUBLIC



## **STUDY ON THE WARM-COOL AND DRY-WET FEELING OF STRAW BOARD SURFACE**

XIANQING XIONG, YITING NIU, QINGRU MA, YUTING PAN  
NANJING FORESTRY UNIVERSITY  
NANJING, CHINA

(RECEIVED APRIL 2019)

### **ABSTRACT**

To expand the application of furniture materials, the warm-cool and dry-wet tactile properties of the rice straw particleboard (RSP) surface were investigated. RSP substrates exhibiting densities equal to 757 and 554 kg·m<sup>-3</sup> were sanded using different types of sandpaper (mesh 180#, 360#, and 600#). Psychological experiments on sensation were then conducted by bubbling for RSP substrates. By observing and comparing changes in warm-cool and dry-wet tactile properties between the RSP and other different materials, the effects of several variables on surface tactile properties, such as sandpaper types, RSP densities, and thermal conductivities of materials, were evaluated.

**KEYWORDS:** Rice straw particleboard, warm-cool feeling, dry-wet feeling, surface tactile properties.

### **INTRODUCTION**

To conform to the development trend of Made in China 2025, China has taken advantage of the great agricultural country, mitigating the shortage of materials in furniture manufacturing by straw board production (Li et al. 2018, Basta et al. 2013). The rice straw particleboard (RSP) is a biomass fiber material made from the crop rice straw fiber and glued using an isocyanate adhesive (Parker 1997, Wu et al. 2019). Owing to the use of a non-aldehyde glue, it releases no free formaldehyde. In addition, the RSP is eco-friendly and exhibits uniform density and a smooth surface (Yang et al. 2003, Yan et al. 2012, Fang et al. 2019).

Warm-cool feeling and dry-wet feeling, two important characteristics of the environmental properties of wood materials, are essential criteria in the selection of furniture in the interior environment (Li et al. 2019). A high or low temperature or a humid environment is not desirable. Indoor temperature and humidity should be kept within a wide comfort range (Wang et al. 2000). The RSP, a wooden artificial board, can directly improve the temperature and moisture content of the material itself, as well as our living environment, through its own functions, namely, heat

preservation, heat insulation, moisture absorption, and dehumidification. The RSP is used as furniture or interior decoration material, improving the quality of life and work efficiency of users (Ahn et al. 2017, Shi et al. 2018).

Several studies have currently focused on the tactile properties of materials. Zhao et al. (2017) used the semantic differential technique to analyze subjective sensations when touching different materials. With this approach, the change in temperature of wood-plastic composites and other heated floor substrates is determined. The report indicated that density considerably affected the warm-cool feeling of the wood material surface and exhibited the opposite trend. That is, the higher the density, the lower the warm-cool feeling of the wood material surface. Mangat et al. (2017) measured the subjective and objective warm-cool feeling of the fabric surface after biopolishing by using human senses and Alambeta instruments. These series of studies showed that the smoothness of the fabric surface was enhanced after polishing. The smooth surface exhibited increased thermal absorption, resulting in a cool sensation when it comes in contact with a human body. Vivekanadan et al. (2011) used five methods to measure four different greige cotton denim fabrics. The fabric structure and physical properties significantly influenced the warm-cool and dry-wet feeling of the clothing surface. The finer the raw material yarn, the colder the fabric surface. The density and washing treatment also positively affected the cooling feeling of the fabric surface. Decreasing the roughness of fabric or increasing its smoothness simultaneously increase the cooling feeling of the fabric surface. Most of the research on tactile properties relate to clothing materials, and experiments on the tactile properties of the surface of wood materials, particularly research on the warm-wet feeling, are rarely reported (Goldie et al. 2001, Hu et al. 2013).

On the basis of the aforementioned reports, the current study examined the two aspects of warm-cool feeling and dry-wet feeling on the surface of RSP (Pac et al. 2001, Inoue et al. 2010, Okuyama et al. 2011, Bellizzi et al. 1992, Mangat et al. 2017). The present study employed sanding treatment with different types of sandpaper for RSPs with densities of 554 and 757 kg·m<sup>-3</sup> to analyze the effects of density and surface roughness on the tactile properties, that is, warm-cool feeling and dry-wet feeling of the RSP surface. The experiment was expected to identify materials suitable for a given temperature and humidity and to determine how to improve the warm-cool feeling and dry-wet feeling of material surfaces. This study aimed to provide a broader range of materials for furniture production.

## MATERIALS AND METHODS

### Materials

RSPs were purchased from Novofibre Co., Ltd. (Yangling, Shanxi, China). The two RSP plates with different densities varied in performance. The density of the first plate was 554 kg·m<sup>-3</sup>, and the moisture content was 8.0%. The density of the second plate was 757 kg·m<sup>-3</sup>, and the moisture content was 7.5%. Experimental specimens measuring 200 × 200 × 10 mm were taken from these two RSP plates with different densities, resulting in 12 specimens with a density of 554 kg·m<sup>-3</sup>, and 10 specimens with a density of 757 kg·m<sup>-3</sup> for a total of 22 specimens. Other experimental specimens 300 × 200 × 10 mm (including poplar medium density particleboard (PB), foam plastic, pine board, and marble) and four pieces were taken. Other auxiliary materials included sanding materials, absorbent papers, fresh-keeping bags, sinks, and homemade metal grid, among others.

## Experimental apparatus

A stainless steel probe-type electronic thermometer was purchased from Hengxing Instrument Co., Ltd. (Hengshui, Hebei, China). This instrument had a measurement accuracy of 0.01°C, a temperature measurement range of -50°C to 300°C, and a measurement time of 60 s (Shen and Lv 2018).

An electronic scale was supplied by Shanghai Yousheng Electronic Weighing Apparatus Co. (Shanghai, China) with a measurement accuracy of 0.01 g and a measurement range of 0-600 g.

## Experiment method

### *Grouping of specimens and preparation*

The prepared specimens were divided into three groups (labeled as MSB-A, MSB-B, and MSB-C), and each group consisted of two specimens. MSB-A and MSB-C had a density of 554 kg·m<sup>-3</sup>, and MSB-B had a density of 757 kg·m<sup>-3</sup>.

In addition, two groups of RSPs with different densities were divided into Groups A and B (Tab. 1). Each specimen was further divided into four pieces and then grouped based on the difference in sandpaper and sanding time. Group A had a density of 554 kg·m<sup>-3</sup>, and Group B had a density of 757 kg·m<sup>-3</sup>, each test was repeated twice. A1-A4 (four groups) and B1-B4 (four groups) were used for numbering groups and marking the back of the specimens. A1 and B1 specimens comprised the control group, representing the specimens that were not subjected to sand treatment.

*Tab. 1: Group number and treatment of specimens.*

Group number	Density of RSP (kg·m <sup>-3</sup> )	Sandpaper models/#	Sanding time (min)
A1	554	0# (Untreated)	0
A2	554	180#	2
A3	554	360#	2
A4	554	600#	2
B1	757	0# (Untreated)	0
B2	757	180#	2
B4	757	600#	2

### *Experiment on interface temperature and humidity*

Three groups (MSB-A, MSB-B, and MSB-C) of RSP specimens were marked and sanded with 180# sandpaper. The MSB-A and MSB-B specimens were sanded for 1 min, and the MSB-C specimens were sanded for 2 min. The principle of grain sanding was applied, and sanding time was controlled with a stopwatch to ensure the accuracy of the experiment (Xiong et al. 2015, Molnar et al. 2017, Magoss et al. 2019). Except for the RSP specimens, all specimens (including PB, foam plastic, pine board, and marble) were not sanded. Hands were placed on the surface of the different materials to be tested. The temperature between the palm of the test subject and the interface of the specimen was measured using an electronic thermometer, and the results were recorded. Contact duration were set to 0, 10, 20, 30, and 40 s.

First, two RSPs with different densities (from MSB-A and MSB-B) were sanded with sandpaper of different models (180#, 360#, 600#) for 2 min. The treated specimens were then kept in a room-temperature environment after 24 h until a weight difference of 0.1% between the specimens was achieved. Subsequently, the constant specimens were weighed, and the value obtained was recorded as the quality before immersion. The specimens were fixed with a metal

grid, immersed in warm water with pH of almost 7 for 24 h, and taken out. The surfaces were subsequently wiped and then placed in a fresh-keeping bag. The weights were determined and then recorded as the quality after immersion. The 24 h water absorption rate of the specimens was calculated based on their quality before and after immersion.

#### *Experiment on psychological quantity*

In the case in which the experimental subjects were blindfolded, the tactile psychological quantity of the treated specimens was measured. The specimens, which were randomly placed on the top of a table, were touched in a uniform grain direction. The MSB-A and MSB-B specimens and other materials were sorted based on their degree of coldness and warmth by using the bubble method. Two adjacent test specimens were compared with respect to the coldness and warmth of the surface, and the warmer surface was placed in front. The comparison continued for the remaining specimens until the order of last specimens. In accordance with the order after sorting, the experimental subjects recorded the position of each specimen and rated the specimens as follows: +4, warmest; +2, warmer; 0, warm; -2, cool; -4, cooler; and -6, coolest. Scores were subsequently assigned. The average of each group was determined, and the value obtained was considered as the final tactile psychological quantity in the warm-cool feeling experiment. The specimens were observed from 0.5 m by the experimental subjects with the naked eye. With reference to the testing method used to determine the tactile psychological quantity, the degrees of coldness and warmth of the specimen were assessed, and the average was assigned as the final visual psychological quantity of the specimen.

Under the same method (from dry to wet), the specimens were rated as follows: +3, driest; +2, drier; +1, dry; 0, generally; -1, wet; -2, wetter; and -3, wettest. Two specimens from Groups A and B and other materials were subsequently assigned scores. The average for each group was ultimately assigned as the final tactile and visual psychological quantities in the dry-wet feeling experiment.

## RESULTS AND DISCUSSION

### Warm-cool feeling experiment

After the sanding treatment, the temperature of specimens was recorded by the above measurement method, and each specimen was tested three times and the average value of the three test results were taken as the final evaluation parameter (Tab. 2). Through the touch of RSP and other materials, as well as the observation of naked eyes, the degree of warm-cool feeling was tested and recorded according to the grading standard, and the averages were taken as the final tactile and visual psychological quantities in the warm-cool feeling experiment (Tab. 3).

*Tab. 2: Surface temperature of different specimens under different sanding treatments.*

Contact duration (s)	Surface temperature (°C)						
	MSB-A	MSB-B	MSB-C	PB	Foam plastic	Pine board	Marble
0	34.21	34.21	34.21	34.21	34.21	34.21	34.21
10	33.65	33.25	33.42	33.35	33.85	33.68	32.53
20	32.75	32.53	32.61	32.68	33.25	32.84	31.55
30	32.30	32.02	32.20	32.15	33.04	32.65	31.05
40	32.08	31.83	31.95	31.90	32.95	32.45	30.02

Tab. 3: Tactile and visual psychological quantities of different specimens in the warm-cool feeling experiment.

Specimen	Tactile psychological quantity	Visual psychological quantity
MSB-A	+0.1	+1.5
MSB-B	-3.2	-2.0
PB	-2.8	-4.0
Foam plastic	+4.0	+4.0
Pine board	+1.9	+0.5
Marble	-6.0	-6.0

The effects of variations in density and roughness on the surface temperature of the RSP specimens are presented in Figs. 1 and 2. The effects on the tactile and visual psychological quantities of the RSP specimens are shown in Fig. 3.

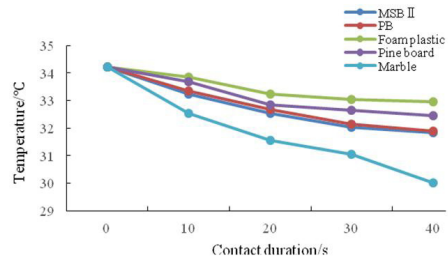
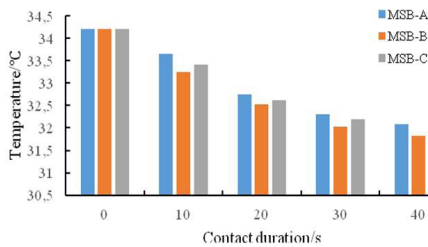


Fig. 1: Surface temperature of RSP specimens with different contact duration.

Fig. 2: Surface temperatures of different materials with different duration.

(1) The temperatures of the palms of the experimental subjects decreased continuously as contact duration with RSP increased (Fig. 1). The maximum change occurred at contact duration with 10 s, which tended to stabilize after 30 s. Roughness exerted an effect to a certain extent, but such was not evident in the warm-cool feeling of the RSP surface. With an increase in sanding time, the roughness of the RSP surface decreased and the warmth increased. At a constant surface roughness, the temperatures of the specimens with a lower density (MSB-A) were always higher than those of the specimens with a higher density (MSB-B). That is, density exerted a more significant influence on the warm-cool feeling of the RSP surface. The higher the density, the cooler the RSP surface. By consulting the literature, it can be seen that Zhao et al. (2017) also concluded that the density was negatively correlated with the surface temperature of the substrates when they study and compare the temperature changes between wood-plastic composites and other heated floor substrates. The same trend exists in related research in different fields, especially the research on the warm-cool feeling of the fabric surface in garment industry. Zhang (2016) of Donghua University has analyzed that the density of fabric has a significant effect on its surface warm-cool feeling by establishing a physical model of the temperature between the fingertip and the fabric, the greater the density, the lower the temperature of fabric surface. Zhang et al. (2017) has tested the warm-cool feeling of 14 different fabrics by a precision instantaneous thermal property tester. The experimental results showed that the smoothness and density had the opposite tendency to the warm-cool feeling of fabric surface.

In Fig. 2, the temperature curve of PB basically coincided with that of the RSP (MSB-B), indicating that the two materials exhibited a similar warm-cool feeling. RSPs had a similar warm-cool feeling as that of the particle board made of other types of wood. In several wood materials, the surface of pine exhibited the lowest change in warm-cool feeling. This finding was mainly attributed to its high internal porosity and low thermal conductivity, which resulted in a lower temperature change between pine and human contact interface than that between other artificial panels and human contact interface. The temperature change in marble was the largest. The highest thermal conductivity of the marble suggested that the marble was not suitable for use in furniture materials, which often are in contact with the human body. Foam plastic exhibited the strongest warm-cool feeling and the highest contact-interface temperature. The temperature change was considerably affected by the environment. Long-term contact affects comfort.

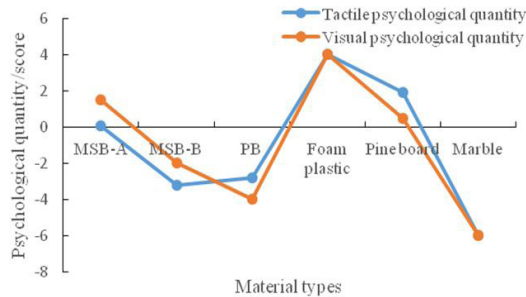


Fig. 3: Psychological quantity of different materials in a warm-cool feeling experiment.

(2) The psychological quantity of the RSP specimens and other wood specimens was between that of the marble and that of the foam plastic (Fig. 3), indicating compared with the RSP specimens, wood materials provided greater comfort as furniture materials. Compared with that of the artificial panel, the pine specimens had a lower density and a softer texture. Therefore, the tactile psychological quantity of pine specimens was higher than those of the RSP and PB specimens. Density significantly influenced the tactile psychological quantity of the RSP specimens. When the sanding time of MSB-A and MSB-B were similar, the MSB-B surface exhibited cooler tactile and visual psychological quantities. The tactile warmth of the RSP specimens was lower than that of PB. The reason was that PB and solid wood exhibited a similar texture, with PB achieving increased tactile warmth after a layer of veneer treatment. With respect to the visual psychological quantity, the surface of the MSB-B specimens exhibited a certain roughness after the sanding treatment. The RSP fiber induced diffused reflection on the surface; in addition, the PB surface was varnished and not sanded in the experiment. Consequently, the PB surface was smoother, and their refractive index was higher, thereby decreasing their visual psychological quantity and cooler tactile quality.

### Dry-wet feeling experiment

The 24 h absorption rate was calculated by recording the quality before and after immersion of the specimens, and each specimen was tested three times and the averages of the three test results were taken as the final evaluation parameter (Tab. 4). Through the touch of RSP and other materials, as well as the observation of naked eyes, the degree of dry-wet feeling was tested and recorded according to the grading standard, and the averages were taken as the final tactile and visual psychological quantities in the dry-wet feeling experiment (Tab. 5).

Tab. 4: 24 h water absorption rate of RSP specimens.

Group number	Quality before immersion (g)	Quality after immersion (g)	24 h water absorption rate (%)
A1	32.05	48.27	50.6
A2	32.14	46.59	44.96
A3	30.12	44.5	44.77
A4	32.93	47.5	44.25
B1	33.46	43.65	30.45
B2	37.35	48.07	28.7
B3	35.31	45.82	28.23
B4	35.84	45.84	27.9

Tab. 5: Tactile and visual psychological quantities of different specimens in the dry-wet feeling experiment.

Specimen number	Tactile psychological quantity	Visual psychological quantity
MSB-A	1.8	+1.5
MSB-B	-2.1	-1.9
MSB-C	+0.1	+0.2
PB	-2.1	-1.5
Foam plastic	+3.0	+3.0
Pine board	+1.9	+1.7
Marble	-3.0	-3.0

The effects of variations in density and surface roughness on the 24 h water absorption rate of the RSP are presented in Fig. 4. The effects on the tactile and visual psychological quantities are shown in Fig. 5.

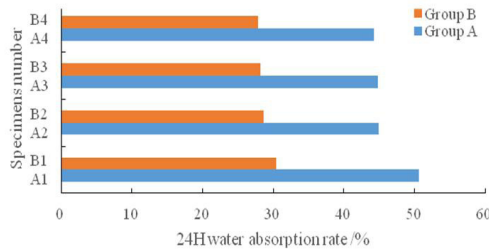


Fig. 4: 24 h water absorption rates of different materials.

(1) Density significantly affected the water absorption performance of the specimens (Fig. 4). Considerable difference in water absorption was found between Groups A and B. The lowest water absorption rate of the specimens in Group A was 44.25%, which was far greater than the highest absorption rate of the specimens in Group B. This finding indicated that the higher the density of the RSP, the poorer the water absorption. The RSP with a greater density had a smaller gap between the fibers, thereby decreasing water absorption. By consulting the literature, we can see that there is a similar relationship between the density and absorption rate in garment industry. Shen (2007) of Xi'an polytechnic university has analyzed that as the density and thickness of the fabric increased, the water absorption ability of the fabric showed

a decreasing trend. Compared with density, the surface roughness affected the water absorption of RSP, but the effect was not apparent. The specific effects exhibited a proportional tendency, and the lower the surface roughness, the poorer the water absorption.

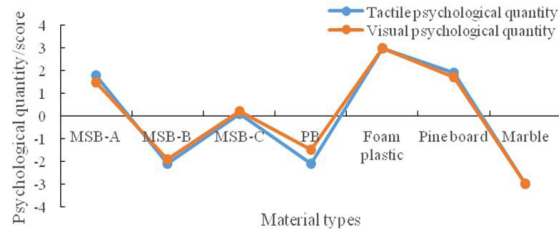


Fig. 5: Psychological quantity of different materials in the dry-wet feeling experiment.

(2) The tactile and visual psychological quantities of wood materials were between that of the marble and that of the foam plastic (Fig. 5). This finding indicates that wood materials had a good dry-wet tactile quality. Contact between the human body and the material could produce tactile and visual comfort. Therefore, wood materials could be used widely in furniture materials. The higher the density, the lower the tactile and visual psychological quantities of the RSP specimens, thus providing humidity to human bodies. With density remaining the same, the higher the surface roughness of the specimen, the drier the surface. The dry-wet feeling of the RSP surface could be improved by veneering, and the comfortable feeling as furniture materials increased. Among the three materials, PB achieved the lowest psychological and visual psychological quantities. The reason is that the surface of PB were treated with veneer and then finished, thus increasing the smoothness of the panel surface. The surface had a poor dry-wet feeling relative to that of the solid wood board.

## CONCLUSIONS

(1) After the RSP specimens with two different densities were sanded using different types of sandpaper and sanding time, the surface tactile properties were evaluated by conducting warm-cool feeling and dry-wet feeling experiments. Density and roughness significantly affected the tactile properties of RSP, and the influence of density is greater than that of the surface.

(2) The surface tactile properties of the RSP are closest to those of the poplar medium-density particleboard. However, the RSP has a preferable water absorption for adjusting indoor humidity.

(3) Among the several materials tested, the solid wood materials exhibited the highest tactile and visual psychological quantities. This superior characteristic is also the reason solid wood is most widely used in furniture and interior decoration.

## ACKNOWLEDGEMENTS

The authors are grateful for Natural Science Foundation of Jiangsu Province (CN) (No. BK20150881).

## REFERENCES

1. Ahn, E., Yeom, D., Lee, K.I., 2017: Experimental research on the indoor environment performance of complex natural insulation material: carbonized rice hull and rice hull. *Journal of Asian Architecture and Building Engineering* 16(1): 239-246.
2. Basta, A.H., Lotfy, V.F., 2013: Performance of rice straw-based composites using environmentally friendly polyalcoholic polymers-based adhesive system. *Pigment & Resin Technology* 42(1): 24-33.
3. Bellizzi, J. A., Hite, R. E., 1992: Environmental color, consumer feelings, and purchase likelihood. *Psychology & marketing* 9(5): 347-363.
4. Fang, L., Zeng, J., Liao, X., Zou, Y., Shen, J., 2019: Tensile shear strength and microscopic characterization of veneer bonding interface with polyethylene film as adhesive. *Science of Advanced Materials* 9: 1223-1231.
5. Goldie, L., Weedall, P.J., 2001: The objective measurement of the 'cool feeling' in fabrics. *The Journal of the Textile Institute, Part 3. Technologies for a New Century* 92(4): 379-386.
6. Hu, S. R., Li, J., 2013: Study on warm-cool feeling of knitted fabric. *Advanced Materials Research* 2735(1643): 309-312.
7. Inoue, T., Nakayama, A., Niwa, M., 2010: Relationship between the warm/cool feeling of fabric and the subjective evaluation of the quality of ladies' knitted fabrics. *International journal of clothing science and technology* 22(1): 7-15.
8. Li, R., Xu, W., Wang, X., Wang, C., 2018: Modeling and predicting of the color changes of wood surface during CO<sub>2</sub> laser modification. *Journal of cleaner production* 183: 818-823.
9. Li, Q., Jiang, H., Tang, Q., Chen, Y., Li, J., Jian, Z., 2018: Smart manufacturing standardization: reference model and standards framework. *Computer Integrated Manufacturing Systems* 101: 91-106.
10. Magoss, E., Molnár, Z., Suri, V., 2019: Evaluating of wetting-induced effects on the surface stability of sanded wood. *Wood Research* 64(3): 401-410.
11. Mangat, A., Hes, L., Bajzik, V., 2017: Effect of biopolishing on warm-cool feeling of knitted fabric: a subjective and an objective evaluation. *Autex Research Journal* 17(2): 95-102.
12. Molnár, Z., Németh, G., Sandor, Héjja, S., Magoss, E., Tatai, S., 2017: The effect of the position of 2D roughness measurement on the roughness parameters by natural wood material. *Wood Research* 62(6): 895-903.
13. Okuyama, T., Hariu, M., Kawasoe, T., Kakizawa, M., Shimizu, H., Tanaka, M., 2011: Development of tactile sensor for measuring hair touch feeling. *Microsystem technologies* 17(5-7): 1153-1160.
14. Pac, M. J., Bueno, M. A., Renner, M., El Kasmi, S. 2001: Warm-cool feeling relative to tribological properties of fabrics. *Textile Research Journal* 71(9): 806-812.
15. Parker, P., 1997: A summary report on building materials produced from wheat straw. *Inorganic Bonded Wood Fiber Composite Material* 5: 47-48.
16. Shen, H., Lv, G., 2018: Calibration Method for surface thermometer. *Metrology & Measurement technology* 1: 93-95.
17. Shen, L., Fan, L., Zhang, L., 2007: Test analyses of heat and moisture property of bamboo fiber fabric. *Cotton Textile Technology* 35(5): 1-4.
18. Shi, L., Zhang, H., Li, Z., Man, X., Wu, Y., Zheng, C., Liu, J., 2018: Analysis of moisture buffering effect of straw-based board in civil defence shelters by field measurements and numerical simulations. *Building and Environment* 143: 366-377.

19. Vivekanadan, M.V., Raj, S., Sreenivasan, S., Nachane, R.P., 2011: Parameters affecting warm-cool feeling in cotton denim fabrics. *Computers & Geosciences* 36(2): 117-121.
20. Wang, S., Lin, F., Lin, M., 2000: Thermal properties of interior decorative material and contacted sensory cold-warmth I: relation between skin temperature and contacted sensory cold-warmth. *Journal of Wood Science* 46(5): 357-363.
21. Wu Y., Bian Y., Yang F., Ding Y., Chen K., 2019: Preparation and properties of chitosan/graphene modified bamboo fiber fabrics. *Polymers* 11: 1540.
22. Xiong, X., Jiang, Y., Xu, W., 2015: The Roughness tactile properties of the straw board surface. *Packing Engineering* 36(3): 42-47.
23. Yan, Y., Li, X., Liu, X., 2012: Study on hot-pressing process of straw particle board. *Journal of Central South University of Forestry & Technology* 32(1): 126-129.
24. Yang, H. S., Kim, D. J., Kim, H. J., 2003: Rice straw-wood particle composite for sound absorbing wooden construction materials. *Bioresource Technology* 86(2): 117-121.
25. Yi, X., Zhao, D., Ou, R., Ma, J., Chen, Y., Wang, Q., 2017: A comparative study of the performance of wood-plastic composites and typical substrates as heating floor. *Bioresources* 12(2): 2565-2578.
26. Zhang, W., 2016: Study on computer modelling of fabric contact thermal sensation. Donghua University, Shanghai, China, pp. 5-15.
27. Zhang, X., Wang, L., Chen, Y., 2017: Formation mechanism and influence factors of warm-cool feeling of knitted underwear fabrics. *Journal of Textile Research* 38(1): 57-60.

XIANQING XIONG<sup>1,2\*</sup>, YITING NIU<sup>1,2</sup>, QINGRU MA<sup>1,2</sup>, YUTING PAN<sup>1,2</sup>  
NANJING FORESTRY UNIVERSITY

<sup>1</sup>CO-INNOVATION CENTER OF EFFICIENT PROCESSING AND UTILIZATION OF FOREST  
RESOURCES

<sup>2</sup>COLLEGE OF FURNISHINGS AND INDUSTRIAL DESIGN  
NANJING FORESTRY UNIVERSITY  
NANJING 210037  
CHINA

\*Corresponding author: xiongxianqing@njfu.edu.cn

## **MECHANICAL AND PHYSICAL PROPERTIES OF MEDIUM DENSITY FIBREBOARD WITH CALCITE ADDITIVE**

OSMAN CAMLIBEL  
KIRIKKALE UNIVERSITY  
YAHSIHAN/ KIRIKKALE, TURKEY

MEHMET AKGUL  
KARAMANOGLU MEHMETBEY UNIVERSITY  
KARAMAN, TURKEY

(RECEIVED MAY 2019)

### **ABSTRACT**

In this study, it is investigated that are calcite filler can be used in the production of medium density fiberboard. Chips have been to the process of cooking for 4-5 minutes in Asplund defibrator with the vapor pressure of 7-7.5 bar, and 180°C temperature. 1.5% paraffin and 1% ammonium sulphate to be pulverized is added to fibers on the output of defibrillator and blowline line. Calcite fillers are prepared in a separate tank in order to use calcite instead of lignocellulosic fibers in the production of 1 m<sup>3</sup> MDF. After that, urea formaldehyde glue is prepared as three different solutions which include the calcite, respectively with 3% (20 kg·m<sup>-3</sup>), 6% (40 kg·m<sup>-3</sup>), 9% (60 kg·m<sup>-3</sup>). The fibers are dried to moisture of 8%-12%. This press applies temperature about 185-190°C and pressure about 32-34 kg·m<sup>-2</sup> to the mixture material for 270 seconds during pressing time. MDF panels (2100 x 4900 x 18 mm) were produced in the process. Both mechanical and physical experiments are performed on boards which are produced.

**KEYWORDS:** MDF, fiberboard, calcite filler, physical properties, mechanical properties.

### **INTRODUCTION**

The wood chips or lignocellulosic materials, cement, water and chemicals can be produced as smooth-surfaced panels by mixing in suitable proportions in forest products industry. Wood composite products with binding calcite materials were generated by using plaster, magnesium cement and Portland cement. Güller (2001) has produced the calcite material-binding fiber boards and particle boards. Kalaycıoğlu et al. (2012) have performed some studies on the cement composites and wood wool. Salari et al. (2012) have produced the OSB board which had added

nanoclays layered silicates as reinforced adhesive with 0%, 2%, 4%, 6%, 8% mixing ratios. They have also performed studies on the physical and mechanical properties. Candan et al. (2012) have investigated the effects of some production parameters on the layer thickness swell properties of the medium density fibreboard (MDF). Özdemir and Ayaz (2017) have investigated the effect of ammonium polyphosphate (app) and boric acid (BA) on the fire resistance of MDF panels as surface coating material. Zahedsheijani et al. (2011) studied the potential use of Nanoclay in MDF production. Özdemir (2019) has produced three different minerals (sepiolite, dolomite and perlite) and five different ratios (3%, 6%, 9%, 12% and 15%) according to the oven-dry wood fiber weight. Taghiyari et al. (2016) have produced MDF from wollastonite fibers, camel-thorn and wood fibers. They have studied the physical and mechanical properties of these boards. Taghiyari and Nouri (2015) have investigated nano-wollastonite (NW) on physical and mechanical properties of medium density fiberboard (MDF). Wang et al. (2016) produced vermiculite added MDF boards. They have investigated the properties of boards, limitation of oxygen index (LOI), simultaneous thermal analysis (TG-DSC), the modulus of rupture (MOR), and the modulus of elasticity (MOE). Akgül et al. (2017) have produced agribased lignocellulosic biomass (okra, tobaccos, hazelnut, walnuts hell, pine cone) in medium density fiberboard (MDF) production. They have investigated on physical and mechanical properties of medium density fiberboard (MDF). Kaya (2018) has investigated the physical and mechanical properties of fiber layers produced by using glass fiber mixture of walnut shells and sunflower stalks in different ratios were investigated. Özdemir (2019) have investigated the use of different mineral material types (sepiolite, dolomite, and perlite) in medium density fiberboard (MDF) production. Çavdar et al. (2019) have investigated ammonium zeolite and ammonium phosphate as fire retardants for microcrystalline cellulose thermoplastic composites. Funk et al. (2017) have studied diatomaceous earth as an inorganic additive to reduce formaldehyde emissions from particleboards. Istek et al. (2013) have worked combustion properties of medium-density fiberboards coated by a mixture of calcite and various fire retardants. Özdemir et al. (2016) have researched the effects of coating with calcite together with various fire retardants on the fire properties of particleboard.

These researchers were about the possibilities of use of the calcite minerals instead of lignocellulosic raw materials. There are millions of tons of the calcite mineral reserves in Turkey. In MDF production process the calcite mineral, which has the mixing ratio 0%, 3%, 6%, 9%, was produced for boards in industrial process scale.

The production of MDF in 2015 was about 5,412.0 million m<sup>3</sup> in Turkey. The production of MDF in 2015 was about 98,098.0 million cubic meters/year in the world. In this study, the experimental investigations handled in order to realize the density and physical and mechanical properties of the produced boards which have calcite mineral according to the control board.

## MATERIAL AND METHODS

### Materials

Beech (*Fagus orientalis* L.) from Duzce province forestry, Oak (*Quercus Robur* L.) from the West Black Sea region and pine (*Pinus sylvestris* L) from Bolu province were supplied for the production of MDF. Calcite consists of 90% CaCO<sub>3</sub> containing limestone with hardness and the specific gravity 2.5-2.7 g·cm<sup>-3</sup> was provided from the region about the province of Aksaray. Calcium oxide is converted into calcium hydroxide by reaction with water. The urea formaldehyde resins, the liquid paraffin and the ammonium sulphate were supplied from Polisan company in Gebze, Mercan Chemistry in Denizli and another company in Gebze, respectively.

## Methods

The solid ratio of the urea-formaldehyde is reduced to 50% solid rate in the production process. The colour of ammonium sulfate crystal grains is off-white. It is prepared for hardener with 20% solution, and then it is injected from a single point to blow line. The colour of liquid paraffin is cream and the fat content is up to 2%. The penetration of liquid paraffin is 32, and then it is stored in reserve tank as liquid state. The liquid paraffin is mixed into dry fiber up to a maximum of 1.5% percent. The mixture described above is added to fiber in Asplund defibrator. The hardener, calcite solution and urea-formaldehyde are injected from blow line to the biomass fiber.

Fibers, which include the calcite and the chemical, are dried at the drier line up to 11-12% of moisture. Dried fibers are made up of mat in the mechanical station. The mat is produced by pressing in the multi hot press. The pressing parameters are 180-190°C, 32-34 kg·m<sup>-2</sup> and 275 second. The dimensions of the panel are 2100 x 4900 x 18 mm. After production of the panels in process, the panels are leaved to rest in pre-storage for 5 days. The panels are acclimatized here. The moisture level is adjusted to 7.5%. After this process, the top and bottom surfaces of panels are sanded with 40, 80, 120 grit size sandpaper. Then all panels were conditioned at 20 + 2°C and 65 +5% relative humidity until 12% moisture content was reached. The MDF product process is presented in Fig. 1.

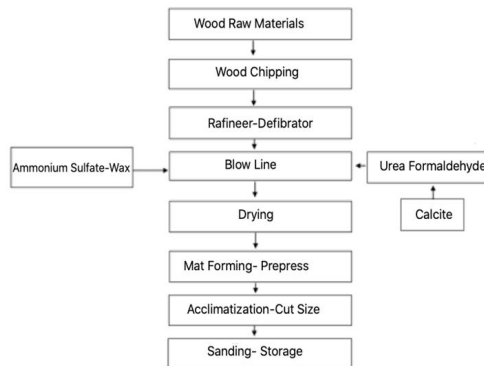


Fig. 1: Product process flow.

The resins and other chemicals are prepared in the glue unit. The calcite mineral solution is prepared in the solution preparing tank. After that these chemicals, which are prepared in the tank, are mixed with each other and this mixture is sent blow line.

## Product parameters

Wood fiber contains 70% hardwoods and 30% softwood fibers in this study. Firstly, the hardwood and softwood species had brought from the Western Black Sea forests, and then these species were chopped and stored one by one in silos according to the production parameters. In Tab. 1, R defines the consumed wood fibers for 1 m<sup>3</sup> board, C defines the consumed calcite minerals for 1 m<sup>3</sup> board. The raw materials formulation for the experimental MDF boards are presented in Tab. 1. This table shows the addition of calcite solution and other chemicals to lignocellulosic biomass. Xing et al. (2006) in a study in MDF production; The effect of wood acidity has been shown to have a direct effect on the gel time and curing behavior of UF resins. In this study; the amount of calcite had no significant effect on the curing of the glue.

Tab. 1: Experimental design.

Board Type	Product Type	Biomass	Resin	Hardener	Paraffin	Calcite filler	Industrial fibers	Ratio
R <sub>100</sub> C <sub>0</sub>	MDF	L	UF	AS	W <sub>ax</sub>	0	100%	0
R <sub>97</sub> C <sub>3</sub>	MDF	L	UF	AS	W <sub>ax</sub>	C	97%	3%
R <sub>94</sub> C <sub>6</sub>	MDF	L	UF	AS	W <sub>ax</sub>	C	94%	6%
R <sub>91</sub> C <sub>9</sub>	MDF	L	UF	AS	W <sub>ax</sub>	C	91%	9%

R: fiber content. MDF: medium density fibreboard, L:lignocellulosic, UF:urea formaldehyde, AS: ammonium sulphate, C:calcite.

**Hot multiple press parameters**

The MDF production hot press diagram is presented in Fig. 2.

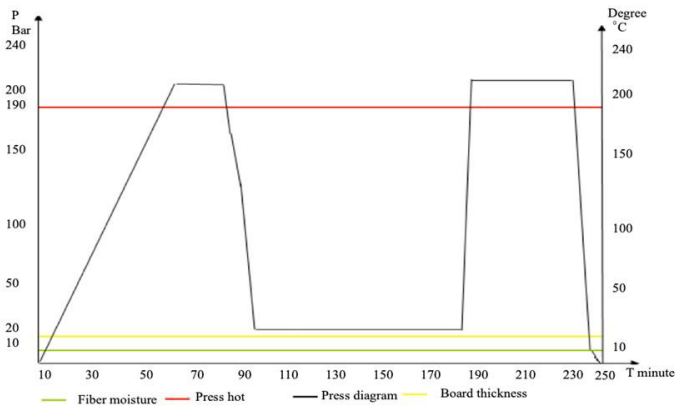


Fig. 2: Press diagram.

**Glue**

The urea-formaldehyde glue with the following technical specification was used: solid (65%), formaldehyde / urea molar ratio (1.25), density at 20°C (1.227 g·cm<sup>-3</sup>), viscosity 20 cPs (185 second), gel time 100°C, 20% (NH<sub>4</sub>)<sub>2</sub>SO<sub>4</sub>: (25-40 sec), pH (7.5 to 8.5), free formaldehyde content 0.5% max, methylol groups 12 - 15% , average shelf life is 45 days.

**Physical testing**

Physical properties were tested according to TS-EN 622-5 (2008) and the density of MDF sheets was tested according to TS-EN-323 (1999). The water absorption and thickness swelling of the specimens were measured according to TS-EN 317 (2008). The sheet surface toluene was tested TS according to the EN 382-1 (1999). Sample thickness and length of specimens were measured by using a digital micrometer and caliber with 0.01 mm gradients.

**Colour properties**

Colour measurements are measured by using the tristimulus photoelectric colorimeter Elrepho Spectrophotometer, with a measuring head 50 mm in diameter, according to ASTM D2244-07e1 standards. The Elrepho spectrophotometer measures the colour of any material in a three-dimensional colour area. This system is called CIE L\*a\*b\* and works according to the

CIE Standard. The part of the coordinate system, which is interested in this work, is the first quadrant which corresponds positive values of  $a^*$  and  $b^*$ . The colour parameters  $L^*$ ,  $a^*$ , and  $b^*$  were determined by the CIEL\*a\*b\* method on the surface fiberboards. Their variations with regard to the treatment ( $\Delta L^*$ ,  $\Delta a^*$ ,  $\Delta b^*$ ) are calculated. The colour sphere is defined as the circle of the cross-section at  $L^* = 50$ . The colour difference,  $\Delta E$  total colour difference is the distance between two colour points in the colour sphere. To the right: Cross section at  $L^* = 50$  showing the axis from green to red ( $a^*$ ) and from blue to yellow ( $b^*$ ), the coordinates chroma ( $C^*$ ) and hue ( $h = \arctan(b^*/a^*)$ ) is the hues of a colour: 0 or 360 is red, 90 is yellow, 180 is green and 270 is blue.  $L^*$  is the lightness; 100 = white and 0 = black.  $C^*$  is the chroma or saturation; 0 represents only greyish colours and 60 (Akgül 2013). The three measured co-ordinates,  $L^*$ ,  $a^*$ , and  $b^*$ , were transformed to  $L^*$ ,  $C^*$ , and  $h$  co-ordinates and  $\Delta E$  values, according to the Eq. 1 (Temiz et al. 2005)

$$\Delta E = \sqrt{(\Delta L)^2 + (\Delta a)^2 + (\Delta b)^2} \quad (1)$$

The  $L^*C^*h$  system has been chosen, since only one color variable is needed to donate hue, i.e. red, green, blue, or yellow and furthermore, this system is easy to refer to our experience of colour characteristics such as lightness, saturation, and hue. Each colour parameter  $L^*$ ,  $C^*$ ,  $h$  and  $\Delta E$ , was measured for each material, time, and temperature. The average colour values, standard deviations, and 5% significance level based on distribution were calculated assuming normal distribution. The lower value of  $\Delta E^*$  indicates that the colour is either not changed or the change is negligible equation (Akgül 2013).

### Mechanical testing

Cutting and sizing according to TS EN 325 (2008), TS EN 326-1 (1999) standard has been performed to specify the properties of MDF sheets with calcite. These tests were; bending strength TS EN 310 (2008), modulus elasticity TS EN 310 (2008), internal bond TS EN 319 (2008). Screw holding ability perpendicular to the plane of panel ASTM D 1037-78 (1994). An universal tester (imal mobiltemp shc22, model ib400) was used to assess mechanical properties. Janka hardness measure vertically to the sheet surface standards have been applied ANSI A 208.1 (1999).

### Statistical analysis

The data concernings physical tests, colour feature tests, mechanical tests were explained  $\pm$  standard deviation and were analyzed using an analysis of variance (ANOVA) method for a entirely completely randomized design. Differences were considered statistically substantial at  $p < 0.05$ . As a result of these tests, SPSS 17 (ANOVA) Duncan results are evaluated by statistical programs.

## RESULTS AND DISCUSSION

The results of ANOVA and Duncan mean separation test for density, the toluene surface, the thickness swelling (TS, 2-24 hours) and water absorption (WA, 2-24 hours) percent of the fiberboards made from calcite addictive fiber and control fiberboards are shown in Tab. 2.

Tab. 2: The results of ANOVA and Duncan mean separation test for density, the toluene surface, the thickness swelling (TS, 2-24 hours) and water absorption (WA, 2-24 hours) percent of the fiberboards made from calcite additive fiberboards and control fibreboard.

Board		Avg. <sup>x</sup>	Std. Deviation	Board		Avg. <sup>x</sup>	Std. Deviation
Calcite				Calcite			
Density (g·cm <sup>-3</sup> )	R <sub>100</sub> C <sub>0</sub>	0.715 <sup>a</sup>	0.01	TS 2 hours (%)	R <sub>100</sub> C <sub>0</sub>	3.81 <sup>a</sup>	0.40
	R <sub>97</sub> C <sub>3</sub>	0.720 <sup>a</sup>	0.02		R <sub>97</sub> C <sub>3</sub>	8.44 <sup>b</sup>	1.82
	R <sub>94</sub> C <sub>6</sub>	0.716 <sup>a</sup>	0.02		R <sub>94</sub> C <sub>6</sub>	11.09 <sup>c</sup>	0.98
	R <sub>91</sub> C <sub>9</sub>	0.712 <sup>a</sup>	0.01		R <sub>91</sub> C <sub>9</sub>	13.15 <sup>d</sup>	1.00
WA 2 hours (%)	R <sub>100</sub> C <sub>0</sub>	21.29 <sup>a</sup>	2.00	TS 24 hours (%)	R <sub>100</sub> C <sub>0</sub>	10.55 <sup>a</sup>	0.28
	R <sub>97</sub> C <sub>3</sub>	33.93 <sup>b</sup>	3.99		R <sub>97</sub> C <sub>3</sub>	16.88 <sup>b</sup>	1.01
	R <sub>94</sub> C <sub>6</sub>	36.61 <sup>b</sup>	4.56		R <sub>94</sub> C <sub>6</sub>	18.28 <sup>c</sup>	0.22
	R <sub>91</sub> C <sub>9</sub>	39.91 <sup>c</sup>	7.51		R <sub>91</sub> C <sub>9</sub>	20.51 <sup>d</sup>	0.85
WA 24 hours (%)	R <sub>100</sub> C <sub>0</sub>	41.68 <sup>a</sup>	2.86	BST (cm)	R <sub>100</sub> C <sub>0</sub>	34.35 <sup>a</sup>	1.08
	R <sub>97</sub> C <sub>3</sub>	70.29 <sup>b</sup>	10.13		R <sub>97</sub> C <sub>3</sub>	31.00 <sup>b</sup>	1.29
	R <sub>94</sub> C <sub>6</sub>	70.67 <sup>b</sup>	6.52		R <sub>94</sub> C <sub>6</sub>	29.00 <sup>c</sup>	1.45
	R <sub>91</sub> C <sub>9</sub>	80.29 <sup>c</sup>	7.41		R <sub>91</sub> C <sub>9</sub>	25.00 <sup>d</sup>	2.47

x- the average value of the samples, 95% confidence interval for the average ANOVA. a, b, c, d- values with the same letter are not significantly different (Duncan's test), (TS) thickness swelling, (WA) water absorption, (BST) board surface test.

The conclusions are shown in Tab. 2. There is no significant difference between densities for calcite added panels R<sub>100</sub>C<sub>0</sub>, R<sub>97</sub>C<sub>3</sub>, R<sub>94</sub>C<sub>6</sub>, R<sub>91</sub>C<sub>9</sub> according to this statistical analysis result. The results of MDF densities stay in 0,65 < MDF < 0,80 g·cm<sup>-3</sup> according to TS EN 622-5 standards. Thus, there is no significant difference in results.

The ratio of the lowest fiberboard density to the average fiberboard density is always desired between 0.85 to 0.95 values. The efficiency of process parameters and applied hot press diagram in MDF production affect the optimum homogenous density of the fiberboard.

### The results of the swell in water for 2 hours test

There is significantly difference between (R<sub>100</sub>C<sub>0</sub>), (R<sub>97</sub>C<sub>3</sub>), (R<sub>94</sub>C<sub>6</sub>) and (R<sub>91</sub>C<sub>9</sub>) according to the percentage of swell in water for 2 hours test. The results are explained in Tab. 2. The ratio for this test is 121.3% for R<sub>97</sub>C<sub>3</sub> according to R<sub>100</sub>C<sub>0</sub>. Therefore, the percentage of swelling increases for R<sub>97</sub>C<sub>3</sub>. Similarly, the ratio is 190.6% for R<sub>94</sub>C<sub>6</sub> according to R<sub>100</sub>C<sub>0</sub>. Therefore, the percentage of swelling increases for R<sub>94</sub>C<sub>6</sub>. The ratio is 244.7% for R<sub>91</sub>C<sub>9</sub> according to R<sub>100</sub>C<sub>0</sub>. Therefore, the percentage of swelling increases for R<sub>91</sub>C<sub>9</sub>. The thickness swelling and water absorption properties of the test panels increased as the amount of mineral filler usage was increased (Özdemir, 2019).

### The results of the swell in water for 24 hours test

There is significantly difference between (R<sub>100</sub>C<sub>0</sub>), (R<sub>97</sub>C<sub>3</sub>), (R<sub>94</sub>C<sub>6</sub>) and (R<sub>91</sub>C<sub>9</sub>) according to the percentage of swell in water for 24 hours test. The results are explained in Tab. 2. The ratio for this test is 60.0% for R<sub>97</sub>C<sub>3</sub> according to R<sub>100</sub>C<sub>0</sub>. Therefore, the percentage of swelling increases for R<sub>97</sub>C<sub>3</sub>. Similarly, the ratio is 73.2% for R<sub>94</sub>C<sub>6</sub> according to R<sub>100</sub>C<sub>0</sub>. Therefore, the percentage of swelling increases for R<sub>94</sub>C<sub>6</sub>. The ratio is 94.4% for R<sub>91</sub>C<sub>9</sub> according to R<sub>100</sub>C<sub>0</sub>. Therefore, the percentage of swelling increases for R<sub>91</sub>C<sub>9</sub>.

### The results of the water absorption for 2 hours test

There is significant difference between ( $R_{100}C_0$ ), ( $R_{97}C_3$ ,  $R_{94}C_6$ ) and ( $R_{91}C_9$ ) according to the percentage of the water absorption for 2 hours test. The results are explained in Tab. 2. The ratio for this test is 59.3% for  $R_{97}C_3$  according to  $R_{100}C_0$ . Therefore, the percentage of water absorption increases for  $R_{97}C_3$ . Similarly, the ratio is 71.9% for  $R_{94}C_6$  according to  $R_{100}C_0$ . Therefore, the percentage of the absorption increases for  $R_{94}C_6$ . The ratio is 87.4% for  $R_{91}C_9$  according to  $R_{100}C_0$ . Therefore, the percentage of the absorption increases for  $R_{91}C_9$ .

### The results of the water absorption for 24 hours test

There is a significant difference between ( $R_{100}C_0$ ), ( $R_{97}C_3$ ,  $R_{94}C_6$ ) and ( $R_{91}C_9$ ) according to the percentage of the water absorption for 24 hours test. The results are explained in Tab. 2. The ratio for this test is 68.6% for  $R_{97}C_3$  according to  $R_{100}C_0$ . Therefore, the percentage of the water absorption increases for  $R_{97}C_3$ . Similarly, the ratio is 69.6% for  $R_{94}C_6$  according to  $R_{100}C_0$ . Therefore, the percentage of the absorption increases for  $R_{94}C_6$ . The ratio is 92.6% for  $R_{91}C_9$  according to  $R_{100}C_0$ . Therefore, the percentage of the absorption increases for  $R_{91}C_9$ . This increase in the thickness swelling and water absorption properties of the boards was due to the material properties of the mineral materials such as hydrophilic properties (Özdemir 2019). It shows that as the resin content increases, mat moisture content increases and continuous press speed increases, the TS values of MDF panels decrease both for 2 hours and 24 hours (Candan et al. 2012).

### The results of toluene on the surface of board test

There is a significant difference between ( $R_{100}C_0$ ), ( $R_{97}C_3$ ), ( $R_{91}C_9$ ) and ( $R_{94}C_6$ ) according to the percentage of toluene on the surface of board test. The results are explained in Tab. 2. The ratio for this test decreases 10.8% for  $R_{97}C_3$  according to  $R_{100}C_0$ . Therefore, the percentage of toluene on the surface of board decreases for  $R_{97}C_3$ . Similarly, the ratio decreases 18.4% for  $R_{94}C_6$  according to  $R_{100}C_0$ . Therefore, the percentage of the absorption decreases for  $R_{94}C_6$ . The ratio is 37.4% for  $R_{91}C_9$  according to  $R_{100}C_0$ . Therefore, the percentage of the absorption increases for  $R_{91}C_9$ . The physical properties of the fiber boards are determined according to the raw material source, quantity and type of additives, resin ratio and press conditions produce in MDF boards (Kaya, 2018). The addition of inorganic filler to the MDF changes the WA and TS of the boards significantly. In fact, the results indicate that the addition of filler might increase WA and TS, which is considering the fact that some parts of hydrophilic wood fibers were exchanged by the inorganic mineral. Owing to the increase in the amount of calcite filling between wood fibers, the bond of wood fibers with each other are decreasing.

### Color properties

ASTM D2244-07e1 standard is applied in this test. The surface color analysis of MDF fiberboards is calculated by using Eq. 1. The results are explained in Tab. 3.

Tab. 3: ANOVA and Duncan average separation test results of surface color analysis of MDF fiberboards.

Board Type		Avg.x	Std. Deviation	Board Type		Avg.x	Std. Deviation
Calcite				Calcite			
$\Delta L_y$	R <sub>100</sub> C <sub>0</sub>	60.47 <sup>a</sup>	0.95	$\Delta b_t$	R <sub>100</sub> C <sub>0</sub>	20.28 <sup>a</sup>	0.38
	R <sub>97</sub> C <sub>3</sub>	59.38 <sup>b</sup>	0.44		R <sub>97</sub> C <sub>3</sub>	18.10 <sup>b</sup>	0.38
	R <sub>94</sub> C <sub>6</sub>	61.26 <sup>a</sup>	2.05		R <sub>94</sub> C <sub>6</sub>	18.67 <sup>b</sup>	0.38
	R <sub>91</sub> C <sub>9</sub>	62.64 <sup>c</sup>	1.53		R <sub>91</sub> C <sub>9</sub>	19.96 <sup>a</sup>	0.38
$\Delta a_z$	R <sub>100</sub> C <sub>0</sub>	5.94 <sup>a</sup>	0.50	$\Delta E_x$	R <sub>100</sub> C <sub>0</sub>	64.10 <sup>a</sup>	0.38
	R <sub>97</sub> C <sub>3</sub>	5.17 <sup>b</sup>	0.07		R <sub>97</sub> C <sub>3</sub>	62.30 <sup>b</sup>	0.38
	R <sub>94</sub> C <sub>6</sub>	5.98 <sup>a</sup>	0.38		R <sub>94</sub> C <sub>6</sub>	64.33 <sup>a</sup>	0.38
	R <sub>91</sub> C <sub>9</sub>	5.88 <sup>a</sup>	0.38		R <sub>91</sub> C <sub>9</sub>	66.02 <sup>c</sup>	0.38

x- the average value of the samples. 95% confidence interval for the average ANOVA. a, b, c, d- values with the same letter are not significantly different (Duncan's test).  $\Delta E_x$  - total color difference,  $\Delta L_y$  - black-white color change,  $\Delta a_z$  - red-green color change,  $\Delta b_t$  - yellow-blue color change.

### The variation of $\Delta L$

There is a significant difference between (R<sub>100</sub>C<sub>0</sub>, R<sub>94</sub>C<sub>6</sub>), (R<sub>97</sub>C<sub>3</sub>), and (R<sub>91</sub>C<sub>9</sub>) in the variation of  $\Delta L$ . The results are explained in Tab. 3. This variation decreases 1.8% for R<sub>97</sub>C<sub>3</sub> according to R<sub>100</sub>C<sub>0</sub>. Similarly, the variation decreases 1.3% for R<sub>94</sub>C<sub>6</sub> according to R<sub>100</sub>C<sub>0</sub>. Therefore, the variation decreases for R<sub>94</sub>C<sub>6</sub>. The variation increases 3.6% for R<sub>91</sub>C<sub>9</sub> according to R<sub>100</sub>C<sub>0</sub>. Therefore, the variation increases for R<sub>91</sub>C<sub>9</sub>.  $\Delta L^*$  is the most important parameter for describing wood surface quality (Temiz et al. 2005).

### The variation of $\Delta a$

There is significantly difference between (R<sub>100</sub>C<sub>0</sub>, R<sub>94</sub>C<sub>6</sub>, R<sub>91</sub>C<sub>9</sub>) and (R<sub>97</sub>C<sub>3</sub>) in the variation of  $\Delta a$ . The results are explained in Tab. 3. This variation decreases 14.9% for R<sub>97</sub>C<sub>3</sub> according to R<sub>100</sub>C<sub>0</sub>. Similarly, the variation increases 0.7% for R<sub>94</sub>C<sub>6</sub> according to R<sub>100</sub>C<sub>0</sub>. Therefore, the variation decreases for R<sub>94</sub>C<sub>6</sub>. The variation decreases 1.0% for R<sub>91</sub>C<sub>9</sub> according to R<sub>100</sub>C<sub>0</sub>. Therefore, the variation decreases for R<sub>91</sub>C<sub>9</sub>.

### The variation of $\Delta b$

There is a significant difference between (R<sub>100</sub>C<sub>0</sub>, R<sub>94</sub>C<sub>6</sub>) and (R<sub>97</sub>C<sub>3</sub>, R<sub>91</sub>C<sub>9</sub>) in the variation of  $\Delta b$ . The results are explained in Tab. 3. This variation decreases 12.0% for R<sub>97</sub>C<sub>3</sub> according to R<sub>100</sub>C<sub>0</sub>. Similarly, the variation decreases 8.6% for R<sub>94</sub>C<sub>6</sub> according to R<sub>100</sub>C<sub>0</sub>. Therefore, the variation decreases for R<sub>94</sub>C<sub>6</sub>. The variation increases 1.6% for R<sub>91</sub>C<sub>9</sub> according to R<sub>100</sub>C<sub>0</sub>. Therefore, the variation decreases for R<sub>91</sub>C<sub>9</sub>.

### The variation of $\Delta E$

There is significantly difference between (R<sub>100</sub>C<sub>0</sub>, R<sub>94</sub>C<sub>6</sub>), (R<sub>97</sub>C<sub>3</sub>) and (R<sub>91</sub>C<sub>9</sub>) in the variation of  $\Delta E$ . The results are explained in Tab. 3. This variation decreases 2.9% for R<sub>97</sub>C<sub>3</sub> according to R<sub>100</sub>C<sub>0</sub>. Similarly, the variation increases 0.4% for R<sub>94</sub>C<sub>6</sub> according to R<sub>100</sub>C<sub>0</sub>. Therefore, the variation increases for R<sub>94</sub>C<sub>6</sub>. The variation increase 3.0% for R<sub>91</sub>C<sub>9</sub> according to R<sub>100</sub>C<sub>0</sub>. Therefore, the variation increases for R<sub>91</sub>C<sub>9</sub>. As the amount of calcite increases in MDF production, value increases. As the use rate for calcite minerals increased, the increased in the bright of boards values continued. The color and lightness differences of the MDF panels increased with increasing burned wood content (Akgül et al. 2013). Color is characterized by the wavelength of visible light reflected from the surface (Çakıcıer et al. 2011).

## Mechanical properties

The results of ANOVA and Duncan mean separation test for bending strength, modulus elasticity, internal bond, surface screw holding ability, Janka hardness measure vertically to the sheet surface of the fiberboards made from calcite additive fiber and control fiberboards are shown in Tab. 4.

Tab. 4: The results of ANOVA and Duncan mean separation test for mechanical properties of the calcite additive fiberboards and control fibreboard.

Calcite Board	Type	Avg.x	Std.	Calcite Board	Type	Avg.x	Std.
			Deviation				Deviation
Modulus elasticity (MOE) (N·mm <sup>-2</sup> )	R <sub>100</sub> C <sub>0</sub>	3,482.91c	218.21	Surface screw holding ability (N)	R <sub>100</sub> C <sub>0</sub>	10.07a	0.30
	R <sub>97</sub> C <sub>3</sub>	3,224.16b	196.77		R <sub>97</sub> C <sub>3</sub>	8.77b	1.21
	R <sub>94</sub> C <sub>6</sub>	2,909.49a	223.48		R <sub>94</sub> C <sub>6</sub>	8.48a	0.88
	R <sub>91</sub> C <sub>9</sub>	2,974.37a	262.33		R <sub>91</sub> C <sub>9</sub>	9.30ab	1.02
Bending strength (MOR) (N·mm <sup>-2</sup> )	R <sub>100</sub> C <sub>0</sub>	36.89c	2.43	Janka hardness (N)	R <sub>100</sub> C <sub>0</sub>	81.05a	1.23
	R <sub>97</sub> C <sub>3</sub>	33.62b	2.78		R <sub>97</sub> C <sub>3</sub>	77.60bc	3.11
	R <sub>94</sub> C <sub>6</sub>	31.30a	2.42		R <sub>94</sub> C <sub>6</sub>	75.40c	2.90
	R <sub>91</sub> C <sub>9</sub>	29.91a	3.02		R <sub>91</sub> C <sub>9</sub>	78.50b	1.27
Internal bond (IB) (N·mm <sup>-2</sup> )	R <sub>100</sub> C <sub>0</sub>	0.58c	0.03				
	R <sub>97</sub> C <sub>3</sub>	0.54b	0.04				
	R <sub>94</sub> C <sub>6</sub>	0.48a	0.02				
	R <sub>91</sub> C <sub>9</sub>	0.50a	0.04				

x - the average value of the samples. 95% confidence interval for the average ANOVA. a, b, c, d - values with the same letter are not significantly different (Duncan's test).

### The results of the bending strength test (MOR)

There is a significant difference between (R<sub>100</sub>C<sub>0</sub>), (R<sub>97</sub>C<sub>3</sub>), (R<sub>94</sub>C<sub>6</sub>, R<sub>91</sub>C<sub>9</sub>) according to the percentage of bending strength test. The results are explained in Tab. 4. The ratio for this test is 8.0% for R<sub>97</sub>C<sub>3</sub> according to R<sub>100</sub>C<sub>0</sub>. Therefore, the percentage of bending strength decreases for R<sub>97</sub>C<sub>3</sub>. Similarly, the ratio is 19.7% for R<sub>94</sub>C<sub>6</sub> according to R<sub>100</sub>C<sub>0</sub>. Therefore, the percentage of bending strength decreases for R<sub>94</sub>C<sub>6</sub>. The ratio is 17.1% for R<sub>91</sub>C<sub>9</sub> according to R<sub>100</sub>C<sub>0</sub>. Therefore, the percentage of bending strength decreases for R<sub>91</sub>C<sub>9</sub>. The increase in the mineral filler content reduced the effect of interconnecting the fibers, causing MOR, MOE resistance to be adversely affected (Özdemir 2019). Tomasz et al. (2019) In the study of GCC filler addition on MDF production; The data of the 550,700 and 850 density boards showed that the bending strength (MOR) properties decreased as the filling amount increased.

### The results of the Internal bond (IB) test

There is a significant difference between (R<sub>100</sub>C<sub>0</sub>), (R<sub>97</sub>C<sub>3</sub>) and (R<sub>94</sub>C<sub>6</sub>, R<sub>91</sub>C<sub>9</sub>) according to the percentage of internal bond (IB) test. The results are explained in Tab. 4. The ratio for this test is 7.2% for R<sub>97</sub>C<sub>3</sub> according to R<sub>100</sub>C<sub>0</sub>. Therefore, the percentage of the internal bond decreases for R<sub>97</sub>C<sub>3</sub>. Similarly, the ratio is 20.0% for R<sub>94</sub>C<sub>6</sub> according to R<sub>100</sub>C<sub>0</sub>. Therefore, the percentage of the internal bond decreases for R<sub>94</sub>C<sub>6</sub>. The ratio is 80.9% for R<sub>91</sub>C<sub>9</sub> according to R<sub>100</sub>C<sub>0</sub>. Therefore, the percentage of the internal bond decreases for R<sub>91</sub>C<sub>9</sub>. Mineral filler type and usage rate have a negative effect on IB values (Özdemir. 2019). As the use rate for calcite minerals increased, the same results in the IB values continued. Tomasz et al. (2019) In the study

of GCC filler addition on MDF production; The data of the 550 and 700 density boards showed that the internal bond (IB) properties decreased as the filling amount increased.

### **The results of the modulus elasticity test (MOE)**

There is a significant difference between ( $R_{100}C_0$ ), ( $R_{97}C_3$ ), ( $R_{94}C_6$ ,  $R_{91}C_9$ ) according to the percentage of modulus elasticity test. The results are explained in Tab. 4. The ratio for this test is 8.0% for  $R_{97}C_3$  according to  $R_{100}C_0$ . Therefore, the percentage of modulus elasticity decreases for  $R_{97}C_3$ . Similarly, the ratio is 19.7% for  $R_{94}C_6$  according to  $R_{100}C_0$ . Therefore, the percentage of modulus elasticity decreases for  $R_{94}C_6$ . The ratio is 17.1% for  $R_{91}C_9$  according to  $R_{100}C_0$ . Therefore, the percentage of modulus elasticity decrease for  $R_{91}C_9$ . Mineral fillers increased the contact surface between the fibers and the glue and also created a barrier effect. It prevented the glue from being placed in the gaps and reduced the mechanical locking of the fiber and glue (Ayrılmış et al. 2017). The intermolecular force and the sliding rubbing force between the constituents of the MDF reduced quickly rapidly, resulting in a reduced MOR and MOE (Wang et al. 2016). As the use rate for calcite minerals increased, the very little reduction result in the modulus elasticity values continued.

### **The results of the surface screw holding ability test**

There is a significant difference between ( $R_{100}C_0$ ), ( $R_{97}C_3$ ), ( $R_{94}C_6$ ) and ( $R_{91}C_9$ ,  $R_{100}C_0$ ,  $R_{97}C_3$ ) according to the percentage of the surface screw holding ability test. The results are explained in Tab. 4. The ratio for this test is 14.8% for  $R_{97}C_3$  according to  $R_{100}C_0$ . Therefore, the percentage of the surface screw holding ability decreases for  $R_{97}C_3$ . Similarly, the ratio is 14.8% for  $R_{94}C_6$  according to  $R_{100}C_0$ . Therefore, the percentage of the surface screw holding ability decreases for  $R_{94}C_6$ . The ratio is 8.2% for  $R_{91}C_9$  according to  $R_{100}C_0$ . Therefore, the percentage of the surface screw holding ability decreases for  $R_{91}C_9$ .

### **The results of Janka hardness test**

There is a significant difference between ( $R_{100}C_0$ ), ( $R_{97}C_3$ ,  $R_{94}C_6$ ,  $R_{91}C_9$ ), ( $R_{94}C_6$ ) and ( $R_{91}C_9$ ) according to the percentage of Janka hardness test. The results are explained in Tab. 4. The ratio for this test decreases 4.4% for  $R_{97}C_3$  according to  $R_{100}C_0$ . Therefore, the percentage of Janka hardness decreases for  $R_{97}C_3$ . Similarly, the ratio decreases 7.4% for  $R_{94}C_6$  according to  $R_{100}C_0$ . Therefore, the percentage of the Janka hardness decrease for  $R_{94}C_6$ . The ratio is 17.7% for  $R_{91}C_9$  according to  $R_{100}C_0$ . Therefore, the percentage of the Janka hardness decreases for  $R_{91}C_9$ . Mechanical properties including MOR, MOE, IB, surface screw holding and janka hardness values of samples very little reduction result in with increasing amount of calcite minerals.

With an increase of calcite mineral interfering with wood fibers and a reduction in the surface present for creating adhesive bond with the wood fibers, a reduction in the created fiber -to- fiber glue bonds is anticipated. In this study, it is seen that mechanical test results are decreased.

## **CONCLUSIONS**

This study evidence that MDF with up to 3%, 6% , 9% wood fiber replaced by calcite mineral can be produced in MDF proses line-scale environment without significantly deteriorating the material properties. As the amount of calcite increases in MDF production, both the percentage of the TS and the percentage of the WA are increasing. This reason is the usage amount of

calcite mineral and its geometrical structure. As the amount of calcite increases in MDF, the quality of the board surface decreases. The question to what degree wood fiber acidity compensate for the buffering capacity of calcite in a wood fibre-urea formaldehyde glue-inorganic filler system recommended to be addressed in the next studies. While the addition of calcite filler at a great number of until 3% and 6% does not have any visible effect on the MDF boards properties, at loads excessive this amount, a meaningful effect is anticipated.

As the amount of calcite increases in MDF, total color difference of the board surface increases in terms of the result of color parameters. As the amount of calcite increases in MDF, the total color difference and whiteness (black-white color change) over the surface board increase. Curative results have been obtained in physical, mechanical, color tests of calcite compounded MDF panels. Therefore, it has been determined that the use of calcite in MDF production is more appropriate in terms of productivity. A reduction in the mechanical properties and an increase in the physical properties, believed to be caused by the reduced quantity of fiber-to-fiber stress connectivity points, is most pronounced. As a result of all tests, it is suggested calcite filling mineral percentage 3% and 6% in MDF production

## ACKNOWLEDGEMENTS

This study was supported by T.C. Ministry of Science Industry and Technology, Düzce University, and Divapan Integrated Wood Company as the project of San-Tez 00653.STZ.2010-2. The authors would like to acknowledge Division of Wood Chemistry and Technology Department in Faculty of Forestry at Duzce University for their help and support.

## REFERENCES

1. Akgül, M., Ayrılmış, N., Çamlıbel, O., Korkut, S., 2013: Potential utilization of burned wood in manufacture of medium density fiberboard. *Journal of Material Cycles and Waste Management* 15(2): 195-201.
2. Akgül, M., Uner, B., Çamlıbel, O., Ayata, U., 2017: Manufacture of medium density fiberboard (MDF) panels from agribased lignocellulosic biomass. *Wood Research* 62(4): 615-624.
3. ANSI A 208.1, 1999: American national standard for particleboard. Composite panel association, Gaithersburg.
4. ASTM D-1037-78, 1994: Standart methods of evaluating the properties of wood-base fiber and particle panel materials.
5. ASTM D2244-07e1, 2007: Standard practice for calculation of color tolerances and color differences from instrumentally measured color coordinates.
6. Ayrılmış, N., Güleç, T., Peşman, E., Kaymakçı, A., 2017: Potential use of cotton dust as filler in the production of thermoplastic composites. *Journal of Composite Materials* 51(30): 4147- 4155.
7. Candan, Z., Akbulut, T., Wang, S., Zhang, X., Sisci A, F., 2012: Layer thickness swell characteristics of medium density fibreboard (MDF) panels affected by some production parameters. *Wood Research* 57(3): 441- 452.
8. Çakıcıer, N., Korkut, S., Korkut, D. S., Kurtoglu, A., Sönmez, A., 2011: Effect of QUV accelerated aging on surface hardness surface roughness, glossiness, and color difference for some wood species. *International Journal of the Physical Sciences* 6(8): 1929-1939.

9. Çavdar, A.D., Torun, S.B., Ertas, M., Mengelöglu, F., 2019: Ammonium zeolite and ammonium phosphate applied as fire retardants for microcrystalline cellulose filled thermoplastic composites. *Fire Safety Journal* 107: 202-209.
10. Güller, B., 2001: Wood composites. *Suleyman Demirel University Forest Faculty Journal Serial: A, Number 2*: Pp 135-160.
11. Funk, M., Wimmer, R., Adamopoulos, S., 2017: Diatomaceous earth as an inorganic additive to reduce formaldehyde emissions from particleboards. *Wood Material Science & Engineering* 12(2): 92–97.
12. Istek, A., Aydemir, D., Eroglu, H., 2013: Combustion properties of medium-density fiberboards coated by a mixture of calcite and various fire retardants. *Turkish Journal of Agriculture and Forestry* 37: 642–648.
13. Kalaycıođlu, H., Yel, H., Çavdar A.D., 2012: Wood wool cement boards and its applications. *Kastamonu University Journal of Forestry Faculty* 12 (1): 122-133.
14. Kaya, N., 2018: Investigation of mechanical and physical properties of glass fiber reinforced fiber plates (MDF) produced from agricultural wastes. *Journal of The Faculty of Engineering and Architecture of Gazı University* 33(3): 905-916.
15. Ozyhar, T., Depnering, T., Ridgway, C., Welker, M., Schoelkopf, Mayer, I., Thoemen, H., 2020: Utilization of inorganic mineral filler material as partial replacement for wood fiber in medium density fiberboard (MDF) and its effect on material properties. *European Journal of Wood and Wood Products* 78(1): 75-84.
16. Özdemir, F., Ayaz, A., 2017: Investigation of the effect on combustion resistance of ammonium polyphosphate and boric acid chemicals added to surface coating. *Kastamonu University. Journal of Forestry Faculty* 17(2): 290-297.
17. Özdemir, F., 2019: Effect of mineral materials content as filler in medium density fiberboard. *Bioresources* 14(1): 2277-2286.
18. Özdemir, F., Tutus, A., 2016: Effects of coating with calcite together with various fire retardants on the fire properties of particle- board. *BioResources* 11: 6407–6415.
19. Salari, A., Tabarsa T., Khazaieian A., Saraeian A., 2012: Effect of nanoclay on some applied properties of oriented strand board (OSB) made from underutilized low quality paulownia (*Paulownia fortunei*) wood. *Journal of Wood Science* 58: 513–524.
20. Taghiyari, H.R., Nouri, P., 2015: Effects of nano-wollastonite on physical and mechanical properties of medium-density fiberboard. *Maderas: Ciencia Y Tecnología* 17 (4): 833-842.
21. Taghiyari, H.R., Behrooz, M.P., Morrell, J.J., 2016: Effects of wollastonite on the properties of medium-density fiberboard (MDF) made from wood fibers and camel-thorn Maderas. *Ciencia Y Tecnología* 18(1): 157 – 166.
22. Temiz, A., Yildiz, U.C., Aydin, I., Eikenes, M., Alfredsen, G., Colakoglu, G., 2005: Surface roughness and color characteristics of wood treated with preservatives after accelerated weathering test. *Applied Surface Science* 250(1-4): 35-42.
23. TS EN 310, 2008: Wood-based-panels determination of modulus of elasticity in bending and of bending strength.
24. TS EN 317, 2008: This standard specifies a method of determining the swelling in thickness of flat pressed or drum pressed particleboards, fibreboards and cement bonded particleboards.
25. TS EN 319, 2008: Particleboards and fibreboards determination of tensile strength perpendicular to the plane of the board.
26. TS EN 323, 2008: Wood-based-panels determination of density.
27. TS EN 325, 2008: Wood-based-panels determination of dimensions of test pieces.

28. TS EN 326-1, 1999: Wood-based-panels sampling, cutting and inspection-part 1: Sampling test pieces and expression of test results.
29. TS EN 382-1, 1999: Fiberboards- determination of surface absorption part 1: Test method for dry process fibreboards.
30. TS EN 622-5, 2008: Fibreboards-specifications-part-5 Requirements for dry process boards (MDF).
31. Wang, J., Wang, F., Gao, Z., Zheng, M., Sun, J., 2016: Flame retardant medium-density fiberboard with expanded vermiculite. *Bioresources* 11(3): 6940-6947.
32. Xing, C., Zhang, S.Y., Deng, J., Riedl, B., Cloutier, A., 2006: Medium-density fiberboard performance as affected by wood fiber acidity, bulk density, and size distribution. *Wood Science and Technology* 40: 637-646.
33. Zahedsheijani, R., Gholamiya, H., Tarmia, A., Yousefi, H., 2011: Mass transfer in medium density fiberboard (MDF) modified by Na<sup>+</sup> montmorillonite (Na<sup>+</sup>Mmt) nanoclay, *Maderas. Ciencia Y Tecnología* 13(2): 163-172.

OSMAN CAMLIBEL  
KIRIKKALE UNIVERSITY  
KIRIKKALE VOCATIONAL SCHOOL  
INTERIOR DESIGN PROGRAM  
YAHSIHAN, KIRIKKALE  
TURKEY

\*Corresponding author: [osmancamlibel@kku.edu.tr](mailto:osmancamlibel@kku.edu.tr)

MEHMET AKGUL  
KARAMANOGLU MEHMETBEY UNIVERSITY  
YUNUS EMRE CAMPUS, 70100  
KARAMAN  
TURKEY



## **FLEXURAL BEHAVIOR OF OSB REINFORCED WOOD TRUSS**

XIAOJUN YANG, QI ZHAO, DAN HAO, JIAYANG WANG, SHUAI FU, LAN MA  
NANJING FORESTRY UNIVERSITY  
NANJING, JIANGSU, CHINA

(RECEIVED JULY 2019)

### **ABSTRACT**

In this paper, oriented strand board (OSB) on both sides of the wood truss was used to strengthen the wood truss. The flexural behavior of the reinforced wood truss was studied. The results showed that OSB was an effective technical member to improve the flexural bearing capacity of wood truss. Besides, wood truss and OSB can be firmly combined by using glue bonding and screw connections. The screws served only to apply pressure to the glued joint. And the reinforced wood trusses had good synergy and overall stability. The initial bending stiffness and ultimate bending load of the reinforced wood trusses were increased by 203.20% and 234.39% respectively. Ultimate bending load and initial bending stiffness were improved a little by making the wood truss wider. Compared with the traditional wood truss, the reinforced wood truss had the advantages of simple connection mode, less wood consumption, no rolling machine and easy fabrication.

**KEYWORDS:** Wood truss reinforced with OSB, flexural behavior, lateral stability, stiffness.

### **INTRODUCTION**

Wood construction has a long history. As early as 3000 years ago, the tenon-mortise structures were mainly used to connect beams and columns, forming a unique architecture style and contributing greatly to the world's architectural history. Nowadays, modern wood constructions are energy-saving, environment-friendly, safe and comfortable, which have been popularized in many areas all over the world (Lou et al. 2015, Liu et al. 2018, Yang et al. 2018, Wang et al. 2019, Zhang et al. 2019). With the rapid development of economy, people attach more and more importance to respecting nature and protecting environment. And higher requirements have been put forward for the living environment, which makes wood buildings have a good development prospect. For example, China is vigorously promoting sustainable development strategy, advocating low-carbon real estate and green buildings, which makes modern wood construction become a powerful factor in the future direction of domestic construction development.

Wood members play an important role in wood construction, including columns, beams, stairs and other wood components. Wood beams are widely used in modern wood construction. The main types of them are solid wood beams and engineered wood beams. Solid wood beams have small range of application because it is easy to deform and crack. Besides, solid wood beams need to consume a lot of wood and its load-bearing performance requires prime wood properties. Engineered wood beams are made by modern wood processing methods, including glue laminated wood beams, laminated veneered lumber beams, parallel laminated wood beams, laminated stand lumber beams and so on (Ribeiro et al. 2009, Shi et al. 2017, Zhou et al. 2015, Ghanfth et al. 2017, Yehia et al. 2018, Wang et al. 2019, Xie et al. 2019). Engineered wood beams not only overcome many shortcomings of solid wood beams, but also can be designed in special sizes according to demand. In addition, they have many kinds of shapes. However, engineered wood beams need to be prefabricated in factories with complex technology. What's more, processing engineered wood beams needs large timber consumption and high cost.

Wood truss is a sort of wood frame system by using truss plates or nails to assemble and connect wood components. It is an important component of wood floor support and roof support. Besides, it has the advantages of light weight, high strength and good seismic performance (Song et al. 2010, Jin et al. 2015, Que et al. 2019). Wood truss mainly contains triangular truss and parallel chord truss. Wood truss has stable structure and changeable style. It can provide good bearing capacity under different conditions. For a long time, there have been many studies on wood truss, mainly in the form of wood truss structure, joint connection of wood truss, bearing capacity of wood truss and system combination effect of multi-trusses, etc. For the purpose of understanding the bearing capacity of light wood truss, the load carrying tests for light wood trusses with 6 meters span were carried out. Test results were compared with Chinese current code for design of wood constructions and several major factors which influence the bearing capacity of light wood truss were analyzed (Xu et al. 2006). In order to quantitatively recognize the properties of light wood truss assembly, the system effect and its influential factors for light wood truss assembly with a random sampling simulation method were analyzed. The result showed that the system effect of light wood truss assembly was mainly influenced by the failure mode, system volume, boundary supporting condition as well as correlation between elastic modulus and strength of dimension lumber (Huang et al. 2011). In Auburn University, a wood truss ladder that moved truss from the ground to the level was examined. A prototype version of the truss ladder was constructed and tested at two residential housing projects. Speed, ease of use, safety, and worker fatigue were investigated for these two projects using qualitative measures. The truss lifter offers potential increases in safety and reduced worker fatigue (Farrow 2009). These studies are almost based on the use of mechanical theory or finite element method with specification timber as members (Hoyle 1985, Hunt 2004, Song et al. 2012, Wu et al. 2018). This paper arranges the wood truss specifications along the wide plane, strengthens the wood truss by applying OSB on both sides of the wood truss to study its initial bending stiffness and develop large cross-section wood beams suitable for construction site, which is of great significance to promote the development of modern wood construction.

## EXPERIMENT AND METHODS

### Materials

The wood species used in the study was pine (*Pinus* spp.) in the category of SPF (spruce-pine-fir). OSB with dimension of 15mm in depth was used as reinforced material, with a static

bending strength ( $//$ ) of 30 MPa, a static bending strength ( $\perp$ ) of 18 MPa, a modulus of elasticity (MOE  $//$ ) 3600 MPa, a modulus of elasticity (MOE $\perp$ ) 1500 MPa and an internal bonding strength of 0.41 MPa.

Chamfer screw (mode: cI- 38  $\times$  2.2 and cI- 80  $\times$  3.4) were used in the test, which were widely used in the joint of wood products with high stiffness. The adhesive used in the test was a single component polyurethane (type: R645/30, producer: H.B. Fuller Co., Ltd). Deformations were measured by 7 resistance strain gauges (type: BF350-6AA, producer: Guangzhou Zheyuan Electronics Co., Ltd) with a nominal resistance of 350  $\Omega$ , a sensitivity of 2.11 + 1%, an accuracy grade A and a base size of 9.6  $\times$  3.5 mm. The resistance strain gauges were fixed by cyanoacrylate adhesive. And the placement was shown in Fig. 3.

The test was carried out using a universal testing machine (type: UTM5105, producer: Shenzhen Suns Technology Stock Co., Ltd.) and resistance strain instrument (type: TDS-530, Producer: Tokyo Sokki Kenyujō Co., Ltd.).

### Experimental design

OSB reinforced wood truss (Fig. 1) was composed of wood truss and OSB boards on both sides. The wood truss was made up of 2  $\times$  4 inches or 2  $\times$  6 inches dimension lumber (*Pinus* spp). It was connected by screw with dimension of 80 mm in length and 3.4 mm in diameter. The spacing of truss internode was 253 mm, the height of truss was 200 mm, the angle between chord and web member was 30°, and the lateral OSB was fixed by screw with dimension of 38 mm in length and 2.2 mm in diameter.

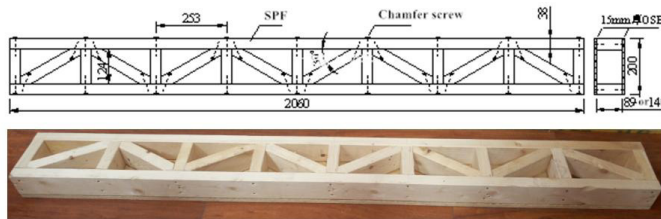


Fig. 1: Structure of reinforced timber truss using OSB.

Tab. 1: Specimen of reinforced timber truss using OSB.

Experimental group	Specification of rod	Connection between rods	Reinforcement pattern	OSB connection mode	OSB nail connection section
C-Z	2x4 inch	Truss plate	—	—	—
D-L	2x4 inch	Chamfer screw	OSB reinforcement	Nailed joint	Chord and web member
J-D-X	2x4 inch	Chamfer screw	OSB reinforcement	Glue connection+ nail connection	chord
J-D-XF	2x4 inch	Chamfer screw	OSB reinforcement	Glue connection + nail connection	Chord and web member
J-D-XF-K	2x6 inch	Chamfer screw	OSB reinforcement	Glue connection + nail connection	Chord and web member

Notes: “—” Indicates no reinforcement or nonexistence.

The wood truss test was divided into five groups (Tab. 1). There were three specimens in each group. The first group to the fourth group were made of 2  $\times$  4 inches lumber. The first

group was not reinforced in accordance to Chinese Nation Standard (JGJ/T 265-2012). It was connected by galvanized truss plate as a reference control group, numbered C-Z. In group 2, OSB reinforcement group was connected with nails, which was fixed by nails at the upper, lower chord and web rod parts. The nail spacing at the chord part was 150 mm, and the nail spacing at the web rod part was 100 mm. The number was D-L. The third group was the OSB reinforcement group with glue and chord nails, which was coated with polyurethane glue on both sides of the wood truss, and fixed OSB reinforcement wood truss with nails at the chord position. The nail spacing was 150 mm, numbered J-D-X. The fourth group was OSB reinforcement group with glue connection + nail connection located in whole truss. The spacing between chord nail and web nail was 150 mm and 100 mm respectively. The number was J-D-XF. The fifth group was the 2 × 6 inches wood truss reinforcement group. The two sides of the wood truss made of 2 x 6 inches dimension lumber were coated with polyurethane glue, and OSB-reinforced wood truss was fixed with nails at the chord and web, the nail spacing at the chord was 150 mm, and the nail spacing at the web was 100 mm, numbered J-D-XF-K. The arrangement of nails fixed in wood truss was shown in Fig. 2.

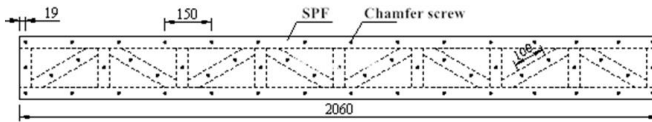


Fig. 2: Layout of screws in wood truss's lateral.

The bending performance test was carried out according to the Chinese National Standard (GB/T 50329-2012). The loading speed was uniform of 10 mm·min<sup>-1</sup>. In order to understand the deformation of the mid-span section along the height of the cross-section, seven strain gauges were arranged in the mid-span of each specimen, one on the upper and lower surfaces of the wood truss, and five on the equal spacing along the height direction, with the spacing of 30 mm. In order to understand the deformation of the wood truss during the loading process, displacement gauge were arranged at the bottom of the specimen span and the side of the wood truss under the pressure head of the testing machine. The bottom displacement gauge were fixed on the base of the testing machine and the lateral displacement gauge were fixed on the cross beam of the pressing head of the testing machine. Two lateral displacement gauge were arranged on both sides of the wood truss, and their position numbers were QS-1, QX-1, BS-2 and BX-2. The arrangement of strain gauges and displacement gauges was shown in Fig. 3.

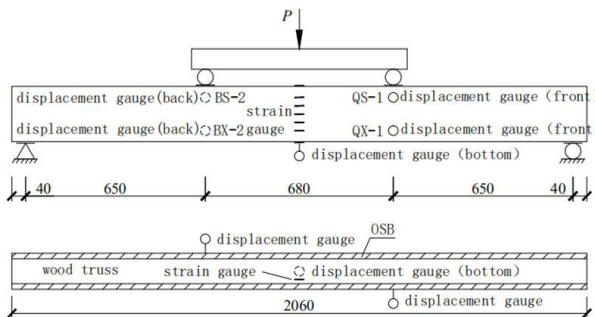


Fig. 3: Layout of displacement gauge and strain gauge.

## RESULTS AND DISCUSSION

As shown in Fig. 4, the load-deflection curve of reinforced wood truss showed almost the same regulation as that of reference group. At the initial stage of loading, the specimen was basically in an elastic state. The load increased linearly with the increase of displacement. At the stage of loading approaching the limit value, the specimen showed a certain plastic deformation. The stiffness decreased and the deformation tended to be obvious. The load decreased rapidly with large sound of local fracture. When the load of each reinforcement group reached the limit value, the deflection was 21.29 mm - 28.68 mm. The slope of the curve in the early stage of loading was significantly different between the reinforcement group and the reference group. The slope of the curve in C-Z group was gentle, while that in J-D-X group, J-D-XF group and J-D-XF-K group was steep, and that in D-L group was in the middle. According to the Chinese National Standard (GB50005-2017), when the deflection limit of C-Z, D-L, J-D-X, J-D-XF and J-D-XF-K wood trusses reached 1/150, the loads of each group were 8.8 kN, 13.37 kN, 25.96 kN, 27.18 kN and 28.25 kN, respectively. Compared with the reference group, the load-bearing capacity of each reinforcement group was greatly improved when the deflection limit was specified.

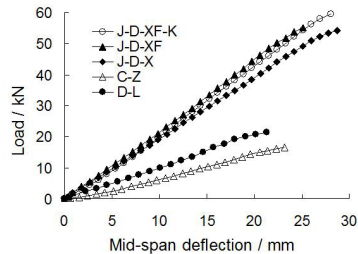


Fig. 4: Load deflection curves of typical wood trusses.

The failure characteristics of wood truss specimens in reinforcement group were shown in Fig. 5. Before the failure, there was obvious screw-bending noise caused by nail yielding in D-L group and obvious lateral deformation of OSB plates on both sides of wood truss. The failure of the specimens showed that the middle part of the tension zone of the OSB plate was broken and the web of the wood truss collapsed obviously. The failure of J-D-X group showed nail bending deformation, cracking of upper edge adhesive layer between OSB and wood truss, breaking of lower edge OSB and intact lower chord. Before the failure of J-D-XF group, there was intermittent sound of wood fiber brittle fracture. After the failure of the sample, the upper edge of OSB was extruded and uplifted. The lower edge of OSB was broken with the lower chord of wood truss, and the fracture location was adjacent. The failure modes of J-D-XF-K were similar to those of J-D-XF group, which showed OSB compression failure at upper and middle edges, OSB and lower chord fracture at lower edges.



(a) D-L group

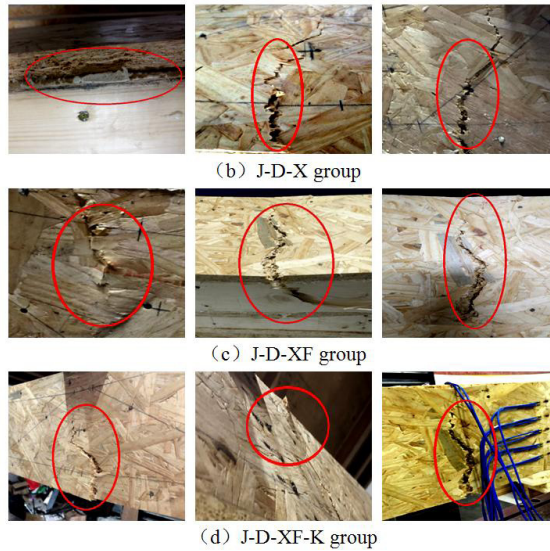


Fig. 5: Typical failure modes of specimens.

According to the load and deflection changes of reinforced wood truss in the elastic range, the initial bending stiffness of reinforced wood truss was calculated. The initial stiffness was the linear slope of 10% to 40% of the ultimate load on the load-displacement curve. The stiffness of each group of specimens was as shown in Tab. 2.

Tab. 2: Flexural capacity and initial stiffness of reinforced timber truss using OSB.

Number	Ultimate load (kN)	1/150 Deflection limit load (kN)	Limited deflections (mm)	Initial stiffness (N·mm <sup>-1</sup> )
C-Z	16.46	8.80	23.18	708.21
D-L	21.39	13.37	21.29	964.95
J-D-X	54.25	25.96	28.68	1942.38
J-D-XF	55.04	27.18	25.09	2147.26
J-D-XF-K	59.71	28.25	28.03	2083.47

From Tab. 2, it could be seen that the ultimate load and initial stiffness of OSB reinforcement group were significantly higher than those of the reference group. The ultimate load of D-L, J-D-X, J-D-XF and J-D-XF-K in the reinforcement group was 29.95%, 229.59%, 234.39% and 262.76% higher than that of the reference group, respectively. The limit load of 1/150 deflection was 51.93%, 195.00%, 208.86% and 221.02% higher than that of the reference group, and the initial stiffness was 36.25%, 174.27%, 203.20% and 194.19%, respectively. The bearing capacity and initial stiffness of the reinforcement groups differed significantly due to the different reinforcement modes. As a conventional method, the flexural capacity and stiffness of reference group wood truss were general. The flexural load-bearing capacity of wood truss could be significantly improved by compounding OSB boards on the side of the truss.

For the D-L group, the flexural capacity was improved the least. For one thing, nail connection was used between the members of wood truss, which was weaker than that of

reference group. For another thing, nail connection composite OSB which was the weak part of destruction was difficult to play the synergistic role between OSB and wood truss. When bending, the interaction between OSB and wood truss on both sides was less. The bearing capacity was mainly provided by OSB side plate. The shear force of nail joint was huge.

For the J-D-X group, the ultimate load and bending stiffness were 2.54 and 2.01 times higher than those of the D-L group, respectively. The polyurethane structural adhesives coated on the chord had remarkable improvement in bending resistance. OSB and wood truss had good synergy. The nails when bonding ensured that OSB and wood truss chord were fully bonded and compounded under certain pressure. In addition, the polyurethane adhesives used in the curing process would foam and expand, which could fully fill some uneven surfaces and cracks on the side of the truss and bond firmly. OSB contributed a lot to the flexural capacity of wood truss.

For the J-D-XF group, the ultimate load and flexural stiffness were 1.01 and 1.11 times higher than those of the J-D-X group, respectively, and the increase was not obvious. The gluing of web members of wood truss contributed a little to the whole, mainly supporting web members and reducing the flexural capacity of nail joints between chord and web members. The web member region played a supporting and connecting role, while the upper and lower chords played a bending role.

For the J-D-XF-K group, both of them adopt the same reinforcement composite method. The former used 2×6 inches of dimension stock and the latter 2×4 inches of dimension stock. When the width of wood truss increased, larger support surface could be obtained. However, the flexural performance could not be improved. The ultimate load of the former was slightly higher than that of the latter, while the initial stiffness of the former was slightly lower than that of the latter. The ultimate load was slightly higher and the initial stiffness was slightly lower, which indicated that the bending stiffness mainly depended on the OSB plates on both sides of the wood truss. The contribution of OSB to flexural capacity was not obvious with the increase of width, and the dimension of width direction was not the key factor affecting the bending performance.

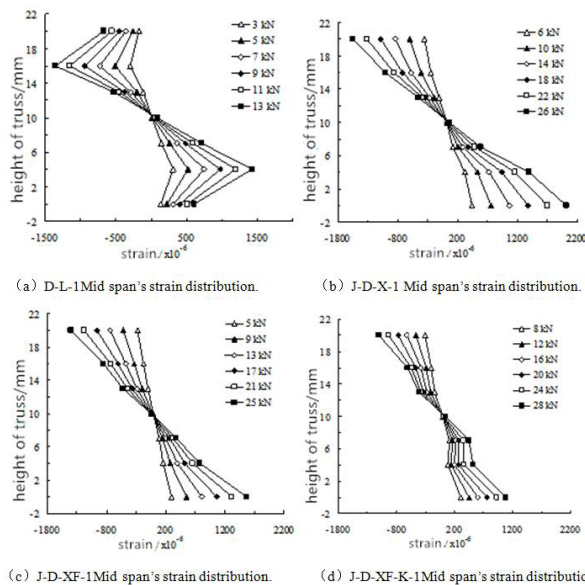


Fig. 6: Mid span's strain distribution of typical wood truss reinforced with OSB.

From Fig. 6, it could be seen that the strain distribution along the cross-section height of D-L group wood truss was significantly different from that of J-D-X group, J-D-XF group and J-D-XF-K group in the process of loading in the elastic range. The strain distribution of upper and lower chords of wood truss was not linear with that of the intermediate strain of wood truss. The key to stress transfer between plates was that the poor rigidity of nail joints easily lead to the inconsistency of the overall synergy between OSB and upper and lower chords of wood truss as well as the obvious difference of strain distribution occurs at lower loads.

The strain distribution in the span of J-D-X group and J-D-XF group was almost the same. Both groups adopt the reinforcement mode of nail connection fixation and structural bonding fixation OSB. The former was glued on the upper and lower chords, while the latter was glued on the chord and web. Structural adhesives were single-component polyurethane adhesives. Structural adhesives were commonly used for structural materials with high bonding strength. OSB and wood truss were firmly bonded. The bonding surface bear the stress transfer between wood truss and OSB board. The linear distribution of mid-span strain indicated that OSB and wood truss have good synergy and synchronization in the process of loading in the elastic range, and the material difference in different parts has little influence on the strain distribution. In the composite process of OSB and wood truss, nails could make the glued OSB and wood truss adhere closely and achieve firm bonding.

The strain in the span of J-D-XF-K group wood truss approximated linear distribution, and the group adopts the reinforcement mode of pin connection fixation and structural glue full surface bonding fixation OSB. The wood truss was made of 2x6 inch large size timber, and the strain value under each load was smaller than that of J-D-XF group wood truss under the same composite condition. The strain distribution of OSB on the side of wood truss was a little irregular. Wider specification timber was used in the wood truss, which accounts for a large proportion in the overall truss. OSB was obviously affected by the web member of the wood truss.

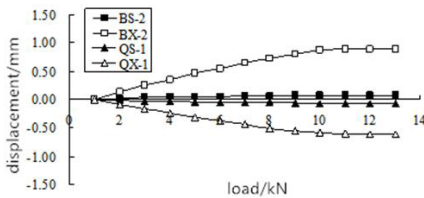


Fig. 7: Lateral displacement variation of typical wood truss in D-L group.

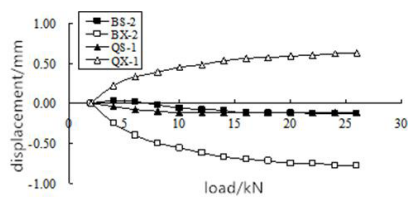


Fig. 8: Lateral displacement variation of typical wood truss in J-D-X group.

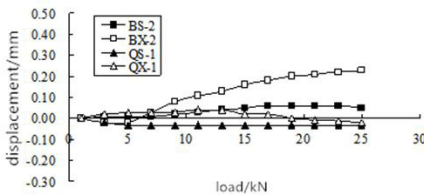


Fig. 9: Lateral displacement variation of typical wood truss in J-D-XF group.

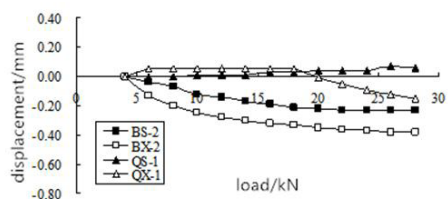


Fig. 10: Lateral displacement variation of typical timber truss in J-D-XF-K group.

From Fig. 7 to Fig. 10, it could be seen that the lateral displacement of each position on both sides of the reinforced wood truss increased with the increase of load. The trend of lateral displacement of the upper edge of the truss was similar. It fluctuated in a small range of (+ 0.1mm). The lower edge of the truss was pulled under compression, the upper edge was compressed. And the bending stiffness of OSB plate in a small plane was found in a small deformation range with the truss under load. The change trend of lateral displacement at the lower edge position was distinct. The lateral displacement of the lower edge of the truss under the indentation head varied greatly in both D-L group and J-D-X group. One side of the truss deformed inward and the other side expanded outward. Truss and OSB plate had smaller mutual restraint force. When OSB plate was bent in plane, the ratio of height to width of section was 13:1. The compression part of OSB plate was prone to buckling along the plane with smaller stiffness. However, because of the continuous restraint of the tension part along the length direction, the compression part would move sideways while driving the whole section to twist, which ultimately lead to a certain degree of bending and torsion deformation of OSB plate. In addition, the composite technology and internal stress of reinforced wood truss were also important factors affecting the overall lateral stability and overall performance of reinforced wood truss. The deformation of the lower lateral protrusion and depression in group D-L was significantly larger than that in group J-D-X. In group J-D-X, structural bonding was used between OSB and truss chord during composite, which partially restrained the lateral deformation of OSB cladding.

J-D-XF group was similar to J-D-XF-K group in wood truss, and lateral displacement varied in a small range. Both groups used nail connection and full surface glue bonding between wood truss and OSB board. The bonding between cladding board and web bar and chord bar was firm. The possibility of lateral deformation was greatly reduced under load. The range of lateral displacement fluctuation was related to the fabrication of wood truss members, the accuracy of joints of wood truss members, the symmetry of cover plates on both sides of the truss and the rebalancing of internal stress. The lateral ultimate displacement of the wood truss in J-D-XF-K group was slightly larger than that in J-D-XF group, but both of them were in the range of  $\pm 0.4$  mm. According to the failure characteristics of the samples, there was no obvious warping or lamination of OSB plates on both sides during the failure. The lateral stability of the wood truss was good. And the small variation of lateral displacement had little effect on the overall workability of the reinforced wood truss.

During the past few decades, researchers and engineers have been constantly exploring engineering wood materials that can replace solid wood beams. The wood truss reinforced with OSB has large bearing capacity and rigidity which is close to other studies analyzing the mechanical properties of CFRP-reinforced wood beams or other composite beams (Issa et al. 2005, Li et al. 2009, Nadir et al. 2016). It is a light-weight high-strength large-section wood beam. In addition, it can be obtained by simple processing of dimension lumbers and also be put into use on-site construction. To some extent, the reinforced wood truss can take the place of some wood beams in wood structure engineering.

## CONCLUSIONS

(1) Using OSB on both sides of the wood truss was an effective technical means to improve the flexural bearing capacity of wood truss. Compared with the common wood truss, the initial bending stiffness and ultimate bending load of the reinforced wood truss was greatly improved by using OSB through screw connection and full surface glue bonding.

(2) Within the elastic range, the strain variation trend of the mid-span section could reflect the synergy between OSB and wood truss. The synergy between OSB and wood truss is better by using nail bonding and chord bonding or full surface bonding. The strain variation of mid-span section along the beam height is always linear. The glued joint is stiff while nailing joints is not. There is no long-term synergy between the screws and adhesives on which we can build a long-term safety. The screws in the glued joints serve only to apply pressure to the glued joint.

(3) The change trend of lateral displacement of wood truss could reflect the lateral stability of wood truss. The lateral stability of wood truss is better by means of nail bonding and full-surface glue bonding. The lateral displacement fluctuates in a small range and the overall effect was strong, showing good overall performance.

(4) Composite mode was the decisive factor of OSB enhancement effect. The reinforcement effect of wood truss was not ideal and the lateral stability was poor when OSB was combined with nail connection. The ultimate bending load and initial bending stiffness of reinforced wood truss was improved significantly by using nail connection and chord glue bonding, but the lateral stability was general, and local OSB delamination and peeling were easy to occur. With nail bonding and full surface glue bonding, the wood truss had the best reinforcement effect and the overall working performance was greatly improved. The bending failure modes of reinforced wood truss were mainly OSB extrusion uplift, OSB at lower edge and OSB at lower chord tie rod break or OSB at lower edge nail break, and no OSB peeling and delamination phenomenon occurs. The ultimate bending load increased slightly with the increase of section width of reinforced wood truss, and the contribution to the initial bending stiffness was small.

(5) The connection of reinforced wood truss was simpler than that of conventional wood truss. Reinforced wood truss did not need truss plate rolling machine. And it was convenient for site construction and consumed less wood. Besides, large cross-section solid wood beam can be replaced by reinforced wood truss. Thus, reinforced wood truss could be used in wood construction engineering.

## ACKNOWLEDGEMENT

This work was supported by Nanjing Senzhihu Construction Engineering Co., Ltd.

## REFERENCES

1. Farrow, C.B., 2009: Evaluation of a prototypical mechanical wood truss ladder. *Automation in Construction* 18: 1114-1122.
2. Ghaneh, M., Behbood, M., Ghanbar, E., 2017: Glulam beam made from hydrothermally treated poplar wood with reduced moisture induced stresses. *Journal of Construction and Building Materials* 135: 386- 393.
3. Hoyle, R.J., Griffith, M.C., Itani, R.Y., 1985: Primary creep in Douglas fir beams of commercial size and quality. *Wood and Fiber Science* 17: 300-313.
4. Huang H., He M.J., Zhou S.R., Cui J., 2011: System effect analysis of light wood truss assembly. *Journal of Shenyang University of Technology* 33(3): 343-348 (In Chinese).
5. Hunt, D.G., 2004: The prediction of long-time viscoelastic creep from short-time data. *Wood Science and Technology* 38: 479-492.

6. Issa C.A., Kmeid Z., 2005: Advanced wood engineering: Glulam beams. *Construction & Building Materials* 19(2): 99-106.
7. Jin M.M., Hu Y.C., Wang B., 2015: Compressive and bending behaviours of wood-based two-dimensional lattice truss core sandwich structures. *Composite Structures* 124: 337-344.
8. Li Y.F., Xie Y.M., Tsai M.J., 2009: Enhancement of the flexural performance of retrofitted wood beams using CFRP composite sheets. *Construction & Building Materials* 23(1): 411-422.
9. Liu, M.B., Sun, Y.F., Sun, C., 2018: Study on thermal insulation and heat transfer properties of wood frame walls. *Journal of Wood Research* 63: 249-260.
10. Lou, W.L., Ren, H.Q., 2015: Characteristics and prospects of wood structure buildings in China. *Journal of Wood Industry* 29: 20-23. (In Chinese).
11. Nadir Y., Nagarajan P., Ameen M., Arif M.M., 2016: Flexural stiffness and strength enhancement of horizontally glued laminated wood beams with GFRP and CFRP composite sheets. *Construction and Building Materials* 112: 547-555.
12. Que Z.L., Hou T.Y., Gao Y.F., Teng Q.C., Chen Q.Y., Wang C.J., Chang C., 2019: Influence of different connection types on mechanical behavior of girder trusses. *Journal of Bioresources and Bioproducts* 4(2): 89-98.
13. Ribeiro, A.S., de Jesus, A.M.P., Lima, A.M., Lousada, J.L.C., 2009: Study of strengthening solutions for glued-laminated wood beams of Maritime pine wood. *Journal of Construction and Building Materials* 23(8): 2738-2745.
14. Shi H.Y., Liu W.Q., Fang H., Bai Y., Hui D., 2017: Flexural responses and pseudo-ductile performance of lattice-web reinforced GFRP-wood sandwich beams. *Composites Part B* 108: 364-376.
15. Song X.B., Lam F., 2012: Stability analysis of metal-plate-connected wood truss assemblies. *Journal of Structural Engineering* 138: 1110-1119.
16. Song X.B., Lam F., Huang H., He M.J., 2010: Stability capacity of metal plate connected wood truss assemblies, *Journal of Structural Engineering* 136(6): 723-730.
17. Wang F.B., Wang X.M., Cai W.Z., Chang C., Que Z.L., 2019: Effect of inclined self-tapping screws connecting laminated veneer lumber on the shear resistance. *BioResources* 14(2): 4006-4021.
18. Wang, Z., Lu, Y., Xie W.B., Gao. Z.Z., Ging Y.W., Fu H.Y., 2019: Shear stress analysis interlayer shear strength test of cross laminated timber (CLT) beam. *Journal of Scientia Silvae Sinicae* 55: 157-164.
19. Wu Y., Xiao, Y., 2018: Steel and glulam hybrid space truss. *Engineering Structures* 171: 140-153.
20. Xie, W.B., Lu, Y., Wang, Z., Wang X.W., Wu, X.L., Gao, Z.Z., 2019: Feasibility of predictive assessment of bending performance of CLT plates of Canadian hemlock. *Journal of bioresources* 14: 6047-6059.
21. Xu X.L., Ma R.L., He M.J., 2006: Static test and load capacity of lightweight wooden truss. *Special Structures* 23(1): 1-4 (In Chinese).
22. Yang, X.J., Ma, L., Zhao, Q., 2018: Screw connection in wood members and WPC members. *Wood Research* 63: 833-841.
23. Yehia A., Zaher A., 2018: Flexural behavior of FRP strengthened concrete-wood composite beams. *Ain Shams Engineering Journal* 9: 3419-3424.
24. Zhang X.F., Luo L.S., Fu H.Y., Sun Y.F., Hui X.R., 2019: Experimental investigation into the flexural behavior of hollow, full, and intermittently stiffened (bamboo-like) glulam beams from larch wood. *BioResources* 14(1): 2171-2185.

25. Zhou, X.Y., Cao, L., Zeng, D., 2015: Flexural capacity analysis of glulam beams. Journal of Building Structures 45: 91-96. (in Chinese).

XIAOJUN YANG\*, QI ZHAO, DAN HAO, JIAYANG WANG, SHUAI FU, LAN MA  
NANJING FORESTRY UNIVERSITY  
CO-INNOVATION CENTER OF EFFICIENT PROCESSING  
AND UTILIZATION OF FOREST RESOURCES  
NANJING, JIANGSU 210037  
CHINA

\*Corresponding author: yxj5460@163.com

## **IMPACT OF ELECTRICAL CABLES EMBEDDED INTO ORIENTED STRAND BOARD ON CRITICAL HEAT FLUX**

JOZEF MARTINKA, TOMÁŠ ŠTEFKO, IGOR WACHTER, PETER RANTUCH  
SLOVAK UNIVERSITY OF TECHNOLOGY IN BRATISLAVA  
FACULTY OF MATERIALS SCIENCE AND TECHNOLOGY IN TRNAVA  
TRNAVA, SLOVAKIA

(RECEIVED AUGUST 2019)

### **ABSTRACT**

The paper deals with the research of electrical cables embedded in surface grooves of OSBs and its impact on the critical heat flux. An OSB type 3 board (structural board for use in dry or humid environments) and an electrical cable with fire reaction class B2<sub>ca</sub> have been investigated. Four different configurations of grooves were investigated. The first configuration consisted of an OSB without grooves (control sample). The second configuration consisted of an OSB with a single groove in the centre in which the electrical cable was mounted. In the third and fourth configurations, there were three and five grooves, respectively in which the electrical cables were mounted (the width of the grooves and the spacing between them was 9 mm). The critical heat flux was calculated from the ignition times at five different heat fluxes (30, 35, 40, 45 and 50 kW·m<sup>-2</sup>) by using a cone calorimeter. The obtained data showed that the OSB without grooves (first configuration) shows the lowest critical heat flux (8.6 kW·m<sup>-2</sup>) and the lowest standard deviation of ± 0.5 kW·m<sup>-2</sup> (lower ignition resistance) compared to the other configurations (critical heat flux in the range from 9 to 10 kW·m<sup>-2</sup> and standard deviation from 3.1 to 3.2 kW·m<sup>-2</sup>).

**KEYWORDS:** Critical heat flux, oriented strand board, electrical cables, fire investigation, fire risk, safety.

### **INTRODUCTION**

Critical heat flux is the minimum heat flux needed to ignite a material or product. The critical heat flux is related to the time interval of its action. As the time interval increases, the critical heat flux decreases (at a longer exposure time, lower heat flux is sufficient to ignite the same material). In practice, 30 minutes time interval for the critical heat flux is most often considered, as the critical heat flux decreases only slightly with increasing time interval above the given value.

The critical heat flux is determined from the material ignition times measured at a minimum of three different heat fluxes (higher than the critical heat flux). It is necessary to identify whether the material is thermally thick or thin before determining the critical heat flux. Thermally thin material is a material which is firstly overheated throughout the cross-section and then ignited as a result of exposure to the heat flux. This means the temperature is distributed uniformly through the sample. Conversely, thermally thick material is ignited by the heat flux before it is heated over its entire cross-section to approximately the same temperature. The difference between thermally thin and thermally thick material is illustrated in Fig. 1.

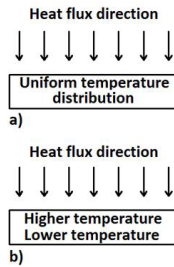


Fig. 1: Temperature distribution along cross section for a) thermally thin and b) thermally thick material.

The thermal thickness of a material depends on a large number of parameters (especially the thickness of the material, its density, thermal conductivity, specific heat capacity, and heat flux applied to the surface of the material and others). For the purposes of calculating the critical heat flux, according to Babrauskas and Parker (1987), the thermal thickness of a material can be estimated from the density of the material and the heat flux to which its surface is exposed, according to Eq. 1:

$$L = 0.6 \frac{\rho}{q} \quad (1)$$

where:  $L$  is the thickness from which the material behaves as thermally thick (mm),  $\rho$  is the density of the material ( $\text{kg}\cdot\text{m}^{-3}$ ) and  $q$  is the heat flux density applied to the surface of the material ( $\text{kW}\cdot\text{m}^{-2}$ ).

The procedure for calculating the critical heat flux of materials is given in the scientific papers of Mikkola and Wichman (1989), Spearpoint and Quintiere (2001), Tewarson (2002) and Mikkola (2009). All cited methods are based on an experimental determination of material ignition time at a minimum three applied heat fluxes. The simplest method of calculation is given by Tewarson (2002), according to which the critical heat flux is calculated from the statistical dependence of the ignition time (raised to the power of  $-1/2$ ) on the heat flux. Critical heat flux is then calculated from this statistical dependence (equation) by substituting 0 in the ignition time (mathematically corresponds to infinite ignition time). A more sophisticated method is given by Mikkola and Wichman (1989) and Mikkola (2009). According to the cited authors, the equation of statistical dependence differs for thermally thin and thermally thick materials. For thermally thin materials, the ignition time is raised to the power of  $-1$  in the equation of the statistical dependence of ignition time on the heat flux. For thermally thick materials, the ignition time is raised to the power of  $-1/2$ . The critical heat flux is calculated as in the Tewarson (2002) method by substituting zero for the ignition time raised to  $-1/2$  (thermally thick materials) or

-1 (thermally thin materials). According to the cited authors, a value of  $3 \text{ kW}\cdot\text{m}^{-2}$  is added to the calculated value representing heat losses and the fact that the critical heat flux is not calculated for the infinite ignition time but for the ignition time of 30 minutes. According to Spearpoint and Quintiere (2001), the value calculated from the equation of statistical dependence is divided by the constant 0.76. The cited authors give a calculation procedure only for thermally thick materials.

In addition to the critical heat flux, the surface temperature at the moment of ignition is very important. Ignition temperature is calculated according to Eq. 2 reported by Spearpoint and Quintiere (2001) or Eq. 2 presented by Xu et al. (2015). Eq. 3 is a simplified form of equation (2) as it neglects heat exchange by convection.

$$q_{cr} = \sigma(T_{ig}^4 - T_0^4) + h_c(T_{ig} - T_0) \quad (2)$$

where:  $q_{cr}$  is critical heat flux ( $\text{kW}\cdot\text{m}^{-2}$ ),  $\sigma$  is the Stefan-Boltzmann constant ( $5.67 \cdot 10^{-8} \text{ W}\cdot\text{m}^{-2}\cdot\text{K}^{-4}$ ),  $T_{ig}$  is ignition temperature (K),  $T_0$  is the ambient temperature (normally assumed  $293.15 \text{ K}$ ) and  $h_c$  is the natural convective heat transfer coefficient (normally assumed  $5 \text{ W}\cdot\text{m}^{-2}\cdot\text{K}^{-1}$ ).

$$T_{ig} = \left(\frac{q_{cr}}{\sigma}\right)^{1/4} \quad (3)$$

Ignition temperature does not coincide with flash-ignition temperature and spontaneous-ignition temperature determined according to ISO 871 (2006). These values for selected lignocellulosic materials are given in scientific papers e.g. Zachar (2010) and Zachar et al. (2012). This is due to the differences in test equipment, test procedure and method for determining ignition temperature on one hand and flash-ignition temperature or spontaneous-ignition temperature on the other hand. The advantage of ignition temperature over flash-ignition temperature or spontaneous-ignition temperature is its higher informative value for the needs of fire modelling. In addition, lignocellulosic materials can be characterized by the temperature from which they begin to thermally decompose. This temperature may be determined by thermogravimetric analysis. The thermogravimetric decomposition temperatures of selected lignocellulosic materials are shown in the scientific works of Kacik et al. (2017) and Markova et al. (2018). Other methods of assessing the fire safety of lignocellulosic materials can be found in the scientific works of Terenova et al. (2018) and Osvaldova et al. (2018).

In addition to the critical heat flux and ignition temperature, the material resistance against initiation is expressed by the Thermal Response Parameter (TRP). TRP is a very useful parameter for engineering calculations to assess resistance to ignition and fire propagation (Khan et al. 2016). TRP is defined as the resistance of a material to generate a combustible mixture (Tewarson et al. 1992, Tewarson 2002 and ASTM E2058 2002). TRP is calculated according to Eq. 4, which was used in the work of Tewarson (2002).

$$t_{ig}^{-1/2} = \frac{q_e - q_{cr}}{\text{TRP}} \quad (4)$$

where:  $t_{ig}$  is the ignition time (s),  $q_e$  is the heat flux applied to the surface of the material ( $\text{kW}\cdot\text{m}^{-2}$ ),  $q_{cr}$  is the critical heat flux ( $\text{kW}\cdot\text{m}^{-2}$ ) and the TRP is the thermal response parameter ( $\text{kW}\cdot\text{s}^{-1/2}\cdot\text{m}^{-2}$ ).

At present, the critical heat flux, ignition temperature and thermal response parameter of all technically significant wood and lignocellulosic materials are known. However, critical heat flux

and other initiation characteristics depend on a large number of external factors. Electrical cables are often mounted on the surface or into the grooves of OSB boards. An unresolved problem is the effect of electrical cables mounted into the grooves of OSBs on the critical heat flux of the resulting configuration. In such grooves, electrical cables with a fire reaction class B2<sub>ca</sub> are often installed. The aim of this paper is therefore to determine the effect of the electrical cables with fire reaction class B2<sub>ca</sub> embedded in the surface grooves of the OSB board on the ignition parameters (critical heat flux, ignition temperature and thermal response parameter).

## MATERIALS AND METHODS

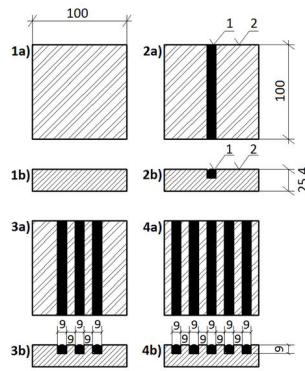
### Materials

The effect of the electrical cable embedded in the surface grooves of the OSB on ignition parameters of resulting configuration was determined for OSB type 3 (construction board for the use in dry or wet environment) according to EN 300 (2006). Basic parameters of examined OSBs are shown in Tab. 1.

*Tab. 1: Basic characteristics of investigated OSB boards.*

Thickness (mm)	25.4
Density (kg·m <sup>-3</sup> )	609 ± 16
Water content (mass %)	5.1 ± 0.3
Emissivity (-)	0.89
Composition (mass %)	93.6 Coniferous wood
	4.7 Polyurethane resin
	1.7 Paraffin

The dimensions of the tested OSB samples were 100 x 100 x 25.4 mm (± 1 mm). The samples were prepared in four configurations. The first control configuration was without any grooves in the OSB surface (comparative sample). In the second configuration, there was one groove with a width and depth of 9 mm (in which one electrical cable was installed) in the centre of the OSB surface. In a third configuration, there were three grooves in the OSB surface (each 9 mm wide and deep). The first groove was positioned as in the second configuration. Position of the second and third groove was on both sides of the central groove with 9 mm spacing (from the edges of a central groove). Electrical cables were installed in all three grooves. The fourth configuration contained five grooves, with equal spacing and dimensions (9 mm). Electrical cables were installed in all grooves. The configuration of the samples is shown in Fig. 2.



1- electrical cable, 2- OSB (dimensions in mm).

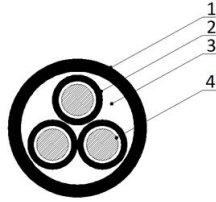
Fig. 2: Configurations of investigated samples: 1a) first configuration – view from above, 1b) first configuration – cross section, 2a) second configuration – view from above, 2b) second configuration – cross section, 3a) third configuration – view from above, 3b) third configuration – cross section, 4a) fourth configuration – view from above, 4b) fourth configuration – cross section.

Tested electrical cable CHKE-R J3x1.5, produced and supplied by VUKI, a.s., Bratislava, Slovakia, was installed in the grooves of the OSB boards. CHKE-R is a three-wire power cable designed for fixed installation, with flame spread resistance. The cable does not show fire circuit integrity. The electrical cable consists of three insulated electrical conductors housed inside the sheath that protect the electrical cable from external influences and its surrounding from electric shock. The space between the insulated conductors and the sheath is filled with bedding. Properties and materials of the CHKE-R cable are illustrated in Tab. 2.

Tab. 2: Basic parameters of investigated electrical cable.

Cable diameter (mm)	8.2
Insulated conductor diameter (mm)	2.6
Conductors diameter (mm)	1.38
Conductors cross section (mm <sup>2</sup> )	1.50
Mass of copper conductors (g·m <sup>-1</sup> )	37.5
Mass of insulation (g·m <sup>-1</sup> )	17.8
Mass of bedding (g·m <sup>-1</sup> )	23.6
Mass of sheath (g·m <sup>-1</sup> )	33.2
Total mass (g·m <sup>-1</sup> )	112.1
Material of conductor (-)	Copper
Material of conductor insulation (-)	Polyethylene copolymer
Material of bedding (-)	Al(OH) <sub>3</sub> + Mg(OH) <sub>2</sub> filled polyethylene copolymer
Material of sheath (-)	Al(OH) <sub>3</sub> + Mg(OH) <sub>2</sub> filled polyethylene copolymer
Rated voltage DC (V)	1000
Rated voltage AC (V)	600
Reaction to fire class (-)	B2 <sub>ca</sub> , s1, d1, a1
Resistance to flame spread (-)	Yes
Circuit integrity during fire (-)	No

The cross-section scheme of the CHKE-R electrical cable is shown in Fig. 3.



1- sheath, 2- insulation, 3- bedding, 4- copper wire.

Fig. 3: Cross section of investigated cable.

## Methods

The critical heat flux was calculated from the ignition times measured at five heat fluxes (30, 35, 40, 45 and 50 kW·m<sup>-2</sup>), according to Mikkola and Wichman (1989), Spearpoint and Quintiere (2001), Tewarson (2002) and Mikkola (2009). Ignition temperature was determined according to Spearpoint and Quintier (2001) and the thermal response parameter by the Tewarson (2002).

Ignition times were determined on a cone calorimeter. The cone calorimeter and test procedure are described in ISO 5660-1 (2015). Investigated heat fluxes (30, 35, 40, 45 and 50 kW·m<sup>-2</sup>) and sample configurations (Fig. 2) were tested at least three times (any outlying values were discarded and the measurement was repeated). As a result, average values are reported.

The cone calorimeter and the samples after their initiation (after the determination of the ignition time) are shown in Fig. 4.

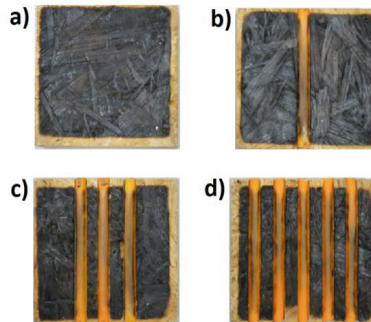


Fig. 4: Photographs of a) first configuration of sample after ignition, b) second configuration of sample after ignition, c) third configuration of sample after ignition and d) fourth configuration of sample after ignition.

## RESULTS AND DISCUSSION

Examined ignition times for all sample configurations and heat fluxes are shown in Tab. 3.

Tab. 3: Time to ignition of different sample configurations using heat fluxes from 30 to 50 kW·m<sup>-2</sup>.

Heat flux (kW·m <sup>-2</sup> ) / Configuration (-)	Time to ignition (s)			
	1 <sup>st</sup>	2 <sup>nd</sup>	3 <sup>rd</sup>	4 <sup>th</sup>
30	60	67	87	67
30	67	70	66	63
30	73	69	66	74
Average time (s)	66.7 ± 5.3	68.7 ± 1.3	73 ± 9.9	68 ± 4.5
35	40	37	35	46
35	38	38	41	41
35	40	37	57	42
Average time (s)	39.3 ± 0.9	37.3 ± 0.5	44.3 ± 9.3	43 ± 2.2
40	33	30	34	30
40	40	27	41	28
40	29	26	37	33
Average time (s)	34 ± 4.5	27.7 ± 1.7	37.3 ± 2.9	30.3 ± 2.1
45	25	21	27	25
45	19	28	28	23
45	29	20	25	23
Average time (s)	24.3 ± 4.1	23 ± 3.6	26.7 ± 1.2	23.7 ± 0.9
50	19	21	22	23
50	19	16	19	13
50	19	16	21	21
Average time (s)	19 ± 0	17.7 ± 2.4	20.7 ± 1.2	19 ± 4.3

The dependence of the average initiation time (raised to the power of -1/2) on the heat flux, together with the equations of statistical dependence, are shown in Fig. 5. Critical heat fluxes calculated from the equations of statistical dependence on Fig. 5 according to Mikkola and Wichman (1989), Spearpoint and Quintiere (2001), Tewarson (2002) and Mikkola (2009) are shown in Tab. 4.

Tab. 4: Critical heat fluxes for investigated configurations.

Method (-) / Configuration (-)	Critical heat flux (kW·m <sup>-2</sup> )			
	1 <sup>st</sup>	2 <sup>nd</sup>	3 <sup>rd</sup>	4 <sup>th</sup>
Tewarson (2002)	5.6 ± 0.5	7 ± 3.2	6 ± 3.2	6.9 ± 3.1
Mikkola and Wichman (1989)	8.6 ± 0.5	10 ± 3.2	9 ± 3.2	9.9 ± 3.1
Spearpoint and Quintiere (2001)	7.4 ± 0.5	9.2 ± 3.2	7.9 ± 3.2	9.1 ± 3.1

According to Scudamore et al. (1991) and Tewarson (2002), the critical heat flux of most organic polymers ranges from 10 to 15 kW·m<sup>-2</sup>, while the critical heat flux of most lignocellulosic materials is approximately 10 kW·m<sup>-2</sup>. Similar critical heat flux values of lignocellulosic materials indicate e.g. and Martinka et al. (2017) and Martinka (2018). These values apply to lignocellulosic materials without grooves in their surface and without the installation of electrical

cables (therefore, the conditions of determination correspond to the first configuration). It follows that the critical heat fluxes of the first configuration of OSB samples calculated according to Mikkola and Wichman (1989) and Spearpoint and Quintiere (2001) are comparable to those published for lignocellulosic materials in the cited papers.

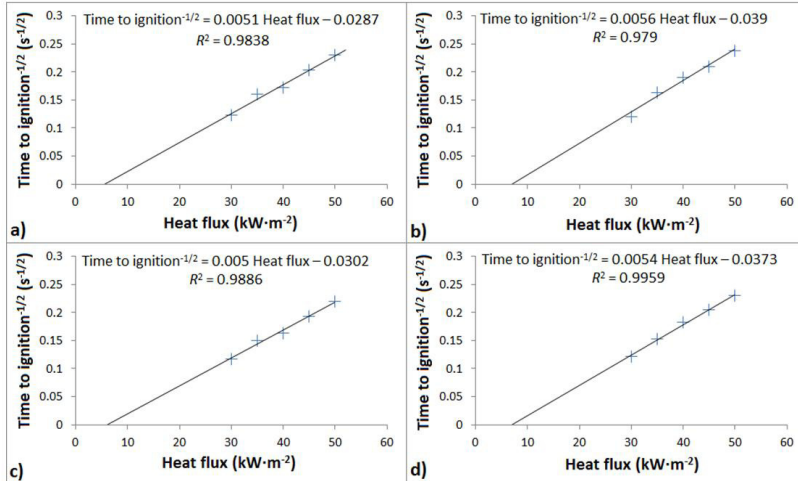


Fig. 5: Dependences of time to ignition<sup>-1/2</sup> on heat flux for a) first configuration, b) second configuration, c) third configuration and d) fourth configuration.

The critical heat flux of halogen-free electrical cables (12 and 21 mm in diameter) is according to Meinier et al. (2018) in the range of 10.6 to 12.8 kW·m<sup>-2</sup>. The cited author's team assumed that the examined electrical cables behaved like thermally thick material during the test. The polymer components of the investigated cables (Tab. 2) were mainly copolymers based on ethylene-vinyl acetate and polyethylene, the sheath was filled mainly with Al(OH)<sub>3</sub> (the composition was therefore similar to the cables examined in the cited study). In the cited scientific paper, the critical heat flux was determined for three electrical cables placed side by side, 12 mm apart and 27 mm apart. According to Fontaine et al. (2015), the critical heat flux of electrical cables is 10.5 kW·m<sup>-2</sup>. The cables examined by the cited authors were 10 mm in diameter, and the composition of the polymer components was similar to the cables in the study by Meinier et al. (2018). Rantuch et al. (2018) determined the critical heat flux of a vertically oriented self-installed electrical cable (fire response class B2<sub>ca</sub>) in the range of 21 to 25 kW·m<sup>-2</sup>. The reason for the substantially higher critical heat flux determined by Rantuch et al. (2018) as compared to Fontaine et al. (2015) and Meinier et al. (2018) is probably the fact that a single electrical cable has a significantly higher critical heat flux than multiple electrical cables of the same type installed side by side.

The critical heat fluxes in the presented paper (Tab. 4) are consistent with the results of the aforementioned papers. The lowest critical heat flux was achieved at samples of the first configuration (OSB without an installed electrical cable). Installation of electrical cables (second to fourth configurations) caused a slight increase in critical heat flow (Tab. 4). The critical heat flux of the first sample configuration is approximately consistent with the results published for lignocellulosic materials in the scientific work of Scudamore et al. (1991), Tewarson (2002),

Martinka et al. (2017) and Martinka (2018). The critical heat flux of the second, third and fourth sample configurations is lower than the critical heat flux of electrical cables as determined by Fontaine et al. (2015), Meinier et al. (2018) and Rantuch et al. (2018) and approximately the same as the critical heat flux of lignocellulosic materials published in the aforementioned works. This is probably due to the fact that the critical heat flux of a product consisting of two different materials on the surface (in this case the OSB with electrical cables mounted in grooves on the surface) is closer to the material with lower critical heat flux.

The statistical significance of the impact of the installation of electrical cables in the grooves on the OSB surface on the critical heat flux cannot be directly assessed from the critical heat flux values (the reason is that each sample configuration has only one critical heat flux and the number of data is insufficient for statistical analysis). For this reason, two-factor analysis of variance (ANOVA) with replication of ignition times was performed. The dependence of the ignition times for all four sample configurations examined (along with a 95% confidence interval) on the heat flux is shown in Fig. 6. Ignition times (at a certain heat flux) are the only input parameter for calculating the critical heat flux. However, based on the ANOVA results, only the effect of the sample configuration on the ignition time (not on the critical heat flux) can be drawn out.

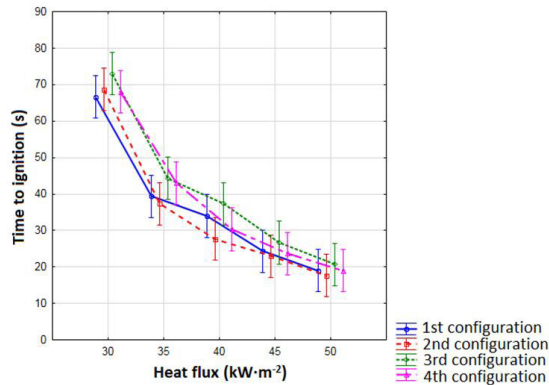


Fig. 6: Dependences of time to ignition on heat flux (with 95% confidence interval) for a) first configuration, b) second configuration, c) third configuration and d) fourth configuration.

ANOVA was performed at significance level  $\alpha = 0.05$ . The ANOVA results ( $p = 0.0328$ ,  $F = 3.33$  and  $F_{crit} = 2.84$ ) demonstrate that the investigated configurations show a statistically significant difference in ignition times. A post hoc Duncan's test was performed to determine which configurations and at which heat fluxes have a statistically significant difference in ignition times. The data obtained show that there is a statistically significant difference in ignition time at a heat flux of  $40 \text{ kW}\cdot\text{m}^{-2}$  (Duncan's coefficient for this heat flux and sample configuration is 0.0347) between the second and third sample configurations. There is no statistically significant difference in initiation times between other sample configurations (at the same heat fluxes).

The ignition temperatures of the investigated sample configurations, calculated by the methods of Spearpoint and Quintier (2001) and Xu et al. (2015) are shown in Tab. 5. In both methods, samples of the first configuration show the lowest ignition temperature (and at the same time the lowest standard deviation). This is due to the higher resistance of electric cables (compared to OSB) to ignition.

Tab. 5: Ignition temperatures of investigated configurations.

Method (-) / Configuration (-)	Ignition temperature $\pm$ SD ( $^{\circ}$ C)			
	1 <sup>st</sup>	2 <sup>nd</sup>	3 <sup>rd</sup>	4 <sup>th</sup>
Spearpoint and Quintiere	245 $\pm$ 8	341 $\pm$ 47	317 $\pm$ 52	339 $\pm$ 45
Xu et al.	328 $\pm$ 8	362 $\pm$ 48	338 $\pm$ 52	360 $\pm$ 45

Data in Tab. 5 calculated by the method of Xu et al. (2015) are consistent with data according to Janssens (1991), which for vertical oriented lignocellulosic materials reports ignition temperature in the range 314 to 394 $^{\circ}$ C. Similar ignition temperature values (in the range of 306 to 372 $^{\circ}$ C) of cork insulation are also reported by Rantuch et al. (2016). Different ignition temperature values of lignocellulosic materials (ranging from 456 to 488 $^{\circ}$ C and for Merbau Hardwood up to 643 $^{\circ}$ C) are reported by Xu et al. (2015). The cause of the substantially higher ignition temperature value determined by Xu et al. (2015) is probably the fact that the cited author's team determined the critical heat flux (input to calculate ignition temperatures) from the ignition times at heat fluxes of 25, 50 and 75 kW $\cdot$ m $^{-2}$  (normally the critical heat flux is calculated from the ignition times measured at heat fluxes in the range of 20 to 50 kW $\cdot$ m $^{-2}$ ). The ignition temperature data of the lignocellulosic material in which the electrical cable is installed have not been published in other scientific papers. Likewise, the published data on the ignition temperature of electric cables were not determined in a similar way for identical electric cables as in presented scientific paper. Gong et al. (2018) report the ignition temperature of commonly used flame retardant electrical cables (based on PVC and XLPE) in the range of 511 to 650 $^{\circ}$ C. However, the cited team did not examine identical electrical cables and used a different methodology. According to Tewarson et al. (2000) and Tewarson (2002) is the ignition temperature of polyethylene (the major component of the polymer of the investigated cables) in the range 377 to 443 $^{\circ}$ C. A comparison of the above data demonstrates that lignocellulosic materials have a lower ignition temperature than electrical cables with polyethylene-based polymer components. Data in Tab. 5 are consistent with this conclusion drawn from the data in the cited scientific papers (the ignition temperature of the second to fourth sample configurations is higher than the ignition temperature of the first (control) sample configuration due to the increasing proportion of electrical cables on the OSB surface).

The thermal response parameters (TRP) of the sample configurations are shown in Tab. 6. Tab. 6 show that TRP decreases with increasing heat flux. This trend is already apparent from Eq. 4. The average TRP of the first sample configuration is higher than the second sample configuration, while lower than the third sample configuration (Tab. 6). This trend can be explained by the fact that installing a cable in the surface of the OSB (creating grooves) will cause the surface to break and consequently reduce the resistance to ignition. On the other hand, the electrical cable (fire reaction class B2 $_{ca}$ ) has, according to Rantuch et al. (2018) significantly higher critical heat flux than OSB. Thus, in the second configuration (one groove), the negative effect (surface disruption) probably prevailed over the positive effect (presence of the element - cable with a higher critical heat flux), since the ratio of the installed electrical cable surface to OSB board surface was too low. In the third configuration, the effect was reversed.

Tab. 6: Thermal response parameters for investigated configurations.

Heat flux (kW·m <sup>-2</sup> ) / Configuration (-)	Thermal response parameter (kW·s <sup>-1/2</sup> ·m <sup>-2</sup> )			
	1 <sup>st</sup>	2 <sup>nd</sup>	3 <sup>rd</sup>	4 <sup>th</sup>
30	344	352	410	353
30	363	360	357	342
30	379	357	357	371
Average TRP (kW·s <sup>-1/2</sup> ·m <sup>-2</sup> )	362 ± 14	356 ± 3	375 ± 25	355 ± 12
35	281	262	260	292
35	274	265	282	276
35	281	262	332	279
Average TRP (kW·s <sup>-1/2</sup> ·m <sup>-2</sup> )	279 ± 3	263 ± 1	291 ± 30	282 ± 7
40	255	236	257	236
40	281	223	282	228
40	239	219	268	248
Average TRP (kW·s <sup>-1/2</sup> ·m <sup>-2</sup> )	258 ± 17	226 ± 7	269 ± 10	237 ± 8
45	222	197	229	216
45	194	228	233	207
45	239	192	220	207
Average TRP (kW·s <sup>-1/2</sup> ·m <sup>-2</sup> )	218 ± 19	206 ± 16	227 ± 5	210 ± 4
50	194	197	206	207
50	194	172	192	155
50	194	172	202	198
Average TRP (kW·s <sup>-1/2</sup> ·m <sup>-2</sup> )	194 ± 0	180 ± 12	200 ± 6	187 ± 23

For comparison, according to Scudamore et al. (1991) and Tewarson (2002) wood materials show (without flame retardant) TRP in the range from 134 to 138 kW·s<sup>-1/2</sup>·m<sup>-2</sup> (flame retardant can increase this value by more than 100 kW·s<sup>-1/2</sup>·m<sup>-2</sup>) and polyethylene-based polymers have reached 224 - 321 kW·s<sup>-1/2</sup>·m<sup>-2</sup>. According to the cited authors power electrical cables (consisting of polymer components based on polyethylene and PVC) show TRP in the range of 221 - 263 kW·s<sup>-1/2</sup>·m<sup>-2</sup>. It should be noted that TRP was determined by the authors on a Fire Propagation Apparatus according to then applicable ASTM E2058 (2002) and only for a narrow group of tree species. However, the cited data show that the TRP of wood and wood-based materials and electrical cables are approximately in the same interval. The obtained data (Tab. 6) are in approximate conformity with the cited papers. Despite the fact that the differences in TRP between the different configurations are measurable (Tab. 6), these differences are practically negligible.

## CONCLUSIONS

The impact of the electrical cables with fire reaction class B2<sub>ca</sub> mounted into the grooves of OSBs surface on the critical heat flux, ignition temperature and thermal response parameters was studied in this paper. The measurements were conducted on samples with 3 different configurations (OSB with 1, 3 and 5 electrical cables mounted into grooves) and on a control sample (OSB without an electrical cable).

The obtained data showed that the configuration without any electrical cable had a lower critical heat flux (8.6 ± 0.5 kW·m<sup>-2</sup>) and lower ignition temperature (328 ± 8°C) compared to

OSBs with electrical cables mounted into the grooves (critical heat flux was determined in the range from 9 to 10 kW·m<sup>-2</sup> and ignition temperature in the range from 338 to 362°C). The effect of electrical cables mounted into the grooves of OSB boards on the TRP is not clear.

Electrical cables (fire reaction class B2<sub>ca</sub>) mounted into grooves in the surface of the OSB boards caused a measurable increase in both critical heat flux and ignition temperature. However, this increase is negligible from a practical point of view. Therefore, on the basis of the obtained data, it can be concluded that the installation of electrical cables with the specified reaction to fire class into the OSB grooves will not cause a significant change in its tendency to ignite by thermal radiation. This conclusion applies to the experimental conditions described in this scientific work.

## ACKNOWLEDGEMENTS

This work was supported by the Slovak Research and Development Agency under the contract No. APVV-16-0223.

## REFERENCES

1. ASTM E2058, 2002: Standard test methods for measurement of synthetic polymer material flammability using a fire propagation apparatus.
2. Babrauskas, V., Parker, W.J., 1987: Ignitability measurements with the cone calorimeter. *Fire and Materials* 11(1): 31-43.
3. EN 300, 2006: Oriented strand boards (OSB). Definitions, classification and specifications.
4. Fontaine, G., Ngohang, F.E., Gay, L., Bourbigot, S., 2015: Investigation of the contribution to fire of electrical cable by a revisited mass loss cone. In: *Fire Science and Technology* (ed. Harada K, Matsuyama K, Himoto K, Nakamura Y, Wakatsuki K). Singapore. Springer, Pp 687-693.
5. Gong, T., Xie, Q., Huang, X., 2018: Fire behaviors of flame-retardant cables part I: Decomposition, swelling and spontaneous ignition. *Fire Safety Journal* 95(1): 113-121.
6. ISO 5660-1, 2015: Reaction to fire tests. Heat release, smoke production and mass loss rate. Part 1: Heat release rate (cone calorimeter method) and smoke production rate (dynamic measurement).
7. ISO 871, 2006: Plastics. Determination of ignition temperature using a hot-air furnace.
8. Janssens, M.L., 2003: Improved method for analyzing ignition data from the cone calorimeter in the vertical orientation. In: *Fire Safety Science* (ed. Evans DD). International Association for Fire Safety Science. London. Pp 803-814.
9. Kacik, F., Luptakova, J., Smira, P., Estokova, A., Kacikova, D., Nasswetrova, A., Bubenikova, T., 2017: Thermal analysis of heat-treated silver fir wood and larval frass. *Journal of Thermal Analysis and Calorimetry* 130(2): 755-762.
10. Khan, M.M., Tewardson, A., Chaos, M., 2016: Combustion characteristics of materials and generation of fire products. In: *SFPE Handbook of Fire Protection Engineering* (ed. Hurley MJ). Pp 1143-1232, Springer, London. Pp 1143-1232.
11. Markova, I., Hroncova, E., Tomaskin, J., Turekova, I., 2018: Thermal analysis of granulometry selected wood dust particles. *BioResources* 13(4): 8041-8060.
12. Martinka, J., 2018: Fire risk of materials and combustible liquids. Ales Cenek Publishing House. Plzen, 142 pp.

13. Martinka, J., Hroncova, E., Kacikova, D., Rantuch, P., Balog, K., Ladomersky, J., 2017: Ignition parameters of poplar wood. *Acta Facultatis Xylogiae Zvolen* 59(1): 85-95.
14. Meinier, R., Sonnier, R., Zavaleta, P., Suard, S., Ferry, L., 2018: Fire behavior of halogen-free flame retardant electrical cables with the cone calorimeter. *Journal of Hazardous Materials* 342(1): 306-316.
15. Mikkola, E., 2009: Ignitability of solid materials. In: *Heat Release in Fires* (ed. Babrauskas V, Grayson SJ). Interscience Communications. London. Pp 225-232.
16. Mikkola E., Wichman, I.S., 1989: On the thermal ignition of combustible materials. *Fire and Materials* 14(3): 87-96.
17. Osvaldova, L.M., Gasparik, M., Castellanos, J.R.S., Markert, F., Kadlicova, P., Cekovska, H., 2018: Effect of thermal treatment on selected fire safety features of tropical wood. *Communications - Scientific Letters of the University of Zilina* 20(2): 3-7.
18. Rantuch, P., Hrusovsky, I., Martinka, J., Balog, K., 2016: Determination of the critical heat flux and the corresponding surface ignition temperature of the expanded cork plates. In: *Conference proceedings of 8<sup>th</sup> International Scientific Conference Wood and Fire Safety 2016*. Vol. 1, University of Zilina. Zilina. Pp 261-268.
19. Rantuch, P., Stefko, T., Martinka, J., Wachter, I., Kobeticova, H., 2018: Impact of initiator placement on ignition of the vertically positioned electrical cable. In: *Conference proceedings of 18<sup>th</sup> International Multidisciplinary Scientific Conference SGEM 2018* (Vol. 18). STEF92 Technology. Sofia. Pp 419-426.
20. Scudamore, M.J., Briggs, P.J., Prager, F.H., 1991: Cone calorimetry – a review of tests carried out on plastics for the association of plastics manufacturers in Europe. *Fire and Materials* 15(2): 65-84.
21. Spearpoint, M.J., Quintiere, J.G., 2001: Predicting the piloted ignition of wood in the cone calorimeter using an integral model - effect of species, grain orientation and heat flux. *Fire Safety Journal* 36(4): 391-415.
22. Terenova, L., Dubravskaa, K., Majlingova, A., 2018: The impact of geometric shape of the log wall construction elements on their fire behaviour. *Wood Research* 63(4): 547-558.
23. Tewarson, A., 2002: Generation of heat and chemical compounds in fires. In: *The SFPE Handbook of Fire Protection Engineering* (ed. DiNenno PJ). National Fire Protection Association. Quincy. Pp 618-697.
24. Tewarson, A., Abu-isa, I.A., Cummings, D.R., Ladue, D.E., 2000: Characterization of the ignition behaviour of polymers commonly used in the automotive industry. In: *Fire Safety Science* (ed. Curtat M). International Assotiation for Fire Safety Science. London. Pp 991-1002.
25. Tewarson, A., Ogden, S.D., 1992: Fire behavior of polymethylmethacrylate. *Combustion and Flame* (89)3: 237-259.
26. Xu, Q., Chen, L., Harries, K.A., Zhang, F., Liu, Q., Feng, J., 2015: Combustion and charring properties of five common constructional wood species from cone calorimeter tests. *Construction and Building Materials* 96(1): 416-427.
27. Zachar, M., 2010: Selected deciduous wood species flash ignition and ignition temperature determination. In: *Fire Engineering* (ed. Mrackova E, Markova I). Technical University in Zvolen. Zvolen. Pp 431-438.
28. Zachar, M., Mitterova, I., Xu, Q., Majlingova, A., Cong, J., Galla, S., 2012: Determination of fire and burning properties of spruce wood. *Drvna Industrija* 63(3): 217-223.

\*JOZEF MARTINKA, TOMÁŠ ŠTEFKO, IGOR WACHTER, PETER RANTUCH  
SLOVAK UNIVERSITY OF TECHNOLOGY IN BRATISLAVA  
FACULTY OF MATERIALS SCIENCE AND TECHNOLOGY IN TRNAVA  
JANA BOTTU 2781/25  
917 24 TRNAVA  
SLOVAKIA  
\*Corresponding author: [jozef.martinka@stuba.sk](mailto:jozef.martinka@stuba.sk)

## **INFLUENCE OF WET AND DRY CYCLE ON PROPERTIES OF MAGNESIA-BONDED WOOD-WOOL PANEL**

BIN NA, HAIQING WANG, TAO DING, XIAOLING LU  
NANJING FORESTRY UNIVERSITY  
CHINA

(RECEIVED JANUARY 2019)

### **ABSTRACT**

In this paper, magnesia-bonded wood-wool panel was subjected to different times of wet and dry cycle to analyze their effects on the physical properties and the sound absorption property of the panel from macro and micro perspective. The results showed that with the increase of the wet and dry circle times, both MOE and thickness swelling decreased and the average absorption coefficient of the specimen increased.

**KEYWORDS:** Magnesia wood-wool panel, wet and dry cycle, sound absorption coefficient, thickness swelling, MOE.

### **INTRODUCTION**

Magnesia-bonded wood wool panel (MWWP) is a panel made of wood-wool as reinforcing material bonded with hydration product after the reaction between magnesia (main content: MgO) and MgCl<sub>2</sub> solution (Na et al. 2012, 2013, 2014b, Wang et al. 2013a,b, Simatupang and Geimer 1990). The hydration product is indeed the magnesium oxychloride cement (Na et al. 2012, 2013, 2014a, 2018). Magnesium oxychloride cement is a rigid gas cementing material, with advantages of fast condensation, high strength, low density, fire resistance etc. However, changes of temperature and humidity will greatly affect the surface stability of magnesium oxychloride cement, causing excessive moisture absorption, back to halogen, efflorescence and so on, and deteriorating physical and mechanical properties of magnesium oxychloride cement products.

Magnesium oxychloride cement is mainly composed of two alternate salt crystals (Zhu et al. 1994) of 5Mg(OH)<sub>2</sub> • MgCl<sub>2</sub> • 8H<sub>2</sub>O and 3Mg(OH)<sub>2</sub> • MgCl<sub>2</sub> • 8H<sub>2</sub>O produced by the reaction of magnesium oxide and magnesium chloride. The two complex salt crystals intertwined joined together with better crystalline rod or gel-like crystals. 5-phase, 3-phase crystals are fibrous, phase 5, showing the rod-shaped is comparatively thicker than 3-phase which presented as needle-like. In terms of crystal morphology (Matkovic and Yong 1973), 5Mg(OH)<sub>2</sub> • MgCl<sub>2</sub> • 8H<sub>2</sub>O is better than 3Mg(OH)<sub>2</sub> • MgCl<sub>2</sub> • 8H<sub>2</sub>O and shows higher strength and stability.

But when it is put in water or in a long-term high humidity environment, the 5-phase crystal will present a poor stability and break free  $\text{MgCl}_2$ . However, studies have shown that in the high-temperature water vapor (Deng 2003, Deng and Zhang 1996), free  $\text{MgCl}_2$  can generate  $\text{Mg}(\text{OH})\text{Cl}$  and precipitation, and thus effectively improve the MOC hygroscopic (Pan et al. 1984, Tong 1995). The crystal morphology of  $\text{Mg}(\text{OH})_2$  is a large bulk crystal (Chen et al. 1996), showing a layered structure. So, when the proportion of  $\text{MgO}$ ,  $\text{MgCl}_2$  and  $\text{H}_2\text{O}$  is appropriate, the 5 phases and  $\text{Mg}(\text{OH})_2$  with high content and stability, magnesia-bonded wood-wool panel will have the highest intensity accordingly (Jiang et al. 2002). In addition, since the excess  $\text{MgO}$  can take further reaction to form  $\text{Mg}(\text{OH})_2$ , therefore a reasonable increase in moles of  $\text{H}_2\text{O}$  will also help to enhance the panel strength.

## MATERIAL AND METHODS

Since magnesia-bonded wood-wool panel is a new material, there is no standard on water sorption test of such material, considering the obvious impact of dry and wet cycles on its water resistance, so the experiment followed china aerated concrete wet-dry cycle test standard GB / T11975-1997 (China Standards Press 2014).

First, put the specimens in electric blast oven at  $(60 \pm 5)^\circ\text{C}$ , and dried to constant mass; taken out and cooled 20 min at temperature of  $(20 \pm 5)^\circ\text{C}$ ; put the specimens in water at temperature of  $(20 \pm 5)^\circ\text{C}$ ; kept the specimen 30 mm below the water surface; removed the specimen 5 min later; put them in the air for 30 min; after then kept the specimens in the oven at  $(60 \pm 5)^\circ\text{C}$  for 7 h.

## RESULTS AND DISCUSSION

Fig. 1 showed, after wet and dry treatment, the cross-sectional structure became obviously looser than before, and the wood-wool swelled. To further study changes of the crystalline phase after wet and dry treatment, SEM and XRD would be used in the following study.



Fig. 1: Cross-sectional view of wood-wool panel before and after wet and dry treatment.

### XRD analyses

Samples from magnesia wood-wool panels were prepared before /after wet and dry treatment respectively. Magnesium oxychloride cement was ground and those with the size of less than 200 mesh were kept. The microscopic analysis was made by X-ray diffraction (XRD) analyzer, the results were obtained as follows, in which: 1- $\text{MgCO}_3$ , 2- $\text{MgO}$ , 3- $\text{Mg}(\text{OH})_2$ , 4- $5\text{Mg}(\text{OH})_2 \cdot \text{MgCl}_2 \cdot 8\text{H}_2\text{O}$ , 5- $3\text{Mg}(\text{OH})_2 \cdot \text{MgCl}_2 \cdot 8\text{H}_2\text{O}$ .

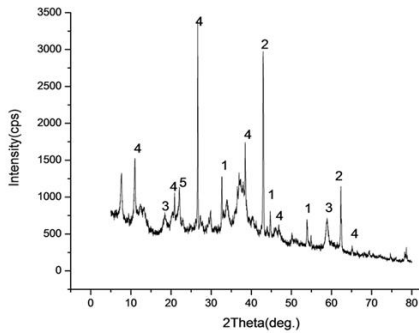


Fig. 2: XRD spectrum of untreated magnesium oxychloride cement panels with  $n = 0$ .

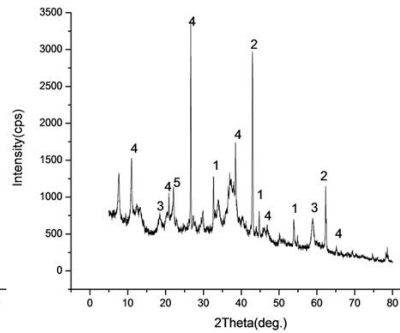


Fig. 3: XRD spectrum of treated magnesium oxychloride cement panels with  $n = 2$ .

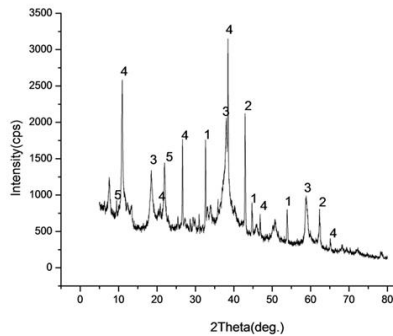


Fig. 4: XRD spectrum of treated magnesium oxychloride cement panels with  $n = 5$ .

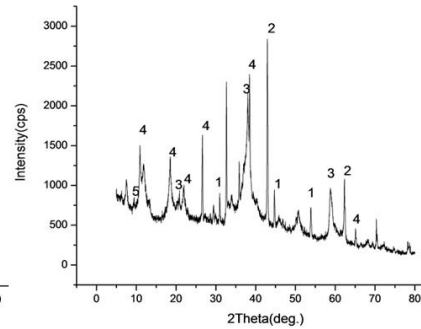


Fig. 5: XRD spectrum of magnesium oxychloride cement panels with  $n = 8$ .

By comparing XRD spectra results of magnesium oxychloride cement under four states, it could be found that  $MgCO_3$  (magnesite),  $MgO$  (periclase),  $Mg(OH)_2$ , five complex salt crystal phase and three-phase double salt crystals were the four main phases (Ji et al. 1995) existing in magnesium oxychloride cement with different times of wet-dry cycle process. By comparing Figs. 2, 3, 4, 5, it could be found that the intensity of diffraction peaks at the position of  $2\theta = 38.48^\circ$ ,  $22.05^\circ$  and  $10.99^\circ$  of the 5-phase were greatly enhanced after 2 wet-dry cycles. With increase of the wet and dry cycle processing times increase, the peak intensity decreased, the peak shape gradually widened, which was especially obvious at  $2\theta = 38.48^\circ$  in Fig. 4 and 5 comparing to Fig. 2 in which the peak appears thin and tall. The results showed that through 2 wet-dry cycles, 5 complex salt crystal phase had been changed with higher degree of crystallinity and higher content, but the rules of the crystal surface became poorer. With the increase of wet-dry cycle process, the content of three complex salt crystal phase in magnesium oxychloride cement decreased, and even close to disappear in some diffraction angle because 3-phase was unstable. The related studies showed when the molar ratio of  $MgO$  to  $MgCl_2$  is 4 or 5, cement hydrates was unstable after flooding due to the dissolution and phase transformation would lead to decomposition of 3-phase hydrate (Guan and Ba 2009). In summary, 5 complex salt crystal

phase (Xia et al. 1994) in magnesium oxychloride cement increased gradually with increase of the wet and dry cycle p times, The crystal grown no better than those were not suffered the wet and dry cycle treatment. This was one of main reasons that the strength of panel was decreased with increase of wet and dry cycle times.

### SEM analyses

Specimens were taken from magnesium oxychloride cements with different times of wet-dry cycle process, and analyzed by scanning electron microscope (SEM). The results of specimens with  $n = 0, 2, 5, 8$  (times of wet and dry cycle) are shown as follows.

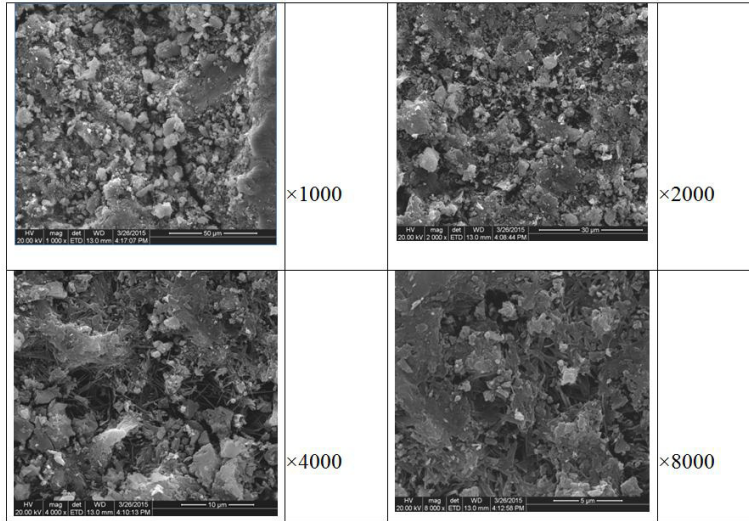


Fig. 6: SEM micrograph of magnesium wood wool panels with  $n = 0$ .

Fig. 6 showed that the surface morphology of magnesium oxychloride cement with  $n = 0$  presented colloidal showing topography, mainly formed by layered, rod-shaped and needle-shaped structure. 5 phase was rod-like; t 3 phase was needle-like and  $Mg(OH)_2$  is bulk crystal with layered structure (Shuxing 2011). The strength and stability of a 5-phase crystals were better than  $Mg(OH)_2$  crystal phase, thus illustrated that there were lots of 3-phase, 5-phase complex salt crystals and  $Mg(OH)_2$  crystalline phase. So under normal circumstances, the higher the content of 5-phase crystals were, the greater the intensity of magnesium oxychloride cement was.

Comparing Fig. 6 and Fig. 7, it can be found that the layered structure on the surface of magnesium oxychloride cement surface reduced after 2 times wet and dry cycles. That means, that the  $\text{Mg}(\text{OH})_2$  phase was reduced. Comparing picture of  $\times 8000$ , it could be found when the pore diameter increased until that the cement structure became relatively loose, but it also made the material porosity increase, thus the sound absorption property of the panel was increased.

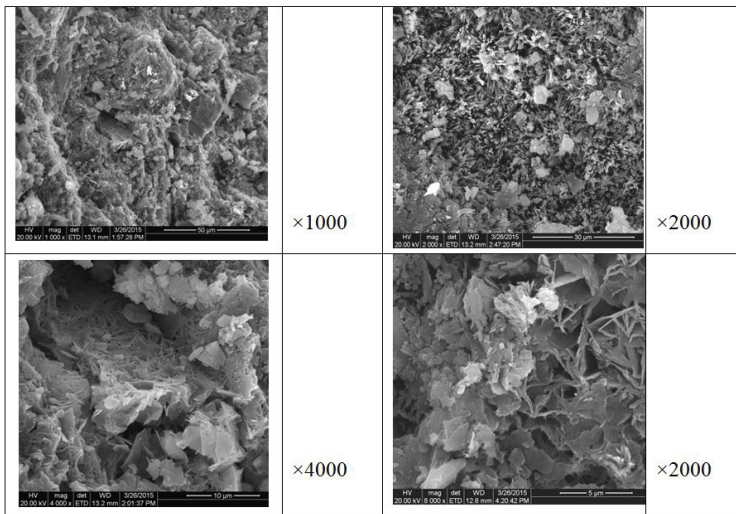


Fig. 7: SEM micrograph of magnesium wood wool panels with  $n = 2$ .

Comparing 2000 times photos of Fig. 6, 7, and 8, it could be found that the layered structure on the surface of magnesium oxychloride cement surface was significantly reduced, that meant, the  $\text{Mg}(\text{OH})_2$  phase was greatly reduced, but the 5-phase crystal rod increased obviously which should have improved the physical strength of the panel.

However, comparing 2000 times and 8000 times photos in Figs. 6 and 8, the following results were found: 5-phase crystal growth basically in holes or voids, and grow radially from the hole edge to centre, or radiate outwardly from the pores. The  $\text{MgCl}_2$  solution and  $\text{MgO}$  particles can easily fill holes and voids, and interaction occurred therein, providing sufficient space to facilitate the growth of 5 phase. This kind of radial crystal in holes had no contribution to the strength of magnesium oxychloride cement because this radial crystal did not form the network crystal structure. On the contrary, the existence of such holes reduced the strength of magnesia cement.

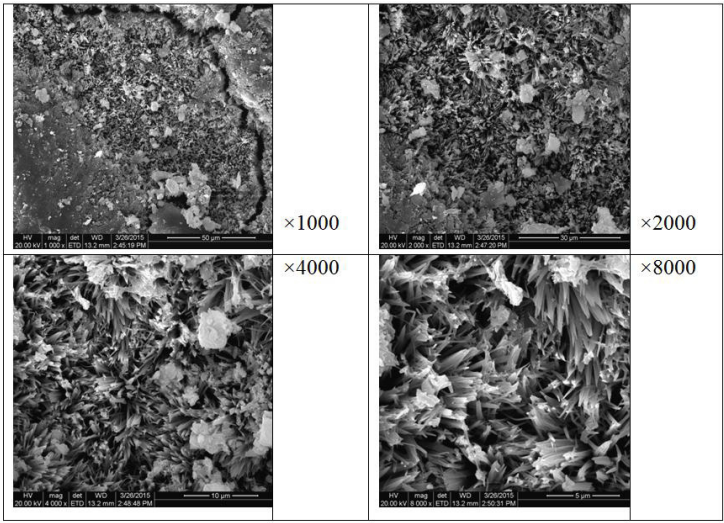


Fig. 8: SEM micrograph of magnesium wood wool panels with  $n = 5$ .

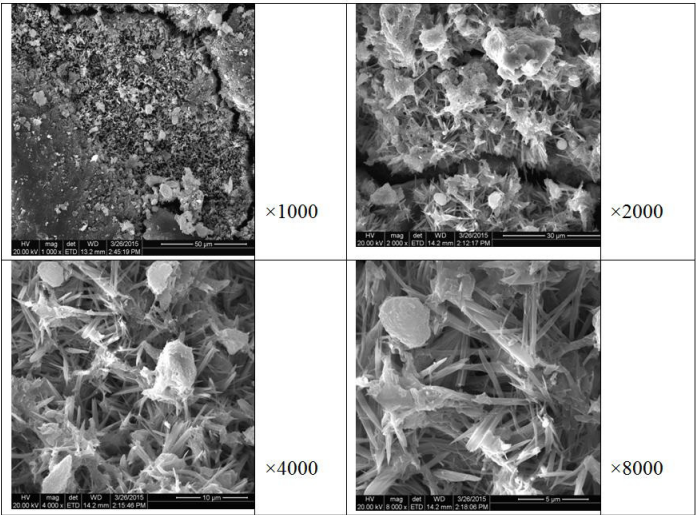


Fig. 9: SEM micrograph of magnesium wood wool panels with  $n = 8$ .

Comparing 4000 times photos of Fig. 8 and Fig. 9, it could be found that in both photos, layered structure became rare, but the later structure was obviously looser than the former. Hardened cement formed by composite-magnesia-cement materials was similar to other kinds of hardened-bodies. The formation of sufficient stable hydrates and the well intersection crossed each other, and a continuous, dense crystalline structure of cement in the whole space, these two were the prerequisites ensuring the cement's physical strength. The loose structure of 5 phase could not cross over with each other, so even the high 5 phase content could not bring high

strength, wood moisture expansion which led to hardened-body cracking is another important reason (Tu 1996).

### Analysis of thickness swelling

From Fig. 10, it could be found that, the longer the panel was soaked, the higher the panel thickness swelling would be. This showed that the water resistance property of magnesium oxychloride cement was poor. Combining the XRD and SEM results, the following reasons could be found: on the one hand, the magnesium oxychloride cement hydration products were unstable in water, especially the 3-phase, which could be dissolved in water. The other reason was the wood-wool's property of moisture absorption. When the wood-wool's expansion reached a certain level, the expansion stress would exceed the MOC's internal stress, and result in the destruction of the internal structure of magnesium oxychloride cement, and the decrease of MOC's physical and mechanical properties, thereby reducing the binding force to the wood fiber. Thus the improvement of the panel's water resistance heavily depended on the improvement of magnesium oxychloride cement's water resistance.

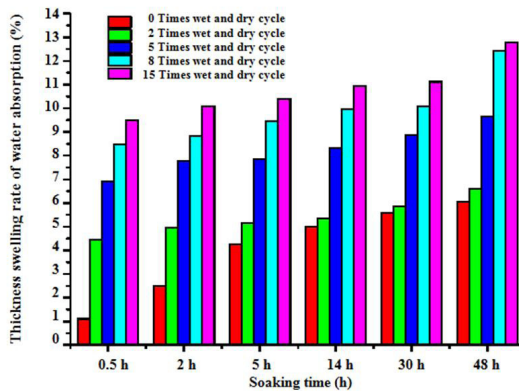


Fig. 10: Effects of wet and dry cycles on thickness swelling.

Further analyse showed that the specimen had not been handled with wet and dry cycles. Its thickness swelling ratio increased rapidly at the initial five hours, after which, the value rose slowly, while this value of those specimen being handled was relatively smaller with time going even their thickness swelling value was larger than the former. This was because the three-phase hydrates hydrolyzed in soaking process, then in the drying process, those active MgO which did not react would combine with free H<sub>2</sub>O to generate Mg(OH)<sub>2</sub> crystals. With the increase of time, the content of 5 phase increased which was relatively stable than 3 phase, so the following soaking process had little effect on its thickness swelling ratio. Thus, the impact of wet and dry cycles on the panel's thickness swelling ratio came mainly from the wood wool's hygroscopic expansion and the decomposition of some hydration products in the cement.

### Mechanical performance analysis

Fig. 11 showed that with the increase of wet and dry cycles, the panel showed a nonlinear decrease of MOE. The slope of the curve with  $n \leq 2$  was significantly greater than  $2 < n \leq 15$ , which indicated that MOE of the panel sharply declined after 2 cycles, and with increase of the circle time, the rate of decline decreased. This change trend was consistent with the change of

thickness swelling, which also indicating that the poor water resistance of magnesium oxychloride cement was the main reason leading to a sharp decline in the MOE of the panel after wet and dry circle. The following relationship between the plate elastic modulus ( $E_b$ ) and the times of wet and dry cycle ( $n$ ) was established by ORIGIN nonlinear fitting:

$$E_b = 51.69429n^2 - 559.37371n + 1633.856 \tag{1}$$

where:  $E_b$ - elastic modulus, (MPa),  
 $n$ - times of wet and dry cycle,  $n \leq 15$ .

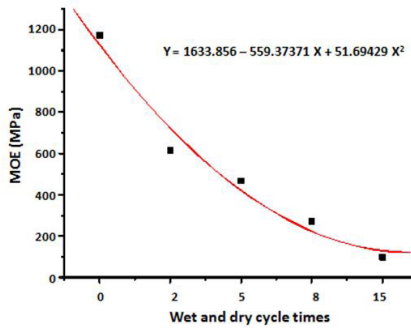


Fig. 11: Effects of wet and dry cycles on MOE.

Fitting results are analyzed as follows. Tab. 1 showed the correlation coefficients between  $E_b$  and  $n = 0.972$ , indicating high correlation between them. At the same time, the table showed the value of standard deviation and fitting deviation were big because of the limited times of wet and dry circle. But in the actual use, the requirements about MOE of the panel itself was not high, and furthermore, MOE of the panel was able to meet the standard requirements for wood-wool panel even with  $n = 8$ . So the simulation results were applicable for a rough estimate of MOE of the panel value with  $n \leq 15$  in engineering application.

Tab. 1: Analysis of fitting results between MOE and wet and dry cycles.

			Y = A + B * X
Parameter	Results	Deviation	
A	1633.856	208.429	
B	-559.371	158.837	
Correlation coefficient R	SD	Number of parameters (N)	P
0.972	97.181	5	< 0.027

**Analysis of sound absorption properties**

A large number of experimental specimens were used, and the following four typical sound absorption characteristics were found.

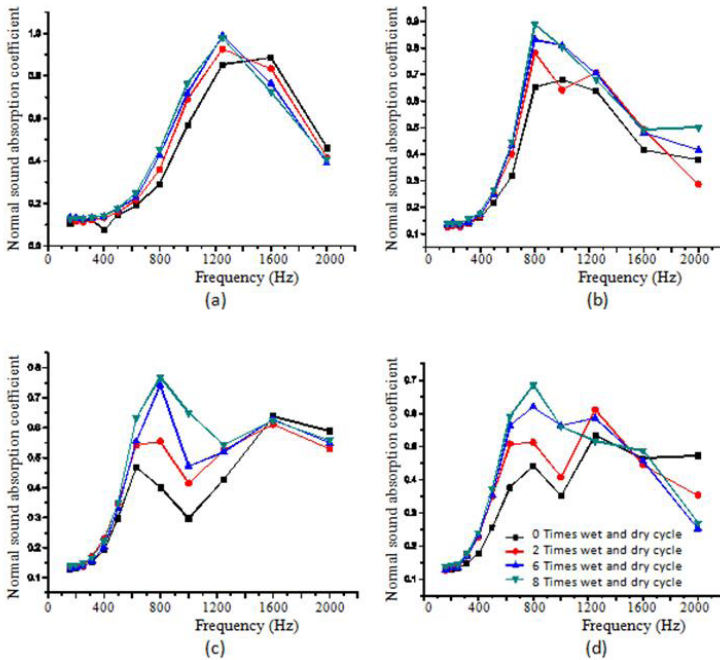


Fig. 12: Four typical sound absorption properties.

In Fig. 12a: (1) the peak value of absorption coefficient before/after wet and dry cycles were at  $f = 1600$  Hz,  $f = 1200$  Hz respectively, that was, after wet-dry cycle the panel's sound coefficient peak value shifted to lower frequency; (2) the panel's sound absorption performance was poor when  $f \leq 600$  Hz.

In Fig. 12b: (1) both the peak value of absorption coefficient before/after wet and dry cycles were at  $f = 800$  Hz; (2) with the increase of  $n$ , sound absorption coefficients at the stage of  $f \leq 800$  Hz continued to improve which was less clear at high frequencies.

In Fig. 12c: (1) there were two peak values of absorption coefficient before /after wet and dry cycles, and the first peak value transferred from 600 Hz to 800 Hz after wet and dry circles. Both the valley values appeared at 1000 Hz; (2) the panel's sound absorption performance was poor when  $f \leq 600$  Hz. (3) before the stage of  $f \leq 1000$  Hz, the absorption coefficient increased substantially with the increase of  $n$ .

In Fig. 12d: (1) there were two peak values of absorption coefficient before/after wet and dry cycles, and the first peak value transferred from 800 Hz to 1250 Hz after wet and dry circles; (2) the panel's sound absorption coefficients increased with the increase of  $n$ , and the value decreases rapidly when  $f = 2000$  Hz.

The following two points were reached by comparing this four figures: (1) poor low frequency sound absorption performance were presented with the increase of  $n$ , but the trend was not apparent at the frequency channel of high frequency; (2) The main difference between the four typical sound absorption characteristic diagrams was that the first two contains only one peak while the latter two peaks.

Mechanism analysis: during the process of wet and dry cycle, the crystal hydration product was hydrolyzed and generated  $Mg(OH)_2$  when the panel was soaked in water because of its high solubility in water, and the  $Mg(OH)_2$  was a bulk crystal (Yang 1999) with layered structure and hardened body much lower in intensity which was composed of the rod-like gel 5-phase crystals and the sharp needle-shaped 3-phase crystals. On the other hand, wood-wool's moisture expansion would result in swelling stress, when 5-phase and 3-phase crystals dissolved, the strength of the panel was lower than the swelling stress, then the panel's deformation was produced, thus the panel's strength decreased rapidly. Therefore, the strength loss of magnesium oxychloride cement wood-wool panel was not only due to the physical action of water, but also mainly led by the solubility characteristics of 5-phase and 3-phase crystals and wood-wool's swelling stress (Delany and Bazley 1970).

## CONCLUSIONS

This paper examined effect of wet and dry cycle on thickness swelling, MOE and normal sound absorption coefficient of the panel from the macro and micro perspective and explored oxychloride changes of microstructure of magnesium cement hydration product during the wet and dry cycle process. The following conclusions were shown as follows:

(1) After the wet and dry cycles, MOE and thickness swelling of the specimens decreased, and with the increase of wet and dry cycles, the decline decreased; the average absorption coefficient of the specimen increased, mainly due to the increased plate thickness and magnesium oxychloride cement in 5-phase crystal structure changes, the porosity increased. The absorption coefficient of the plate were particularly sensitive to the microstructure of the panel, But on the whole, the low-frequency sound absorption property of magnesia-bonded wood-wool panel was poor. At around 1000 Hz, sound absorption property of the panel was the best which applied to sound insulation for civil building.

(2) For the magnesium oxychloride cement before/after wet-dry cycles, the ARD and SEM results showed that: with the increase of wet and dry cycles, magnesium oxychloride cement  $Mg(OH)_2$  crystals gradually reduced, and finally almost completely disappeared, hydrolysis of 3-phase double salt crystals occurred in the soaking process, the five-phase double salt crystals gradually increased. However, after the wet and dry cycles, disappear of  $Mg(OH)_2$  in the panel crystals of ledto pore diameter in magnesium oxychloride cement larger, the crystal structure of a 5-phase complex salt crystals from the original high strength and gelled into a rod from gap around the radial centre of the structure to improve the strength of the panel, which led to an increase in 5-phase complex salt crystals, but the physical strength of the panel was reduced.

## ACKNOWLEDGEMENTS

This study was funded by northern Jiangsu scientific and technological development plan of China (BC2012417). The authors would also like to thank the support of the Priority Academic Program Development of Jiangsu Higher Education Institutions of China.

## REFERENCES

1. China Building Material Academy, 2003: Green building material and technologies reaching it. Chemical Industry Press, Beijing.
2. Chen, X., Cao, J., Liu, Y., 1996: Looking into the ways of solving water tolerant behaviour of magnesite materials. *Hunan Chemical Industry* 26(3): 34-37.
3. Deng, D., 2003: The mechanism for soluble phosphates to improve the water resistance of magnesium oxychloride cement. *Cement and Concrete Research* 33 (9): 1311-1317.
4. Deng, D., Zhang, C., 1996: Theoretical mechanism of hygroscopicity of magnesium oxychloride cement and technical methods to lower it. *Neo-Building Materials* (10): 24-27.
5. Delany, M.E., Bazley, E.N., 1970: Acoustic properties of fibrous absorbent materials. *Applied Acoustics* (3): 105-116.
6. Guan, F., Ba, H., 2009: Study on phase stability of magnesium oxychloride cement. *Journal of Harbin Engineering University* 30(11): 1213-1218 (in Chinese).
7. China Standards Press, 2014: Standard complication of cement products in building materials. *China Concrete and Cement Products* (2): 43 (in Chinese).
8. Ji, Y., Wu, Z., Zhang, F., 1995: Influence of the additive on the microstructure and performance of the new water-resisting magnesium cement. *Journal of Inorganic Materials* 10(2): 241-247.
9. Jiang, J., Luo, Y., Lan, X., 2002: Novel thermal insulation and soundproofing building material. Chemical Industry Press, Beijing.
10. Matkovic, B., Yong, J.F., 1973: Microstructure of magnesium oxychloride cements. *Natural Physical Science* 246: 79-80.
11. Na, B., Wang, Z., Wang, H., Lu, X., 2012: Study on improvement of hygroscopicity property of low density magnesia-bonded wood-wool panel. *Journal of Building Materials* 15(5): 660-664 (in Chinese).
12. Na, B., Zhao, Y., Wang, Z., Lu, X., 2013: Effects of additives on mechanical property and hygroscopicity property of low density magnesia-bonded wood wool-panel. *Journal of Northwest Forestry University* 28(2): 168-172 (in Chinese).
13. Na, B., Wang, Z., Wang, H., Ding T., Lu, X., 2014a: Study on hydration mechanism of low density magnesia-bonded wood wool panel. *Wood Research* 59(1): 137-148.
14. Na, B., Wang, Z., Wang, H., Lu, X., 2014b: Wood-cement compatibility review. *Wood Research* 59(5): 813-826.
15. Na, B., Wang, H., Ding, T., Lu, X., 2018: Study on factors affecting the sound absorption property of magnesia-bonded wood wool panel. *Wood Research* 63(4): 617-624.
16. Pan, G., Zhao, Z., Liu, Ch., 1984: Chemical reactive manual. Liaoning People's Publishing House 5: 26-30 (in Chinese).
17. Simatupang, M.H., Geimer, R.L., 1990: Inorganic binder for wood composites: feasibility and limitations. In: *Wood Adhesives 1990*. Wisconsin, 8 pp.
18. Shuxing, J., 2011: Study on hydration phase and microscopic characteristic of the composite magnesium oxychloride cement. *Non-Metallic Mines* 34(5): 42-44 (in Chinese).
19. Tu, P., 1996: Application of water in magnesium oxychloride cementitious material. *China Building Materials* (2): 42-43 (in Chinese).
20. Tong, Y., 1995: Study on factors affecting the water resistance property of magnesium oxychloride cement by orthogonal experiment. *New Building Materials* (2): 42-43 (in Chinese).

21. Xia, S., Wang, J., Huang, J., Chen, R., 1994: Influence of additives on dimensional stability of magnesium oxychloride cement. *Journal of Salt & Chemical Industry* 23(6): 18-22.
22. Yang, S., 1999: Thermal insulation and soundproofing building material. China Planning Press, Beijing.
23. Wang, Z., Sun, D., Chen, X., Zhao, X., Na, B., Lu, X., 2013a: Study on the sound absorption and thermal conductivity properties of low density magnesia-bonded wood wool panel. *Journal of Southwest Forestry University* 33(3): 97-101.
24. Wang, Z., Sun, D., Chen, X., LiQ, Liu H., 2013b: Steam-pressing mechanism of low density magnesia-bonded wood wool panel. *Journal of Northwest Forestry University* 28(6): 165-168.
25. Zhu, Z., Dong, X., Yiong, X., Cao P., 1994: Study on MgO-MgCl<sub>2</sub>-H<sub>2</sub>O solid phase system. *Journal of Shandong Institute of building materials* 8(1): 8-18.

\*BIN NA, HAIQING WANG, TAO DING, XIAOLING LU  
COLLEGE OF MATERIALS SCIENCE AND ENGINEERING  
NANJING FORESTRY UNIVERSITY  
NANJING, 210037  
CHINA

\*Corresponding author: nabin8691@126.com

## **GENETIC AND SELECTION ASSESSMENT OF THE SCOTS PINE (*PINUS SYLVESTRIS* L.) IN FOREST SEED ORCHARDS**

ELVIRA KHANOVA, VLADIMIR KONOVALOV, AZAT TIMERYANOV  
REGINA ISYANYULOVA, DINA RAFIKOVA  
BASHKIR STATE AGRARIAN UNIVERSITY  
UFA, RUSSIA

(RECEIVED AUGUST 2019)

### **ABSTRACT**

Cultivation of highly productive stands of the Scots pine is a priority task of the forestry industry. This task should be solved using the methods based on the molecular genetic analysis. Following these methods carefully will allow improving the work quality and efficiency in the forest seed farming, to control successfully the stand phytosanitary condition, as well as to use DNA markers in the in vitro culture reproduction of tree species. Our studies have shown a high level of the Scots pine genetic diversity in forest seed orchards, which is confirmed by insignificant spread of values between similar studied characteristics when analyzing the Scots pine with high morphological characteristics, selected from natural populations. Thus, genetic monitoring of the objects of permanent forest seed base of this tree species should be introduced into practice of the forest selection seed farming.

**KEYWORDS:** Gene resources, forest seed orchards, clone, plus tree, stand origin, genetic markers.

### **INTRODUCTION**

An urgent problem of the forest seed selection farming is the search for effective measures to preserve the gene of valuable forest-forming tree species (Ivanovskaia 2004, Tsarev 2013, Vidiakin 2003), especially coniferous ones (Tsarev 2006, Vidiakin 2008).

Forest seed farming involves a number of measures to create a forest seed base on the selection and genetic basis for cultivation of highly productive and sustainable forest stands (Redko et al. 2008).

The work under Federal Target Program "Development of forest seed selection farming for the period 2009-2020" (The Federal Target Program of the Forest Seed Production development

for the period from 2009 to 2020 2009) resulted in entity generation of a high quality unified genetic and selection complex of, including forest seed orchards (FSO), created by using vegetative and seed material of plus and elite trees. Therefore, one of the priority areas is the study and assessment of the selected plus forest gene, and proposals for further forest seed farming development (Besschetnov and Besschetnova 2012, Ivanovskaia 2014, Vidiakin 2010).

The most important condition for maintaining forest ecosystems resistance to external forcing (climatic, anthropogenic) is the conservation and reproduction of biodiversity (Gabbrakhimov et al. 2015, Sultanova et al. 2018). Special attention in solving this problem should be paid to the study of the intraspecific and genetic potential of the main forest-forming species of woody plants, the Scots pine (*Pinus sylvestris*) being one of them (Prishnivskaia et al. 2016). The ability of a population to adapt to extreme environmental conditions in the process of natural selection depends on its genetic diversity. At low rates of intrapopulation polymorphism, the number of possible combinations of genes promoting adaptation to the environment decreases, which reduces the possibility of new adapted genotypes to occur in this population (Copenheaver et al. 2002, Wieser et al. 2018). Thus, the population in natural conditions should have an appropriate level of genetic diversity to be able to survive under the pressure of constantly changing biotic and abiotic components of the ecosystem (Grushetskaia et al. 2013).

The problem of the genetic diversity conservation should not be disregarded when implementing tree species breeding programs. During different selection cycles phenotypic selection and production of seeds and seedlings should be done very carefully (El-Kassaby 1995). Otherwise, at the stage of phenotypic selection the level of genetic diversity can be reduced.

Genetic diversity defines the ability of living organisms to adapt to environmental changes and determines the variability of their features and properties.

However, different kinds of variance are not sufficiently used in economic activities, which may finally lead to the genetic potential constriction of forest seed objects. Thus, making correct selection and characterization of genetic resources are the main tasks in modern woody plants selection (Shigapova and Shigapov 2009, Swamy et al. 2018).

Use of the Ex Situ method can help to preserve the forest species genetic diversity (Feng et al. 2006). Clone and seed plantations are the center of the conservation of forest genetic resources, as the relationship between the population size and the percentage of the retained heterozygosity are reduced to a minimum loss of the total additive genetic variance. Kajba (Kajba and Andric 2019) notes that in Croatia they have started the works on the phenotypic selection and vegetative reproduction of plus trees. In addition, in order to produce forest seeds of high genetic quality, the creation of clone plantations has been started. That was the beginning of the genetic assessment of mother trees and of genotypic selection in order to obtain higher genetic growth.

Up to the present moment, most researches on the Scots pine genetic variance have been aimed to study the growth (DeSiervo et al. 2018), morphological characteristics (Copenheaver et al. 2002, Seo et al. 2013) and plantability of this species (Porth and El-Kassaby 2014). The studies of genetic variance are mainly concentrated on the isoenzymes analysis. Some articles describe species variance at the DNA level, as well as of the variance of the genes encoding ribosomal units. Outstanding features of the DNA analysis technology are its high informative value, no need for genome pre-sequencing to develop primers, possible primers universality for different species, and relatively low cost. The ISSR technology is considered to be reliable due to the use of longer primers (Nkongolo et al. 2002).

Reliability of the phenotypic evaluation of the genotype in forest selection research works is most commonly identified with the assessment of genetic polymorphism. Evaluation of genetic polymorphism is becoming more common in the forest breeding science. Genetic variance helps

to determine the resistance of forest stands to environmental conditions. It is also a source of information for the improvement of breeding programs (Zheng et al. 2015).

The method of studying forest seed farming includes the work on valuable tree species breeding, their accounting and gene resource analysis. Relaxation of the forest stands gene resource is primarily associated with such phenomena as inbreeding and reduction of climax forest with representative genes bank. As a whole, all this can lead to a decrease in the stands resistance to environmental conditions and to human impact.

With reference to the above mentioned, the issue of natural gene resource conservation in order to enhance breeding properties of tree species is becoming a priority in the research in the field of genetics and selection of woody plants.

The aim of the study was to determine the genetic variance of the Scots pine clones at the sites of a unified genetic-breeding complex, including forest seed orchards (FSO). For this purpose, the following tasks were set and successfully solved: one-site investigation of FSO and definition of their main mensurational indicators; collection of needles from the Scots pine clones for further genetic analysis and DNA isolation; polymerase chain reaction with the use of five ISSR primers; electrophoretic separation of polymerase chain reaction products (PCR); data analysis and development of recommendations.

## MATERIALS AND METHODS

### Research object.

The research was conducted in forest seed orchards of vegetative origin (1980-1989), located in Angasiaksk forest division of the Diurtiuli district forestry of the Republic of Bashkortostan.

### Data collection and analysis.

The research was based on the sample plot method. All sample plots were laid and processed by general forest inventory methods. The data were processed by the methods of variation statistics and with the use of the Statistica 6 software package. For laboratory research on the scientific problem to be developed, source material was selected by the recommended CTAB method (Cetyl Trimethyl Ammonium Bromidium) (El-Kassaby 1995). Fresh needles of the Scots pine from seed plantations were used as a source material for genetic studies.

While studying seed production patterns of the Scots pine clones we carried out the works on the phenological observation of the process. Seed production level was assessed according to three phases: early flowering of reproductive organs, seed-bud early formation and conelet early formation inside the clone.

Tab. 1 presents a brief description of five ISSR primers which were used to isolate DNA from needles.

*Tab. 1: Characteristics of the used ISSR-primers.*

No.	Primer	Sequence (5-3)
1	(CA) <sub>6</sub> AGCT	CACACACACAAGCT
2	(CA) <sub>6</sub> AG	CACACACACAAGG
3	(CA) <sub>6</sub> GT	CACACACACAGT
4	(CA) <sub>6</sub> AS	CACACACACAAC
5	(AG) <sub>8</sub> T	AGAGAGAGAGAGAGT

The experimental part of the study on the polymerase chain reaction evaluation was carried out using test tubes with the MJ Mini™ Gradient Thermal Cycler (BIO-RAD) amplifier. The recommended Encyclo PCR reagents kit was used for the experiments.

Basic requirements met at the laboratory research stage were as follow: the reaction mixture of 10 µl contained 1 µl of PCR buffer; 0.2 µl of 10 Mm dNTPs; 0.1 µl of 100 µM of primer; 1 µl of DNA sample; 0.1 µl of Taq polymerase (2 u/µl); 7.6 µl of water. The following amplification regime was chosen: 5 min denaturation at 94°C; 0.5 min denaturation at 94°C; 45 sec annealing (45 - 60°C); 2 min elongation at 72°C; 7 min extension at 72°C. The entire amplification process consisted of 45 successive cycles.

Later the separation of PCR products was carried out. It was carried out during 45-60 min in a horizontal electrophoretic chamber (Power Pac™ Universal (BIO-RAD)) using 1.5% agarose gel and adding ethidium bromide at a voltage of 70 mV. DNA 100+DNALadder length mark was laid out in the farthest track. TVE buffer in the form of a complex mixture was used for electrophoresis: tris-HCl (pH = 8.3) – 12.1 g; boric acid – 5.1 g; EDTA (sodium salt) – 0.37 g; distilled water – 1000 ml.

DNA visualization, processing and analysis of the obtained images were performed using GelDoc 2000 (BIO-RAD) gel-documentation system and Quantity One® Version 4.6.3 software package.

Popgene Version 1.32 program was used to calculate genetic parameters of the Scots pine trees. The program determines the proportion of polymorphic loci, the total (observed) number of alleles (na), the effective number of alleles (ne), Ney genetic diversity (N), the proportion of interpopulation genetic diversity in the total diversity, or the population subdivision index (Gst). Having analyzed the electrophoregrams, a binary matrix was compiled. "1" was the symbol to mark the present PCR fragments of the matrix and "0"- for the missing ones.

## RESULTS

The studied stands of the Scots pine proved to be high-bonitat plantings clean in composition. The main forest inventory indicators of the stands are presented in Tab. 2.

Tab. 2: Biometric indicators of the Scots pine seed plantations.

Indicators	M	± m	σ	V, %	P, %
FSP (Forest Seed Plantation) No. 32					
Trunk diameter, cm	25.01	1.21	4.86	19.43	4.84
Bole height, m	14.98	0.64	2.70	18.02	4.27
Crown width, m	6.62	0.30	1.80	27.19	4.53
Crown length, m	13.01	0.62	5.50	42.28	4.77
FSP No. 18					
Trunk diameter, cm	27.79	1.88	4.52	16.26	6.77
Bole height, m	17.14	0.82	3.10	18.09	4.78
Crown width, m	8.04	0.58	1.90	23.63	7.21
Crown length, m	14.24	0.90	6.30	44.24	6.32
FSP No. 24					
Trunk diameter, cm	32.33	1.94	4.76	14.72	6.00
Bole height, m	13.50	0.92	2.26	16.74	6.81

Crown width, m	10.25	0.78	1.92	18.73	7.61
Crown length, m	10.67	0.72	7.10	66.54	6.75
FSP No. 28					
Trunk diameter, cm	37.42	1.59	3.90	10.42	4.25
Bole height, m	12.75	0.57	1.41	11.06	4.47
Crown width, m	9.83	0.40	0.99	10.07	4.07
Crown length, m	12.31	0.89	5.90	47.93	7.23

The main indicators of the Scots pine stands in forest seed plantations are characterized by high features variability under identical growth conditions. The height variability coefficient within clones varies from 11.06% to 18.09%, the diameter coefficient from 10.42% to 19.43%, the crown diameter from 10.07% to 27.19%, the crown length variability coefficient varies from 42.28% to 66.54%. The studied stands are generally characterized by a good trunk state and crown development.

During the phenological observation it was noted that the studied clones of the Scots pine growing in the forest seed orchard No. 32 of vegetative origin are characterized by a high rate of seed-bud and conelet formation. The main morphometric features of conelets are given in Tab. 3.

Tab. 3: Main indicators of the Scots pine conelets.

Characteristics to be measured	Average statistical values				
	M	$\pm m$	$\sigma$	V (%)	P (%)
Length, cm	5.1	0.1	1.02	20.0	2.0
Diameter, cm.	3.5	0.11	0.65	13.3	2.2
Weight, g	16.4	0.68	4.22	25.7	4.1

The greatest variability is characteristic for the conelets weighing ( $V = 25.7\%$ ). The conelets length and width are more stable ( $V = 20.0\%$  and  $13.3\%$  respectively). When the variability values of the conelets linear indicators are low, their weight ranges greatly. This is due to a large amount of empty and germless seeds inside the conelets.

According to the results of the ISSR-analysis of DNA isolated from the Scots pine needles, the following results were obtained: 96 amplified fragments were identified when using five ISSR primers. 20 of these 96 fragments are accounted for (CA)  $6AGCT$  and (CA)  $6GT$ , 23 – for (CA)  $6AG$ , 18 – for (CA)  $6AS$ , 15 – for (AG)  $8T$ . The results of DNA analysis of the Scots pine are shown in Tab. 4.

Tab. 4: Results of PCR analysis of the Scots pine trees DNA.

Primer	The number of DNA fragments		Amplified fragments size, bp
	Totally	polymorphic	
(SA) $6AGCT$	20	16	230 -1220
(CA) $6AG$	23	20	200 - 1270
(CA) $6GT$	20	17	260 - 1240
(CA) $6AS$	18	14	230 - 1700
(AG) $8T$	15	12	290 - 1200
Totally	96	79	200 - 1700

The share of polymorphic loci varied from 12 to 20 DNA fragments. 96 DNA fragments were isolated in total, 79 of them being polymorphic ones. The variability in the size of DNA fragments ranged from 200 to 1700 nucleotide pairs.

According to the results of the analysis and estimation of the clones' genetic variability conducted on the FSP to be studied, we managed to establish the occurrence frequency of alleles of the detected loci. It was found that the effective number of alleles ( $N_e$ ) on the studied seed plantations was 1.385. The total genetic diversity ( $H$ ) amounted to 0.239.

## DISCUSSION

At present, the method of molecular genetic analysis is increasingly used to identify the most valuable forest plantations in regard to genetics, to identify individual forms of tree species with high trunk quality, growth rate and other valuable features. This method allows estimating the level of genetic diversity in natural populations and its possible losses during artificial reforestation (Tsarev 2006). It also helps to identify populations from different geographical regions, to determine the level of stands inbreeding, to appreciate genetic quality of their seeds (Sheikina 2014), as well as to identify plants resistant to pathogens and various pollutants (Feng et al. 2006, Hui-yu et al. 2005, Sultanova et al. 2018). The purpose of the practical application of molecular genetic analysis is not only to assess the genetic resources state of, but also to develop a strategy for the genetic diversity conservation of an appropriate species (DeSiervo et al. 2018, Provan et al. 1998).

According to (Ivanovskaia 2014), a reliable parameter characterizing the level of genetic variability of indicators of the tree species population is average heterozygosity which can be observed  $H_o$  (actual) and expected  $H_e$  (calculated from allele frequencies). It is important to take into account the size of the samples of the studied tree species. They should be representative, which will ensure high accuracy of calculating the average value of the observed and expected heterozygosity.

When assessing the level of genetic variability of the Scots pine phenotypic characteristics, we paid attention to research articles of scientists dealing with this problem. Thus, in the studies of (Novikov and Sheikina 2012) the value of the average expected heterozygosity  $H_e$  in plus Scots pine stands was 0.273. According to the studies of Ivanovskaya S. I., the same value was equal to 0.250 (Ivanovskaia 2014). In the work of Nowakowska J. this parameter was 0.289 (Nowakowska et al. 2014). Comparative data on the levels of genetic variability of the Scots pine trees on forest seed sites are given in Tab. 5.

Tab. 5: Main indicators of genetic variability.

Indicators of genetic variability	Research data	Novikov, Sheikina (2012)	Ivanovskaia (2014)	Nowakowska (2014)
Share of polymorphic loci (P,%)	82	94	85	84
Expected heterozygosity ( $H_e$ )	0.239	0.273	0.250	0.289

Thus, the results of the study prove a high level of genetic diversity and variability of stands of the Scots pine on the studied seed plantations created by vegetative material. This fact is confirmed by slight differences between the final data of our studies and the data of other scientists (Tab. 5). It should be noted that the level of genetic variability of trees on forest seed sites is not inferior to the level of genetic variability detected in Italy ( $H_e = 0.347$ ) (Copenheaver

et al. 2002), Romania and Sweden ( $H_e = 0.297$ ) (Floran et al. 2010), Finland ( $H_e = 0.312$ ) (Zheng et al. 2015), Scotland and Spain ( $H_e = 0.297$ ) (Provan et al. 1998).

The most important condition for obtaining genetic diversity of tree species is the presence on the forest seed plantations of such number of unlike clones as necessary to ensure a high level of genetic variability (Feng et al. 2006, Kajba and Andric 2019, Seo et al. 2013). Average values of heterozygosity of the Scots pine grown on forest seed plantations differ significantly from the same values of this species grown in natural populations (Floran et al. 2010, Nowakowska et al. 2014).

According to Wójkiewicz et al. (2016), a better understanding of the formation of the Scots pine population is important in developing programs to conserve the species genetic resources as well as evaluating the role of natural selection across the species' range.

The Scots pine is characterized by a high level of population genetic diversity and a low divergence degree within the species in the studied part of the area (Raj et al. 2006, Wieser et al. 2018). Seo et al. (2013) in his studies gives the analysis to the nature of rare alleles spacing and of the distribution of intraspecific genetic diversification, which is illustrative of relative gene resources throughout the species range. The Scots pine populations exchange genetic material to support the genetic basis of the species as a whole (Nkongolo et al. 2002). The results of our research on the PCR analysis of the Scots pine trees DNA are confirmed by Hui-yu (Hui-yu et al. 2005).

Authors proved great importance of molecular genetic analysis when studying gene resources of populations (Copenheaver et al. 2002, Feng et al. 2006, Kajba and Andric 2019). Based on these studies, it is possible to determine the main characteristics of the main forest-forming species.

Z. Hong, M. R. G Gil note that studies which are based on the genetic approach will allow to understand the essence of the influence of natural selection on the genomic patterns of forest tree species, to gain new knowledge about the evolutionary processes that affect the nature of pine genetic variability.

## CONCLUSIONS

Molecular genetic analysis with the use of ISSR-markers allowed us to obtain new data on the gene resources state of the Scots pine on forest seed plantations of the Republic of Bashkortostan. On the basis of our studies we revealed that the effective number of alleles ( $N_e$ ) on the studied seed plantations was 1.385. The total genetic diversity ( $H$ ) amounted to 0.239. The share of polymorphic loci varied from 12 to 20 DNA fragments. 96 DNA fragments were isolated in total, 79 of them being polymorphic ones.

The results of our research prove a high degree of genetic variability of the Scots pine clones, which suggests that vegetative material for seed plantations was chosen properly. Continuous monitoring of forest seed objects at genetic and breeding level is necessary in order to conserve high-quality gene resources of the Scots pine tree species. When creating new objects of a unified genetic and breeding complex, it is necessary to provide intensive control on the quality and genetic diversity of the planting material.

## REFERENCES

1. Belletti, P., Ferrazzini, D., Piotti, A., Monteleone, I., Ducci, F., 2012: Genetic variation and divergence in Scots pine (*Pinus sylvestris* L.) within its natural range in Italy. *European Journal of Forest Research* 131(4): 1127-1138.
2. Besschetnov, V., Besschetnova, N., 2012: Complex assessment of the Scots pine plus trees according to their needles parameters. *Bulletin of Kazan State University* 2(24): 88-91.
3. Copenheaver, C., Grinter, E., Lorber, J., Neatrour, M., Spinney, M., 2002: A dendroecological and dendroclimatic analysis of *Pinus virginiana* and *Pinus rigida* at two slope positions in the Virginia Piedmont. *Costanea* 67(3): 302-315.
4. DeSiervo, M., Jules, E., Bost, D., De Stigter, E., Butz, R., 2018: Patterns and drivers of recent tree mortality in diverse conifer forests of the Klamath mountains, California. *Forest Science* 64(4): 371-382.
5. Doyle, J.J., Doyle, J.L., 1987: A rapid DNA isolation procedure for small quantities of fresh leaf tissue. *Phytochemical Bulletin* 19: 11-15.
6. El-Kassaby, Y., Namkoong, G., 1995: Genetic diversity of forest tree plantations: consequences of domestication. In: *Consequences of changes in biodiversity*. IUFRO World Congress, Tampere, Finland 2: 218-228.
7. Feng, F., Han, S., Wang, H., 2006: Genetic diversity and genetic differentiation of natural *Pinus koraiensis* population. *Journal of Forestry Research* 17(1): 21-24.
8. Floran, V., Ganea, S., Sestras, R., Rosario, M., Gil, G., 2010: Genetic variability in populations of Scots pine from Romania and Sweden. *Bulletin of University of Agricultural Sciences and Veterinary Medicine Cluj-Napoca. Horticulture* 67(1): 481.
9. Gabdrakhimov, K., Khairtdinov, A., Sultanova, R., Konashova, S., Kononov, V., Sabirzianov, I., Gabelkhakov, A., Isianiulova, R., Martynova, M., Blonskaia, L., 2018: Reproduction of stable pine forests in the Southern Urals. *Journal of Engineering and Applied Sciences* 13(S8): 6494-6499.
10. Gil, M.R.G., Floran, V., Östlund, L., Gull, B.A., 2015: Genetic diversity and inbreeding in natural and managed populations of Scots pine. *Tree genetics & genomes* 11(2): 28.
11. Grushetskaia, Z., Nikitinskaia, T., Kubrak, S., Dziuban, O., Kukhareva, L., Poliksenova, V., Titok, V., Lemesh, V., Parfenov, V., Khotyleva, L., 2013: The use of the ISSR analysis for the study of intra- and interspecific genetic polymorphism of different taxa of higher plants. *Bulletin of Bashkir State Agrarian University* 1(3): 50-56.
12. Hong, Z., Fries, A., Wu, H.X., 2015: Age trend of heritability, genetic correlation, and efficiency of early selection for wood quality traits in Scots pine. *Canadian Journal of Forest Research* 45(7): 817-825.
13. Huiquan, Z., Hongjing, D., Dehuo, Hu, Yun, L., Yubao, H., 2015: Genotypic variation of *Cunninghamia lanceolata* revealed by phenotypic traits and SRAP markers. *Dendrobiology* 74: 85-94.
14. Hui-yu, L., Jing, J., Gui-frng, L., Xu-jun, M., Jing-Xiang, D., Shi-Jie, L., 2005: Genetic variation and division of *Pinus sylvestris* provenances by ISSR markers. *Journal of Forest Research* 16(3): 216-218.
15. Iarullin, R., Aipov, R., Gabitov, I., Linenko, A., Akchurin, S., Safin, R., Mudarisov, S., Khasanov, E., Rakhimov, Z., Rakhimov, Z., Masalimov, I., 2018: Adjustable driver of grain cleaning vibro-machine with vertical axis of eccentric masses rotation. *Journal of Engineering and Applied Sciences* 13: 6398-6406.

16. Ivanovskaia, S., 2014: Evaluation of the gene resources of the Scots pine (*Pinus sylvestris* L.) in the plus stands of Belarus according to isoenzyme analysis. Proceedings of Bryansk State Technical University. Forestry 165(1): 130-134.
17. Kajba, D., Andric, I., 2019: Ex situ conservation. Case study Croatia. Forests of Southeast Europe under a Changing Climate 5: 259-269.
18. Nkongolo, K., Michael, P., Gratton, W., 2002: Identification and characterization of RAPD markers inferring genetic relationships among pine species 45(1): 51-58.
19. Novikov, P., Sheikina, O., 2012: The ISSR-analysis of the Scots pine trees (*Pinus sylvestris*) of different breeding categories. Scientific journal of Kuban State Agrarian University 82(8): 100-112.
20. Nowakowska, J., Zachara, T., Konecka, A., 2014: Genetic variability of Scots pine (*Pinus sylvestris* L.) and Norway spruce (*Picea abies* L. Karst.) natural regeneration compared with their maternal standards. Forest Research Papers 75(1): 47-54.
21. Porth, I., El-Kassaby, Y., 2014: Assessment of the genetic diversity in forest tree populations using molecular markers. Diversity 6(2): 283-295.
22. Prishnivskaia, I., Nechaev, I., Krasilnikov, V., Boronnikova, S., 2016: Molecular and genetic analysis of four populations of the *Pinus sylvestris* L. in the East of the Russian Plain on the basis of polymorphism of ISSR markers. Bulletin of Orenburg State University 2(190): 88-93.
23. Provan, J., Soranzo, N., Wilson, N., McNicol, J., Forrest, G., Cottrell, J., Powell, W., 1998: Gene-pool variation in caledonian and European Scots pine (*Pinus sylvestris* L.) revealed by chloroplast simple-sequence repeats. Proceedings. Biological Sciences 265(1407): 697-705.
24. Raj, D., Govindaraju, D., Orians, C., 2006: Genetic variation among pitch pine *Pinus rigida* families from Walden Woods: heritability and path analysis of developmental variation of phenotypic traits. Rhodora 108(936): 356-369.
25. Redko, G., Merzlenko, M., Babich, N., Danilov, I., 2008: Forest crops and protective afforestation. Publishing center "Academy". Moscow, 400 pp.
26. Scalfi, M., Piotti, A., Rossi, M., Piovani, A., 2009: Genetic variability of Italian Southern Scots pine (*Pinus sylvestris* L.) populations: the rear edge of the range. European Journal of Forest Research 128(4): 377-386.
27. Seo, Y., Lee, Y., Lumbres, R., Pyo, J., Kim, R., Son, Y., 2013: Influence of stand age class on biomass expansion factor and allometric equations for *Pinus rigida* plantations in South Korea. Scandinavian Journal of Forest Research 28(6): 566-573.
28. Sheikina, O., 2014: Forest biotechnology. Study guide. Ministry of Education and Science of the Russian Federation, Federal State Budgetary Educational Institution of Higher Professional Education Povolzhskiy State Technological University. Ioshkar-Ola, 76 pp.
29. Shigapova, A., Shigapov, Z., 2009: Genetic diversity of the Scots pine populations *Pinus sylvestris* L. Bulletin of Orenburg State University 6: 445-447.
30. Sultanova, R., Gabdrakhimov, K., Khairtdinov, A., Konashova, S., Konovalov, V., Blonskaia, L., Sabirzianov, I., Martynova, M., Isianiulova, R., Gabdelkhakov, A., 2018: Evaluation of ecological potential of forests. Journal of Engineering and Applied Science 13(S8): 6590-6596.
31. Swamy, L., Drazen, E., Johnson, W., Bukoski, J., 2018: The future of tropical forests under the United Nations sustainable development goals. Journal of Sustainable Forestry 37(2): 221-256.
32. The Federal Target Program of the Forest Seed Production development for the period from 2009 to 2020, 2009. Federal Forestry Agency. Moscow, 86 pp.

33. Tsarev, A., 2013: Forest breeding programs (in Russia and abroad). Monograph. Moscow State Forest University. Moscow, 164 pp.
34. Tsarev, A., Laur, N., 2006: Issues and problems of plus-breeding. Forest bulletin 9(3): 118-123.
35. Vidiakin, A., 2003: Problems of the conservation of genetic diversity of forest woody plants and some ways to solve them on the example of the Scots pine (*Pinus sylvestris* L.). Selection, genetic resources and conservation of the gene resources of forest woody plants (the Vavilov readings). Collection of scientific articles of Forest Institute of the National Academy of Sciences of Belarus. Gomel. Forest Institute of the National Academy of Sciences of Belarus 59(1): 98-101.
36. Vidiakin, A., 2008: Pine and spruce plus breeding: results and prospects of the development. Forestry information. In: Proceedings of scientific and technical conference on forestry 3(4): 33-38.
37. Vidiakin, A., Shigapov, I., 2010: Efficiency of woody plants plus breeding. The conifers of the boreal zone 27(1/2): 18-24.
38. Wieser, G., Gruber, A., Oberhuber, W., 2018: Growing season water balance of an inner alpine Scots pine (*Pinus sylvestris* L.) forest. IForest 11(4): 469-475.
39. Wójkiewicz, B., Cavers, S., Wachowiak, W., 2016: Current approaches and perspectives in population genetics of Scots pine (*Pinus sylvestris* L.). Forest Science 62(3): 343-354.

ELVIRA KHANOVA\*, VLADIMIR KONOVALOV, AZAT TIMERYANOV  
REGINA ISYANYULOVA, DINA RAFIKOVA  
FEDERAL STATE BUDGETARY EDUCATIONAL INSTITUTION OF HIGHER EDUCATION  
BASHKIR STATE AGRARIAN UNIVERSITY  
50-LETIIA OKTIABRIA ST., 34  
450001 UFA  
RUSSIA

\*Corresponding author: elvirakhanova@rambler.ru

## **MECHANICAL PROPERTIES AND SET RECOVERY OF COMPRESSED POPLAR WITH GLYCERIN PRETREATMENT**

BO-HAN XU, KE LIU  
DALIAN UNIVERSITY OF TECHNOLOGY  
DALIAN, PEOPLE'S REPUBLIC OF CHINA

ABDELHAMID BOUCHAÏR  
UNIVERSITE CLERMONT AUVERGNE  
CLERMONT-FERRAND, FRANCE

(RECEIVED MAY 2019)

### **ABSTRACT**

In order to improve the mechanical properties of low-density wood, the densified wood was fabricated. Northeast China fast-growing poplar was firstly immersed in 50% glycerin for 24 h, and then compressed under 150°C to attain 60% compression ratio with different thermal modification time (0.5, 1, and 2 h). The set recovery, modulus of elasticity (MOE), modulus of rupture (MOR) and hardness of compressed wood were tested to assess the influence of thermal modification time and wet/dry cycles on mechanical properties and set recovery of compressed poplar with glycerin pretreatment. It can be found that the thermal modification time of 1 h can be more appropriate, the first wet/dry cycle has a significant effect on mechanical properties and set recovery of compressed wood due to the dilution of glycerin during the soaking.

**KEYWORDS:** Glycerin pretreatment, thermal modification time, wet/dry cycles, mechanical properties, set recovery, poplar.

### **INTRODUCTION**

The mechanical properties of wood, such as the surface hardness, MOE and MOR, are positively associated with its density (Gong et al. 2010, Rautkari et al. 2011). The density of the wood depends on the cell wall thickness and size of lumen, and the densities of cell wall are approximately the same ( $1500 \text{ kg}\cdot\text{m}^{-3}$ ) regardless of the wood species or cell type (Kellogg and Wangaard 1969). Thus, density can be increased by compressing the porous structure in the transverse direction (Laine et al. 2016), when deformations in the densification process are

largely the result of the viscous buckling of cell walls without major fracture taking place (Kutnar et al. 2008). In general, wood cannot be compressed directly, because cracking may occur. Before compression, wood needs to be softened from a rigid state to a thermoplastic flow state (Wang and Huang 2011). After compression, the densified wood has a tendency to return to its original dimensions, which is known as set recovery (Rautkari et al. 2010), therefore, it is necessary to fix permanently the compressive deformation through some pretreatment methods for uncompressed wood (Rezayati Charani et al. 2007, Li et al. 2013) and post-treatment methods for compressed wood (Laine et al. 2013, Navi and Heger 2004).

The melamine formaldehyde resin or phenol formaldehyde resin impregnation is a pretreatment method widely studied (Inoue et al. 1991, Wallstrom and Lindberg 1999, Yano et al. 2000, Ohmae et al. 2002, Inoue et al. 2007b), which contributes to dimensional stability by swelling the cell wall and forming a rigid cross-linked network upon curing. However, the high cost of resin limits its application in the wood densification processes.

The pretreatment with glycerin is also an alternative process to fabricate the densified wood. As glycerin is adsorbed to hydroxyl groups through hydrogen bonding in amorphous region, wood enters in swollen state and the molecules are easy to slip (Yan et al. 2010). The glycerin can accelerate the degradation of wood component, and form a chemical cross-linkage between molecules of the matrix constituents, which contributes to fix deformation of compressed wood (Yan et al. 2011). In addition, the stress relaxation is also aggravated by glycerin (Yan et al. 2011).

The post-treatment at high temperature after densification is one of common processes used to fix the compressive deformation (Rautkari et al. 2010, Esteves et al. 2017), due to the release of stresses stored in the cell wall polymers by their decomposition and the formation of some cohesive structures (Higashihara et al. 2004). The steam post-treatment is being receiving more attention (Ito et al. 1998, Skyba et al. 2009, Fang et al. 2012, Kutnar and Kamke 2012, Rautkari et al. 2013). However, most deal with thin wood samples due to efficient steam injection (Dwianto et al. 1999, Navi and Heger 2004, Inoue et al. 2007a). The closed steam system limits its application to batch production. High temperature post-treatment in the absence of steam is also effective in reducing compression-set recovery, due to changes in the polar side groups on the molecular structures of cellulose, hemicelluloses, lignin, and extractives (Hillis 1984, Morsing 2000).

Many attempts have been made to develop a suitable process for the densification of different wood species by assessing the improvements in mechanical properties, dimensional stability and durability (Ulker and Burdurlu 2016, Esteves et al. 2017, Kúdela et al. 2017).

In general, the pretreatment with glycerin and thermal post-treatment are used together to reduce set recovery. Though some studies have reported the mechanical properties and set recovery of compressed wood using those two treatment processes (Yan 2010, Cai et al. 2013), few studies focused on the mechanical properties and set recovery of compressed wood exposed to humid or wet condition, which may destroy the cohesive structures formed in hot treatment. Especially, as the compressed wood is soaked in the water, the glycerin may be diluted, which may affect the mechanical properties and set recovery of compressed wood.

This aim of this paper is to investigate the influence of thermal modification time during densification on mechanical properties and set recovery of compressed poplar with glycerin pretreatment. Northeast China poplar was firstly immersed in 50% glycerin for 24 h, then compressed under 150°C to attain 60% compression ratio with different thermal modification time (0.5 h, 1 h, and 2 h). In order to assess the impact of moisture changes, the compressed specimens were subjected to five cycles of water soaking and drying, and their mechanical properties and set recovery were compared with those without bearing environmental changes. An analysis of variance (ANOVA) was used to evaluate statistical significance of the parameters, and the result is considered statistically significant for  $p < 0.05$ .

## MATERIALS AND METHODS

### Materials and pretreatment

The clear specimens without knots, cracks, decay and other visible defects were made from Chinese white poplar (*Populus tomentosa*) from northeast China, with a length of 600 mm (longitudinal) and width of 160 mm (tangential). They were firstly placed in an environmental-controlled room (20°C, 65% relative humidity) until equilibrium moisture content of approximately 12% was achieved, and then planned to thickness of 45 mm (radial). The measured wood density was equal to 400 kg·m<sup>-3</sup>. After that, the specimens were impregnated in 50% glycerin solution at 50°C, which is the optimal concentration to control the set recovery (Yan 2010), for 23 h and at 100°C for 1 h.

### Compression process

The specimens were compressed at 150°C with a speed of 10 mm·min<sup>-1</sup> along the radial direction (Fig. 1) to a target thickness of 18 mm in order to obtain 60% compression ratio (CR), which can be calculated according to Eq. 1. The wood was densified following the process shown in Fig. 2, and then platens were maintained in the same position for 0.5 h, 1 h, and 2 h, respectively, in order to investigate the influence of thermal modification time.

$$CR = \frac{t_1 - t_c}{t_1} \times 100\% \quad (1)$$

where:  $t_1$  is the original thickness (mm), and  $t_c$  is the target compressed thickness (mm).

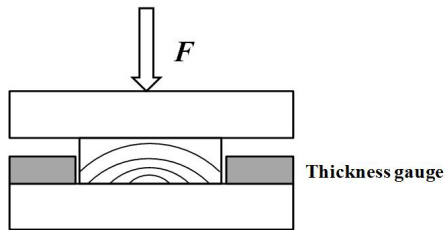


Fig. 1: Schematic diagram of the compression.

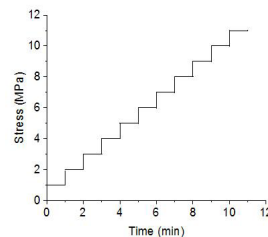


Fig. 2: Schematic diagram of the densification process.

### Set recovery

To measure set recovery, the small specimens (50 mm longitudinal, 15 mm tangential) were cut from compressed wood, which had been conditioned in an environment-controlled room (20°C, 65% relative humidity) until equilibrium moisture content was achieved. Then, the specimens were dried in a convection oven at 103°C, and their thickness was measured as  $t_c$  (mm). After that, the specimens were soaked in water for 24 h and again oven-dried, and their thickness was measured as  $t_s$  (mm). The percentage of set recovery (SR) can be determined using Eq. 2:

$$SR = \left[ \frac{t_s - t_c}{t_1 - t_c} \right] \times 100\% \quad (2)$$

**Wet/dry cycles**

In order to assess the impact of moisture changes, a process of wet/dry cycles was performed, in which soaking in water for 24 h and again oven-drying is defined as one wet/dry cycle, and the set recovery and mechanical properties of compressed wood were measured after one, three and five wet/dry cycles.

**Mechanical properties**

Before testing, all specimens were firstly conditioned in an environment-controlled room (20°C, 65% relative humidity) until equilibrium moisture content was achieved. The three-point bending tests for 6 replicates of specimens were performed to measure the modulus of elasticity (MOE) and modulus of rupture (MOR) of compressed wood according to ASTM D143 – 14 (2015). The specimens (Fig. 3) with 312 mm in length were cut from compressed wood, and the test span is 252 mm in order to meet a minimum span-to-depth ratio of 14 (ASTM 2015). MOE (MPa) and MOR (MPa) were calculated according to Eq. 3 and Eq. 4 (ASTM 2014):

$$MOE = \frac{pl^3}{4bd^3\Delta} \quad (MPa) \quad (3)$$

$$MOR = \frac{3P_{max}l}{2bd^2} \quad (MPa) \quad (4)$$

where:  $p$  is the increment of applied load below proportional limit (N),  $P_{max}$  is maximum load (N),  $l$  is the span between the two supports (mm),  $b$  is the width of specimen (mm),  $d$  is the height of specimen (mm), and  $\Delta$  is the increment of deflection corresponding to  $p$  (mm).



Fig. 3: Schematic diagram of the bending test.

Four replicates of specimens with 150 mm in length and 60 mm in width cut from the compressed wood were used to measure Brinell hardness (HB) according to standard EN 1534 (2000) with minor modifications, similar to that carried out by Rautkari et al. (2011). Six points on each sample were tested. A steel ball of 10 mm diameter ( $D$ ) is intended in the wood surface at such a rate that maximum load ( $F$ ) of 1 kN is reached in 15 s, and then the load is held for 25 s, finally the load is released over a period of 15 s. Because it is difficult to measure accurately the diameter of the indentation, therefore, the maximum depth of the indentation ( $h_{max}$ ) is adopted, which was measured automatically by the universal testing equipment. The HB is calculated according to Eq. 5:

$$HB = \frac{F}{\pi Dh_{max}} \quad (MPa) \quad (5)$$

Hardness recovery (HR) was also measured using Eq. 6, which represents the percentage of wood recovery directly after indentation:

$$HR = \frac{h_{max} - h_r}{h_{max}} \times 100\% \quad (6)$$

where:  $h_r$  (mm) is the recovered indentation after releasing the load.

## RESULTS AND DISCUSSION

### Influence of thermal modification time

The set recovery of compressed wood with different thermal modification time is illustrated in Fig. 4. With the increase of thermal modification time, the set recovery decreases. The set recovery for compressed wood with the thermal modification of 1 h and 2 h is much less than that for specimens with the thermal modification time of 0.5 h. The set recovery at various thermal modification times ( $p = 0.000$ ), shows highly significant differences, which has also been found in previous studies (Yan et al. 2010).

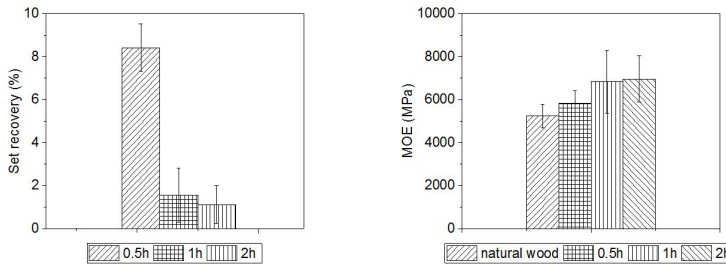


Fig. 4: Set recovery of compressed wood with different thermal modification time.

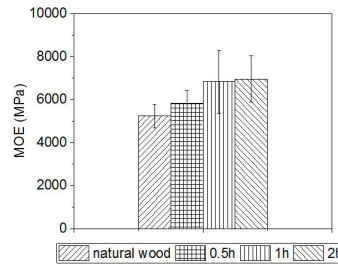


Fig. 5: MOE of specimens.

The density of compressed wood can be up to  $1000 \text{ kg}\cdot\text{m}^{-3}$ . The MOE and MOR of compressed wood with different thermal modification time and those of natural wood are illustrated in Figs. 5 and 6.

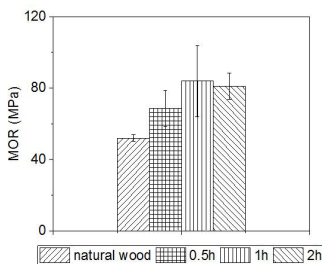


Fig. 6: MOR of specimens.

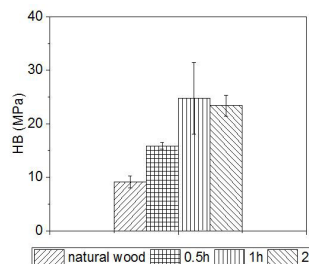


Fig. 7: Brinell Hardness of specimens.

The MOE ( $p = 0.183 > 0.05$ ) and MOR ( $p = 0.156 > 0.05$ ) at various thermal modification times, are not statistically significant. However, in previous studies, Yan et al. (2010) found that the MOE at various thermal modification times (0.5 h and 1 h), has significant differences.

The HB and HR of specimens are illustrated in Figs. 7 and 8. The HB ( $p = 0.000$ ) and HR ( $p = 0.000$ ) at various thermal modification times, show highly significant differences. The set recovery of compressed wood after wet/dry cycles is illustrated in Fig. 9. The Brinell hardness is highest for specimens with the thermal modification time 1 h. A long thermal modification time may result in the degradation of wood components, which will decrease mechanical properties of wood. The observation is consistent with the previous studies (Yan et al. 2010, Laine et al. 2016). It can be seen that the HR is lowest for the specimens with the thermal modification time of 1 h. These results can imply that the thermal modification time of 1 h can be more appropriate.

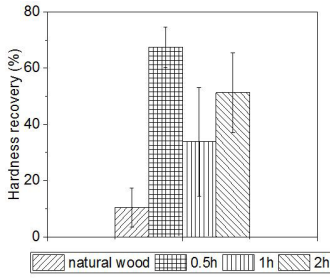


Fig. 8: Hardness recovery of specimens.

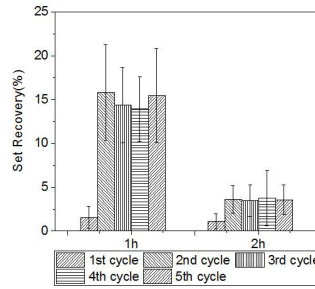


Fig. 9: Set recovery of compressed wood after different wet/dry cycles.

**Influence of wet/dry cycles**

Tab. 1 summarizes the *p*-value to present the statistical significance of wet/dry cycle with respect to density, set recovery and mechanical properties of compressed wood. At different wet/dry cycles, only the density, set recovery and HR of compressed wood with the thermal modification time of 1 h have statistical significance; the density and HB of compressed wood with the thermal modification time of 2 h are statistically significant.

Tab. 1: Statistical significance ANOVA, *p*-value. Units (-).

Thermal modification time	Density	Set recovery	MOE	MOR	HB	HR
1 h	0.014	0.000	0.469	0.535	0.984	0.008
2 h	0.000	0.200	0.589	0.286	0.032	0.084

After the second wet/dry cycle, the set recovery of compressed wood increases significantly. From the second wet/dry cycle, the set recovery changes rarely. For wood compressed under saturated steam, the set recovery reaches a plateau after the third cycle (Kutnar and Kamke 2012).

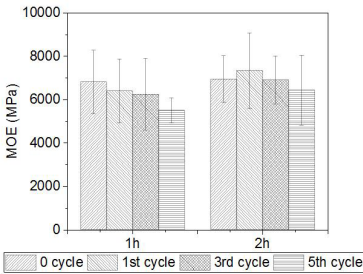


Fig. 10: MOE of compressed wood after different wet/dry cycles.

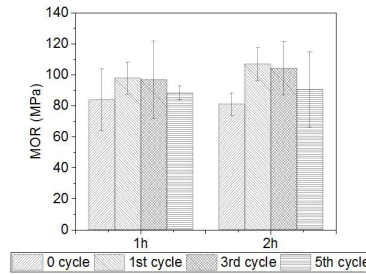


Fig. 11: MOR of compressed wood after different wet/dry cycles.

As shown in Figs. 10 and 11, after the first wet/dry cycle, the MOE and MOR decrease gradually with the increase of wet/dry cycles. For wood compressed under saturated steam, the wet/dry cycle also causes a decrease in the MOE and MOR (Kutnar and Kamke 2012).

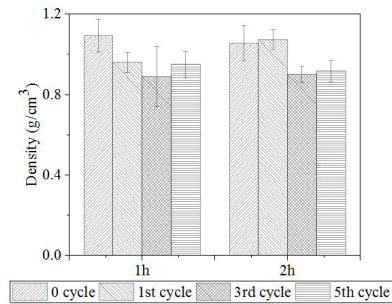


Fig. 12: Density of compressed wood after different wet/dry cycles.

Density of glycerin is equal to  $1261 \text{ kg}\cdot\text{m}^{-3}$ , which is greater than that of compressed wood. Due to the dilution of glycerin during the soaking, the density of compressed wood decreases (Fig. 12), therefore, the HB of compressed wood also decreases. After the first wet/dry cycle, the HB of compressed wood with the thermal modification time of 1 h has nearly no change, and HB of compressed wood with the thermal modification time of 2 h decreases gradually with the increase of wet/dry cycle as shown in Fig. 13. Fig. 14 illustrates the HR of compressed wood compressed after different wet/dry cycles, and the first wet/dry cycle significantly results in the increase of HR.

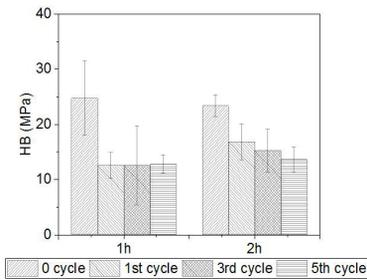


Fig. 13: Brinell Hardness of compressed wood after different wet/dry cycles

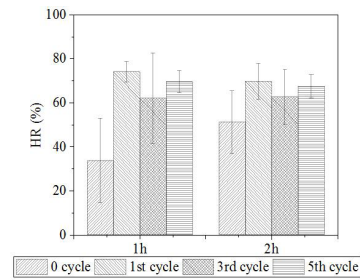


Fig. 14: Hardness recovery of compressed wood after different wet/dry cycles

## CONCLUSIONS

This paper presented the influence of thermal modification time and wet/dry cycles on set recovery and mechanical properties of compressed poplar with glycerin pretreatment. The set recovery decreases with the increase of the thermal modification time, however, the set recovery of compressed wood with the thermal modification time of 1 h is just slightly higher than that of 2 h. The MOE and MOR at various thermal modification times are not statistically significant. For compressed wood with the thermal modification time of 1 h, the HB is highest and the HR is lowest. In conclusion, the thermal modification time of 1 h is suitable for compressed wood used in normal condition.

After the second wet/dry cycle, the set recovery of compressed wood clearly increases, and from the second wet/dry cycle, the set recovery of compressed wood changes rarely. The set

recovery of compressed wood with the thermal modification time of 1 h is obviously higher than that of 2 h. Thus, compressed wood with the thermal modification time of 2 h is more appropriate for humid or wet condition, due to the favorable deformation fixation.

After the first wet/dry cycle, the MOE and MOR of compressed wood decrease with the increase of wet/dry cycles. The first wet/dry cycle significantly results in the decrease of the HB and the increase of HR. Therefore, the first wet/dry cycle has significant effect on mechanical properties of compressed wood due to the dilution of glycerin during the soaking.

## ACKNOWLEDGEMENTS

The authors gratefully acknowledge the support of “National Natural Science Foundation of China (No. 51878114)” and “Creative Research Groups of the National Natural Science Foundation of China (Grant No. 51421064)”.

## REFERENCES

1. ASTM D198-14, 2014: Standard test methods of static tests of lumber in structural sizes.
2. ASTM D143-14, 2015: Standard test methods for small clear specimens of timber.
3. Cai, J., Yang, X., Cai, L., Shi S.Q., 2013: Impact of the combination of densification and thermal modification on dimensional stability and hardness of poplar lumber. *Drying Technology* 31(10): 1107-1113.
4. Dwianto, W., Morooka, T., Norimoto, M., Kitajima, T., 1999: Stress relaxation of sugi (*Cryptomeria japonica* D. Don) wood in radial compression under high temperature steam. *Holzforschung* 53(5): 541-546.
5. EN 1534, 2010: Wood flooring. Determination of resistance to indentation. Test method.
6. Esteves, B., Ribeiro, F., Cruz-Lopes, L., Ferreira, J.V., Domingos, I., Duarte, M., Duarte, S., Nunes, L., 2017: Densification and heat treatment of maritime pine wood. *Wood Research* 62(3): 373-388.
7. Fang, C.H., Mariotti, N., Cloutier, A., Koubaa, A., Blanchet, P., 2012: Densification of wood veneers by compression combined with heat and steam. *European Journal of Wood and Wood Products* 70(1-3): 155-163.
8. Gong, M., Lamason, C., Li, L., 2010: Interactive effect of surface densification and post-heat-treatment on aspen wood. *Journal of Materials Processing Technology* 210(2): 293-296.
9. Higashihara, T., Morooka, T., Norimoto, M., 2000: Permanent fixation of transversely compressed wood by steaming and its mechanism. *Mokuzai Gakkaishi* 46(4): 291-297.
10. Hillis, W.E., 1984: High temperature and chemical effects on wood stability. *Wood Science and Technology* 18(4): 281-293.
11. Inoue, M., Morooka, T., Norimoto, M., Rowell, R.M., Egawa, G., 1991: Permanent fixation of compressive deformation of wood. II. Mechanisms of permanent fixation. *Wood Research & Technical Notes* 27(4): 1859-1866.
12. Inoue, M., Norimoto, M., Tanahashi, M., Rowell, R.M., 2007a: Steam or heat fixation of compressed wood. *Wood & Fiber Science* 25(3): 224-235.
13. Inoue, M., Ogata, S., Kawai, S., Rowell, R.M., Norimoto, M., 2007b: Fixation of compressed wood using melamine-formaldehyde resin. *Wood & Fiber Science* 25(4): 404-410.

14. Ito, Y., Tanahashi, M., Shigematsu, M., Shinoda, Y., 1998: Compressive-molding of wood by high-pressure steam-treatment: Part 2. Mechanism of permanent fixation. *Holzforschung* 52(2): 217-221.
15. Kellogg, R.M., Wangaard, F.F., 1969: Variation in the cell-wall density of wood. *Wood and Fiber Science* 3(3): 180-204.
16. Kúdela, J., Rešetka, M., Rademacher, P., Dejmál, A., 2017: Influence of pressing parameters on surface properties of compressed beech wood. *Wood Research* 62(6): 939-950.
17. Kutnar, A., Kamke, F.A., Sernek, M., 2008: The mechanical properties of densified VTC wood relevant for structural composites. *Holz als Roh- und Werkstoff* 66(6): 439-446.
18. Kutnar, A., Kamke, F.A., 2012: Influence of temperature and steam environment on set recovery of compressive deformation of wood. *Wood Science and Technology* 46(5): 953-964.
19. Laine, K., Rautkari, L., Hughes, M., Kutnar A., 2013: Reducing the set-recovery of surface densified solid Scots pine wood by hydrothermal post-treatment. *European Journal of Wood and Wood Products* 71(1): 17-23.
20. Laine, K., Segerholm, K., Wälinder, M., Rautkari, L., Hughes, M., 2016: Wood densification and thermal modification: hardness, set-recovery and micromorphology. *Wood Science and Technology* 50(5): 1-12.
21. Li, L., Gong, M., Yuan, N., Li, D., 2013: An optimal thermo-hydro-mechanical densification (THM) process for densifying balsam fir wood. *Bioresources* 8(3): 3967-3981.
22. Morsing, N., 2000: Densification of wood—the influence of hygrothermal treatment on compression of beech perpendicular to the grain. Department of structural engineering and materials, Technical university of Denmark, Series R 79, 139 pp.
23. Navi, P., Heger, F., 2004: Combined densification and thermo-hydro-mechanical processing of wood. *Mrs Bulletin* 29(5): 332-336.
24. Ohmae, K., Minato, K., Norimoto, M., 2002: The analysis of dimensional changes due to chemical treatments and water soaking for Hinoki (*Chamaecyparis obtusa*) wood. *Holzforschung* 56(1): 98-102
25. Rautkari, L., Properzi, M., Pichelin, F., Hughes, M., 2010: Properties and set-recovery of surface densified Norway spruce and European beech. *Wood Science and Technology* 44(4): 679-691.
26. Rautkari, L., Kamke, F.A., Hughes M., 2011: Density profile relation to hardness of viscoelastic thermal compressed (VTC) wood composite. *Wood Science and Technology* 45(4): 693-705.
27. Rautkari, L., Laine, K., Kutnar, A., 2013: Hardness and density profile of surface densified and thermally modified Scots pine in relation to degree of densification. *Journal of Materials Science* 48(6): 2370-2375.
28. Rezayati Charani, P., Mohammadi Rovshandeh, J., Mohebbi, B., Ramezani O., 2007: Influence of hydrothermal treatment on the dimensional stability of beech wood. *Caspian Journal of Environmental Sciences* 5(2): 125-131.
29. Skyba, O., Schwarze, F.W.M.R., Niemz, P., 2009: Physical and mechanical properties of thermo-hygro-mechanically (THM)-densified wood. *Wood Research* 54(2): 1-18.
30. Ulker, O., Burdurlu, E., 2016: Some mechanical properties of densified and laminated lombardy poplar (*Populus nigra* L.). *Wood Research* 61(6): 959-970.
31. Wallstrom, L., Lindberg, K.A.H., 1999: Measurement of cell wall penetration in wood of water-based chemicals using SEM/EDS and STEM/EDS technique. *Wood Science and Technology* 33(2): 111-122.

32. Wang, Y.W., Huang, R.F., 2011: Research status of wood densification. *Forestry Machinery and Woodworking Equipment* 39(8): 13-16.
33. Yan, L., 2010: Mechanism and application of compressive deformation fixation of poplar by glycerin pretreatment. Ph.D. Thesis, Beijing Forestry University, China, 118 pp.
34. Yan, L., Cao, J.Z., Jin, X.J., 2010: Deformation fixation, mechanical properties and chemical analysis of compressed *Populus cathayana* wood pretreated by glycerin. *Forestry Studies in China* 12(4): 213-217.
35. Yan, L., Cao, J., Gao, W., Zhou, X., Zhao, G., 2011: Interaction between glycerin and wood at various temperatures from stress relaxation approach. *Wood Science and Technology* 45(2): 215-222.
36. Yano, H., Mori, K., Collins, P.J., Yazaki, Y., 2000: Effects of element size and orientation in production of high strength resin impregnated wood based materials. *Holzforschung* 54(4): 443-447.

BO-HAN XU\*, KE LIU  
DALIAN UNIVERSITY OF TECHNOLOGY  
STATE KEY LABORATORY OF COASTAL AND OFFSHORE ENGINEERING  
OCEAN ENGINEERING JOINT RESEARCH CENTER OF DUT-UWA  
DALIAN 116024  
PEOPLE'S REPUBLIC OF CHINA  
\*Corresponding author: bohanxu@dlut.edu.cn

ABDELHAMID BOUCHAÏR  
UNIVERSITE CLERMONT AUVERGNE  
CNRS, SIGMA CLERMONT  
INSTITUT PASCAL, F-63000  
CLERMONT-FERRAND  
FRANCE

## **BLUE STAIN IN LUMBER INDUSTRY AND LOSSES CAUSED BY CUTTING METHODS**

OSMAN KOMUT  
GUMUSHANE UNIVERSITY  
GUMUSHANE, TURKEY

(RECEIVED MAY 2019)

### **ABSTRACT**

In this study, it is aimed to determine the waste and productivity losses of Scots pine (*Pinus sylvestris* L.) logs that were exposed to blue stain degradation. In this context, a total of 39 timber production processes were analyzed in 7 different lumber managements using prism cutting and sharp cutting method. The main product yield and additional processing requirements were determined for flawed and flawless logs in blue stain damage. As a result of the study, it was determined that the blue stain degradation decreased the main product efficiency by 17% in the prism cutting method and by 33% in the sharp cutting method. Statistically significant differences were discovered between the efficiency values obtained as a consequence of cutting flawed and flawless logs with prism and sharp cutting methods. In addition, additional processing requirements were determined in the sharp mowing method.

**KEYWORDS:** Blue stain, scots pine log, lumber productin, loss of productivity.

### **INTRODUCTION**

The processing of wood-based products supplied from forest resources in such a way that will minimize waste has a significant contribution to the sustainability of forest resources (Kantay and Köse 2009, Khalili et al. 2015). A considerable part of wood-based plants in forests are not suitable for use in industrial production. On the other hand, there is a vast scale of loss during the conversion of the obtained wood products to the final products (Gladstone and Ledig 1990). While the use of efficient and profitable production methods is increasing the likelihood of economic success of managements, it will reduce the consumption pressure on forest resources (Fuwape 2001, Sloan and Sayer 2015).

Significant raw material losses occur during the processing phase of logs (Eshun et al. 2010). It is reported that these losses can reach to approximately 80% beginning from cuttings of the tree to the final product (Dionco-Adetayo 2001, Eshun et al. 2012). That most of these wastes are not used directly for industrial production reduces the added value potential of the resources and

leads to significant economic losses. However, it is known that there is a considerable amount of hardship in reducing the waste amount in the lumber industry (Eshun et al. 2015).

As well as the heterogeneous structure of the wood material, its nature is easily affected by environment and storage conditions which have important effects on the losses occurring during the processing of logs (Blanchette et al. 1989, Şen et al. 2018). On the other hand, factors like the production technique, the suitability of the machine-equipment used and the competence of machine operator increase these losses (Daian and Ozarska 2009, Tunçel and Koç 2017).

Logs are exposed to many harmful effects such as foremost discoloration, crack formation, dot and insect damage until they are taken to production in the forest industry managements (Kantay and Köse 2009, Ahmad et al. 2018). Discoloration of wood material may occur due to different reasons such as sunlight, humidity, temperature, contact with metals and microorganisms (Tolvaj et al. 2011, Li et al. 2019). Fungi are reported to be effective on about one third of the annual industrial wood production (Örs and Keskin 2001, Hong et al. 2019). Especially the blue stain degradation caused by the effect of fungus in the sapwood part of coniferous wood logs leads to significant losses due to its rapid development and visual anomalies it causes (Örs and Keskin 2001). On the other hand, the waste amount generated during the processing of the logs depends on the production method and the technological foundation, hence it depends on the production efficiency (FAO 2014, Gligoraş and Bor 2015). The waste amount in question may vary between different companies in the same country (FAO 2014).

In this study, it is aimed to determine the waste amount generated during the industrial processing of Scots pine logs exposed to sapwood discoloration and their productivity loss in the context of the production method variable.

## MATERIAL AND METHODS

The study was carried out in 7 small and medium-sized lumber production managements operating in Gumushane province, Turkey. The said forest industry managements provide their raw material needs from planted tree sale auctions conducted by the Forestry Directorate of Gümüşhane and Torul affiliated to the General Directorate of Forestry. In the study, the production process of 7 managements, 3 of which use the sharp cutting method and 4 use the prism cutting method, were examined.

Although discoloration and mold fungi do not affect the structural features of wood, the deterioration they cause leads to aesthetic and economic losses (Zeleniuc 2008). In this study, the effects of blue staining caused by coloring fungi on the sapwood part of Scots pine (*Pinus sylvestris* L.) logs were investigated. In this context, firstly, the defect detected in the logs was measured as shown in Fig. 1 and calculated by Eq. 1: (Komut and et al. 2013).

$$\text{Degradation width} = (\sum_{m=1}^n x_m)/n \quad (1)$$

Prism and sharp cutting methods were applied for the production of flawed with blue staining - flawed in terms of appearance (FTA) and flawless without blue staining (flawless in terms of appearance (FssTA) in the processing of Scotch pine logs (Fig. 2). Prism cutting method is preferred in the production of lumber with equal width; sharp cutting method is preferred in timber production with equal thickness (Colakoglu and Colak 2003).



Fig. 1: Cross-section of the blue stained log and the measurement of degradation width (Komut and Ozturk 2018).

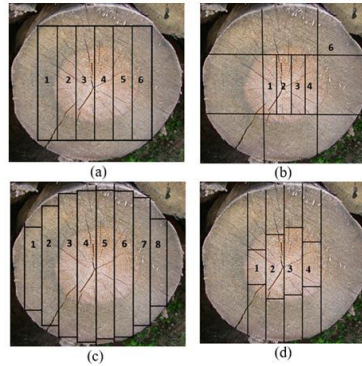


Fig. 2: Cutting methods used in efficiency calculation (a) FTA timber production with rism cutting method, (b) FssTA timber production with Prism cutting method, (c) FTA timber production with sharp cutting method, (d) FssTA timber with sharp cutting method.

Eq. 2 was used to calculate the production efficiency for timber obtained with different production methods.

$$R = \frac{V_{log}}{\sum_{x=1}^n e_x \cdot g_x \cdot l_x} \quad (2)$$

where:  $R$  - production efficiency (%),  $V_{log}$  - log volume ( $\text{cm}^3$ ),  $e_x$  - lumber thickness (cm),  $g_x$  - lumber width (cm),  $l_x$  - lumber length (cm).

Additional processing was observed to be performed in the side pick-up and multi-slitting machines in order to remove the degraded part of the FTA timbers obtained from logs exposed to blue staining. In the study, the durations (energy consumption and labor times) required by the additional procedures were measured with the help of a stopwatch.

IBM SPSS (20,0) package program was used in the analysis of data concerning cutting methods. In the study, since the number of samples was less than 30, Mann-Witney U test with two independent variables from non-parametric tests was used (Kalaycı 2010). Microsoft Office Excel 2010 package program has been utilized to make comparisons of frequency, ratio etc.

## RESULTS AND DISCUSSION

**Findings regarding the managements using prism cutting method**

In this study, the efficiency values obtained during the process of cutting of healthy and blue stained logs in 4 different lumber managements by prism cutting method are given in Tab. 1. A total of 9 cleaned (not irrigated) round wood pieces, which was obtained as a result of processing of FssTA Scotch pine logs, was measured and the average main product efficiency was calculated as 59%. For the timber production of FssTA timber by cleaning the part with blue staining in cross section area, 14 logs were cut, and the main product efficiency value was determined as 42%.

*Tab. 1: The efficiency values obtained in Prism cross-cutting method.*

Workplace	Log diameter (cm)	Log length (m)	Measured distortion (cm)	Total volume (m <sup>3</sup> )	Main product volume (m <sup>3</sup> )	Main product efficiency (%)	Main product efficiency loss (%)
1	32	3	0	0.241	0.154	64	0
	30	3	5	0.212	0.135	44	15
	26	3	7	0.159	0.101	34	25
	42	3	7	0.416	0.265	44	15
	45	3	10	0.477	0.304	39	20
	36	3	0	0.305	0.194	59	0
	43	3	0	0.436	0.277	60	0
2	27	2	4	0.115	0.073	46	13
	32	2	0	0.161	0.102	62	0
	28	2	0	0.123	0.078	55	0
	37	2	5	0.215	0.137	48	11
	35	2	5	0.192	0.123	47	12
3	20	3	4	0.094	0.060	41	18
	28	3	7	0.185	0.118	36	23
	26	3	0	0.159	0.101	58	0
	35	3	0	0.289	0.184	55	0
	28	3	8	0.185	0.118	32	27
	31	3	9	0.226	0.144	32	27
4	45	3	10	0.477	0.304	39	20
	26	3	0	0.159	0.101	57	0
	22	3	0	0.114	0.073	58	0
	38	3	5	0.340	0.217	48	11
	56	3	5	0.739	0.470	53	6

\* Average product efficiency was taken as 59%.

In the prism cutting method, the efficiency loss for the main product is observed to increase as the blue stained area width and the log diameter increase in the log cross section (Fig. 3). On the other hand, differences were observed between the 4 managements in terms of average main product efficiency (respectively 50.2%, 53%, 43%, 51%).

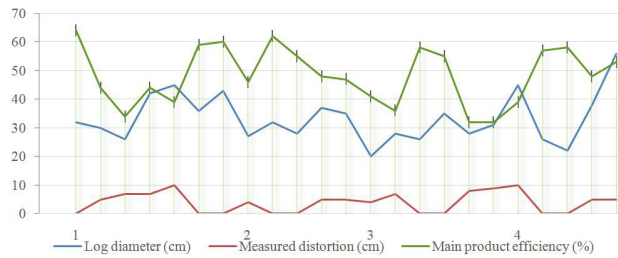


Fig. 3: The effect of discoloration on the efficiency of the main product in the prism cutting method.

**Findings concerning the managements using sharp cutting method**

In the study, efficiency values obtained by cutting FTA and FssTA sample logs with sharp cutting method are given in Tab. 2. Six of processed logs were FssTA Scots pine logs, while 10 of them was selected as FTA logs. The average efficiency of non-irrigated lumber produced as a result of cutting of FssTA logs with sharp cutting method is calculated as 71%. The average efficiency of the main product for logs cleared from non-irrigated and stained parts produced from the damaged logs was determined as 38%.

Tab. 2: The efficiency values obtained in the application of sharp cutting method.

Workplace	Log diameter (cm)	Log length (m)	Measured distortion (cm)	Total volume (m <sup>3</sup> )	Main product volume (m <sup>3</sup> )	Main product efficiency (%)	Main product efficiency loss (%)
1	40	3	4	0.377	0.215	57	14
	35	3	6	0.289	0.115	40	31
	31	3	6	0.226	0.095	42	29
	30	3	5	0.212	0.072	34	37
	34	3	0	0.272	0.207	76	0
	28	3	0	0.185	0.133	72	0
2	27	3	9	0.172	0.041	24	47
	28	2	8	0.123	0.032	26	45
	33	2	12	0.171	0.050	29	42
	36	2	10	0.204	0.081	40	31
	29	2	0	0.132	0.087	66	0
	30	3	0	0.212	0.146	69	0
3	42	4	0	0.554	0.399	72	0
	26	4	5	0.212	0.096	45	26
	32	3	7	0.241	0.094	39	32
	32	3	0	0.241	0.166	69	0

\*Average efficiency of the main product is taken as 71%.

In the logs cut by the sharp intersection method, as the log diameter increased, while the main production efficiency increased, the increase in the measured decay limited the increase in productivity (Fig. 4).

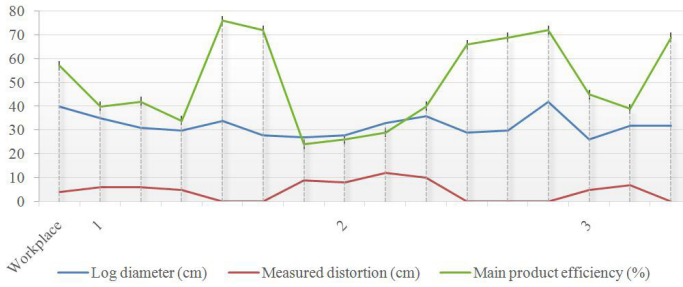


Fig. 4: The effect of color change on the main product efficiency in sharp cutting method.

**Findings concerning the comparison of prism cutting-sharp cutting methods**

In this study, 15 FssTA and 24 FssTA Scots pine logs were ensured to be cut in 7 different managements. Of these logs, 23 were cut with prism and 16 were cut with sharp cutting method. The mean width of the discoloration on the cross-sectional surface of the cut logs was 6.5 cm in the prism cutting method and 7.2 cm in the sharp cutting method. There were statistically significant differences ( $p < 0.05$ ) in terms of efficiency and waste ratio between the cutting of logs with and without the blue stain degradations with the prism and sharp cutting method (Tab. 3). The cutting method used is observed as one of the factors affecting the production efficiency (Alvarez and Vera 2014). It is reported that the differences in productivity between managements occur as a result of the usage of inefficient processes and methods as well as the lack of equipment (Adhikari and Ozarska 2018, Eshun et al. 2012). On the other hand, there are studies that report results regarding that decrease in efficiency may depend on the properties of the supplied log (Örs and Keskin 2001, Choi et al. 2013, Pang et al. 2015).

Tab. 3: Mann-Whitney U test results concerning the cutting method during the processing of logs.

Variable	Cutting Method	(N)	Mean Rank	Mann-Whitney U	Wilcoxon W	Z	Asymp. Sig. (2-tailed)
Efficiency Loss for Flawed Logs	Prism Cutting	14	8.29	11.00	116.00	-3.458	0.001*
	Sharp Cutting	10	18.40				
	Total	24					
Efficiency for Flawless Logs	Prism Cutting	9	5.00	0.00	45.00	-3.193	0.001*
	Sharp Cutting	6	12.50				
	Total	15					

\* $p < 0.05$

While the production efficiency was higher in the sharp cutting method in the FssTA logs, thus the waste amount was lower, the efficiency loss occurred during the cutting of FTA logs was higher. The efficiency in the timber production process varies significantly depending on the log defects. In order to increase the efficiency, it is important to determine these defects correctly (Todoroki 2003). Fungus-originated color changes also affect the log quality (Vanzetti et al. 2018). However, although it is not considered as a log defect, the change in log diameter and length is also reported to be effective on the efficiency thereby on losses (Yang and Jenkins 2008, Vanzetti et al. 2018).

### Findings concerning other losses

The FTA obtained from the logs cut with the sharp cutting method has been shown to require additional processing in the multi-slitting machine to remove this flaw. The distance of the additional processing machines to the main processing machine was measured as 4 m in management 1, as 5.5 m in management 2 and as 6.5 m in management 3. According to this, transport times, machine processing and additional stacking times of timber were measured for additional processing (Tab. 4). In the production of aesthetically flawless lumber by cutting a total of 10 logs with blue-stained degradation in three managements, a work loss of 47.73 min was calculated. On the other hand, an additional 20.07 min machine processing time has formed.

Tab. 4: Measurements for additional processing times.

Workplace	Log diameter (cm)	Log length (m)	Measured distortion (cm)	Number of timber (width 3 cm)	Transport time to machine (min)	Processing time (min)	Re-stacking time (min)	Total lost time (min)
1	40	3	4	7	2.57	4.08	2.33	8.98
	35	3	6	5	1.83	2.92	1.67	6.42
	31	3	6	5	1.83	2.92	1.67	6.42
	30	3	5	5	1.83	2.92	1.67	6.42
2	27	3	9	1	0.50	0.47	0.33	1.30
	28	2	8	3	1.50	1.40	1.00	3.90
	33	2	12	1	0.50	0.47	0.33	1.30
	36	2	10	3	1.50	1.40	1.00	3.90
3	26	4	5	3	1.80	1.75	1.00	4.55
	32	3	7	3	1.80	1.75	1.00	4.55
Total				36	15.67	20.07	12.00	47.73

In the sharp cutting method, the production efficiency decreases as the cross sectional area of the flawed part and color degradation measured horizontal to the log section increases with increase in the obtained log amount. On the other hand, the increase in total loss time duration remains limited. In this application, it was observed that the number of obtained flawless lumber increased as the loss time increased (Fig. 5). There are a number of studies reporting that the insect damage, crack etc cause significant economic losses due to losses in the production process (Zeleniuc 2008, Loeffler and Anderson 2018, Vanzetti et al. 2018).

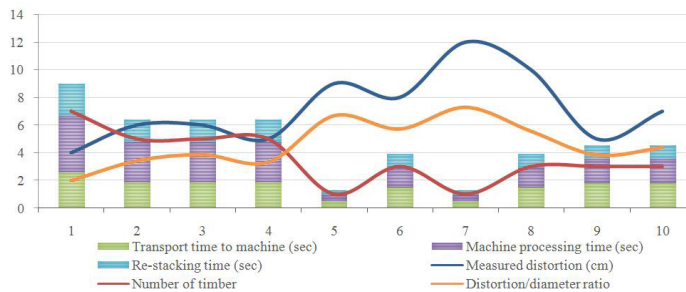


Fig. 5: Total number of flawless lumbers, degradation amount and lost time condition according to the the ratio of degradation to the cross-sectional area variables.

As the number of timbers that require additional processing and the timber length increase, the lost time increases. On the other hand, as the degradation on the cross-sectional surface of the timber increases, the number of flawless lumber obtained decreases, thus decreasing the lost times (Fig. 6).

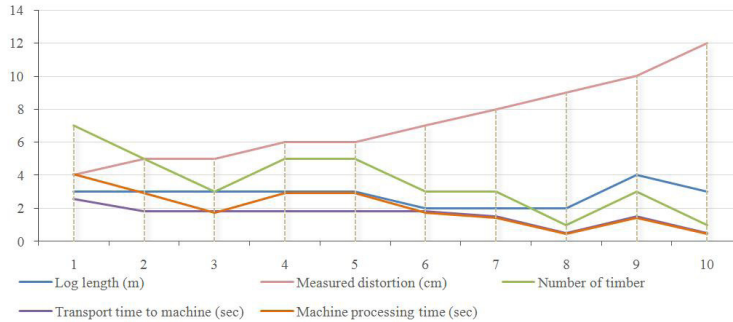


Fig. 6: The effect of lumber length, number and degradation amount on lost time.

## CONCLUSIONS

Blue stain is the appearance defect that can develop in all production and waiting processes of wood material. Blue stain greatly increases the loss in the timber industry sector, therefore leads to a decrease in the main product yield. The amount of loss occurs at a higher level at the sharp cutting method than the prism cutting method. If sharp cutting is chosen as the cutting method, the occurrence of additional production processes causes an increase in economic losses. On the other hand, differences in the main product efficiency may occur in different managements using the same production method.

It is clear that the most effective way to prevent loss is to prevent the formation of blue staining. Therefore, an effective and efficient inventory control system can reduce waiting times (Zeleniuc 2008). However, the application of the prism cutting method for the blue stained logs as well as the preference for the logs with low sapwood width will benefit for a decrease in the losses. The efficient and effective usage of the products obtained from forest resources will contribute greatly to the sustainability of these resources.

## REFERENCES

1. Adhikari, S., Ozarska, B., 2018: Minimizing environmental impacts of timber products through the production process "From Sawmill to Final Products". *Environmental System Research* 7: 6.
2. Ahmad, A., Elserogy, A., Al-Muheisen, Z., Villeneuve, F., El-Oqlah, A., 2018: The conservation of a wooden nabataean coffin box from Jordan-application of non-destructive ultrasonic technique. *Wood Research* 63(1): 2018: 1-14.
3. Alvarez, P.P., Vera, J.R., 2014: Application of robust optimization to the sawmill planning problem. *Annals of Operations Research* 219: 457-475.

4. Blanchette, R.A., Nilsson, T., Daniel, G., Abad, A., 1989: Biological degradation of wood. Chapter 6, Pp. 141-174, Archaeological Wood.
5. Choi, S.I., Kang, H.M., Lee, C.K., Sato, N., 2013: Study on current status and task of sawmills located in the woodland of Korea. Journal of the Faculty of Agriculture Kyushu University 58(1): 183-190.
6. Çolakoğlu, G., Çolak, S., 2003: Molding techniques lecture notes, Karadeniz Technical University Faculty of Forestry Course Lecturers, Series No: 70, Trabzon.
7. Daian, G., Ozarska, B., 2009: Wood waste management practices and strategies to increase sustainability standards in the Australian wooden furniture manufacturing sector. Journal of Cleaner Production, 17(17): 1594-1602.
8. Dionco-Adetayo, E.A., 2001: Utilization of wood wastes in Nigeria: a feasibility overview. Technovation, 21 (2001): 55-60.
9. Eshun, J.F., Potting, J., Leemans, R., 2010: Inventory analysis of the timber industry in Ghana. The International Journal of Life Cycle Assessment 15(2010): 715-725.
10. Eshun, J.F., Potting, J., Leemans, R., 2012: Wood waste minimization in the timber sector of Ghana: a systems approach to reduce environmental impact. Journal of Cleaner Production 26: 67-78.
11. Fuwape, J.A., 2001: Forest resources and economic development in Ondo State. Paper presented at Ondo State economic summit, Pp. 1-15.
12. Gligoraş, D., Bor, S.A., 2015: Factors affecting the effective time consumption, wood recovery and feeding speed when manufacturing lumber using a fbo-02 cut mobile bandsaw. Wood Research 60(2) 2015: 329-338.
13. Hong, J.H., An, S., Song, K.Y., Kim, Y., Yarin, A.L., Kim, J.J., Yoon, S.S., 2019: Eco-friendly lignin nanofiber mat for protection of wood against attacks by environmentally hazardous fungi. Polymer Testing 74: 113-118.
14. Kantay, R., Köse, C., 2009: Forest warehouses and storage techniques. Istanbul University Faculty of Forestry Journal 59(1): 75-92.
15. Kalaycı, Ş., 2010: SPSS applied multivariate statistical techniques. Asil Publishing Distribution Ltd. Sti. Ankara, 426 pp.
16. Khalili, N.R., Duecker, S., Ashton, W., Chavez, F., 2015: From cleaner production to sustainable development: the role of academia. Journal of Cleaner Production 96: 30-43.
17. Komut, O., İmamoğlu, S., Öztürk, A., 2013: Blue colouration damage on *Pinus sylvestris* L. logs and their effects on sales price. Artvin Coruh University Journal of Faculty of Forestry 14(2): 283-291.
18. Komut, O., Öztürk, A., 2018: The effects of blue dyeing damage on the industrial processing properties of logs. Natural Disasters and Environment Journal 4 : 8-14.
19. Li, H., Lei, X., Wu, Y., Li, H., Guo, X., Wen, R., Hu, Y., 2019: Study of the discoloration behaviour of Teak wood (*Tectona grandis* Linn. fil.) caused by simulated sunlight. Wood Research 64(4): 625-636.
20. Loeffler, D., Anderson, N., 2018: Impacts of the mountain pine beetle on sawmill operations, costs and product values in Montana. Forest Products Journal 68(1): 15-24.
21. Örs, Y., Keskin, H., 2001: Wood Material Science. T.C. The Ministry of Industry and Commerce KOSGEB Small and Medium Industry Development and Support Administration, Castle Offset Printing, Ankara, Turkey, 183 pp.
22. Pang, S., H'ng, P., Chai, L., Lee, S., Paridah, T., 2015: Value added productivity performance of the Peninsular Malaysian wood sawmilling industry. BioResources 10(4): 7324-7338.

23. Sloan, S., Sayer, J.A., 2015: Forest resources assessment of 2015 shows positive global trends but forest loss and degradation persist in poor tropical countries. *Forest Ecology and Management* 352: 134-145.
24. Şen, S., Fidan, M. S., Alkan, E., Yaşar, Ş. Ş., 2018: Determination of certain properties of scotch pine (*Pinus sylvestris* L.) wood which is impregnated with boron compounds and Quechua. *Wood Research* 63(6): 1033-1044.
25. Todoroki, C., 2003: Accuracy considerations when optimally sawing pruned logs: internal defects and sawing precision. *Nondestructive Testing and Evaluation* 19(1-2): 29-41.
26. Tolvaj, L., Molnár, S., Németh, R., Varga, D., 2010: Color modification of black locust depending on the steaming parameters. *Wood Research* 55(2): 81-88.
27. Tunçel, S., Koç, H., 2017: The paradox of productivity in forest products industry, IV. National Forestry Congress, 15-16 November 2017; Antalya, pp. 523-529.
28. Vanzetti, N., Broz, D., Corsanoac, G., Montagnaa, J.M., 2018: An optimization approach for multiperiod production planning in a sawmill. *Forest Policy and Economics* 97: 1-8.
29. Yang, P., Jenkins, B.M., 2008: Wood residues from sawmills in California. *Biomass and Bioenergy* 32(2): 101-108.
30. Zeleniuc, O., 2008: Anti-sapstain treatment of timber for sustainable development. *Pro Ligno* 4(4): 41-55.

OSMAN KOMUT\*  
GUMUSHANE UNIVERSITY  
GUMUSHANE VOCATIONAL HIGH SCHOOL  
DEPARTMENT OF FORESTRY  
29100, GUMUSHANE  
TURKEY

\*Corresponding author: [osmankomut@gumushane.edu.tr](mailto:osmankomut@gumushane.edu.tr)

## **TEST ANALYSIS AND VERIFICATION OF THE INFLUENCE OF MILLING CUTTER BLADE SHAPE ON WOOD MILLING**

YANG CHUNMEI, LIU QINGWEI, JIANG TING, SONG MINGLIANG  
MA YAN, LIU JIUQING  
NORTHEAST FORESTRY UNIVERSITY  
HARBIN, CHINA

(RECEIVED MAY 2019)

### **ABSTRACT**

In this paper, the influence law of cutting tools with different blade shapes in the process of wood milling was studied. Keeping the cutting speed, cutting depth, cutting width unchanged, the blade shapes of milling cutter were the research object, the cutting force, cutting vibration, and chip morphology change under different feed rate were discussed, the surface roughness of the processed material was analyzed under down milling and up milling. The results showed that when the feed rate increased from  $6 \text{ m}\cdot\text{min}^{-1}$  to  $14 \text{ m}\cdot\text{min}^{-1}$ , the cutting force in up milling was less than that in downing milling, the cutting vibration of upright milling cutter with spiral curved blade was the smallest, it increased gradually in the range of  $13.6 \text{ m}\cdot\text{s}^{-2}$  -  $27.4 \text{ m}\cdot\text{s}^{-2}$  in up milling. On the whole, the surface roughness of the workpiece in down milling was better than that in up milling. The experimental study on the cutter milling blade shapes had a guiding significance for improving the precision of surface machining and provided a theoretical reference for the selection of process parameters in the milling process.

**KEYWORDS:** Milling cutter blade, wood cutting, cutting parameter, cutting force.

### **INTRODUCTION**

Wood is a kind of natural polymer material which composed of complex organic matters, it is a typical heterogeneous anisotropic material, and widely used in furniture manufacturing, handicraft carving, home decoration and other fields (Ma 2007, Ramasamy and Ratnasingam 2010). Milling is one of the main methods of wood surface processing, and it is also the key link of product profile processing (Song et al. 2006, Engin et al. 2000). In order to obtain the high surface quality when wood processing, the forming surface of the workpiece is usually processed with milling cutter blade at one time, which with good surface smoothness and high production

efficiency (Deng et al. 2014, Li 2008, Eblagon et al. 2007). In the milling process, cutting force, cutting vibration and chip formation are directly affected by the type of the milling cutter blade (Zhu 2015, Päivinen and Heinimaa 2003, Bayoumi and Bailey 1985), and in a cutting layer, the greater the change in cutting force, the greater the mechanical shock on the blade (Zhang et al. 2011, Åbele et al. 2013). Therefore, it is great significance to master the milling properties of wood for optimizing milling parameters, reducing tool wear and improving machining technology.

In recent years, domestic and foreign scholars had studied the milling cutter in the process of wood milling. Jung et al. (2011) provided an effective method to calculate the cutting load from the geometric angle of cutter blade, which is used to predict the area where the dimension error is too large due to the increase of cutting force and cutting load in the processing process, so as to reduce the occurrence of tool fracture or excessive deflection. Palmqvist et al. (2003) studied the changing rules of the parallel cutting force and the normal cutting force on the tool tip when cutting parameters changed in the milling process, and found out the optimal set of normal force parameters to avoid wood damage. Ekevad et al. (2012) studied the effects of different geometric shapes of cutter teeth and cutting direction on the transverse cutting force when cutting wood with six kinds of serrated tools. Jiang et al. (1994) discussed the cutting performance of cutting blade through the cutting force experiment, and provided the methods to improve the cutting performance of the milling cutter from the aspects of tool material, cutting blade structure and tool geometric angle. Zhang et al. (2010) studied the influence of the same tool wear condition on the cutting force under the same cutter parameter, and discussed the influence mechanism. Zhao et al. (2015) studied the influence of cutting parameters on milling composite force, and established the milling force model by response surface design test, which provided theoretical basis for optimizing the selection of cutting parameters, controlling and predicting milling force.

At present, the research on wood milling performance mainly focuses on tool material, tool geometric angle, cutting parameters and other aspects (Zhang 2011, Aknouche et al. 2009, Guo et al. 2009). There are few studies on the influence of milling cutter blade structure on wood milling from the published literature (Guo et al. 1999). The paper used single factor experiment to discovery the influence of milling cutter blade on surface quality and milling performance under different cutting conditions, which provided reference for improving the stability of machining quality and selection of forming tools.

## MATERIAL AND METHODS

### Experiment materials

The machine tool in experiment was from MIKRON UCP710 CNC milling machining center. The test tools selected three typical end milling cutters, which were often used in wood milling produced by the Germany Leitz company. The Fig. 1 presents the cutting tools in test, and tools parameters are shown in Tab. 1. At the same time, the solid wood of *Fraxinus mandshurica* was selected as the experimental material with the size (length × width × thickness) of 500 × 120 × 20 mm, moisture content of 9%, and density of 0.532 g·cm<sup>-3</sup>.

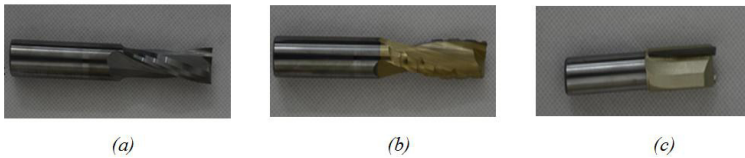


Fig. 1: Cutting tools in test: (a) The integral cemented carbide upright milling cutter with spiral blade, (b) The integral cemented carbide upright milling cutter with spiral curved blade, (c) The integral cemented carbide upright milling cutter with straight blade.

Tab. 1: Type and parameters of the wood milling tool.

Name	Type	Material	Outside diameter of cutting blade(mm)	Shank diameter × length (mm × mm)	Tool length (mm)	Tooth number
a Upright milling cutter with spiral blade	042761	cemented carbide	φ16	φ16 × 50	100	Z = 2
b Upright milling cutter with spiral curved blade	240202	cemented carbide	φ16	φ16 × 50	100	Z = 2
c Upright milling cutter with straight blade	072106	cemented carbide	φ16	φ16 × 50	90	Z = 2

## Experimental methods

Wood is a kind of anisotropic biological material, in the milling process, chip thickness is changed from large to small during down milling, and chip thickness is from small to large transformation during up milling (Su et al. 2002). Therefore, conducted experimental research to the above three tools, with the feed rate as the change vector and other parameters fixed, the comparative experiments were carried out respectively according to the cutting methods of down milling and up milling, and the influence rules of different cutting tools on the milling process were analyzed (Yan. et al. 2002 and Guo et al. 2011), the Tab. 2 presents milling parameters.

Tab. 2: Wood milling experiment parameters.

	Cutting speed $v_c$ (m·min <sup>-1</sup> )	Feed rate $f$ (m·min <sup>-1</sup> )	Cutting depth $a_p$ (mm)	Cutting width $a_e$ (mm)
1	600	6	20	4
2	600	10	20	4
3	600	14	20	4

## RESULTS AND DISCUSSION

### The effect of the tool blade shape on the cutting force

In order to explore the effect rule of cutter blade shape on the cutting force, the milling forces in three directions of XYZ under different feed rate in down and up milling conditions are

statistically analyzed. The Fig. 2 presents a histogram of the change of cutting force with feed rate for *a*, *b* and *c* cutting tools when cutting speed  $v_c = 600 \text{ m}\cdot\text{min}^{-1}$ , cutting depth  $a_p = 20 \text{ mm}$  and cutting width  $a_e = 4 \text{ mm}$ , the down milling status is shown in Fig. 2a, the up milling status is shown in Fig. 2b. It can be seen from the figure that during down milling, with the increasing of feed rate, the composite forces in X, Y and Z directions of each tool have a gradually increasing trend. Because the blade types of cutters a and b are spiral edge, the cutting force  $F_z$  in the Z direction of these two blades is greater than  $F_x$  and  $F_y$ . In the case of up milling, when the feed rate is  $6 \text{ m}\cdot\text{min}^{-1}$ , c tool emerges a sudden force in the X direction during cutting, which may be caused by the hard point of the material encountered in the cutting process, so it is not discussed. In addition, with the increase of the feed rate, the cutting force of the three tools in various directions also increases gradually, and the trend is more regular.

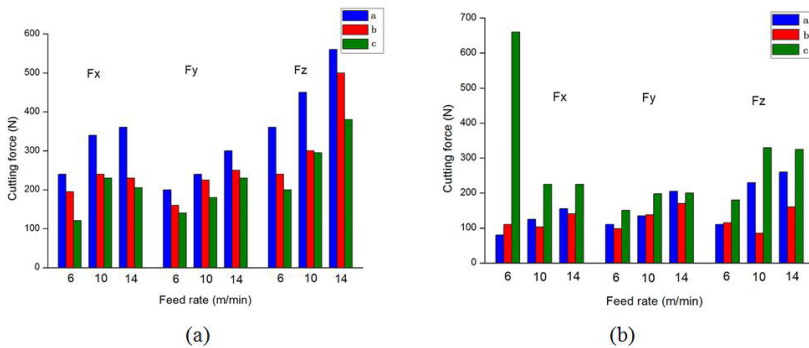


Fig. 2: The effect rules of the feed rate on the cutting forces of the cutting tools *a*, *b*, and *c* in milling: (a) Down milling, (b) Up milling.

After measurement and calculation, the cutting composite force of the cutting tools in down milling is shown in Tab. 3. In the case of the same feed rate and the same direction, the cutting composite force of three kinds of tools shows a gradual decrease trend, and the value of the cutting composite force has a relation:  $F_a > F_b > F_c$  ( $F_a$  - the cutting composite force of the tool *a*;  $F_b$  - the cutting composite force of the tool *b*;  $F_c$  - the cutting composite force of the tool *c*; the same below).

Tab. 3: Cutting composite force of the three cutting tools in the down-milling.

Tool type	Cutting composite force (N)
a	497-637.5
b	389.6-648.7
c	272.3-509.8

The cutting composite force of the three cutting tools in up milling is shown in Tab. 4. Excluding the sudden change of the tool *c* in the X direction, in the case of the feed rate is  $6 \text{ m}\cdot\text{min}^{-1}$ , the cutting composite force value of the three cutting tools does not fluctuate much. When the feed rate increases from  $10 \text{ m}\cdot\text{min}^{-1}$  to  $14 \text{ m}\cdot\text{min}^{-1}$ , the value of the cutting composite force has a relation:  $F_c > F_a > F_b$ . Due to the cutting blade of the tool *b* is the unique helical blade and wave blade, this cutting blade improves the cutting efficiency and optimizes the cutting effect in the cutting process. Compared with the straight line blade of the tool *c* and the helical blade of the tool *a*, the tool *b* also plays a role in reducing the cutting force in the up milling process.

Tab. 4: Cutting composite force of the three cutting tools in the up-milling.

Tool type	Cutting composite force (N)
a	253.1-496.7
b	167-523.3
c	286.6-550.8

In the condition of the same feed rate, by analyzing and comparing the cutting force under the two milling methods, it can be known that the cutting force of the cutting tools a and b in down milling is greater than that in up milling under the same cutting parameters. The cutting force of the tool c in the process of down milling is less than that in the process of up milling. Therefore, it can be seen that the milling method also has an impact on the cutting force when the tool is cutting the material.

### The effect of the tool blade shape on the cutting vibration

In order to explore the effect rule of cutter blade shape on the cutting vibration, the cutting vibration in three direction of XYZ under different feed rate in down and up milling conditions are statistically analyzed. The Fig. 3 presents a histogram of the change of cutting vibration with feed rate for a, b and c cutting tools when cutting speed  $v_c = 600 \text{ m}\cdot\text{min}^{-1}$ , cutting depth  $a_p = 20 \text{ mm}$  and cutting width  $a_e = 4 \text{ mm}$ , the down milling status is shown in Fig. 3a, the up milling status is shown in Fig. 3b. It can be seen from the figure that during down milling, due to the increase of the cutting force caused by the increase of the feed rate, the vibration values in X, Y and Z directions of each tool have a gradually increase trend. In the case of the tool a, the cutting vibration in the X direction (feed direction) will be relatively small when the feed rate is  $6 \text{ m}\cdot\text{min}^{-1}$ , and the main sources of the cutting vibration are Y direction (cutting width direction) and Z direction. Similar to the down milling process, the vibration value of the three directions also increases gradually.

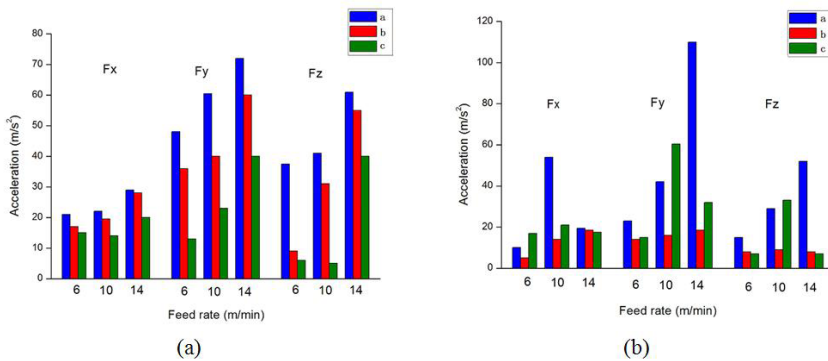


Fig. 3: The effect rules of the feed rate on the cutting vibration of the cutting tools a, b, and c in milling: (a) Down milling, (b) Up milling.

After measurement and calculation, the sum of cutting vibration in X, Y and Z directions during down milling is obtained; the total vibration value is shown in Tab. 5. In the case of the same feed rate and the same direction, the cutting vibration of the three kinds of tools shows a gradually decrease trend, and the relationship is: the cutting vibration of the tool a is greater than the tool b, and the cutting vibration of the tool b is greater than the tool c, but the difference is relatively less.

Tab. 5: Cutting vibration values of the three cutting tools in the down-milling.

Tool type	Cutting vibration (m·s <sup>-2</sup> )
a	63.8-99.1
b	41.9-90.8
c	22.1-61.6

The total vibration value of the three cutting tools in up milling is shown in Tab. 6. Under the same cutting parameters, the cutting vibration of the tool *a* is slightly larger than the tool *b*, but the difference is very subtle. However, due to the reasons of the unique wave blade design of the tool *b*, the cutting vibration of the tool *b* is significantly smaller than that of the tools *a* and *c*.

Tab. 6: Cutting vibration values of the three cutting tools in the up-milling.

Tool type	Cutting vibration (m·s <sup>-2</sup> )
a	30.3-125.3
b	13.6-27.4
c	23-70.4

**Effect of the tool blade on chip formation**

In order to explore the effect rule of the cutter blade shape on the chip formation, the chip formation under different feed rate in down and up milling conditions are statistically analyzed. The Fig. 4 presents the change diagram of chip formation of *a*, *b* and *c* cutting tools in down milling states when cutting speed  $v_c = 600 \text{ m}\cdot\text{min}^{-1}$ , cutting depth  $a_p = 20 \text{ mm}$  and cutting width  $a_e = 4 \text{ mm}$ . The chips of tool *a* and *c* show spiral curled shape, and the chips produced by tool *c* are generally more straight. The chips of the tool *b* presents irregular spiral, and have certain radian and present different size stripes. It can be known from the test that the size of the tool chip will increase with the feed rate increasing.



Fig. 4: The chip shapes comparison of the different tool milling in the down-milling.

The Fig. 5 presents the chip formation at different feed rate with different cutting tools in up milling state. Similar to the down milling state, the chips of the tool *a* and *c* increase with the feed rate increasing, and the chips of the tool *b* appear scattered strip.

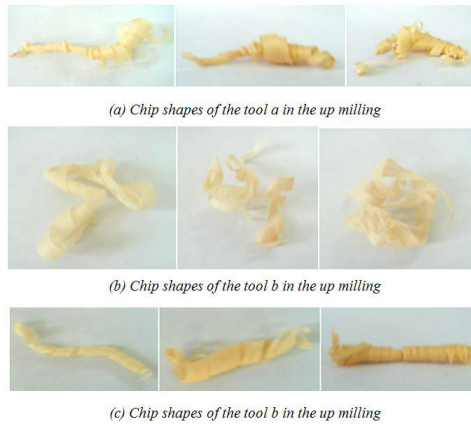


Fig. 5: The chip shapes comparison of the different tool milling in the up-milling.

### Effect of the tool blade on the surface quality of the workpiece

The surface quality of the cut-in and the cut-out of the workpiece cut by the tools *a*, *b*, and *c* is measured and compared by the TR240 surface profile tester. The Fig. 6 presents the rule of the surface roughness of the tool *a*, *b*, and *c* with the changing of feed rate in the down milling.

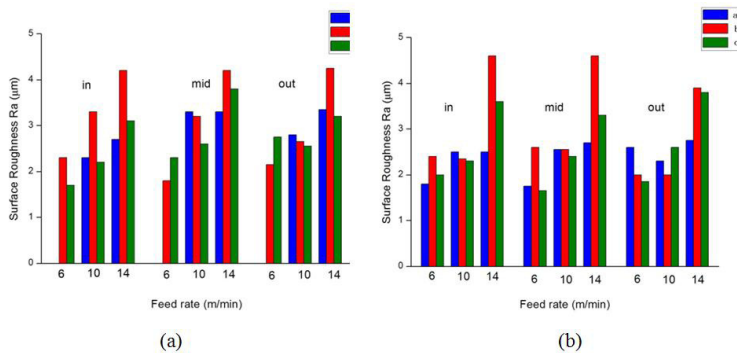


Fig. 6: The effect rules of the surface roughness of the cutting tools *a*, *b*, and *c* with the changing of feed rate in the down milling: (a) Down milling, (b) Up milling.

Each group of experiments collected the surface of the cutting-in, cutting-mid, and cutting-out to detect, so as to reach the purpose of minimizing the error and ensure the accuracy of the measurement data. When the specimen is processed, keeping the cutting speed  $v_c = 600 \text{ m}\cdot\text{min}^{-1}$ , cutting depth  $a_p = 20 \text{ mm}$  and cutting width  $a_e = 4 \text{ mm}$  remain unchanged, the feed rate is set at  $6 \text{ m}\cdot\text{min}^{-1}$ ,  $10 \text{ m}\cdot\text{min}^{-1}$ , and  $14 \text{ m}\cdot\text{min}^{-1}$ . The result shows that the surface roughness appears gradually increasing trend with the increase of the feed rate when the three tools perform down milling and up milling, and the value of the surface roughness increases obviously when the feed rate reaches  $14 \text{ m}\cdot\text{min}^{-1}$ . By comparison under the same feed rate, the surface roughness of the workpiece of the tool *a* is slightly better than that of the tool *c*. Due to the non-uniformity of material removal in the process of the wave blade cutting, the surface roughness of the tool *a* and

c are obviously better than that of the tool b. In the whole, the surface roughness of the workpiece after the down milling is better than that after up milling.

## CONCLUSIONS

In this paper, single factor milling tests were carried out on the tools with different cutting blades, and the influence rules of three kinds of cutting tools on cutting force, cutting vibration, chip state and surface quality were compared under different feed rate. The following conclusions were drawn from the comparison and observation:

- (1) With the increase of feed rate during down milling, the cutting composition force of the three cutting tools increases gradually in all directions, and the trend is more regular. At the same feed rate and the same direction, the cutting composition force of the three kinds of cutting tools successively presents a decreasing trend in the up milling. The unique helical blade and wave blade of tool b can reduce the cutting force in the up milling.
- (2) In the downing milling, the cutting vibration produced by the helical blade and straight blade with vibration damping groove structure is less than that of the helical blade without damping groove structure. In the up milling, because the upright milling cutter with spiral curved blade has a wavy damping groove, which can reduce the cutting resistance and minimize the cutting vibration.
- (3) Through the experiment on chip deformation mechanism, the influence relationship between the cutting parameters on chip morphology is obtained. The shape of the chip is related to the cutter blade shape, and the helical blade produces helical chip, while the straight blade produces linear chip, and the helical blade with the vibration groove produces block chip.
- (4) It can be seen from the detection of workpiece surface quality, the feed rate has a great influence on the surface roughness. In the case of down and up milling, the surface roughness of the workpiece increases with the increase of feed rate, and the surface quality of the milling tool with helical blade is better. In contrast, the milling surface roughness of the helical blade without damping groove is smaller.

## ACKNOWLEDGEMENTS

The research was supported by Research on Key Equipment for Multi-interface Machining of Small Diameter Lumber (2018YFD06003054); and Fundamental Research Funds for the Central Universities (2572018CG06). The authors would like to take this opportunity to express their sincere appreciation.

## REFERENCES

1. Ābele, A., Mioncinskis, U., Tuhern H., 2013: Determination of cutting tool wear and surface roughness of straight milled aspen wood. *Pro Ligno* 9(4): 751-759.
2. Aknouche, H., Outahyon, A., Nouveau, C., Marchal. R., Zerizer, A., Butaud, J.C., 2009: Tool wear effect on cutting forces: In routing process of Aleppo pine wood. *Journal of Materials Processing Technology* 209(6): 2918-2922.

3. Bayoumi, A.E., Bailey, J.A., 1985: Comparison of the wear resistance of selected steels and cemented carbide cutting tool materials in machining wood. *Wear* 105(2): 131-144.
4. Deng, N., Li, C., Liu, M., Lin, L., 2014: Research on processing technology of wave milling. *Tool Technology* 48(8): 102-103.
5. Engin, S., Altintas, Y., Ben, A.F., 2000: Mechanics of routing medium density fiberboard. *Forest Products Journal* 50(9): 65-69.
6. Ekevad, M., Cristóvão, L., Marklund, B., 2012: Lateral cutting forces for different tooth geometries and cutting directions. *Wood Material Science & Engineering* 7(3): 126-133.
7. Eblagon, F., Ehrle, B., Graule, T., Kuebler, J., 2007: Development of silicon nitride/silicon carbide composites for wood-cutting tools. *Journal of the European Ceramic Society* 27(1): 419-428.
8. Guo, F., Wang, Q.Y., Lei, W.M., 1999: Numerical control grinding technology and tool position calculation for front face of spiral blade cutter. *China Mechanical Engineering* 19(1): 10-11.
9. Guo, X.L., Liu, H.N., Cao, P.X., 2011: Formation mechanism of chip flow in the milling of wood based materials. *Journal of Nanjing Forestry University (Natural Science Edition)* 35(5): 74-78.
10. Guo, X.R., Lu, H.M., Gou, X.L., Du D.F., 2009: Study on virtual simulation of wood cutting process based on three-dimensional model and geometric parameter optimization for wood tool. *Machine Tool & Hydraulics* 37(6): 30-33.
11. Jung, Y.H., Kim, J.S., Hwang, S.M., 2001: Chip load prediction in ball-end milling. *Journal of Materials Processing Technology* 111(1): 250-255.
12. Jiang, J.P., Huang, K.Z., Ai, X., Ding, Z.H., Gao, H.D., 1994: Discussion on improving cutting performance of wood forming milling cutter. *Journal of Qingdao Institute of Architecture and Engineering* 1: 1-5.
13. Li, L., 2008: Choice and application of wood milling tools. *Wood Processing Machinery* 19(5): 47-52.
14. Ma, Y., 2007: The new development of theory research in design of timber cutter abroad. *Forestry Machinery and Woodworking Equipment* 35(3): 4-8.
15. Palmqvist, J., 2003: Parallel and normal cutting forces in peripheral milling of wood. *Holz als Roh-und Werkstoff* 61(6): 409-415.
16. Päivinen, M., Heinimaa, T., 2003: The effects of different hand tool blade coatings on force demands when cutting wood. *International Journal of Industrial Ergonomics* 32(3): 139-146.
17. Ramasamy, G., Ratnasingam, J., 2010: A review of cemented tungsten carbide tool wear during wood cutting processes. *Journal of Applied Sciences* 10(22): 2799-2804.
18. Song, C., Song, K.F., Song, H.M., 2006: The microscopic process at the cutting edge of the cutting tool during wood cutting. *International wood industry* 36(4): 19-25.
19. Su, W.C., Wang, Y., 2002: Effect of the helix angle of router bits on chip formation and energy consumption during milling of solid wood. *Journal of Wood Science* 48(2): 126-131.
20. Yan, B., Xu, A.P., Zhang, D.W., Huang, T., Zeng, Z.P., 2002: A new milling force model of spiral edge ball end milling cutter is presented. *China Mechanical Engineering* 13(2): 160-163.
21. Zhu, H.B., 2015: Influencing factors of milling vibration based on cutting parameters and tool wear. *Mechanical Research and Application* 4: 57-59.
22. Zhang, Z.K., Peng, X.R., Li, W.G., Zeng, J., Wang, B.G., 2011: Influence of cutting parameters on cutting forces in wood sawing. *China Wood Industry* 25(6): 7-9.

23. Zhang, J.L., Li, B.Z., Pang, J.Z., 2010: Study on cutting force characteristics in tool wear process. *Manufacturing Technology and Machine Tools* 5: 111-113.
24. Zhao, Y.C., Tu, J.X., 2015: Influence of cutting parameters on milling force of ebony wood. *Machine Design and Manufacturing Engineering* 5: 1-5.
25. Zhang, Z.C., 2011: Face milling cutter for plane machining and its parameter selection. *Metal Working (cold working)* 21: 43-46.

YANG CHUNMEI, LIU QINGWEI, JIANG TING, SONG MINGLIANG, MA YAN\*  
NORTHEAST FORESTRY UNIVERSITY  
FORESTRY AND WOODWORKING MACHINERY ENGINEERING TECHNOLOGY CENTER  
HAPING 6TH STREET, HAPING ROAD, HEILONGJIANG PROVINCE  
HARBIN, 150040  
CHINA

\*Corresponding author: myan@vip.163.com

LIU JIUQING\*  
NORTHEAST FORESTRY UNIVERSITY  
COLLEGE OF MECHANICAL AND ELECTRICAL ENGINEERING  
HARBIN, 150040  
CHINA

\*Corresponding author: nefujdljq@163.com

## TIMBER COLUMN SEISMIC RESPONSE DESIGN

ABDOULLAH NAMDAR<sup>1, 2</sup>

<sup>1</sup>HUAIYIN INSTITUTE OF TECHNOLOGY, HUAI'AN, CHINA

<sup>2</sup>TON DUC THANG UNIVERSITY, HO CHI MINH CITY, VIETNAM

(RECEIVED APRIL 2019)

### ABSTRACT

The timber column seismic response has been analyzed when it has been subjected to near-fault ground motion. The cyclic displacement and cyclic strain have been investigated. It needs to indicate in most of the literature acceleration history of earthquake used in the numerical analysis is not well clear for the reader. The results showed that the damping ratio, strain energy, and nonlinear deformation were changed in respect to the frame geometry. The innovation of this paper is to develop cycling graphs by means ABAQUS for study timber column seismic response and improve the concept of strain energy in understanding displacement mechanism.

KEYWORDS: Timber column, cyclic displacement, strain energy, nonlinear deformation.

### INTRODUCTION

The earthquake is one of the natural hazards needs to investigate appropriately to enhance the infrastructural seismic design. On the other hand, each near-fault ground motion has specific characteristics. The timber beam seismic design has numerically been simulated when subjected to near-fault ground motion, with reference to small displacement theory. The inertial interaction, energy dissipation, and nonlinear deformation are analyzed. The ABAQUS has been used to simulate a number of engineering problems including timber beams and timber structure (Namdar et al. 2019, Namdar et al. 2016a, Namdar et al. 2016b, Namdar 2016a, Namdar 2016b). The numerical, experimental, analytical and theoretical methodologies have been used to explain concepts of seismic timber design, seismic resistance evaluation of traditional timber-frame damping mechanism, construction quality of composite timber-steel frame, traditional timber construction, use timber as an eco-friendly strengthening system and mechanical properties of the timber (Namdar et al. 2019, Namdar et al. 2016a, Jayne 1959, Sandoz 1989, Yeh et al. 1971, Rajčić and Bjelanović 2005, Ayala and Wang 2006, Pizzo et al. 2004, Arun 2009, Galassi et al. 2018, Androić et al. 2008, Daniūnas and Gečys 2015, Stepinac et al. 2017, Aktas et al. 2014). Among construction materials, the wood is used in the structure, and it has shown satisfactory seismic resistance (Soltis 1984, Liu et al. 2018). But the seismic design of timber column subjected to near-fault ground motions and developing cycling graph using ABAQUS and also

the explanation of seismic behavior of timber column never has been reported in the literature. In the present study, the column is located in a single span and single floor of a timber frame with 3-meter height. The columns of two frames with 1.5 m and 3 m span have been compared. The seismic load response-cyclic displacement, seismic load response-cyclic strain, and cyclic strain-cyclic displacement have been investigated to evaluate the damping ratio, strain energy, and nonlinear deformation.

### METHOD AND MATERIALS

The timber frame is subjected to near-fault ground motion. The ABAQUS is used to executing the numerical analysis. Fig. 1 shows the near-fault ground motion is used in the numerical simulation. To explain results, a critical time of the near-fault ground motion has been zoomed and these critical times of acceleration history of the earthquake were used in numerical analysis. In the many kinds of literature acceleration history of earthquake used in the numerical analysis is not well clear for the reader. In the present study, the near-fault ground motion is zoomed. This technique simplifies the interpretation of timber column seismic behavior. Fig. 1b shows the near-fault ground motion has maximum loading in 24.05 sec and maximum reloading occurs in 24.14 sec. In the peak acceleration, there is 0.09 sec for change direction of seismic loading. When the near-fault ground motion reached the peak level, the highest vibration is applied to the model. The seismic excitation widespread released by small-magnitude earthquakes is insignificant in seismic design of structure compared to a major earthquake. Therefore, the near-fault ground motion from 22 sec till 26 sec is used in the numerical analysis. The seismic load response-cyclic displacement, seismic load response-cyclic strain, and cyclic strain-cyclic displacement of the column shown in Fig. 2 have been investigated to evaluate the damping ratio, strain energy, and nonlinear deformation. The details of the timber frame have been depicted in Fig. 2. The geometry of the timber frame has been used at the numerical analysis is shown in Fig. 2. The mechanical properties of timber have been used in the numerical shows in Tab. 1.

Tab. 1: Timber material properties (Dackermann et al. 2016).

Young's modulus (N·m <sup>-2</sup> )	Poisson's ratio	Density (kg·m <sup>-3</sup> )
14,750 *106	0.3	620

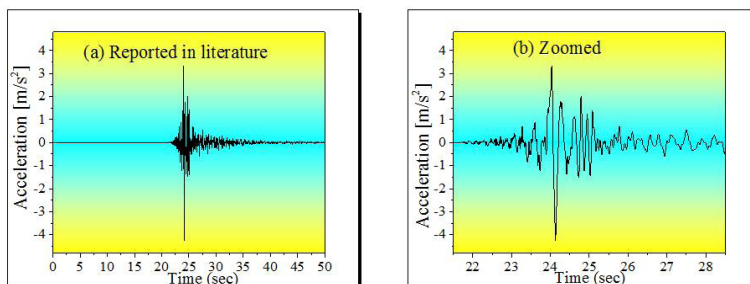


Fig. 1: Acceleration history of the earthquake has been reported in the literature (Center for Engineering Strong Motion data. <https://strongmotioncenter.org>).

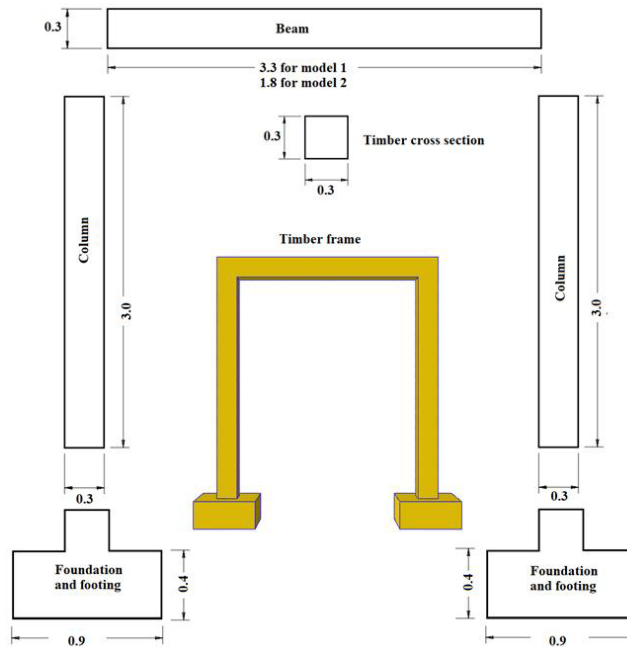


Fig. 2: The structural elements of the timber frame (dimension in meters).

## RESULTS AND DISCUSSION

The cyclic nonlinear displacements have numerically been estimated using finite element method. The deformation mechanism is explained based on cyclic nonlinear displacements observed along the timber column when simulated seismic excitation was applied to the models. The seismic wave travels along the timber beams causes lateral, vertical and residual displacements, it occurs with respect to the seismic wave velocity, construction material characteristics, and frame geometry. The displacement morphology of timber column effect to timber frame seismic resistance. It has been observed that the main reason for timber frame failure was timber geometry. Fig. 3 shows the higher seismic load response and displacement were developed to timber column at model 2. The load-displacement curves show the higher nonlinear deformation in the column at model 2. The seismic wave traveling path is changed at each model. The seismic excitation widespread and cyclic nonlinear displacements cause to the reduction of timber span seismic stability and subsequently significant damage or fully collapse occurs. The deformed shape of timber column at any instant of motion represents in terms of dynamic displacement and changing with time. When the timber frame is subjected to seismic excitation the initial displacement is created. The seismic resistance of timber column is opposite an initial displacement. The geometry of frame supports in time and type of an initial displacement occurrence. It can be observed that the response cyclic load to displacement governs the timber frame vibration mechanism and modify damping ratio at each model. In comparison two models two different shapes of nonlinear displacement shown in Fig. 3. The higher nonlinear

displacement appears at model 2, it is due to resonance and subsequently, significantly timber column seismic resistance reduces, displacement mechanism of timber frame is changed and results in faster timber frame collapse. The peak displacement response in model 2 is higher than in model 1. When the yield displacement capacity of the lateral load resisting system is exceeded, the strain energy internal elastic force and base shear force at each model causes modification nonlinear deformation mechanism and the cyclic load-displacement path for each model formed differently. When the timber column is subjected to seismic excitation the cyclic softening area occurs on the column and it causes specific nonlinear deformation for each column at models 1 and 2. This type of nonlinear behavior leads to the deterioration of seismic resistance of timber frame and developing large displacements. The timber column stiffness degrading hysteretic with respect to larger displacements is minimized seismic resistance of timber. Accordingly, the nonlinear deformation has been formed at softening area.

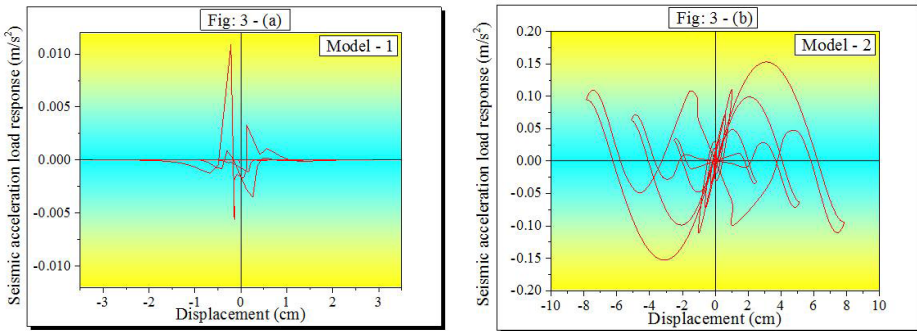


Fig. 3: Seismic response versus displacement found in timber column models 1 and 2, when the model has been subjected to near-fault ground motion.

The interpretation strain-displacement cyclic graph simplified understanding the variation of elastic displacement ratio in numerical analysis. The strain hardening is shown in Fig. 4. The strain-displacement cyclic paths show how strain energy creates displacement. The displacement deforms corresponding to change releasing strain energy. It can be observed that the high difference in peak displacement, and on another hand from the strain-displacement cyclic paths has been understood that the types of seismic excitation at each model has specific characteristics, and its effects on seismic load transferring and deterioration seismic resistance of the model. The seismic excitation type has a meaningful relationship with elastic strain and displacement. The unequal cyclic nonlinear displacements are applicable for seismic assessment and design of timber column and timber frame as well. The near-fault ground motion response in corporative with timber frame geometry induces elastic and inelastic displacement, and the yield point for each timber column is changed. The damping modified with related to the displacement mechanism. The seismic excitation releasing the strain energy and accumulating strain energy in each timber frame column causes nonlinear deformation at different parts of timber column. However, in the present study, the measurement of dissipation strain energy has been made for an evaluation damping ratio of timber column. The strain energy in model 2 is raised compared to model 1, from this phenomenon can understand that the damping ratio in model 1 is considerably higher than model 2. The results of numerical analysis shown dissipation strain energy at a timber column with the same material and shape significantly were affected by the geometry of the timber frame. The concept of sharing loading has governed strain energy and damping ratio of

a structural element consequently, and strain energy dramatically increases. In the design point of view arrangement, a single structural element significantly affects the safety of the structure. On the other hand in model 2 having the same mechanical properties as model 1, the cyclic nonlinear strain was found to dramatically increases in model 2 with increasing frame span and constant height of timber column. The condition of strain-displacement cyclic paths was observed in model 1 has the lower inclination at peak level. However, sudden release strain energy increases seismic excitation of timber frame model 2. Consequently, the seismic excitation mechanism in timber frame supports to predict frame nonlinear cyclic mobility. Furthermore, the cyclic nonlinear strain versus cyclic nonlinear displacement graph shows in a timber frame subjected to a complex seismic excitation mechanism, and the permanent loss in shear strength is expected.

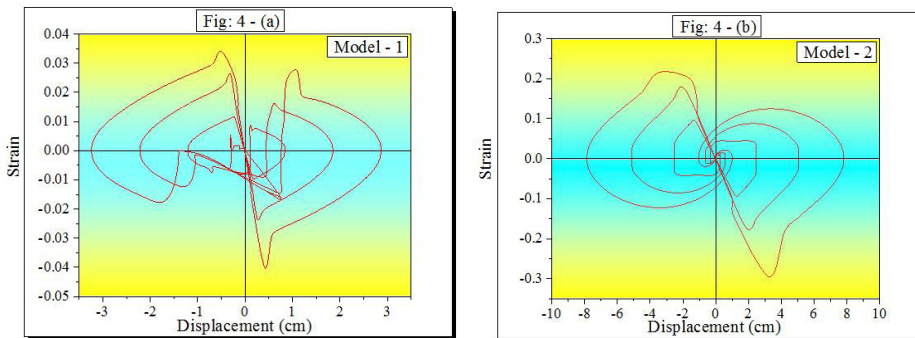


Fig. 4: Strain versus displacement found in timber column models 1 and 2, when the model has been subjected to near-fault ground motion.

The seismic load response versus cyclic nonlinear strain on timber column models 1 and 2 are plotted in Fig. 5. The near-fault ground motion induced cyclic nonlinear displacement and cyclic nonlinear strain, the level of strain and displacement depend on a number of seismic excitation loading. The sensitivity geometry of timber frame allows an earthquake to induce more shaking and it leads to reduction frame strength. A seismic excitation loading applied to the timber frame with the same magnitude produces different strain and settlement mechanism with specific peak level. However, it may cause a dramatic drop-off in the strength of the timber frame at each model differently. When the seismic simulated loading is applied to the model, the most critical condition develops when timber frame is subjected to the mechanical resonance and the strain energy dissipation occurs with a delay due to high oscillate produced by storage strain energy at the model and vibrating model at a specific frequency. The increase in strain energy is intended to provide accelerations in the timber frame. The amplitude at resonance controls the damping ratio. The resonance creates a large displacement and inertia force, however, it leads to failure of timber frame due to the reduction of inertial resistance and developing the mechanical damping and forming the elastic deformation after the meaningfully reducing strength of the timber. The plastic area at timber column leading to decrease storage strain energy in remaining time the near-fault ground motion is applied to the model. The strain energy behavior is important in timber structure seismic response analysis and it significantly depending on frame geometry to be used in a construct timber structure. According to the energy sharing mechanism, when sudden release strain energy it built up deformation and shake model with noticeable magnitude.

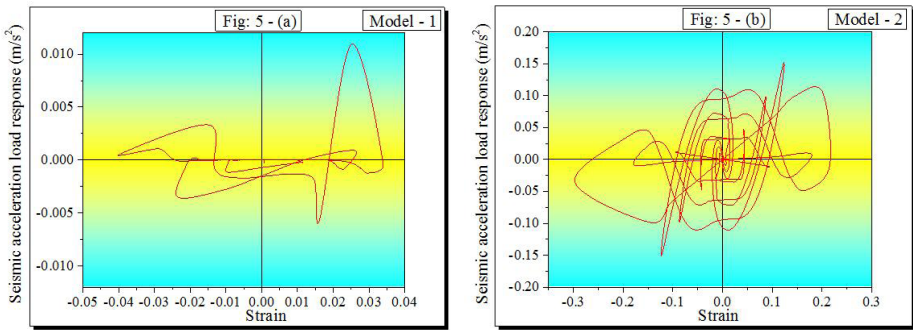


Fig. 5: Seismic response versus strain found in timber column models 1 and 2, when the model has been subjected to near-fault ground motion.

Fig. 6 shows that the larger lateral nonlinear displacement is induced in column characterized by longer frame span. The larger nonlinear deformation has been observed in model 2. The nonlinear cyclic deformation with higher concentration is observed in model 2.

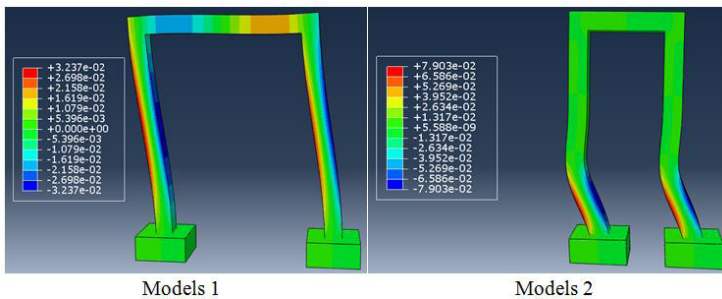


Fig. 6: The cyclic lateral displacement of timber frame (dimension in meters).

The morphology of nonlinear cyclic deformation has been produced based on strain energy characteristics. Significant nonlinear cyclic deformation has occurred within the timber frame and both beam and column experience damage. The noteworthy enlargement wave propagation develops resonance in the majority of the shared load in the form of shearing force mechanism at model 2. The shearing force mechanism is important at design criterion in relation to the timber frame seismic stability. The inappropriate shearing force mechanism leads to the noteworthy enlargement seismic wave propagation effect to the model. The strain energy built up the multidirectional cyclic inertia forces and acts to the mass of timber frame if timber frame exhibit with insufficient inelastic deformation capacity and the unsustainable damage expected. In the present study has been observed that the same near-fault ground motion causes differences multidirectional cyclic inertia forces are subjected to each model, and it leads to developing differences seismic response of these timber frames and different type of failure mechanism at each model. The elastic force and elastic displacement have been occurred with sharing seismic excitation. The damage states in multidirectional cyclic inertia forces refer to strain energy characteristics, and this phenomenon induces cracking, crushing and collapse with minimizing strength and stiffness of timber. The strain energy characteristics are responsible for developing

softening area at timber beam and column, and it is characterized by failure hardening response and occurrences cyclic nonlinear deformation.

### Related work

In the timber beam, seismic resistance has been reported that the greater displacements occur with the increasing length of the timber beam, and subsequently, the strain energy dissipation, inertial interaction and deformation geometry have been modified (Namdar et al. 2019). With attention to the result of the present study, it can be concluded that with select a timber frame with appropriate span significantly support seismic resistance of timber frame and results in suitable cyclic load sharing in frame elements.

The different types of displacements of the concrete footing have been mitigated with increasing soil-concrete footing interface area (Namdar and Dong, 2019). In the present study, the footing is placed on a rigid surface, the displacements of timber frame alter with change soil-footing interface.

The hysteresis loading influences to the load-bearing capacity of the frame (Stepinac et al. 2019), in the present study, at model 2, the results of the numerical simulation have coincided with those is presented in the literature.

The combination of a nonlinear finite element analysis and a complex constitutive model will lead to convergence stability problems (Zucchini 2007). Fig. 7 shows in the most wood system at an initial loading no pinching occurs and in second loading cycle pinching starts (Foliente 1995, Baber and Noori 1986).

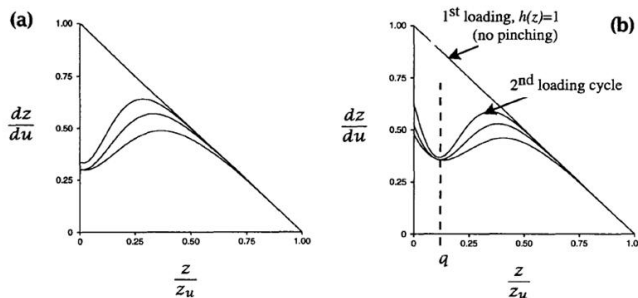


Fig. 7: The pinching under hysteresis mechanism: (a) pinching-function result (Baber and Noori 1986), and (b) pinching for timber (Foliente1995).

The behavior of proposed pinching function for wood systems shows the loading and unloading process leads to initiate fatigue in timber material. It is expected that the model 2 is more vulnerable to fatigue compared to the model one. The reduction of timber structural element fatigue is possible with appropriate timber frame seismic design. Fig. 8 shows, during excitation of the timber frame due to applying cyclic loading, the loading, unloading, and reloading process, the different types of the pinching occur. The following the nature of cyclic loading, three stages of the pinching mechanism included the pinching in the negative direction, positive direction and pinching reach to zero levels have been observed when the timber is subjected to the cyclic loading. During changing the direction of cyclic loading the pinching shape has been changing, while the magnitude of the pinching is related to the nature of the applied load and strength of the timber. Fig. 6 shows, the results of the present numerical analysis

is in good agreement with Fig. 8. It observed that the results of the present numerical analysis show the seismic timber behavior during the timber frame subjects to pinching. According to Fig. 8, the three stages of pinching mechanism leads to the developing fatigues in the timber frame structural elements if the released strain energy is higher than shear strength and ductility cyclic resistance of the timber structural element and timber frame as well.

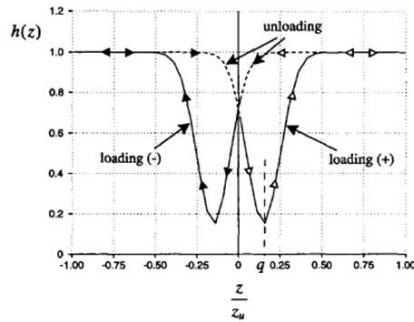


Fig. 8: The pinching mechanism for timber structure (Foliente1995).

After the retrofit a timber structure needs to numerically simulate and design that, it is due to change of timber structure seismic load response-cyclic displacement, seismic load response-cyclic strain, and cyclic strain-cyclic displacement after the retrofit process. The new resonance appears with new characteristic and develops displacement and inertia force which is different from before retrofit, however, the failure mechanism of timber frame meaningfully modifies, in considering inertial resistance, the mechanical damping ratio, forming the elastic deformation in respect to changing strength and stiffness of the timber.

Timber has high flexibility and seismic resistance compared to other building materials. Where damping ratio, strain energy, and nonlinear deformation are not satisfied, the geometry of timber frame must be modified and it leads to change damping ration and effects to the flexibility and leads to modifying seismic resistance of timber frame. The flexibility of timber frame changes related to the modification of timber frame geometry. The seismic resisting of the timber frame is desirable with architectural space designing through providing sufficient timber frame flexibility. This process is responsible for avoiding frame instabilities due to unallowable P- $\Delta$  produce at all structural elements. The architecture designer has to consider maximum safe lateral, vertical and rotational flexibility of each frame members with attention to shapes and sizes of the member in order to control damping ratio, strain energy, and nonlinear deformation of the timber frame. The timber structures seismic resistance mechanism is referred to near-fault ground motion, site geomorphology and building architectural design. The multidirectional flexibility of structural elements has a direct relationship with strain energy concentration. The advantageous flexibility of a structural element affects to completed timber frame seismic resistance. The high flexibility of timber frame causes a long period of vibration, in order to have a timber frame with suitable seismic and wind resistance, it needs to design a timber frame with the right flexibility. Although some structural elements have much higher flexibility than others.

The several timber frame structures have been reported in the literature (Namdar et al. 2019, Namdar et al. 2016a, Halicioglu et al. 2014, Palinić and Bjelanović 2016), they have included modern and heritage building and showed to resist well to seismic loading. The results existing in the present study support to design a flexible structure with high seismic resistance characteristic. Using recycled aggregates to make concrete with acceptable durability

performance, high-performance and self-compacting can be investigated to make the composite timber-concrete structure in the future. It supports to minimize the carbon footprint producing due to construction activities. The timber is eco-friendly and easily recyclable materials as well. However, making a composite timber-concrete cross-section, while the concrete has been made by recycling materials has never been reported in the literature, and can be investigated in the future.

## CONCLUSIONS

The timber elastic frame has been subjected to the near-fault ground motion, and corresponding cyclic nonlinear displacement and cyclic nonlinear strain model have been analyzed. The seismic load response-cyclic displacement, seismic load response-cyclic strain, and cyclic strain-cyclic displacement have been investigated. The critical time of the near-fault ground motion has been zoomed and used in numerical analysis. In the present study the follows goals have been achieved:

- The seismic excitation widespread and cyclic nonlinear displacements cause to the reduction of timber span seismic stability and subsequently significant damage or fully collapse occurs.
- It can be observed that the high difference in peak displacement, and on the other hand from the strain-displacement cyclic paths has been understood that the types of seismic excitation at each model has specific characteristics, and its effects to seismic load transferring and deterioration seismic resistance of the model.
- The results of numerical analysis shown dissipation strain energy at a timber column with the same material and shape significantly were affected by the geometry of the timber frame.
- The sensitivity geometry of timber frame allows an earthquake to induce more shaking and it leads to reduction frame strength.
- The resonance creates a large displacement and inertia force, however, it leads to failure of timber frame due to the reduction of inertial resistance and developing the mechanical damping and forming the elastic deformation after the meaningfully reducing strength of the timber.
- The same near-fault ground motion differences multidirectional cyclic inertia forces are applied to the models, and it leads to developing differences seismic response of timber frames and occurrences different failure mechanism for each model.

## REFERENCES

1. Aktas, Y.D., Akyüz, U., Türer, A., Erdil, B., Sahin Güçhan, N., 2014: Seismic resistance evaluation of traditional Ottoman timber-frame himis houses: Frame loadings and material tests. *Earthquake Spectra* 30(4): 1711-1732.
2. Androić, B., Čizmar, D., Rajčić, V., 2008: Reliability analysis for laminated timber girders. *Građevinar* 60(6): 513-518.
3. Arun, G. 2009: Traditional timber construction in Turkey. In: Proceedings of international symposium "Timber structures from antiquity to the present". Istanbul: T.C. Haliç University Press, Pp 113-124.

4. Ayala, D. D., Wang, H., 2006: Conservation practice of Chinese timber structures: no originality to be changed, or conserve as found. *Journal of Architecture Conservation* 12: 7–26.
5. Baber, T., Noori, M. N., 1986: Modeling general hysteresis behavior and random vibration application. *Journal of Vibration, Acoustics, Stress and Reliability in Design* 108: 411–420.
6. Dackermann, U., Li, J., Rijal, R., Crews, K., 2016: A dynamic-based method for the assessment of connection systems of timber composite structures. *Construction and Building Materials* 102(2): 999–1008.
7. Daniūnas, A., Gečys, T., 2015: Use of component method in the analysis of timber-steel connections. *Građevinar* 67(11): 1087–1092.
8. Foliente, G.C., 1995: Hysteresis modeling of wood joints and structural systems. *Journal of Structure Engineering* 121(6): 1013–1022.
9. Galassi, S., Ruggieri, N., Dipasquale, L., Tempesta, G., 2018: Assessment of the Moroccan vernacular timber roof: a proposal for an eco-friendly strengthening system. *Journal of Architectural Conservation* 24(3): 224–248.
10. Halicioglu, F. H., Cakir, F., Demirkesen, S., 2014: Structural assessment of traditional stone-timber houses in Turkey. *Građevinar* 66(8): 727–737.
11. Jayne, B.A., 1959: Vibrational properties of wood as indices of quality. *Forest Product Journal* 5: 259–301.
12. Liu, Y., Xiong, H., Kang, J., 2018: Seismic evaluation of wood frame construction based on nail connection deflection status. *Wood research* 63(6): 979–992.
13. Namdar, A., 2016a: A numerical investigation on soil-concrete foundation interaction. *Procedia Structural Integrity* 2: 2803–2809.
14. Namdar, A., 2016b: Failure analysis of concrete frame - A numerical analysis. *Procedia Structural Integrity* 2: 2796–2802.
15. Namdar, A., Darvishi, E., Feng, X., Ge, Q., 2016a: Seismic resistance of timber structure - a state of the art design. *Procedia Structural Integrity* 2: 2750–2756.
16. Namdar, A., Darvishi, E., Feng, X., Zakaria, I., Yahaya, F.M., 2016b: Effect of flexural crack on plain concrete beam failure mechanism - A numerical simulation. *Frattura ed Integrità Strutturale* 36(10): 168–181.
17. Namdar, A., Dong, Y., 2019: Seismic resistance and displacement mechanism of the concrete footing. *Shock and Vibration*, Vol. 2019, Article ID 5498505, 9 pp.
18. Namdar, A., Dong, Y., Liu, Y., 2019: Timber beam seismic design. A numerical simulation. *Frattura ed Integrità Strutturale* 47(13): 451–458.
19. Palinić, N., Bjelanović, A., 2016: Wooden structures in the historic port of Rijeka. *Građevinar* 68(10): 801–814.
20. Pizzo, B., Macchioni, N., Lavisci, P., Ciechi, M. De. 2004: On-site consolidation systems of old timber structures. In: C. Bertolini Cestari, T. Marzi, E. Seip, P. Touliatos (Eds.), 2004: *Proceedings Interaction between science, technology and architecture in timber construction*. Elsevier Science, Heritage Series, Collection Patrimoine, Pp 323–352.
21. Rajčić, V., Bjelanović, A., 2005: Classification of timber. *Građevinar* 57(10): 779–784.
22. Sandoz, J.L., 1989: Grading of construction timber by ultrasound. *Wood Science and Technology* 23: 95–108.
23. Soltis, L. A., 1984: Low-rise timber building subjected to seismic, wind and snow. *Journal of Structure Engineering* 110(4): 744–753.
24. Stepinac, M., Rajčić, V., Barbalić, J., 2017: Inspection and condition assessment of existing timber structures. *Građevinar* 69(9): 861–873.

25. Stepinac, M., Rajčić, V., Žarnić, R., 2019: Timber-structural glass composite systems in earthquake environment. *Građevinar* 68(3): 211-219.
26. Yeh, T. C., Hartz, B. J., Brown, C. B., 1971: Damping sources in wood structures. *Journal of sound and vibration* 19(4): 411-419.
27. Zucchini, A., 2007: Mechanics of masonry in compression: results from a homogenisation approach. *Computers & Structures* 85(3-4): 193-204.

ABDOULLAH NAMDAR\*<sup>1,2</sup>

<sup>1</sup>HUAIYIN INSTITUTE OF TECHNOLOGY  
FACULTY OF ARCHITECTURE AND CIVIL ENGINEERING  
HUAI'AN  
CHINA

<sup>2</sup>TON DUC THANG UNIVERSITY  
ADEPT. FOR MANAGEMENT OF SCIENCE AND TECHNOLOGY DEVELOPMENT  
BEACULTY OF ENVIRONMENT AND LABOUR SAFETY  
HO CHI MINH CITY  
VIETNAM

\*Corresponding author: [abdoullah.namdar@tdtu.edu.vn](mailto:abdoullah.namdar@tdtu.edu.vn)



## DEVELOPMENT OF CROSS-LAMINATED TIMBER (CLT) PRODUCTS FROM STRESS GRADED CANADIAN HEM-FIR

PEIXING WEI<sup>1,2</sup>, BRAD JIANHE WANG<sup>3</sup>, ZHONG LI<sup>4</sup>, RONGHUA JU<sup>4</sup>

<sup>1</sup>SOUTHEAST UNIVERSITY NANJING, CHINA

<sup>2</sup>JIANGSU VOCATIONAL COLLEGE OF AGRICULTURE AND FORESTRY JURONG, CHINA

<sup>3</sup>NINGBO SINO-CANADA LOW-CARBON TECHNOLOGY RESEARCH INSTITUTE NINGHAI, CHINA

<sup>4</sup>NANJING FORESTRY UNIVERSITY NANJING, CHINA

(RECEIVED MAY 2019)

### ABSTRACT

To explore the feasibility of hem-fir for CLT products, this work addressed the exploratory and pilot plant studies of hem-fir cross-laminated timber (CLT) products through mechanical tests. The hem-fir lumber was procured and then stress-graded based on dynamic modulus of elasticity (MOE). The resulted 5-ply prototype CLT products were then tested non-destructively and 3-ply pilot plant hem-fir CLT was tested destructively. The results showed that bending performance of hem-fir CLT panel can be predicted. Considering cost-competitiveness and end applications of hem-fir CLT products, the panel structure can be optimized based on the stress-graded data of hem-fir lumber.

**KEYWORDS:** Hem-fir, cross-laminated timber (CLT), modulus of elasticity (MOE), modulus of rupture (MOR), stress-graded lumber.

### INTRODUCTION

At present, forest resource is changing worldwide over time from old-growth to second growth with an increasing volume of shorter rotation plantations (Middleton and Munro 2001, Alteyrac et al. 2005, Liu and Zhang 2005, Beaulieu et al. 2006, Wei et al. 2013, Yang et al. 2018). To maximize the value return from the resource currently available, forest stands should be managed to produce trees with desired attributes for end products. For product development and market access, characteristics of the second growth plantations should be competitive not only to those of old-growth, but also to those of competing species (Wang et al. 2015, Gong et al. 2016, Liao et al. 2017).

Hem-fir is a combination of western hemlock (*Tsuga heterophylla* (Raf.) Sarg) and amabilis fir (*Abies amabilis* (Dougl.) Forbes) and represents the largest component of forests in coastal forest region of British Columbia (BC), Canada (Chen et al. 2009). These two species are generally

harvested and processed together and marketed as “hem-fir” (called coast hem-fir), which are generally used to produce both solid wood products and pulp and paper. Hem-fir solid wood is used primarily as structural lumber and plywood in home and commercial building construction. Products include framing lumber, joinery, windows, doors, staircases, cabinet doors, ladders, floors, roof decking, railway ties, boxes, interior woodworking and finishes, veneer/plywood, and laminating stock or glulam (Wang and Dai 2008).

Despite the widespread use, opportunities exist to recover more value from the short rotation hem-fir through increased utilization in engineered wood products (EWPs) because they present opportunities for potentially transformative product developments and process improvements. The key advantage of EWPs is that their performance is not necessarily limited by fiber quality. Potential EWPs include structural composite lumbers such as laminated veneer lumber (LVL), thick light-weight strand panels, and cross-laminated timber (CLT) that can replace concrete slabs in residential and non-residential constructions (Wang and Dai 2013). CLT is a solid wood-based composite product made by laminating and gluing multiple wood layers with adjacent layers normally oriented at 90° (Brandner et al. 2016). CLT is manufactured according to a wide range of specifications for such structural applications as floor, ceiling, wall and roof (Kanócz and Bajzecerová 2019).

While various proprietary processes are currently adopted, a typical manufacturing process of CLT products generally includes lumber selection, lumber grouping and planning, adhesive application, panel lay-up and pressing, product quality control, cutting and packaging, and so on (Liao et al. 2017). In North America, CLT product standard and plant qualification standard have been established to help fabricate products with desired grade and superior adhesive bond quality.

Unlike glulam with a column-beam structure (Glisovic et al. 2016), CLT panels were often used as floors, roofs and walls (Song and Hong 2018). For floor and roof applications, key characteristics of bending deflection must first be taken into account requiring higher modulus of elasticity (MOE) of CLT elements (Gagnon and Pirvu 2011). For wall applications, in-plane and out-of-plane shear performance of CLT elements needs to be emphasized with slightly lower MOE of CLT being used (Song and Hong 2018).

Based on the intended end uses of CLT, raw materials, specifically lumber and adhesive, and manufacturing technology can be adjusted. CLT panels can be designed with varying lumber grades and macro characteristics (Wang et al. 2018), thickness and lay-ups for desired engineering performance (Gagnon and Pirvu 2011).

Spruce-pine-fir (SPF) and Norway spruce are respectively the common species for CLT manufacturing in North America and Europe (Brandner et al. 2016). The North American standard of performance-rated CLT suggests softwood species with a minimum specific gravity (SG) of 0.35 for CLT manufacturing (ANSI/APA PRG 320 2018). Although hem-fir has a higher SG ( $\geq 0.35$ ) than SPF and has tremendous strength properties, currently it is not included in the recommended species group for CLT by APA-The Engineered Wood Association because information is lacked regarding whether coast hem-fir is suitable for CLT manufacturing. Thus, research is urgently needed to explore the feasibility of hem-fir for CLT products through adhesive bond quality and mechanical tests.

The previous work demonstrated that CLT products manufactured from BC hem-fir lumber could achieve good bond quality and durability (Wang and Pirvu 2010). In the hem-fir CLT manufacturing, the adhesive type and applied pressure significantly affected percent wood failure (WF) and delamination. For PUR adhesive, a pressure higher than 0.83 MPa could be used to achieve good delamination resistance (Wang et al. 2018). The key objective of this work was

to demonstrate the feasibility of manufacturing CLT products from BC coast hem-fir lumber through exploratory study in Canada and pilot plant mechanical tests in China. The study was intended to provide immediate guidance for the Canadian and Chinese CLT manufacturers to fabricate consistent products, increase CLT performance and reduce manufacturing costs.

## MATERIALS AND METHODS

This work was carried out in FPIInnovations (Canada) and in the pilot plant of Ningbo Sino-Canada Low-Carbon Technology Research Institute (China). The purpose of the exploratory study of hem-fir CLT in FPIInnovations was to illustrate the influence of lumber MOE on the final product MOE to what extent. And then the pilot plant study was continued in China based on the initial results and gained experience of exploratory study.

### Exploratory study

#### *Material preparations*

In FPIInnovations, hem-fir lumber samples were directly purchased from a sawmill in BC with the following three categories:  $4000 \times 38 \times 140$  mm (Kiln-dried No. 1 grade),  $4000 \times 38 \times 140$  mm (Kiln-dried No.3 grade), and  $2700 \times 19 \times 140$  mm (Kiln-dried prior grade). At the time of purchase, the moisture content (MC) was maximum 23% for all hem-fir lumber.

Visual grading of hem-fir lumber stock was first performed in accordance with NLGA rule (2003). In FPIInnovations, the E-rating of hem-fir lumber was done with a transverse vibration method over a 3600 mm span using E-computer equipment (Metriguard 239) (Fig. 1).

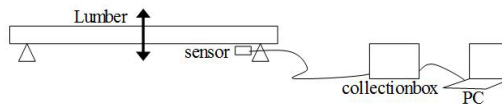


Fig. 1: Dynamic MOE testing by E-computer testing.

To help establish the relationship between CLT product MOE and lumber MOE, three hem-fir CLT construction grades (A, B and C) were distinguished based on the measured dynamic modulus of elasticity (MOE) of lumber within a certain range. The selected lumber was planed to 34 mm thick for  $38 \times 140$  mm and 15 mm thick for  $19 \times 140$  mm, and then grouped for different layers of CLT manufacturing. In the meantime, control western SPF and eastern SPF lumber pieces were grouped to make SPF CLT.

### Prototype hem-fir CLT panel manufacturing

In FPIInnovations, to reveal the relationship between CLT product MOE and lumber MOE, 5-ply prototype hem-fir CLT panels with a target size of  $4000 \times 1200 \times 132$  mm were designed with lay-up configurations shown in Tab. 1. Three hem-fir CLT construction grades (A, B and C) were considered with symmetrical lay-ups, with the outer main laminations (top and bottom faces) having higher MOE rating than the inner main laminations (center). The MOE boundaries indicated in Tab. 1 are based on the designations in the glulam standard for different glulam grades (AITC 2007), which were adapted to the actual MOE range obtained for the hem-fir sample and the number of pieces obtained for each MOE group. The resulted panel lay-up sequence was 34 - 15 - 34 - 15 - 34 (mm) in thickness laminated with adjacent layers oriented at  $90^\circ$  to each other, as shown in Fig. 2.

Tab. 1: The lay-up configurations of 5-ply prototype hem-fir CLT panels.

CLT layer	Lumber visual grade	Lumber thickness (mm)	CLT panel grade			
			A	B	C	
			Required lumber MOE (MPa)			
1	Top face	No.2 & better	34	$11721 \leq MOE < 13792$	$9652 \leq MOE < 11721$	$6896 \leq MOE < 9652$
2	Top cross	No.2 & better	15	$MOE \geq 6896$	$MOE \geq 6896$	$MOE \geq 6896$
3	Centre	No.2 & better	34	$9652 \leq MOE < 11721$	$6895 \leq MOE < 9652$	$MOE < 8274$
4	Bottom cross	No.2 & better	15	$MOE \geq 6896$	$MOE \geq 6896$	$MOE \geq 6896$
5	Bottom face	No.2 & better	34	$11721 \leq MOE < 13792$	$9652 \leq MOE < 11721$	$6896 \leq MOE < 9652$

The grade A CLT was made from lumber with the highest possible MOE with potentially lowest recovery of lumber stock. The grade C CLT was made from lumber with the lowest possible MOE with potentially highest recovery of lumber stock. The grade B CLT was made as a medium grade CLT with relatively high utilization of lumber stock. For each CLT panel, each of the three longitudinal layers (top face layer #1, centre layer #3 and bottom face layer #5) was formed by 9 pieces of 4000 mm long  $34 \times 140$  mm whereas each of the two cross-layers (top cross layer #2 and bottom cross layer #4) was formed by 29 pieces of 1200 mm long  $15 \times 140$  mm. Each grade of CLT panel was repeated three times.

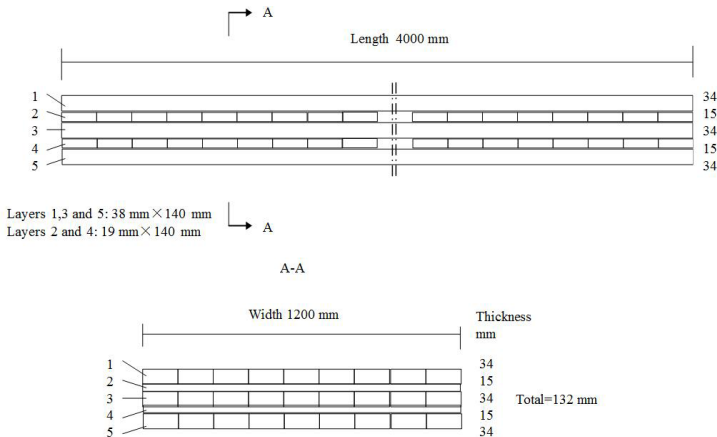


Fig. 2: The lay-up structure of prototype hem-fir CLT panel.

Based on the visual requirements in combination with MOE values of lumber as set out in Tab.1, lumber were selected and placed in MOE groups from where they were randomly selected for various layers of the three CLT panels. For use as cross laminations, each 2700 mm long  $15 \times 140$  mm hem-fir piece was trimmed into two 1200 mm short pieces. At the manufacturing site where an industrial press ( $4000 \times 1200$  mm) was used, all pieces were further face- and edge-planed to the target sizes within 24 h of glue application and pressing.

A commercial polyurethane (PUR) resin was acquired from an adhesive supplier. The CLT panel's lay-up arrangement and sequence, such as the number and location of each lumber

piece per layer, was recorded for each CLT panel. During CLT manufacturing, the ambient temperature was about 7-8°C and the average glue application rate was about 200 g·m<sup>-2</sup>. The panel assembly time was about 15 min without edge-gluing lumber pieces within each layer. However, to minimize the potential gaps between lumber pieces in the top face, center and bottom face layers, a maximum allowable side pressure of 0.35 MPa was applied during pressing. The vertical pressure applied was 0.38 MPa (maximum value offered by the press) with a pressing time of 150 min. After unloading, all CLT panels were stored at ambient temperature and relative moisture content for about two months before flexure testing.

#### *Flexure test of prototype hem-fir CLT panel*

The effective bending stiffness of CLT ( $EI_{eff}$ ) for the major strength axis with alternating orthogonal layers shall be calculated as follows (Gagnon and Popovski 2011):

$$EI_{eff} = \sum_{i=1}^n E_i b_i \frac{t_i^3}{12} + \sum_{i=1}^n E_i b_i t_i z_i^2 \quad (1)$$

where:  $b_i$ - width of the panel for the major strength axis, (mm)  
 $E_i$ - modulus of elasticity of laminations in the  $i$ -th ply, (MPa)  
 $E_{\parallel}$  - for laminations in the longitudinal layers, (MPa)  
 $E_{\perp}$  - for laminations in the transverse layers, which is 1/30 of MOE of lumber in the direction parallel to grain  $E_{\parallel}$ , (MPa)  
 $n$ - number of layers in the panel  
 $t_i$ - thickness of laminations in the  $i$ -th layer, (mm)  
 $z_i$ - distance between the center point of the  $i$ -th layer and the neutral axis, (mm).

For 5-ply hem-fir CLT in this work,  $n = 5$ ,  $b_i = 1200$  mm,  $t_i = 34$  mm ( $i = 1, 3, 5$ ) or 15 mm ( $i = 2, 4$ ),  $z_{i=1} = 49$  mm ( $i = 1, 5$ ) or 24.5 mm ( $i = 2, 4$ ) or 0 mm ( $i = 3$ ) and  $I = b_i (t_1 + t_2 + t_3 + t_4 + t_5)^3 / 12 = 229996800$  mm<sup>4</sup>. Thus, the Eq. 1 can be further derived as follows:

$$E_{eff} = 0.44(E_1 + E_5) + 0.048(E_2 + E_4) + 0.017 E_3 \quad (2)$$

Based on the coefficient of lumber MOE in the Eq. 2, it can be derived that lumber MOE of face and back layers largely determined the final CLT product MOE.

Each 4000 × 1200 mm CLT panel was tested three times non-destructively under four-point loading in bending over a span of 3600 mm to determine stiffness and MOE.

## **Pilot plant study**

### *Material preparations*

In China, hem-fir lumber samples were directly imported from a sawmill in BC of Canada with a size of 38 × 140 mm (5490 mm). All hem-fir lumber was dried in a kiln to reach a measured MC of 12% before using.

Considering the grade outturn and practical applications, all the hem-fir lumber with a sample number of 557 in this work was classified into three grades ( $E_1$ ,  $E_2$ ,  $E_3$ ) based on the dynamic MOE values which were determined by another transverse vibration method using FFT spectrum analyzer (AZ CRAS, Nanjing, China) (Fig. 3). And then lumbars prepared for manufacturing CLT were planed to 35 mm thick.

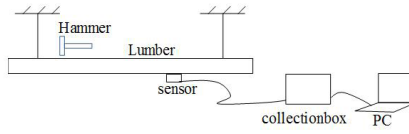


Fig. 3: Dynamic MOE testing by FFT spectrum analyzer.

*Pilot plant hem-fir CLT panel manufacturing*

In China, the panel lay-up sequence was 35 - 35 - 35 (mm) in thickness laminated with adjacent layers oriented at 90° to each other. And two configurations of hem-fir CLT were designed for different applications (floor and wall) based on the lumber E grade, as shown in Tab. 2. For each CLT panel, each of the two longitudinal layers (top face layer #1 and bottom face layer #3) was formed by 9 pieces of 5490 mm long 35 × 140 mm whereas the cross-layer (Centre layer #2) was formed by 39 pieces of 1280 mm long 35 × 140 mm. Two hem-fir CLT replicates were manufactured for each configuration with the same processing parameters as the above description for exploratory study.

Tab. 2: The lay-up configurations of 3-ply pilot plant hem-fir CLT panels.

CLT layer		Lumber visual grade	Lumber thickness (mm)	Required lumber grade	Required lumber grade
Floor panel	1	Top face	No.2 & better	35	E1
	2	Centre	No.2 & better	35	E3
	3	Bottom face	No.2 & better	35	E1
Wall panel	1	Top face	No.2 & better	35	E2
	2	Centre	No.2 & better	35	E3
	3	Bottom face	No.2 & better	35	E2

*Bending test of pilot plant hem-fir CLT panel*

For each 5490 × 1280 mm 3-ply CLT panel, two pieces of CLT bending specimens were cut from both symmetrical sides along with the fiber direction of the top face. Six CLT specimens of wall panel with a size of 3150 × 298 × 105 mm were obtained. Similarly, another six CLT specimens of floor panel with a size of 3150 × 298 × 105 mm were also obtained. Bending tests were conducted flatwise (loads were applied perpendicular to the face layer of CLT) in accordance with the four-point load method. The load continued to increase at a speed of 2 mm·min<sup>-1</sup> until the CLT failure occurred (Fig. 5). The deflection of the specimen at the center of the span was measured via linear variable differential transformers (LVDTs). Both the MOE and MOR of CLT in the major strength direction were evaluated at a span-to-depth ratio of 30 according to ASTM D198 (2015).

**RESULTS AND DISCUSSION**

**Exploratory study**

Fig. 4 shows the frequency distributions of dynamic MOE for both 38 × 140 mm and 19 × 140 mm hem-fir dimension lumber pieces in FPInnovations. Based on the target MOE range (6896 MPa -13792 MPa), hem-fir seemed to have a low reject rate and high grade outturn. The average MOE of 38 × 140 mm hem-fir lumber was 11170 MPa with a standard deviation of

2413 MPa. Based on a parallel study (Wang and Pirvu 2010), the average MOE of  $38 \times 140$  mm western SPF lumber was 10135 MPa with a standard deviation of 2137 MPa. For this study with limited number of hem-fir samples, it was estimated that: 1) only about 1% of total hem-fir lumber has a MOE value below 6896 MPa; and 2) about 29% of total hem-fir lumber (24% for  $38 \times 140$  mm and 33% for  $19 \times 140$  mm) has a MOE value equal or greater than 13792 MPa. The hem-fir grade outturn was about 70%. These high MOE lumber pieces can be used to make higher grade CLT. Amabilis fir only accounted for a small proportion (average 7.1%) of the total hem-fir lumber stock.

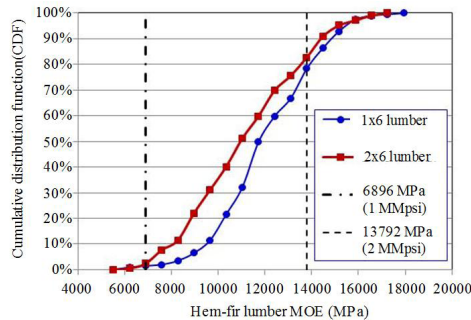


Fig. 4: Frequency distributions of hem-fir lumber dynamic MOE for exploratory study.

As shown in Fig. 5, the CLT bending performance is mainly governed by the lumber MOE in the tension/compression layers (i.e. outer face and back layers), which agrees well with the theoretical derivation.

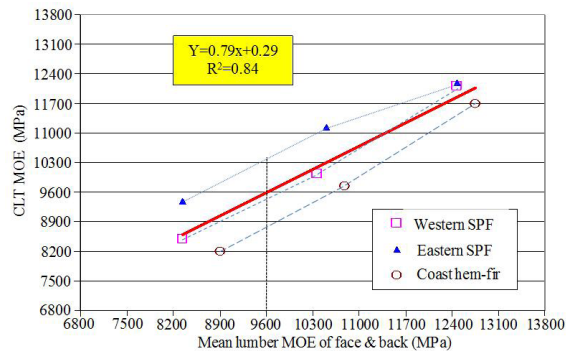


Fig. 5: The relationship between lumber MOE and final hem-fir CLT MOE.

There was a good correlation between the hem-fir CLT panel MOE and average MOE of dimension lumber used for the face and back layers ( $R^2 = 0.84$ ). The higher the lumber MOE in the outer layers, the higher the CLT MOE. Similarly, for spruce-pine-fir (SPF) commonly used for CLT manufacturing in North America, CLT bending performance was also determined by the lumber MOE of outer layers. In addition, according to the trend lines when lumber with the same MOE was used for the outer layers, the eastern SPF-CLT had the greatest bending modulus, western SPF-CLT followed and hem-fir CLT was the last. This difference to a great extent can

be attributed to wood texture feature that affected the mechanical properties of wood along the grain. Development of different CLT grades based on the MOE rating of dimension lumber is beneficial for structural applications as floor and roof components. For wall components, the bending MOE may not be as critical as other properties, such as shear and compression. Thus, selection of the hem-fir dimension lumber for use in CLT should be based on the end application of CLT panels. The use of hem-fir lumber for CLT panels provided promising results. However, given the limited sample size, further studies are needed to confirm appropriateness of hem-fir as a species for CLT manufacturing and acceptance in the Canadian CLT standard.

It was found that the CLT bending performance was basically governed by the lumber MOE of outer layers ( $R^2 = 0.84$ ), namely the lumber closer to the core layer influenced less on the final CLT bending performance. The shear stiffness of core-layers, which can be viewed as another main factor, affected the deformation of CLT owing to its lower stiffness of lumber in the cross-section (Gagnon and Pirvu 2011). Thus, the number of layers can be reduced under the premise of end application and the species which has higher shear stiffness in the cross-section can be selected as the core-layers to make hybrid CLT.

### Pilot plant study

The frequency distributions of dynamic MOE for both  $38 \times 140$  mm hem-fir dimension lumber pieces in Ningbo Sino-Canada Low-Carbon Research Institute are shown in Fig. 6. About 30% of total hem-fir lumber has a MOE value below 9120 MPa and about 35% of total hem-fir lumber has a MOE value equal or greater than 11600 MPa. The two MOE boundaries were selected to achieve a mean lumber MOE of 13800 MPa for E1 grade and a mean lumber MOE of 10340 MPa for E2 grade. Thus, the hem-fir lumbars were classified into three grades, namely, E<sub>1</sub> (MOE  $\geq 11600$  MPa), E<sub>2</sub> ( $9120 \text{ MPa} \leq \text{MOE} \leq 11600 \text{ MPa}$ ), and E<sub>3</sub> (MOE  $< 9120 \text{ MPa}$ ).

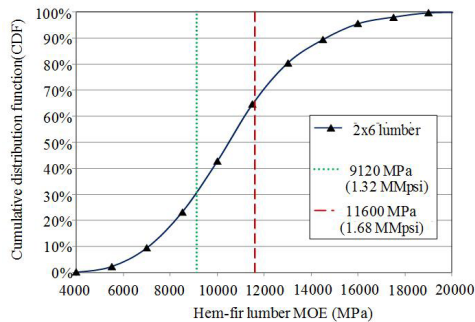


Fig. 6: Frequency distributions of hem-fir lumber dynamic MOE for pilot plant study.

The MOE and MOR of 3-ply pilot plant hem-fir CLT are listed in Tab. 3. Although there was not a good correlation between the hem-fir CLT panel MOE and average MOE of dimension lumber used for the face and back layers owing to the limitations of specimen's number, it was no doubt that the higher the lumber MOE in the outer layers, the higher the CLT MOE and MOR. According to the publication (Liao et al. 2017), at least the 3-ply pilot plant hem-fir floor CLT panel in this study can meet the requirements of CLT grade E1 in the major strength direction and the 3-ply pilot plant hem-fir wall CLT panel can meet the requirements of CLT grade E2, which provided a strong evidence that hem-fir had a feasibility of manufacturing CLT, so called value-added EWP.

Tab. 3: Bending properties of 3-ply hem-fir CLT.

CLT configuration	MOE (MPa)				MOR (MPa)		
	Mean lumber MOE of face & back	Measured CLT MOE	CLT grade E <sub>1</sub> *	CLT grade E <sub>2</sub> *	Measured CLT MOR	CLT grade E <sub>1</sub> *	CLT grade E <sub>2</sub> *
Floor panel	14993.30 (703.99)**	12044.34 (1373.19)**	11721.5	10342.5	39.91 (5.33)**	28.24	23.89
Wall panel	10312.25 (329.02)**	10833.24 (899.60)**			34.78 (2.47)**		

Note: \* The data indicate required characteristic test value for PRG 320 CLT in the major strength direction.

\*\*The data in the brackets indicate the standard deviations.

As indicated by Fig. 6 and Tab. 3, the grade outturn of hem-fir lumber was estimated at 35% each for E<sub>1</sub> and E<sub>2</sub> grades, which can be successfully used to make E<sub>1</sub> and E<sub>2</sub> grade CLT respectively in accordance with ANSI/APA PRG 320 standard (2018).

## CONCLUSIONS

Based on the exploratory and pilot plant studies, it can be concluded that it was feasible to manufacture CLT using BC coast hem-fir lumber. The main findings were summarized as following:

- (1) BC coast hem-fir lumber stock could be used to manufacture CLT products with distinct product MOE classes (grades). The high MOE hem-fir lumber pieces can be used for higher grade CLT. The grade outturn of hem-fir lumber was estimated at 35% each for E<sub>1</sub> and E<sub>2</sub> grades, which can be successfully used to make E<sub>1</sub> and E<sub>2</sub> grade CLT respectively in accordance with ANSI APA PRG 320-2018 standard.
- (2) According to the trend lines when lumber with the same MOE was used for the outer layers, the eastern SPF-CLT had the greatest bending MOE, western SPF-CLT followed and hem-fir CLT was the last. This difference to a great extent can be attributed to wood texture feature that affected the mechanical properties of wood along the grain.
- (3) The final hem-fir CLT product can be designed for cost-effectiveness and predictable bending performance. A good correlation was found between the hem-fir CLT product MOE and MOR and average MOE of hem-fir lumber used for the outer layers.
- (4) The final hem-fir CLT product can be designed based on the end applications such as floor or wall panels. The 3-ply pilot plant hem-fir floor CLT panel in this study can meet the requirements of CLT grade E<sub>1</sub> in the major strength direction and the 3-ply pilot plant hem-fir wall CLT panel can meet the requirements of CLT grade E<sub>2</sub> in accordance with the current ANSI APA PRG 320-2018 CLT standard, which provided a strong evidence that hem-fir had a feasibility of manufacturing CLT.

## ACKNOWLEDGEMENTS

This work was supported by Jiangsu Planned Projects for Postdoctoral Research Funds (2018K121C) and Scientific Project of National Engineering Research Center of Biomaterials, This work was also funded by Natural Resources Canada (Canadian Forest Service), the Province

of British Columbia, and Ningbo Sino-Canada Low-Carbon Technology Research Institute. And the authors would like to thank following staff from FPInnovations of Canada and Ningbo Sino-Canada Low-Carbon Technology Research Institute of China: C. Pirvu, C. Lum, C. Dai, Z. Gao, and S. Zhang.

## REFERENCES

1. Alteyrac, J., Zhang, S.Y., Cloutier, A., Ruel, J.C., 2005: Influence of stand density on ring width and wood density at different sampling heights in black spruce (*Piceamariana* (Mill.) B.S. P.). *Wood and Fiber Science* 37(1): 83-94.
2. ANSI/AITC A190.1, 2007: Structural glued laminated timber.
3. ANSI/APA PRG 320, 2018: Standard for performance-rated cross-laminated timber.
4. ASTM D198-15, 2015: Standard test methods of static tests of lumber in structural sizes.
5. Beaulieu, J., Zhang, S.Y., Yu, Q., Rainville A., 2006: Comparison between genetic and environmental influences on lumber bending properties in young white spruce. *Wood and Fiber Science* 38(3): 553-64.
6. Brandner, R., Flatscher, G., Ringhofer, A., Schickhofer, G., Thiel, A., 2016: Cross laminated timber (CLT): overview and development. *European Journal of Wood and Wood Products* 74(3): 331-351.
7. Chen, Y., Barrett J.D., Lam, F., 2009: Mechanical properties of Canadian coastal Douglas-fir and Hem-fir. *Forest Products Journal* 59(6): 44-54.
8. Gagnon, S., Pirvu, C., 2011: CLT Handbook: Cross-laminated Timber. Vancouver, British Columbia: FPInnovations, 380 pp.
9. Glisovic, I., Stevanovic, B., Todorovic, M., Stevanovic, T., 2016: Glulam beams externally reinforced with CFRP plates. *Wood Research* 61(1): 141-154.
10. Kanócz, J., Bajzecerová, V., 2019: Analysis of composite action of various mass timber structural panels with concrete layer. *Wood research* 63(6): 1091-1099.
11. Liu, C., Zhang, S.Y., 2005: Equations for predicting tree height, total volume, and product recovery for black spruce (*Picea mariana*) plantations in northeastern Quebec. *Forest Chron* 81: 808-14.
12. Liao, Y.C., Tu, D.Y, Zhou, J.H., Zhou, H.B., Yun, H., Gu, J., Hu, C.S., 2017: Feasibility of manufacturing cross-laminated timber using fast-grown small diameter eucalyptus lumbers. *Construction and Building Materials* 132: 508-515.
13. Middleton, G.R., Munro, D., Dai, C., Morris, P., Lum, C., Williams, D., Watson, P., Gee, W., Johal, S., Reath, S., Yuen, B., Hussein, A., 2001: Second-growth western hemlock product yields and attributes related to stand density. Forintek, Canada Corp. 139 pp.
14. National Lumber Grade Authority, 2003: NLGA standard grading rules for Canadian lumber. National Lumber Grades Authority. Burnaby, BC, Canada.
15. Song, Y.J., Hong, S.L., 2018: Performance evaluation of the bending strength of larch cross-laminated timber. *Wood Research* 63(1): 105-115.
16. Wang, Z.Q., Dong, W.Q., Wang, Z.Z., Zhou, J.H., Gong, M., 2018: Effect of macro characteristics on rolling shear properties of fast-growing poplar wood laminations. *Wood Research* 63(2): 227-238.
17. Wang, B.J., Dai, C., 2008: Present utilization and outlook of BC hem-fir for composite products. BC coastal forest sector development program report. Department of Engineered Wood Products, FPInnovations, Vancouver, Canada, 15 pp.

18. Wang, B.J., Dai, C., 2013: Development of structural laminated veneer lumber from stress graded short-rotation hem-fir veneer. *Construction and Building Materials* 47: 902-909.
19. Wang, B.J., Pirvu, C., 2010: Manufacturing and demonstration of Canadian cross laminated timber (CLT). Department of Engineered Wood Products, FPIInnovations, Vancouver, Canada, pp 11.
20. Wang, B.J., Wei, P.X., Gao, Z., Dai, C., 2018: The evaluation of panel bond quality and durability of hem-fir cross-laminated timber (CLT). *European Journal of Wood and Wood Products* 76(3): 833-841.
21. Wei, P.X., Wang, B.J., Zhou, D.G., Dai, C., Wang, Q.Z., Huang, S.W., 2013: Mechanical properties of poplar laminated veneer lumber modified by carbon fiber reinforced polymer. *BioResources* 8(4): 4883-4898.
22. Yang, R., Zhang, J., Wang, S.Q., Mao, H.Y., Shi, Y.L., Zhou, D.G., 2018: Effect of hydrophobic modification on mechanical properties of Chinese fir wood. *BioResources* 13(1): 2035-2048.
23. Gong, Y.C., Wu, G.F., Ren H.Q., 2016: Block shear strength and delamination of cross-laminated timber fabricated with Japanese larch. *BioResources* 11(4): 10240-10250.
24. Liao, Y.C., Tu, D.Y., Zhou, J.H., Zhou, H.B., Yun, H., Gu, J., Hu, C.S., 2017: Feasibility of manufacturing cross-laminated timber using fast-grown small diameter eucalyptus lumbers. *Construction and Building Materials* 132: 508-515.
25. Wang, Z.Q., Gong, M., Chui, Y.H., 2015: Mechanical properties of laminated strand lumber and hybrid cross-laminated timber. *Construction and Building Materials*, 101: 622-627.

PEIXING WEI<sup>1,2\*</sup>, BRAD JIANHE WANG<sup>2\*</sup>, ZHONG LI<sup>3</sup>, RONGHUA JU<sup>3</sup>

<sup>1</sup>SCHOOL OF CIVIL ENGINEERING SOUTHEAST UNIVERSITY, NANJING CHINA 210096

<sup>2</sup>JIANGSU VOCATIONAL COLLEGE OF AGRICULTURE AND FORESTRY NO 19 WENCHANG EAST ROAD, JIANGSU PROVINCE JURONG CHINA 212400

\*Corresponding authors: wayne0448123@163.com and bradwang@shaw.ca

<sup>3</sup>NINGBO SINO-CANADA LOW-CARBON TECHNOLOGY RESEARCH INSTITUTE NINGHAI CHINA 315600

<sup>4</sup>NATIONAL ENGINEERING RESEARCH CENTER OF BIOMATERIALS NANJING FORESTRY UNIVERSITY

NANJING  
CHINA 210037



**SHORT NOTE****ELASTIC CONSTANTS OF SIX WOOD SPECIES  
MEASURED WITH THE RESONANT BEAM TECHNIQUE**

SINN GERHARD<sup>1</sup>, JÜRGEN MAIERHOFER<sup>2</sup>, DIETER LOIDL,  
STEPHAN PUCHEGGER<sup>3</sup>, STEFANIE STANZL-TSCHEGGI

<sup>1</sup>UNIVERSITY OF NATURAL RESOURCES AND LIFE SCIENCES, VIENNA, AUSTRIA

<sup>2</sup>MATERIALS CENTER LEOBEN FORSCHUNG GMBH, LEOBEN, AUSTRIA

<sup>3</sup>UNIVERSITY OF VIENNA, VIENNA, AUSTRIA

(RECEIVED OCTOBER 2019)

**ABSTRACT**

The elastic properties of six wood species were determined using the resonant beam technique. By stimulation of transverse vibrations and analyzing the responding oscillations of carefully prepared rectangular beams of wood, simultaneous determination of one Young's modulus and two shear-moduli on one specimen is possible. Using three different cutting orientations along the principal material directions all three Young's moduli and three shear moduli can be determined. This paper presents the application of this technique to six wood species: two softwoods, two hardwoods and two tropical woods.

**KEYWORDS:** Resonant beam technique, wood, elastic constants.

**INTRODUCTION**

In the literature on wood mechanics, wood is generally treated as an orthotropic material (Bodig and Jayne 1993, United States Department of Agriculture 2010 (5/1–5/2 pp), Wagenführ and Scholz 2008, Kollmann and Côté 1968). Usually three orthogonal directions are used to describe the material: the longitudinal direction L – macroscopically parallel to the stem and microscopically parallel to the fibre direction, the radial direction R – pointing from the pith to bark and the tangential direction T – tangentially to the circumference of the stem and anatomically parallel to the year-rings. The full elastically description of such an orthotropic material requires 9 independent parameters: 3 Young's moduli, 3 shear moduli and 3 Poisson's ratios. Knowledge of these parameters is necessary to model the deformations and stresses in wood under mechanical loads in the elastic range for e. g. wooden constructions, but these data

is often available only partially or not at all for rarer wood species. This paper aims to add the mechanical data of six wood species to the available datasets.

As testing method, the resonant beam technique (RBT) was chosen. With the resonant beam technique (Bucur 2006, Hearmon 1958, Hearmon 1946, Hearmon 1957, Hearmon and Barkas 1941, Kollmann and Krech 1960, Lins et al. 1999), it is possible to determine six of the nine parameters of an orthotropic material with three carefully prepared prismatic specimens oriented in principal material axes L, R and T. The resonance beam technique is therefore a very efficient method to measure elastic constants, especially for the determination of the shear moduli. Reliable data on elastic constants is prerequisite for numerical modelling of wood.

## MATERIALS AND METHODS

### Resonant beam technique

The resonant beam technique works by analysing the free transverse vibration spectra of prismatic beams (specimen). One modulus of elasticity along the beam and two shear moduli perpendicular to each other can be obtained from a single specimen by turning the specimen by 90° along its longitudinal axis. The specimen is suspended on two loops of fibre bundles connected to piezoelectric transducers and to allow free transversal vibrations. On one end, the specimen is excited by a piezoelectric transducer with a sinusoidal signal of defined frequency; on the other end, the oscillations of the specimen are registered with a piezoelectric receiver. Sweeping the excitation frequency slowly from low to high (0.1 kHz – 60 kHz) and measuring the vibrations at the receiver side, a spectrum will be obtained. This experimental spectrum shows several resonance peaks, which are further compared to the theoretical resonances obtained by solving numerically Timoshenko's beam theory for an initial guess of parameters (Timoshenko 1922, 1921, Hearmon 1958). Timoshenko's beam theory is a further development of the classical Euler-Bernoulli-beam-theory taking account for rotatory inertia and shear deformations (Hearmon 1958). The model parameters are then varied to minimize the sum of squares between the modelled and the measured resonance frequencies. The experimental technique applied for this work is described in more detail by Lins et al. (1999) and Puchegger et al. (2003a, 2003b, 2005, and 2006).

### Wood

For this study, six wood species covering a wide range of densities and properties were chosen. The softwoods were Western red cedar (*Thuja plicata*) and European larch (*Larix decidua* Mill.), the two hardwoods from temperate climates were oak (*Quercus robur*) and beech (*Fagus sylvatica*) and the two tropical hardwoods were wenge (*Milettia laurentii*) and courbaril (*Hymenaea courbaril*).

All raw materials were stored in standard climate at 20°C and 65% relative humidity to allow the moisture content to be in equilibrium with the atmosphere before specimen preparation. Specimens were then prepared from planks of stem wood and raw densities were measured. Care was taken to prepare specimens with their material axis parallel to the cutting planes of the prismatic specimens (Fig. 1). The size of the specimens was not uniform, as it depended on orientation and uniformity of growth. A typical size e. g. of longitudinal specimens was 100 x 10 x 12 mm. A minimum of six samples were prepared and scanned for each species.

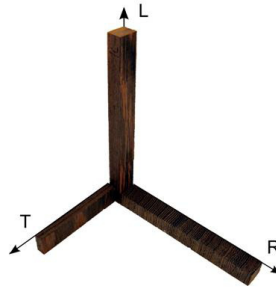


Fig. 1: Prismatic specimens of wenge cut in principal material directions.

## RESULTS AND DISCUSSION

The results of the mechanical constants from the fitting procedure are summarized in Tab. 1 and the results from literature data are summarized in Tab. 2.

Tab. 1: Experimental results for raw-density and elastic constants of investigated wood species.

	$\rho$ ( $\text{kg}\cdot\text{m}^{-3}$ )	$E^L$ (GPa)	$E^R$ (GPa)	$E^T$ (GPa)	$G^{LR}$ (GPa)	$G^{LT}$ (GPa)	$G^{RT}$ (GPa)
Western red cedar	370 (19)	9.36 (0.17)	1.18 (0.14)	0.67 (0.17)	0.91 (0.25)	0.38 (0.31)	0.18 (0.10)
European larch	583 (14)	13.89 (1.60)	1.37 (0.37)	1.02 (0.07)	0.64 (0.27)	0.64 (0.18)	0.51 (0.94)
Beech	764 (32)	21.24 (0.60)	1.92 (0.04)	1.06 (0.07)	1.20 (0.35)	1.74 (1.03)	0.49 (0.09)
Oak	636 (26)	13.09 (0.27)	1.97 (0.06)	0.96 (0.01)	1.20 (0.29)	1.01 (0.34)	0.32 (0.01)
Wenge	836 (58)	19.93 (1.60)	2.80 (0.03)	1.62 (0.30)	1.53 (0.15)	1.61 (0.41)	0.52 (0.09)
Courbaril	955 (11)	16.29 (0.32)	3.47 (0.06)	2.77 (0.70)	2.16 (0.52)	1.52 (0.85)	0.72 (0.28)

\*(Standard deviations in parenthesis).

Moduli of elasticity perpendicular to grain and shear moduli could not be found for all investigated species in literature, especially shear moduli were missing (compare Tab. 2). This confirms the necessity of this work. To compare at least averaged data for softwoods and hardwoods with literature, averages of the elastic constants were calculated and normalized by the longitudinal Young's modulus. The literature values were calculated from table 5-1 of (United States Department of Agriculture 2010). Ratios of averaged parameters from experimental data for softwood and hardwood agree reasonably well with the ratio from literature (Tab. 3), neglecting the influence of density for this rough approximation. Remarkable in Tab. 3 is the increasing ratio of the radial modulus of elasticity to the longitudinal modulus of elasticity, which reflects the increasing amount of ray tissue from softwood to tropical wood. Whereas the moduli of elasticity can be determined in an accurate way from transverse vibrations the shear moduli

are more difficult to determine due to the anisotropic structure of the material. The methodical error increases if the shear modulus is of the same order as the Young's modulus (Puchegger et al. 2005). This is valid especially for G<sup>RT</sup>, where the specimen length orientation is either allocated to the radial or the transverse direction of wood. Additional sources of errors are density gradients within the samples due to the annual structure and grain deviations like interlocked grain observed e. g. for Wengé and Courbaril. These inhomogeneities in density strongly influence the shear coupling in free vibration. Therefore, the spectra measured were distorted and damped, which made identification of some of the resonance peaks more difficult and increased the measurement error. See also Lins et al. (1999) for a deeper discussion on measurement errors.

Tab. 2: Raw-density and elastic constants of investigated wood species from literature.

	$\rho$ (kg·m <sup>-3</sup> )	E <sup>L</sup> (GPa)	E <sup>R</sup> (GPa)	E <sup>T</sup> (GPa)	G <sup>LR</sup> (GPa)	G <sup>LT</sup> (GPa)	G <sup>RT</sup> (GPa)
Western red cedar	370* 310***	8.0* 7.7***	-	-	-	-	-
European larch	590*	12.0*	-	-	-	-	-
Beech	890*	14.0*	2.28*	1.16*	1.64*	1.08*	-
Oak	690*	13.0*	1.5*	0.82*	0.88*	0.62*	-
Wenge	860**	17.5**	-	-	-	-	-
Courbaril	950** 800***	15.7** 14.9***	-	-	-	-	-

\*(Niemz 1993, 217-220 pp.), \*\*(Wagenführ 2000, (399-400 pp., 121-122 pp.)), \*\*\* (United States Department of Agriculture 2010 (2/22 pp., table 5-5a)).

Tab. 3: Average ratios of elastic constants referenced to the longitudinal modulus of elasticity. Ratios calculated from United States Department of Agriculture (2010) table 5-1 and compared to average experimental data from Tab. 1.

	E <sup>T</sup> /E <sup>L</sup> , (%)	E <sup>R</sup> /E <sup>L</sup> , (%)	G <sup>LR</sup> /E <sup>L</sup> , (%)	G <sup>LT</sup> /E <sup>L</sup> , (%)	G <sup>RT</sup> /E <sup>L</sup> , (%)
softwood	5.7	9.6	8.2	7.7	0.9
exp. softwood	7.3	11.0	6.7	4.4	3.0
hardwood	5.7	11.4	8.9	6.7	1.8
exp. hardwood	5.9	11.3	7.0	8.0	2.4
Exp. tropical wood	12.1	17.3	10.2	8.6	3.4

## CONCLUSIONS

The resonant beam technique is a reliable and fast method to determine Young's moduli and shear moduli of orthotropic materials like wood with a relatively low effort regarding the shape and the number of specimens. The experimental results for the moduli of elasticity correspond reasonably well with literature data, while no complete set of reference values could be found for the investigated species. The resonance beam technique applied to other wood species could be a powerful tool to help filling these gaps.

## REFERENCES

1. Bodig, J., Jayne, B.A., 1993: Mechanics of wood and wood composites. Krieger, Pp 110-118.
2. Bucur, V., 2006: Acoustics of wood. Berlin, Springer, Pp 65-69.
3. Hearmon, R.F.S., 1946: The fundamental frequency of vibration of rectangular wood and plywood plates. Proceedings of the Physical Society 58: 78-92.
4. Hearmon, R.F.S., 1957: Some applications of physics to wood. British Journal of Applied Physics 8: 49-58.
5. Hearmon, R.F.S., 1958: The influence of shear and rotatory inertia on the free flexural vibration of wooden beams. British Journal of Applied Physics 9: 381-388.
6. Hearmon, R.F.S., Barkas, W.W., 1941: The effect of grain direction on the Young's moduli and rigidity moduli of beech and Sitka spruce. Proceedings of the Physical Society 53: 674-680.
7. Kollmann, F., Krech, H., 1960: Dynamische Messung der elastischen Holzeigenschaften und der Dämpfung. Ein Beitrag zur zerstörungsfreien Werkstoffprüfung. Holz als Roh- und Werkstoff 18: 41-54.
8. Kollmann, F.F.P., Côté, W.A., 1968: Principles of wood science and technology, Vol. 1: Solid wood, Berlin, Springer, pp. 293-297.
9. Lins, W., Kaindl, G., Peterlik, H., Kromp, K., 1999: A novel resonant beam technique to determine the elastic moduli in dependence on orientation and temperature up to 2000°C. Review of Scientific Instruments 70: 3052-3058.
10. Niemz, P., 1993: Physik des Holzes und der Holzwerkstoffe. DRW-Verlag Weinbrenner GmbH & Co, Pp 217-220.
11. Puchegger, S., Bauer, S., Loidl, D., Kromp, K., Peterlik, H., 2003a: Experimental validation of the shear correction factor. Journal of Sound and Vibration 261: 177-184.
12. Puchegger, S., Loidl, D., Kromp, K., Peterlik, H., 2003b: Hutchinson's shear coefficient for anisotropic beams. Journal of Sound and Vibration 266: 207-216.
13. Puchegger, S., Loidl, D., Kromp, K., Peterlik, H., Weiß, R., 2005: Extension of the resonant beam technique to highly anisotropic materials. Journal of Sound and Vibration 279: 1121-1129.
14. Puchegger, S., Loidl, D., Peterlik, H., Kromp, K., 2006: Determination of elastic modules in dependence on orientation by the resonant beam technique. Materials Science Forum 514-516: 815-824.
15. Timoshenko, S.P. 1921: LXVI. On the correction for shear of the differential equation for transverse vibrations of prismatic bars. The London, Edinburgh, and Dublin Philosophical Magazine and Journal of Science 41: 744-746.
16. Timoshenko, S.P., 1922: X. On the transverse vibrations of bars of uniform cross-section. The London, Edinburgh, and Dublin Philosophical Magazine and Journal of Science 43: 125-131.
17. United States Department of Agriculture, F.S.F.P.L., 2010: Wood handbook: wood as an engineering material. Centennial edition. Madison, WI: U.S. Dept. of Agriculture, Forest Service, Forest Products Laboratory.
18. Wagenführ, A., Scholz, F., 2008: Taschenbuch der Holztechnik, Carl Hanser Verlag, Pp 93-99.
19. Wagenführ, R., 2000: Holzatlas, Fachbuchverlag Leipzig, 720 pp.

SINN GERHARD\*, DIETER LOIDL, STEFANIE STANZL-TSCHEGG  
BOKU – UNIVERSITY OF NATURAL RESOURCES AND LIFE SCIENCES  
INSTITUTE OF PHYSICS AND MATERIALS SCIENCE  
DEPARTMENT OF MATERIAL SCIENCES AND PROCESS ENGINEERING  
PETER-JORDAN-STRASSE 82  
A-1190 VIENNA  
AUSTRIA

\*Corresponding author: [gerhard.sinn@boku.ac.at](mailto:gerhard.sinn@boku.ac.at)

JÜRGEN MAIERHOFER  
MATERIALS CENTER LOEBEN FORSCHUNG GMBH  
ROSEGGERSTRASSE 12  
A-8700 LOEBEN  
AUSTRIA

STEPHAN PUCHEGGER  
UNIVERSITY OF VIENNA  
FACULTY CENTER FOR NANO STRUCTURE RESEARCH  
BOLTZMANNGASSE 5  
A-1090 VIENNA  
AUSTRIA